BUILDING-SPECIFIC SEISMIC RESILIENCE ASSESSMENT FRAMEWORKS CONSIDERING CONTENT SLIDING AND INJURY

By
Trevor Zhiqing Yeow

A THESIS SUBMITTED IN PARTIAL FULFILMENT
OF THE REQUIREMENTS FOR THE DEGREE OF
DOCTOR OF PHILOSOPHY

AT

THE DEPARTMENT OF CIVIL AND NATURAL RESOURCES ENGINEERING

UNIVERSITY OF CANTERBURY
CHRISTCHURCH, NEW ZEALAND
2017

Abstract

In this thesis, frameworks are developed to: (i) quantify the severity of content movement; (ii) predict injuries caused by people losing balance and falling over, or from movement of building contents; and (iii) assess structural damage and injury-related losses caused by earthquakes. These frameworks are then applied to various structural forms to assess which has lower overall life-cycle costs and higher seismic resilience.

The first stage of this research investigated the influence of structural form on building structural and non-structural damage direct-repair costs using existing seismic loss estimation frameworks. In general, it was found that the stiffer building and stronger building considered incurred lower expected annual losses compared to more flexible buildings and weaker buildings. However, cost-benefit assessment showed that stiffer buildings and stronger buildings had higher life-cycle costs when initial construction costs were included.

The second stage focused on quantifying the severity of content movement; in particular content sliding. Existing numerical content sliding models were validated using shaking table tests of realistic furniture on common flooring materials subjected to sinusoidal floor motion. A new equation for predicting the peak sliding displacement of contents was then developed. This equation was found to be more sufficient and efficient compared to other existing prediction equations. Furthermore, it was found that sliding of contents within stiffer buildings were generally less severe compared to more flexible buildings. In contrast, contents in stronger buildings exhibited greater sliding response compared to weaker buildings.

A framework for predicting injuries caused by people falling, content movement, and building collapse was developed in the third stage of this research. Outputs from this framework were found to be consistent with anecdotal injury data. It was found that fall-related injuries were more likely to occur in stiffer buildings and stronger buildings. In

addition, lesser content movement-related injuries occurred in stiffer buildings compared to more flexible buildings. However, more content movement-related injuries occurred in stronger buildings compared to weaker buildings. Lesser collapse-related injuries occurred in stiffer buildings and stronger buildings.

The final stage of this research investigated the influence of structural forms on life-cycle costs including initial construction costs, building damage direct-repair costs, and injury costs. Cost-benefit analyses showed that stiffer buildings generally have lower overall life cycle costs, and the highest seismic resilience, of all buildings considered.

Acknowledgements

First and foremost, I would like to thank my supervisory team; Associate Professor Gregory MacRae (main supervisor), Professor Rajesh Dhakal (co-supervisor), and Professor Brendon Bradley (associate supervisor). They had always found time to provide guidance and support despite their busy schedules, and presented opportunities for me to gain experiences outside of my PhD research. They had also rigorously reviewed my work and provided valuable constructive criticism to guide me towards achieving a high standard for myself. All three are inspirations in my life, and I am grateful to have the opportunity to be their student.

I would like to show my appreciation to the University of Canterbury, the New Zealand Society of Earthquake Engineering, and the New Zealand Earthquake Commission (EQC) for their financial support during various stages of my PhD. I also want to acknowledge the MBIE Natural Hazards Platform for funding the experimental phase of my research. Having financial security enabled me to focus solely on the research, and has no doubt helped in improving its overall quality.

I would also like to acknowledge the technicians who had provided tremendous help with my experimental work; especially John Maley and Alan Poynter. Many thanks as well to the University Warehouse who supplied the furniture used in the experiments, and the Geomechanics Laboratory for allowing the use their very expensive high-speed camera at a short moment's notice. I also want to thank Brandon Hutchinson who had provided me with access to multiple servers which allowed me to complete my computational analyses in a timely manner. Special thanks as well to Greg Preston and Robert Finch for providing me with a nice and quiet office space at the Quake Centre when I was in the final stages of writing my thesis.

My life as a PhD student would not have been as enjoyable without the company of amazing friends within the department; both past and present. Firstly, to my fellow peers

from my undergraduate days who made the jump with me to postgraduate studies together, thank you for helping make the daunting transition that much easier to handle. To those who had been around for a while when I first started, thank you for showing me the ropes and providing much valuable advice to guide me through the first few years which are always the roughest. My sincerest gratitude as well to those who had joined the department during my tenure as a postgraduate student, had the patience to deal with my wise-man tales, and yet supported me when I needed it.

I also want to acknowledge my many friends outside the department who had also supported me through the years; whether it be providing words of encouragement, reminding me to take breaks and look after my health, dragging me out to travel the world during the few opportunities I had available, or just keeping me company while I worked even at some unfathomable hour of the night. I would not have been able to accomplish this feat without all your support. I am glad that I have such amazing friends to remind me that there is more to life outside of research during my time as a PhD student.

Finally, I want to give my heartfelt thanks to my parents and my extended family. They had supported me the most through the year and always made me feel proud of my achievements no matter how small they are. They had brought me into this world, and steered me in the direction of the person I am today. I embarked on this journey not just for myself, but to pay off all the hard work which they had done over the past quarter of a century. From the bottom of my heart, thank you. I am blessed to have such a caring and wonderful family.

Table of Contents

List of Tables

List of Figures

1. Introduction

1.1 MOTIVATION AND OBJECTIVES

During the 2010-11 Canterbury earthquake sequence, it was observed that majority of well-designed buildings satisfied life-safety and collapse-prevention performance objectives. However, many buildings were significantly damaged, and over 1,240 buildings were demolished within the central business district alone [1]. The financial impact of commercial building damage was estimated to be $16 billion in New Zealand Dollars [2]. In addition, 9,430 total injuries were incurred during the 4th September 2010 and 22nd February 2011 shaking events, of which 185 were fatal. Similar observations that large financial losses and injury numbers may still be incurred despite the buildings meeting minimum code requirements had also been made during the 1994 Northridge event. As a result of this event, direct economic loss to the commercial/industrial sector was estimated to be $15.2 billion USD [3], and up to 246,000 people were injured [4].

One approach to reduce this socioeconomic burden in future events is to encourage the design and construction of certain structural forms which are more likely to have a better performance than others. This is based on past observations, such as (i) the stiff Japan Industrial bank building incurring significantly less structural damage during the 1923 Great Kanto earthquake compared to more flexible buildings of similar age [5, 6], and (ii) the poor performance of unreinforced masonry buildings during the 2010-11 Canterbury sequence of earthquakes [7].

There are several methods available to assess the benefits of selecting one structural form over another. One qualitative method proposed by Chanchi et al. [8] is to assign ratings to various structural forms based on their performance in numerous categories; such as drift damage, element replaceability, floor damage, and permanent displacement. A limitation of

this approach is the ratings are subjective, and it is difficult to quantify if any improvement in performance warrants an increase in construction cost.

An alternative approach is to apply seismic loss estimation frameworks to quantify the financial impact of seismic events. One such approach is that by the Pacific Earthquake Engineering Research (PEER) center [9], where losses were estimated in four steps: (i) predict the severity of ground shaking; (ii) analyze the building's response; (iii) assess the extent of damage; and (iv) quantify resulting losses categorized by damage, death and injury, and downtime. While this approach is rigorous and provides useful information for decision-making purposes, there are several aspects which require improvement.

One such aspect is the assumption that damage to generic building contents, such as furniture and machinery, are correlated to the floor's peak total floor acceleration [10]. However, contents are unlikely to be damaged until it moves far enough to impact other objects, and as such the content's response itself is important in determining if damage will occur. The two most common modes of content movement are rocking and sliding. Rocking response has been investigated in detail in past studies (e.g. [11-14]), especially due to its applicability to certain structural members such as freestanding masonry walls. Experimental and numerical studies on content sliding are far less common, and those which exist are generally based on assumptions which had not been verified using realistic contents on common flooring materials.

Another aspect that could be improved is the prediction of injuries. Most existing approaches uses sample injury rates based on interpretation of sparse injury data, and usually focus mostly on fatalities and/or are correlated to the building's global damage state [15-17]. However, a past study by Porter et al. [18] had found that non-fatal injuries comprised of 96% of total injury cost during the 1994 Northridge earthquake, demonstrating that non-fatal injuries can have a much larger impact on society compared to fatalities. In addition, 55%

and 47% of injuries occurring during the 1994 Northridge and the 2011 Canterbury earthquake sequence, respectively, were due to people losing balance and falling over and/or from impact with projectiles (e.g. non-structural contents) [19, 20]. These sources of injury may not necessarily be dependent on the building's global damage state and are not explicitly considered in existing models.

Though the PEER framework and other loss assessment approaches exist, there are very few studies that use these tools to compare the seismic performance of various structural forms. Those which exist [16, 21-23] do not consider the consequence of selecting particular values of key parameters for design, such as a building's fundamental period, T, or the force reduction factor, R. These do not consider injuries either.

Based on this, it is clear that more advanced methods to evaluate content sliding and injuries need to be developed and validated to provide better estimate of losses in seismic events. These methods then need to be applied to a range of structural forms to identify which are more likely to have a better performance than others in terms of limiting building damage-repair costs, content movement, and injuries. In order to address these needs, the key objectives of this research are as follows:

i) **Building damage-repair costs:** Identify which structural form is best to limit building damage-repair costs.

ii) **Content sliding:** (i) Validate numerical content sliding models using shaking-table test findings, (ii) develop a parametric equation for predicting the extent of content sliding and test this using the numerical models, and (iii) identify which structural form is best to limit content sliding.

iii) **Injury modelling:** (i) Develop a framework for predicting building-specific indoor injury rates including those caused by people losing balance and falling over and/or impact with moving contents, (ii) demonstrate its application for

assessing the effectiveness of mitigation strategies (i.e. anchoring contents) or for deriving sample injury rates for use in less sophisticated injury prediction approaches [15-17], and (iii) identify which structural form is best to limit injury-related losses.

iv) **Combined building damage-repair and injury costs:** Identify which structural form is best to limit combined damage-repair and injury-related loss.

Note that downtime effects are not included in this research as most models are still in its infancy at the time of writing. For example, some methodologies, such as FEMA P-58 [24], are unable to consider the effect of repair sequencing; such as priority being given to repair the structure to a state where interior repairs can be performed safely. While there are ways to account for sequencing (i.e. Gnatt chart approach [25]), investigation into factors determining the order of repair sequence is required. This is in addition to complexities regarding estimating the duration between the earthquake event to the start of repair time (i.e. mobilization time [26]); such as understanding the influence of insurance. As there are limited resources available considering the other objectives already being included, further advancements to downtime modelling were not explored in this thesis.

1.2 ORGANISATION OF THESIS

This thesis is a collection of seven technical chapters which addresses the key objectives outlined in **Section 1.1**, along with a final concluding chapter and appendices. Note that each of the technical chapters is written as stand-alone publications for submission to journals and conferences. While parts have been edited so that the individual chapters are linked, there is unavoidable repetition of background material and findings across several chapters. No dedicated literature review chapter was provided, as this is covered within each relevant technical chapter.

Chapters 2 and **3** demonstrate the use of the PEER loss assessment framework considering only initial construction and building damage direct-repair costs for (i) assessing the relative performance of a frame and a wall building, and (ii) quantifying the effect of a wall building's stiffness and strength on its seismic performance, respectively. The buildings' structural response and incurred losses are scrutinized in detail to highlight the benefits and disadvantages of selecting one form over another.

Chapter 4 details shaking-table tests of office-type furniture on realistic flooring surfaces to identify the parameters which affect content sliding. Validation of numerical analysis approaches for predicting the sliding response of contents against the recorded response from experiments is performed.

In **Chapter 5**, a new parametric equation for estimating the maximum sliding displacement of contents during seismic events is developed. This is then compared against other existing parametric equations using a numerical case study of content sliding within several elastic five-storey frame buildings to investigate which equation is the most sufficient and efficient.

Chapter 6 applies sliding numerical models to a range of wall buildings of varying stiffness, strength, and number of floors to investigate the effect of structural properties on the extent of sliding. The new parametric equation from **Chapter 5** is also tested here to observe its applicability to inelastic buildings. A method to include this equation in design is proposed.

In **Chapter 7**, a new framework for predicting injuries which explicitly considers injuries caused by people losing balance and falling over and content-movement, and also estimates injury severity and associated costs (i.e. treatment, decreased quality of life), is developed. A case study is examined to demonstrate its usage, and its findings are compared to historical injury data to validate the model. An additional case is also examined to quantify

the benefits of anchoring contents on reducing injuries, and to derive sample injury rates for use in less advanced models.

Chapter 8 applies the injury prediction framework to the case study from **Chapter 3** to investigate the effect of a wall building's stiffness and strength on injuries. Damage repair cost findings from **Chapter 3** are also included to investigate the significance of injury-related losses with respect to damage repair costs, and whether considering injuries may alter decision-making outcomes compared to considering damage losses on its own. Additional sample injury rates are derived and proposed.

Chapter 9 summarizes the key findings and contributions from this thesis, and provides recommendations on optimal structural forms for use in engineering practice to improve seismic resilience. Recommendations for possible future extensions of this work are also discussed.

1.3 REFERENCES

1. Gates, C. (2015). 1240 central Christchurch buildings demolished video. The Press: Fairfax New Zealand Limited.
2. Wood, A., Noy, I., & Parker, M. (2015). The Canterbury rebuild five years on from the Christchurch earthquake. Bulletin of the Reserve Bank of New Zealand, 79(3), 3-16.
3. Petak, W. J., & Elahi, S. (2001). The Northridge Earthquake, USA and its Economic and Social Impacts. Paper presented at the EuroConference on Global Change and Catastrophe Risk Management Earthquake Risks in Europe, IIASA, Laxenburg Austria.
4. Seligson, H. A., & Shoaf, K. I. (2003). Human impacts of earthquakes. In Earthquake Engineering Handbook. CRC Press, Boca Raton, FL: W F Chen, C R Scawthorn.
5. Freeman, J. R. (1932). Earthquake Damage and Earthquake Insurance. New York, US: McGraw-Hill.
6. Berg, G. V. (1983). Seismic Design Codes and Procedures (Vol. 6). Berkeley, California, US: Earthquake Engineering Research Institute.
7. Cooper, M., Carter, R., & Fenwick, R. (2012). Volume 4 - Earthquake-prone buildings: Canterbury Earthquake Royal Commission.
8. Chanchi, J., MacRae, G. A., Chase, G. J., Rodgers, G. W., & Clifton, C. G. (2012). Methodology for Quantifying Seismic Sustainability of Steel Framed Structures. Paper presented at the STESSA 2012, Santiago, Chile.
9. Deierlein, G. G., Krawinkler, H., & Cornell, C. A. (2003). A Framework for Performance-based Earthquake Engineering. Paper presented at the 2003 Pacific Conference on Earthquake Engineering, Christchurch, New Zealand.
10. Aslani, H., & Miranda, E. (2005). Probabilistic Earthquake Loss Estimation and Loss Disaggregation in Buildings: Department of Civil and Environmental Engineering, Stanford University.
11. Aslam, M., Godden, W. G., & Scalise, D. T. (1978). Rocking and Overutrning Response of Rigid Bodies to Earthquake Motions: University of California, Berkeley.
12. Spanos, P. D., & Koh, A.-S. (1984). Rocking of Rigid Blocks due to Harmonic Shaking. Journal of Engineering Mechanics, 10, 1627-1642.

13. Zhang, J., & Makris, N. (2001). Rocking Response of Free-Standing Blocks under Cycloidal Pulses. Journal of Engineering Mechanics, 127(5), 473-483.
14. Sorrentino, L., AlShawa, O., & Decanini, L. D. (2011). The relevance of energy damping in unreinforced masonry rocking mechanisms. Experimental and analytic investigations. Bulletin of Earthquake Engineering, 9(5), 1617-1642.
15. Coburn, A. W., Spence, R. J. S., & Pomonis, A. (1992). Factors determining human casualty levels in earthquakes: Mortality prediction in building collapse. Paper presented at the Tenth World Conference in Earthquake Engineering, Madrid, Spain.
16. Mitrani-Reiser, J. (2007). An Ounce of Prevention: Probabilistic Loss Estimation for Performance Based Earthquake Design. PhD Thesis, California Institute of Technology, Pasadena, California.
17. FEMA. (2015). Hazus(R) - MH 2.1 Technical Manual - Earthquake Model: Department of Homeland Security, Mitigation Division, Washington, D.C.
18. Porter, K. A., Shoaf, K. I., & Seligson, H. A. (2006). Value of Injuries in the Northridge Earthquake. Earthquake Spectra, 22(2), 555-563.
19. Shoaf, K. I., Sareen, H., Nguyen, L. H., & Bourque, L. B. (1998). Injuries as a result of California Earthquakes in the Past Decade. Disasters, 22(3), 218-235.
20. Johnston, D., Standring, S., Ronan, K., Lindell, M., Wilson, T., Cousins, J., Aldridge, E., Ardagh, M. W., Deely, J. M., Kirsch, S. J. T., & Bissell, R. (2014). The 2010/2011 Canterbury earthquakes: context and cause of injury. Natural Hazards, 73(2), 627-637.
21. Wen, Y. K., & Kang, Y. J. (2001). Minimum Building Life-Cycle COst Design Criteria. II: Applications. Journal of Structural Engineering, 127(3), 338-346.
22. Ramirez, C. M., Liel, A. B., Mitrani-Reiser, J., Haselton, C. B., Spear, A. D., Steiner, J., Deierlein, G. G., & Miranda, E. (2012). Expected earthquake damage and repair costs in reinforced concrete frame buildings. Earthquake Engineering and Structural Dynamics, 41(11).
23. Moehle, J., Bozorgnia, Y., Jayaram, N., Jones, N. P., Rahnama, M., Shome, N., Tuna, Z., Wallace, J., Yang, T., & Zareian, F. (2011). Task 12 Report for the Tall Buildings Initiative: Case Studies of the Seismic Performance of Tall Buildings Designed by Alternative Means: Pacific Earthquake Engineering Research Center.

2. Seismic Direct Repair Cost Assessment of Structural Systems

2.0 SUMMARY

Probabilistic building component-based seismic loss assessments of a reinforced concrete (RC) frame building and an RC wall building is performed to identify which is more seismically resilient. Both buildings are 10-stories tall, and were designed to minimum allowable standards according to New Zealand seismic codes. Inelastic response history analyses were performed using ground motion records selected following the Generalized Conditioning Intensity Measure approach. It was found that the wall building, which is stiffer and stronger compared to the frame building, has greater (i) initial construction costs, (ii) total floor accelerations, and (iii) acceleration-related damage; but incurs lower (i) interstorey drifts, (ii) drift-related damage, and (iii) probability of requiring full-replacement. Drift-related damage accounted for over 90% of direct damage-repair costs in both buildings, despite acceleration-sensitive contents contributing to over half of the initial construction costs; resulting in the wall building's expected annual direct-repair costs being lower. Despite this, cost-benefit analyses showed that the frame building has lower life-cycle costs considering both initial construction and direct-repair costs. However, loss-hazard curve comparisons including construction costs showed that the wall building has lower losses for events with return periods rarer than 910 years. This decreases to 550 years if acceleration contents were adequately braced, but increases to 1,620 years if the building has few drift-sensitive non-structural elements (i.e. car parking buildings). The selection of the "optimal" building would therefore depend on the risk appetite of stakeholders (i.e. a risk-adverse decision maker may be more concerned with losses in rarer events), and building usage-type.

2.1 INTRODUCTION

Major seismic events worldwide have illustrated that losses associated with damage repair, death/injuries and business disruption can have major economic and social impacts on society. For example, the total financial implication as a result of the 2010-11 series of earthquakes in Canterbury, New Zealand, on commercial buildings was estimated to be $16 billion [1]. A large proportion of buildings in the city centre were severely damaged, some of which had to be demolished. This resulted in significant downtime for many businesses. Similar impacts were observed following the 1994 Northridge, 2009 L'Aquila, and 2010 Maule earthquakes, among others.

One observation from past events is that some structural systems perform better than others. For example, unreinforced masonry buildings generally perform worse than modern ductile frame buildings in major seismic events [2]. Hence, one method to reduce the burden on society from seismic events is to highlight the structural systems which are more likely to perform well. This can be done by utilizing loss estimation methods to quantitatively predict the building performance in terms of the three categories of losses; damage, death/injury and downtime.

While several variations of loss estimation are available in literature, most typically consist of predicting (i) the intensity of ground shaking (measured using an intensity measure, *IM*), (ii) the response of the structure (defined by an engineering demand parameter, *EDP*), (iii) the extent of damage (categorized by a damage measure, *DM*), and (iv) the resulting losses (referred to as decision variables, *DV*). One of the most widely used loss estimation frameworks was formulated by the Pacific Earthquake Engineering Research (PEER) center [3, 4]. Several enhancements to this framework have been made over the past decade, including the ability to perform loss estimation at a component level [5, 6], deaggregate losses [6], compute expected annual losses using a quadruple integration approach [7],

improve computational efficiency [8], and more [9-11]. Several computational programs based on the overall methodology have also been developed [9, 12, 13]. The robustness of these programs and the detailed computed loss information helps provide stronger basis for stakeholders to make decisions.

Studies utilizing loss estimation methodologies to compare the relative seismic performance of different buildings are present in literature [9, 14-16]. The first three studies only considered a single type of structural system as their focus was on the influence of strength detailing. The latter examined the performance of three 42-storey buildings comprising of different lateral load resisting systems; a reinforced concrete (RC) core wall system with perimeter post-tensioned gravity frames, an RC core wall and special moment frame dual system, and a composite buckling-restrained braced (BRB) frame system. It was found that the BRB system had the lowest expected annual loss, followed by the dual frame system and the core wall system. However, cost-benefit assessments considering construction cost and insurance premiums (assumed equal to expected annual losses) had the opposite trend due the core wall system having significantly lower initial construction costs.

There are two limitations to the methodology used by Moehle et al. [16] and the other studies referenced. The first is that the building's performance was often quantified using expected annual losses in one form or another. This measure does not properly convey loss information from larger events, as the biggest contributors to expected annual losses arises from smaller events due to their more frequent occurrence [6, 17]. This information is therefore not sufficient for risk-adverse decision makers. As a decision makers' risk-appetite may be influenced by factors such as prior experience with natural disasters [18], there is a need for the reported losses to be usable for all risk-appetites [19]. While methods such as utility theory [20] or stochastic dominance criteria [21] can be used, these may not be easily

performed in engineering practice. A simpler approach, such as modifying the loss-hazard curve, may be sufficient to achieve this.

The second limitation is that the ground motion record selection methodology used is not site-specific and/or are obtained by scaling to a uniform hazard spectra. This results in the seismic hazard not being properly represented, which is a key requirement in time-based assessments. Although enforcing seismic hazard consistency ensures that the losses incurred are more representative of the site of interest, it may not necessarily change the hierarchy of different structural systems in terms of losses. Nonetheless, this should be considered by using state-of-the-art seismic hazard consistent approaches, such as the Generalized Conditioning Intensity Measure approach [22, 23].

This chapter examines a case study comparing the seismic performance of two 10-storey reinforced concrete (RC) office buildings. One building uses a moment-resisting frame lateral load resisting system, while the other uses cantilever walls. These were selected due to their common usage in New Zealand. For fair comparisons, both have similar plan layout, are designed for Christchurch subsoil class C conditions, and were designed to just meet minimum requirements in design standards where possible. This study seeks to provide rigorous structural behaviour and loss comparisons to provide insight into the influence of a structural system's characteristics on its performance. Note that injury and downtime losses were not considered due to their corresponding modelling approaches still being in its infancy as discussed in **Chapter 1**. In particular, answers to the following questions were sought:

1. How does the selection of structural system affect damage-related and acceleration-related losses?
2. Which building has lower life-cycle cost considering construction and direct-repair costs only?
3. How would the selection of building change with differing risk-appetites?

4. Would the findings change if mitigation strategies were implemented or if the building's usage-type was changed?

2.2 CASE STUDY BUILDING DETAILS

2.2.1 Building Design and Layout

The RC frame building considered in this study was based off the Red Book [24] design example which follows the New Zealand concrete standard, NZS3101:2006 [25]. The building is 10-stories tall, with storey heights of 4 m for the ground floor and 3.6 m for other floors as shown in as shown in **Figure 2.1a**. The lateral load resisting system consists of two perimeter frames in each orthogonal direction, as shown in **Figure 2.1b**. The exterior frames were designed for Christchurch subsoil class C conditions prior to the 2010-2011 Canterbury earthquakes (i.e. a zone factor of 0.22) following the Equivalent Static Method from the New Zealand earthquake loading standard, NZS1170.5:2004 [26]. The force reduction factor, which is the ratio of the design 10% probability of exceedance in 50 year elastic base shear demand to the design base shear demand, was taken as 4.0. While the gross section geometry of interior gravity frame members were provided in the Red Book [24], the reinforcing details were not provided. Hence, these members were not included in the models.

The RC wall building has the same floor geometry and height dimensions as the RC frame building, but the exterior frames were replaced with exterior rectangular walls as shown in **Figure 2.1c**. The ratio between the combined cross sectional area of the walls resisting seismic action in a given orthogonal direction to the floor plan area per storey level was approximately 1%, which is considered the minimum allowable in literature [27, 28]. A minimum allowable reinforcement ratio of 0.53% based on NZS3101:2006 [25] within the plastic hinge region at the base of the wall was assumed. The section geometry and detailing within the plastic hinge region satisfies all strength and stability requirements in the design

standards. As such, it is the detailing requirements which govern the design of the wall rather than minimum required strength.

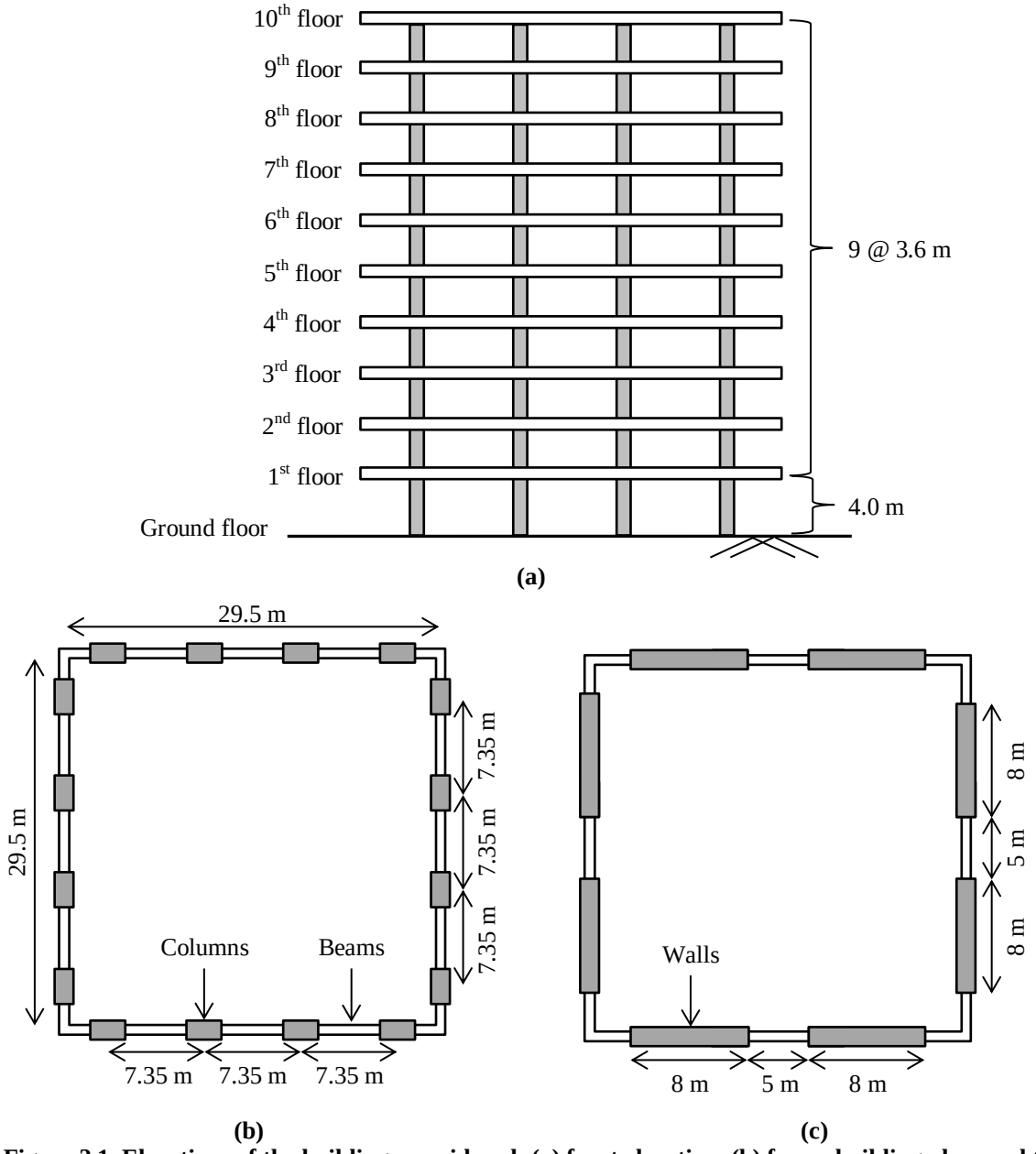

Figure 2.1. Elevations of the buildings considered; (a) front elevation, (b) frame building plan, and (c) wall building plan

2.2.2 Content Inventory and Fragility

The buildings' content inventory considered in this study is listed in **Table 2.1**, and was based on that used by Bradley et al. [17]. The non-structural components and content layout are identical in both buildings; with the exception of the exterior glazing as there is less open exterior space available for the wall building. Costs associated with structural components

were obtained from the Rawlinsons New Zealand construction handbook [29], while non-structural component costs were assumed equal to the estimated full-replacement cost given by the references in **Table 2.1**.

The Seismic Loss Assessment Tool (SLAT) [12], which was used to compute the direct repair cost of the buildings, includes a library of fragility functions based on the references in **Table 2.1**. These fragility functions are used to estimate the probability of the i^{th} building component incurring the j^{th} damage state, DS_j, such as dislodging of ceiling tiles, for a given *EDP*, $P_{DSj|EDP}(ds_j|edp)$. Loss functions, which can be defined by the mean and standard deviation of repair costs for the i^{th} component incurring the j^{th} damage state, $\mu_{Li|DSj}(ds_j)$ and $\sigma_{Li|DSj}(ds_j)$ respectively, are also available. The loss and fragility functions can be combined to compute the mean and standard deviation of the i^{th} component repair costs for a given *EDP*. The equations for this are shown in **Eq. 2.1a** and **2.1b**, respectively; where N_{DS} is the total number of damage states for the i^{th} building component. Note that **Eq. 2.1** and other equations related to loss assessment provided later were obtained from Bradley et al. [17], despite there being preceding research with similar equations [3-6, 9, 30]. This is because SLAT, which was used to perform loss estimation in this study, was developed using the equations in the form provided by Bradley et al. [16].

$$\mu_{Li|EDP}(edp) = \sum_{j=1}^{N_{DS}} \mu_{Li|DSj}(ds_j).P_{DSj|EDP}(ds_j \mid edp) \qquad \textbf{(2.1a)}$$

$$\sigma_{Li|EDP}(edp) = \sqrt{\sum_{j=1}^{N_{DS}} \left[\mu^2_{Li|DS}(ds_j) + \sigma^2_{Li|DS}(ds_j)\right] P_{DSj|EDP}(ds_j \mid edp) - \mu^2_{Li|EDP}(edp)} \qquad \textbf{(2.1b)}$$

Table 2.1 Building components inventory costs ($ million) [fragility function reference in square brackets]

Component	Description	Cost (Frame)	Cost (Wall)
Beam [12]		1.39	0.96
Column [12]		0.67	0.13
Wall (specification B1044.093 [13])		0	1.17
Slab Connection [6]		1.42	1.42
Partition [9]	721 m^2/floor	1.29	1.29
Exterior Glazing [5]	1 pane/2.7 m^2	0.13	0.08
Drywall Paint [9]	721 m^2/floor	0.12	0.12
Generic Drift Sensitive Non-structural component [6]	$100,000/floor	1.00	1.00
Ceiling Systems Suspended acoustical tile [12]	693 tiles/floor	2.01	2.01
Automatic sprinklers [9]	23 sections/floor	0.21	0.21
Desktop Computers [31]	$93000/floor	0.93	0.93
Servers and network equipment [12]	$200,000/floor	2.00	2.00
Roof mounted equipment [12]	$600,000 on roof	0.60	0.60
Conveying - hydraulic elevator [32]		0.11	0.11
Generic acceleration sensitive non-structural component [6]	$100,000/floor	1.00	1.00
Total Building Value		12.88	13.03

Note that while $\mu_{Li|DSj}(ds_j)$ and $\sigma_{Li|DSj}(ds_j)$ from references in **Table 2.1** were used for non-structural contents, only $\sigma_{Li|DSj}(ds_j)$ from the references were used for structural elements. This was because the full-replacement cost of structural elements were obtained from Rawlinson & Co [29], and thus the mean repair cost would likely differ with that from the referenced fragility functions. For these cases, $\mu_{Li|DSj}(ds_j)$ was estimated by multiplying the estimated full-replacement cost from Rawlinson & Co [29] by the ratio between the damage state repair costs to the full-replacement cost for the respective fragility function referenced. For example, the ratio of the wall building repair cost to replacement cost for damage states 1, 2, and 3 from Naeim and Hagie [13] are 0.20, 0.67, and 1.00, respectively; which would correspond to approximately $5,760, $19,700, and $29,300 per wall per floor based on the replacement cost obtained using Rawlinson & Co [29]. This assumes that the repair cost of components is directly related to its replacement cost. $\mu_{Li|DSj}(ds_j)$ and $\sigma_{Li|DSj}(ds_j)$ were used in later sections for estimating the global building losses.

2.3 STRUCTURAL MODELLING

2.3.1 Structural Model and Analysis

Inelastic non-linear response history analyses of the two structures were performed on Ruaumoko2D [33] using two-dimensional models of the lateral load resisting systems. Note that the adopted approach results in torsional or bi-directional action effects on structural members being excluded. These effects are however assumed to be minor as (i) the plan elevations are regular so torsional effects are likely to minimal, and (ii) there are no corner columns in either building so bi-directional effects should not be a significant issue. A constant damping ratio of 5% was assigned to all modes using Caughey damping [34], masses were lumped at the nodes of the building model, and P-delta were accounted for using large displacement analyses [35].

The beams and columns in the frame structure were modelled using concrete beam-column elements to include moment-axial force interaction effects (details available in Ruaumoko manual [35]). The hysteretic behavior of the structural members were modelled using the Modified Takeda hysteretic rule [36].

The structural walls were modelled allowing a plastic hinge to form only at its base using a lumped plasticity element. Preliminary analyses using ground motion records corresponding to a 1 in 2,500 year event showed that this approach is reasonable as (i) the gravity loads acting on the walls remains relatively constant, and (ii) the moment demand does not exceed the wall's capacity in regions assumed elastic. The hysteretic behaviour of the walls were modelled using the SINA hysteresis rule [37], which is a better fit to past experimental findings compared to the Modified Takeda model [38-41].

Fiber section analysis of the structural elements was performed on SAP2000 [42] to obtain the moment capacity, elastic stiffness, and moment-curvature post-elastic stiffness ratio, r_{ϕ}, of each element. In experimental studies, however, the behaviour of elements are

usually expressed as force-displacement or moment-rotation, and past results (e.g. [38-41, 43, 44]) have shown that the post-elastic force-displacement stiffness ratio, r_{Δ}, of a well-designed ductile RC structural element is generally within the range of 2-5%. Therefore, the equation for the plastic hinge length, L_p, considered in this study follows that derived by Tagawa [45], as this expression considers both r_{ϕ} and r_{Δ} in its derivation. This equation is shown in **Eq. 2.2**, where L is the length of the member, and α is 3 and 6 for elements in single and double curvature, respectively. For this study, r_{Δ} of 2% was assumed for all members.

$$L_p = \frac{r_{\phi} L}{\alpha r_{\Delta}} (1 - r_{\Delta}) \qquad \textbf{(2.2)}$$

P-delta actions arising from gravity loads on interior frames were considered by attaching a leaning column to the models. The gravity loads not taken up by the lateral load resisting system per floor was then applied to each of the leaning column's nodes. This method of analysis was selected over explicitly modelling the interior frame because (i) exact reinforcing layout of interior members were not provided in the Red Book [24], (ii) the difference in the results between the two methods were minor (within 5%) if a minimum allowable reinforcing ratio was assumed for the interior frames, and (iii) the computational time was considerably reduced due to having 40% less nodes and elements.

It should be noted that degradation of each member's strength and stiffness with repeated inelastic action during a seismic event was not considered. The reason for this is due to a lack of data to calibrate such models for structural walls. Instead, drift limits were used to identify if a building was damaged to the point of requiring full-replacement. This is discussed further in **Section 2.3.3**. Other changes in the building's strength and stiffness with time, such as deterioration from exposure to the environment, were not considered.

Structural analyses were performed using a ground motion suite consisting of eleven sets of record; each representing a certain hazard level. Selection of these records is described

in **Section 2.4**. Linear interpolation of building response between each hazard level was then performed, and the cumulative distribution function of an *edp* being exceeded given a certain *im* level, $G_{EDP|IM}(edp|im)$, can be calculated using **Eq. 2.3** [17]. Here, *FR* denotes cases requiring the building to be fully replaced after a shaking event, while *NFR* is for cases in which full-replacement is not required. Note that this differs from past studies which considered collapse instead of full-replacement. The main difference is that full-replacement cases also consider events where the building may not collapse but requires demolition. The reasoning behind this change will be discussed in **Section 2.3.3**.

$$G_{EDP|IM}(edp \mid im) = G_{EDP|IM,NFR}(edp \mid im)[1 - P_{FR|IM}(im)] + P_{FR|IM}(im) \quad \textbf{(2.3)}$$

2.3.2 Structural Properties from Modal and Pushover Analyses

General structural properties were obtained by conducting (i) modal analyses to obtain periods and contribution of modes dominating elastic response, and (ii) cyclic adaptive pushover analyses to obtain the global force-displacement behavior of each building on Ruaumoko2D [33]. The periods and cumulative effective mass percentage of the first three modes obtained from modal analyses are shown in **Table 2.2**, while their corresponding mode shapes are shown in **Figure 2.2**. It can be seen that the response is predominantly dominated by the first two modes for the frame building and the first three modes for the wall building based on number of modes required to reach 90% cumulative effective mass. The wall building has lower modal periods due to being stiffer than the frame structure while having similar mass.

Table 2.2. Fundamental periods and cumulative mass of first three modes of each building

Mode	Frame		Wall	
	Period	% Cumulative Effective Mass	Period	% Cumulative Effective Mass
1	2.00s	82	1.45s	65
2	0.65s	92	0.24s	86
3	0.36s	96	0.09s	93

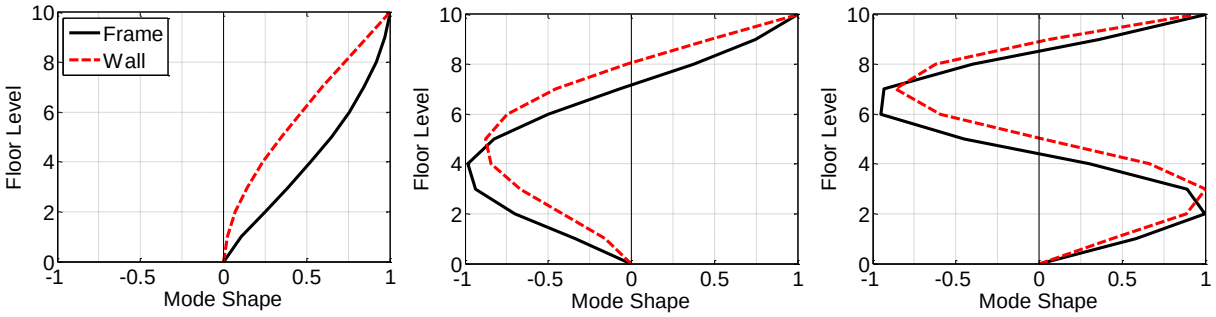

Figure 2.2. Mode shapes for case study buildings; (a) first mode, (b) second mode, and (c) third mode

The base shear versus roof drift curves obtained via roof displacement controlled cyclic adaptive pushover analyses are shown in **Figure 2.3**. The minimum strength requirements from NZS1170.5:2004 [26] are also shown. In both cases, the structure's capacity is greater than the minimum strength required as per NZS1170.5:2004 [26]. The ratio of the approximate yield strength to the minimum required strength is higher for the wall building (2.5 for the wall versus 2.0 for the frame) due to detailing requirements governing the wall building's design as discussed previously.

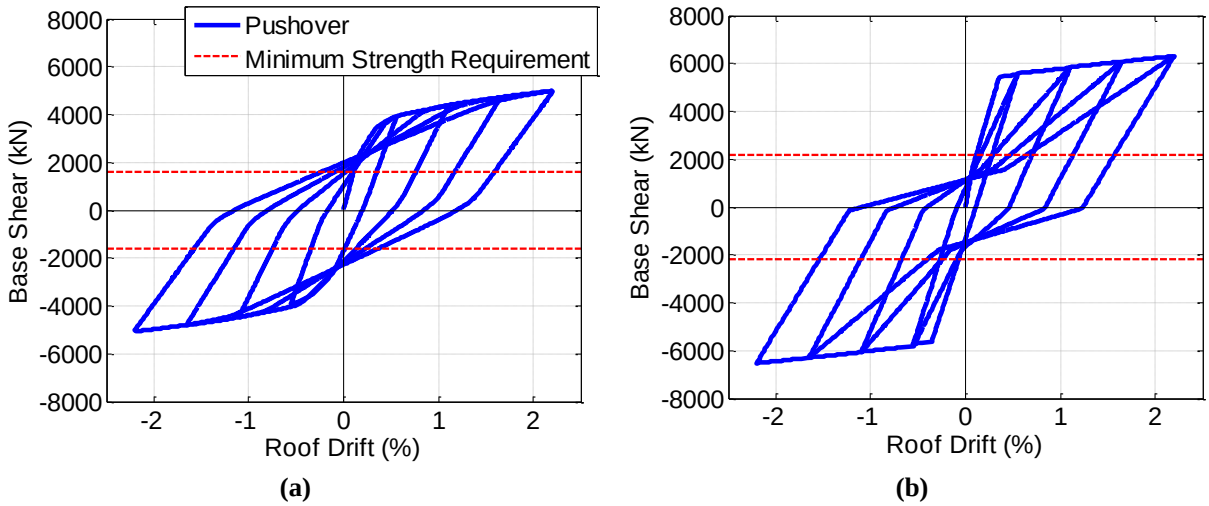

Figure 2.3. Cyclic adaptive pushover analyses; (a) frame building and (b) wall building

2.3.3 Consideration of Full-Replacement

Three global building damage states were considered when assessing the overall state of structures at the completion of seismic shaking. These states are: (i) "collapse"; (ii) "non-collapse – repairable"; and (iii) "non-collapse – irreparable"; the last of which requires demolition. In this study, it was assumed that the direct repair costs resulting from demolition

and collapse are the same, as the savings from salvaging contents from an irreparable building may balance-out the cost of planning and resources required for demolition. These two global damage states were combined and termed the "full-replacement" state.

Traditionally, residual drifts have been used to determine the onset of demolition in loss assessments [46-49]. However, Yazgan [50] highlighted difficulties in assessing residual drifts due to their sensitivity to many modelling assumptions and parameters. In addition, it was observed from the Christchurch earthquake that the extent of structural damage, the subsequent repair costs, and insurance often dictated the decision to demolish [51]. One such example is the Westpac Tower building in Christchurch, which had minor residual displacements but had extensive structural damage and was subsequently demolished [52].

Based on these observations, peak interstorey drift, *PID*, was used as an indicator of the need for full-replacement as it was a better measure of structural damage for beams and columns. FEMA 356 [53] states that *PID* of 2% and 1% for the frame and wall buildings respectively triggers the life safety damage state, where the building may be beyond economical repair. The 1% limit is only applied to the *PID* between the ground and 1st floor of the wall building as this was where the inelastic damage is concentrated, while the 2% limit is considered for other floors in the wall building and for all floors in the frame building as a measure of global structural stability.

2.4 SEISMIC HAZARD AND GROUND MOTION SELECTION

In loss assessment procedures, it is important that the selected ground motion record suites are representative of the seismic hazard at the site of interest. It is known however that use of Uniform Hazard Spectra to select records do not satisfy this requirement [54, 55]. Therefore, the Generalized Conditioning Intensity Measure (GCIM) approach developed by Bradley [22, 23] was adopted for ground motion record selection. This is because the

resulting *EDP*-hazard relationships obtained using records selected following the GCIM approach have been shown to be unbiased to the conditioning intensity measure selected [56, 57]. This allows comparisons between the response of different buildings to be made fairly using the same suite of ground motion records for all buildings so that all are subjected to the same events. The spectral acceleration at the wall building's fundamental period, *Sa*(1.5s), was selected as the conditioning *IM*.

The first step of the ground motion selection procedure is to perform probabilistic seismic hazard analysis (PSHA) to generate hazard curves, $\lambda_{IM}(im)$, for *Sa*(1.5s) considering the Christchurch region (43.53°S, 172.62°E) using New Zealand-specific rupture forecast models [58] and attenuation equations [59]. This was performed on OpenSHA [60]. A ground shear wave velocity, V_{s30}, of 300 m/s is assumed. The difference between the PSHA curve and that from NZS1170.5:2004 [26] is shown in **Figure 2.4a**, where the PSHA annual exceedance rates are lower. The conservatism in NZS1170.5:2004 [26] arises from simplification in the zone factor, *Z*, and the spectral shape factors for Class C soils [61]. It should be noted that a similar level of conservatism was also observed at *Sa*(2.0s) demonstrating that the design of the frame building is also conservative. As the buildings were designed to NZS1170.5:2004 [26], there is inherent conservatism in the designs.

The next step was to compute the theoretical probabilistic distribution of other intensity measures, IM_i, conditioned to a fixed value of *Sa*(1.5 s); the details of which are provided in **Appendix A Section A2**. This was performed at *Sa*(1.5 s) values corresponding to 99%, 80%, 50%, 20%, 10%, 5%, 2%, 1%, 0.5%, 0.2%, and 0.1% probability of exceedance in 50 years. The IM_i selected and their respective prediction equations were: (i) 5% damped spectral acceleration at vibration periods of T = 0.05s, 0.1s, 0.2s, 0.3s, 0.5s, 0.75s, 1.0s, 2.0s, 3.0s and 5.0s [59], (ii) peak ground acceleration, *PGA* [59], (iii) 5-75% and 5-95% significant durations, D_{s575} and D_{s595} [62], and (iv) cumulative absolute velocity, *CAV* [63].

For each hazard level, a set of ground motion records, all scaled to match the target value of S_a(1.5s) at the hazard level of interest, were selected such that the conditional distribution of IM_i matches the theoretical distributions. The record selection procedure follows that outlined by Bradley [23], where Kolmogorov-Smirnov (KS) tests [64] were used for statistical checks of the conditional distributions at each hazard level.

20 ground motion records, each containing two horizontal components and one vertical component, were selected to represent each of the 11 hazard levels; leading to 220 records being used in total. Using fewer records would have increased uncertainty in the building response from structural analyses, while using more would make it difficult to pass the KS test due to the smaller critical KS statistic associated with a larger record set [56]. Structural analyses were performed considering each record's horizontal components individually with no vertical component applied.

An example of records selected for a 10% in 50 year hazard is shown in **Figure 2.4b**, where the median (50th percentile), and the 16th and 84th percentile spectral curves of the selected record suite matches the theoretical distributions well. The list of selected records and their scaling factors are provided in **Appendix A Section A3**.

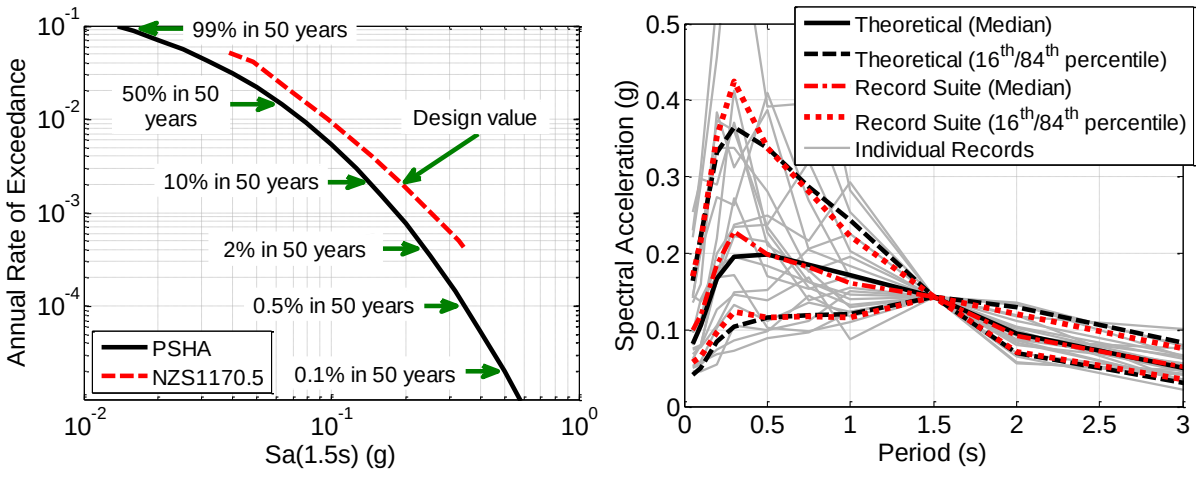

(a) **(b)**

Figure 2.4. Seismic hazard and selected ground motion records; (a) IM-hazard, (b) spectral curves of selected record suite for 10% in 50 year probability of exceedance

2.5 STRUCTURAL RESPONSE DEMAND

2.5.1 Response Excluding Full-Replacement Cases

Generally two types of *EDP*s are of interest in loss assessments; (i) peak total floor acceleration, A_{FT}, which is considered to be a sufficient measure of content and horizontal non-structural component damage, and (ii) peak interstorey drift, *PID*, which is a measure of structural and vertical non-structural component damage. The median, 16th, and 84th percentile A_{FT} and *PID EDP*-floor response of both buildings in a 10% in 50 year *IM* event based on PSHA is shown in **Figures 2.5a** and **2.5b**, respectively, assuming a lognormal distribution.

It can be seen from **Figure 2.5a** that the wall building's A_{FT} was larger than that of the frame building on all floors. This was due to: (i) greater amplification of high-frequency ground motion in the stiffer wall building, and (ii) inertia forces/accelerations not being limited to the same extent as that of the frame building due to the wall building having higher yield strength. In both buildings, the maximum A_{FT} occurred on the roof. However, a local maximum is observed at the 4th floor in the wall building, which was not observed in the frame building to the same extent. Interestingly, both buildings also had a decrease in A_{FT} around the 8th floor. The 4th floor increase and 8th floor decrease are likely due to higher-order mode effects as discussed further in **Section 2.5.2**.

The maximum *PID* occurred between the 2nd and 3rd floor in the frame building, and between the 9th and 10th floor in the wall building, as shown in **Figure 2.5b**. The difference in drift patterns were due to their corresponding deformation patters as shown in **Figure 2.6**; where the frame building deformed in a shear pattern while the wall building deformed as a cantilever. The frame building has the largest maximum value of *PID* (0.72%) compared to the wall building (0.52%) which led to a larger peak displacement at its effective height. However, the wall building has larger *PID* over the top half of the building, and thus it was

not immediately clear which building would incur higher drift-related losses. It is interesting to note however that the drift response does not appear to be affected by higher-order modes to the same extent as the acceleration response.

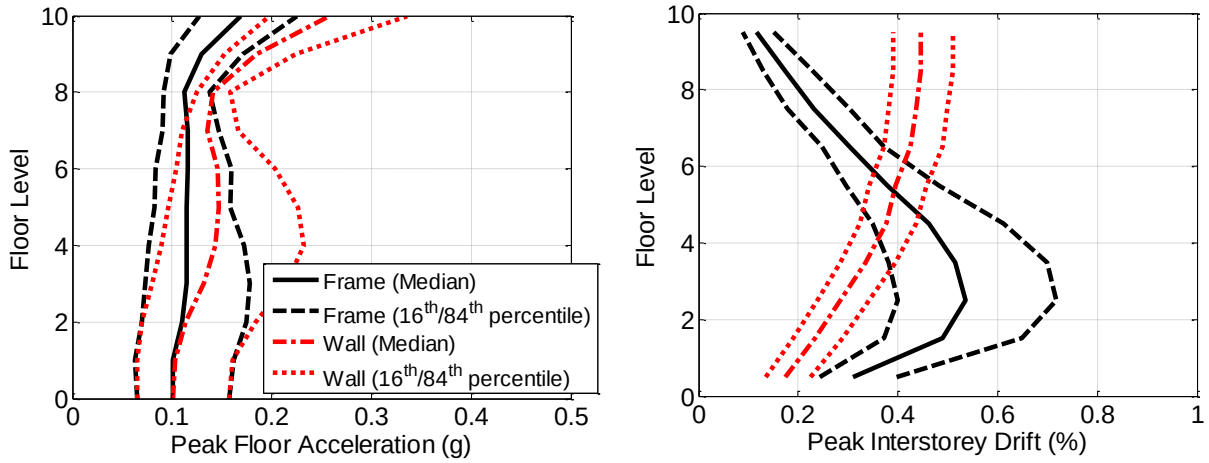

(a) **(b)**

Figure 2.5. *EDP*-floor profiles for *Sa*(1.5s) corresponding to a 10% in 50 years probability of exceedance; (a) peak total floor acceleration, (b) peak interstorey drift

(a) **(b)**

Figure 2.6. Building deformation profile; (a) frame, (b) wall

2.5.2 Effect of Higher-Order Modes

The building's response subjected to a ground motion from the 10% in 50 year set was examined to assess the effect of higher-order modes. The record's spectral accelerations and displacements corresponding to the first three modal periods of each building are shown in **Table 2.3**, where the spectral acceleration response of higher-order modes are generally greater than that of the first mode. In contrast, the spectral displacement response decreases at higher-order modes, which explains why the drift response of both buildings was dominated by the first-mode response.

Table 2.3. Spectral acceleration and displacement corresponding to first three modal periods of frame and wall building (CDMG east-west recording from 1994 Northridge event scaled by 0.31)

Building	Mode	Period	Participation Factor	Spectral Acceleration	Spectral Displacement
Frame	1	2.00 s	1.29	0.080 g	0.076 m
	2	0.65 s	-0.44	0.362 g	0.035 m
	3	0.36 s	0.26	0.634 g	0.019 m
	4	0.27 s	0.18	0.531 g	0.007 m
	5	0.16 s	0.14	0.402 g	0.003 m
Wall	1	1.45 s	1.49	0.185 g	0.093 m
	2	0.24 s	-0.72	0.613 g	0.009 m
	3	0.09 s	0.39	0.277 g	0.001 m
	4	0.05 s	0.27	0.189 g	< 0.001 m
	5	0.04 s	0.18	0.181 g	< 0.001 m

Structural analyses were performed using two approaches; one modelling the entire building, and the other modelling single-degree-of-freedom (SDOF) systems with periods matching those from **Table 2.3**. Both were elastic analyses excluding P-delta effects to allow for modal superposition. The total floor accelerations with time, $a_{FT}(t)$, can be calculated using **Eq. 2.4** for the second approach; where $a_g(t)$ is the ground acceleration with time, ϕ_i is the i^{th} mode shape, PF_i is the i^{th} participation factor obtained from modal analyses (provided in **Table 2.3**), $a_{rel,i}(t)$ is the SDOF mass's acceleration relative to the ground for the i^{th} mode, and n is the number of modes considered.

$$a_{FT}(t) = a_g(t) + \sum_{i=1}^{n} \phi_i . PF_i . a_{rel,i}(t) \qquad \textbf{(2.4)}$$

The peak total floor acceleration response on all floors, A_{FT}, is shown in **Figure 2.7**, where the first mode response underestimates the actual response of the building. Interestingly, the frame required more modes to converge to the solution compared to the wall, despite higher modes having a lower contribution to total mass in the frame building as shown in **Table 2.2**. This is because the spectral accelerations at the higher modes considered from **Table 2.3** was at least 4.5 times that of the first mode for the frame building. In contrast, only the 2nd and 3rd mode spectral acceleration response was noticeably larger than that of the 1st mode for the wall building. As the wall building's second mode has the highest spectral

accelerations of all the modes considered, and has a sizeable participation factor, the actual building's response have similarities with to the second mode shape shown in **Figure 2.2b**. Note that due to the inelastic response of the actual building, the location of the localized peak is not identical to those examined in **Figure 2.7a**, though the overall concept of higher order modes having an effect on A_{FT} is still applicable.

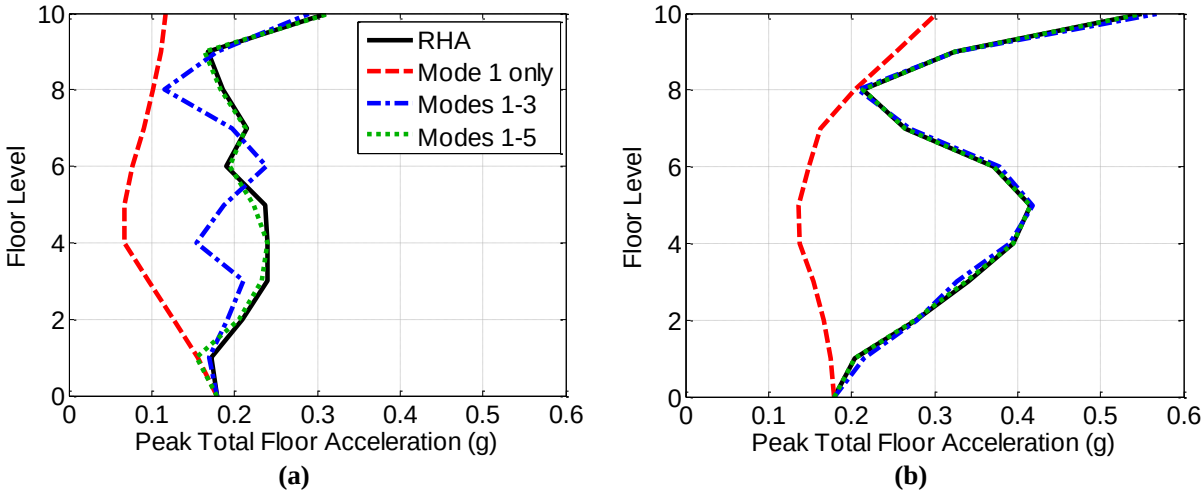

Figure 2.7. Effect of higher-order mode response on AFT response; (a) frame, and (b) wall

2.5.3 Full-Replacement Probability

The probability of requiring full-replacement for a given *IM*, $P_{FR|IM}(im)$, is shown in **Figure 2.8**, where the raw data points were obtained from deterministic assessment at each hazard level. A cumulative probabilistic density function was then fitted to the raw data points to estimate the median and dispersion of *Sa*(1.5s) causing full-replacement to be required. It is shown in **Figure 2.8** that the frame building has a higher probability of requiring full-replacement, and hence is more likely to incur higher full-replacement losses. Note that the probability that full-replacement is not required, $P_{NFR|IM}(im)$, is simply 1-$P_{FR|IM}(im)$ as these are mutually exclusive events.

It should be noted that treating the drift limits as a random variable rather than following a deterministic approach produced similar results if a dispersion of 0.2 or lower was used based on initial checks. While the full-replacement probabilities tended to increase

with larger dispersion values, it was assumed that the deterministic approach was sufficient as there is no information on what dispersion value should be considered for reasonable estimates. Also note that the full range of collapse probabilities (i.e. up to 100%) is not required as *Sa*(1.5s) greater than 0.5 g was extremely rare based **Figure 2.4a** and will have little impact on losses.

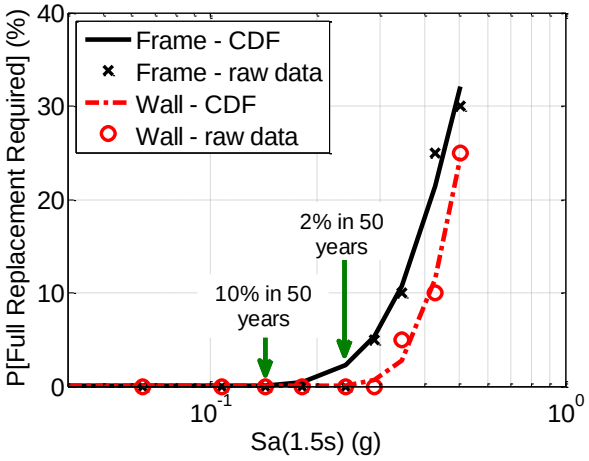

Figure 2.8. Probability of requiring full-replacement

2.5.4 Effect of Selected Conditioning Intensity Measure on *EDP*-Hazard

The key incentive for adopting the GCIM ground motion selection approach is to ensure unbiasedness in the resultant *EDP*-hazard response to the selected conditioning intensity measure. This allows for fair comparisons to be made using a single set of ground motion records, even if the fundamental periods of the buildings are different. To validate this, additional analyses were performed for the frame building using a set of records which adopted *Sa*(2.0s), the spectral acceleration corresponding to the fundamental period of the frame building, as the conditioning intensity measure instead of *Sa*(1.5s).

The annual rate of exceeding a given value of *EDP*, λ_{EDP}, is calculated following **Eq. 2.5** [17]. Here, *FR* and *NFR* denotes cases where full-replacement is or is not required, respectively; $P_{FR|IM}$ is the probability of full-replacement being required at a given *IM* value; $G_{EDP|IM,NFR}$ is the conditional distribution of *EDP* at a given *IM* for cases where full-replacement was not required; and λ_{IM} is the annual exceedance rate of *IM*.

$$\lambda_{EDP}(edp) = \int \left[G_{EDP|IM,NFR}(edp \mid im)[1 - P_{FR|IM}(im)] + P_{FR|IM}(im) \right] \left| \frac{d\lambda_{IM}(im)}{dIM} \right| .dIM \quad \textbf{(2.5)}$$

The *EDP*-hazard response for (i) roof peak total acceleration, (ii) 2nd-3rd floor interstorey drift, and (iii) 9th floor-roof interstorey drift are shown in **Figures 2.9a** to **2.9c**, respectively. These *EDP*s were selected as they represented the peak acceleration or drift response in the frame and/or wall building. It can be seen that the frame's response is nearly identical using either ground motion set, with only small differences in the annual exceedance rate corresponding to the full-replacement damage state (flat portion of *EDP*-Hazard curve) being observed. The similarities in the *EDP*-hazard response of the frame building demonstrate its unbiasedness to the selected conditioning intensity measure. Similar findings were also observed for other *EDP*s not shown here.

Based on the *EDP*-hazard response, the wall building has greater roof accelerations and 9th floor-roof interstorey drift up until the annual exceedance rate corresponding to the full-replacement damage state. In contrast, the wall building had smaller drifts on the 2nd-3rd floor. This is consistent with findings from **Section 2.5.1**. Other *EDP*s also showed the same consistency, and hence the discussions from **Section 2.5.1** can be used to explain damage and loss trends in the following sections.

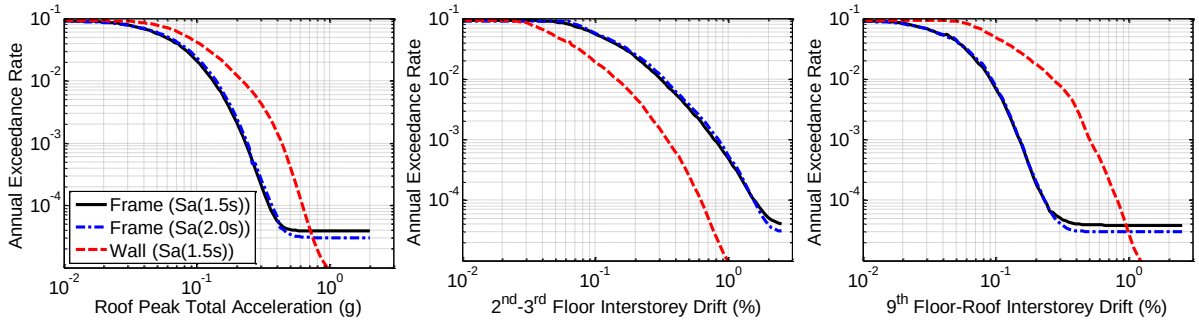

Figure 2.9. *EDP*-hazard response curves including building collapse cases; (a) roof peak total acceleration, (b) 2nd-3rd floor interstorey drift, and (c) 9th floor-roof interstorey drift

2.6. INTENSITY-BASED LOSS ASSESSMENT

One method for comparing the losses for the two buildings was to obtain the distribution of losses at various levels of ground motion shaking intensity. This is referred to as an "intensity-based loss assessment". This approach was performed in two steps. The first step was to calculate the mean and standard deviation of the i^{th} component damage cost for a given *IM* ($\mu_{Li|IM}(im)$ and $\sigma_{Li|IM}(im)$, respectively) following **Eq. 2.6a** and **2.6b** [17]. Here, the conditional probability density function of the *EDP-IM* relationship, $f_{EDP|IM}(edp|im)$, was calculated using **Eq. 2.6c**. These equations were used for all components outlined in **Table 2.1** for each floors. The exception was for wall members, as the damage was assumed to be concentrated over the bottom three floors as observed from past experimental studies [65-67].

$$\mu_{Li|IM}(im) = \int \mu_{Li|EDP}(edp).f_{EDP|IM}(edp \mid im).dEDP \quad \textbf{(2.6a)}$$

$$\sigma_{Li|IM}(im) = \sqrt{\int \left[\mu^2_{Li|EDP}(edp) + \sigma^2_{Li|EDP}(edp)\right].f_{EDP|IM}(edp \mid im).dEDP - \mu^2_{Li|IM}(im)} \quad \textbf{(2.6b)}$$

$$f_{EDP|IM}(edp \mid im) = -\frac{dG_{EDP|IM,NFR}(edp \mid im)}{dEDP} \quad \textbf{(2.6c)}$$

The next step would be to calculate the mean and standard deviation of total building damage loss for a given *IM* ($\mu_{LT|IM}(im)$ and $\sigma_{LT|IM}(im)$ respectively). This was done using **Eq. 2.7a** and **2.7b**, respectively [17]. Here, $\mu_{LT|FR}$ and $\sigma_{LT|FR}$ is the mean and standard deviation of full-replacement cost, and *Nc* is the number of contents. Note that the full-replacement cost

was assumed to be lognormally distributed with a median equal to its initial construction cost and a dispersion of 0.3.

$$\mu_{LT|IM}(im) = \left(\sum_{i=1}^{Nc} \mu_{Li|IM}(im)\right).P_{NFR|IM}(im) + \mu_{LT|FR}.P_{FR|IM}(im) \quad \textbf{(2.7a)}$$

$$\sigma^2_{LT|IM}(im) = \left(\sum_{i=1}^{Nc} \sigma^2_{Li|IM}(im)\right).P_{NFR|IM}(im) + \sigma^2_{LT|FR}.P_{FR|IM}(im) + \left[\left(\sum_{i=1}^{Nc} \mu_{Li|IM}(im)\right) - \mu_{LT|FR}\right]^2.P_{FR|IM}(im).P_{NFR|IM}(im) \quad \textbf{(2.7b)}$$

The median, 16th and 84th percentile total damage loss-*IM* relationships for both buildings are shown in **Figure 2.10a**, where (i) the 16th percentile loss curves were similar in both cases, and (ii) the median and 84th percentile curves were higher for the frame building. The median direct repair cost of the wall building was approximately \$87,000 and \$258,000 less than that of the frame building for a 10% and 2% in 50 year seismic event, respectively. As the wall building's initial construction cost was \$150,000 more than that of the frame building (**Table 2.1**), this implied that the increased construction cost of wall buildings is likely to only be offset by an event that has an exceedance probability lower than 10% in 50 years.

Before deriving and examining loss-hazard information, it is important to use the Loss-*IM* relationships to identify the source of these losses using deaggregation methods [6]. This information is helpful to understand where losses are incurred, and which mitigation strategies can be implemented. **Figure 2.10b** shows the expected loss of the buildings incurred for an event corresponding to a 10% exceedance probability in 50 years deaggregated by component group categories. While the frame building incurred larger total expected losses overall, the wall building incurred higher acceleration-related losses, both in terms of absolute value and contribution to total expected loss. This was due to the wall building experiencing higher acceleration response as shown in **Figure 2.5a**. In some specific

cases, the increased acceleration-related loss may have a larger influence on decisions, especially if the acceleration-sensitive content has more worth than its replacement cost alone; such as the functionality of medical equipment following an earthquake. Interestingly the wall building had similar absolute non-structural drift-related damage losses but lower structural drift-related damage compared to the frame building.

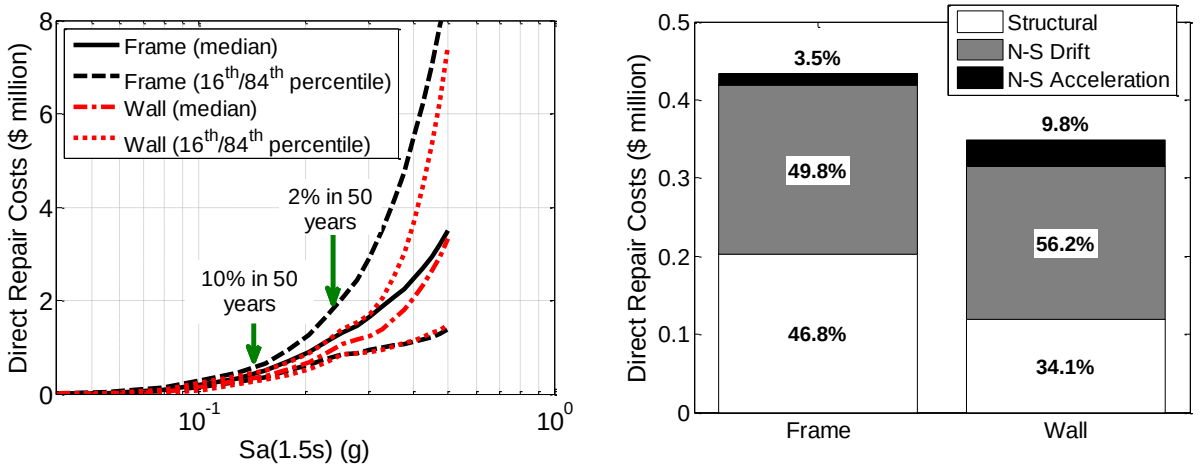

Figure 2.10. Total building repair costs; (a) total damage cost-*IM*, (b) breakdown of expected loss in 10% in 50 year seismic event by component category

Figures 2.11a and **2.11b** shows the deaggregation of expected losses by floor level for acceleration-related and drift-related losses, respectively, to identify if higher losses were incurred on certain floors than others. **Figure 2.11a** shows that the wall incurred higher acceleration response on most floors; while **Figure 2.11b** shows that the frame building incurred higher drift-related losses below floor 6 but lower losses above this level. In both cases, the expected loss-floor profiles were consistent with the *EDP*-floor profiles from **Figure 2.5**. This information is useful for decision makers to plan the configuration of contents throughout a building. For example, rather than distributing servers and network equipment among all floors, the equipment could potentially be grouped on the 7th or 8th floor where the acceleration-related losses are the lowest.

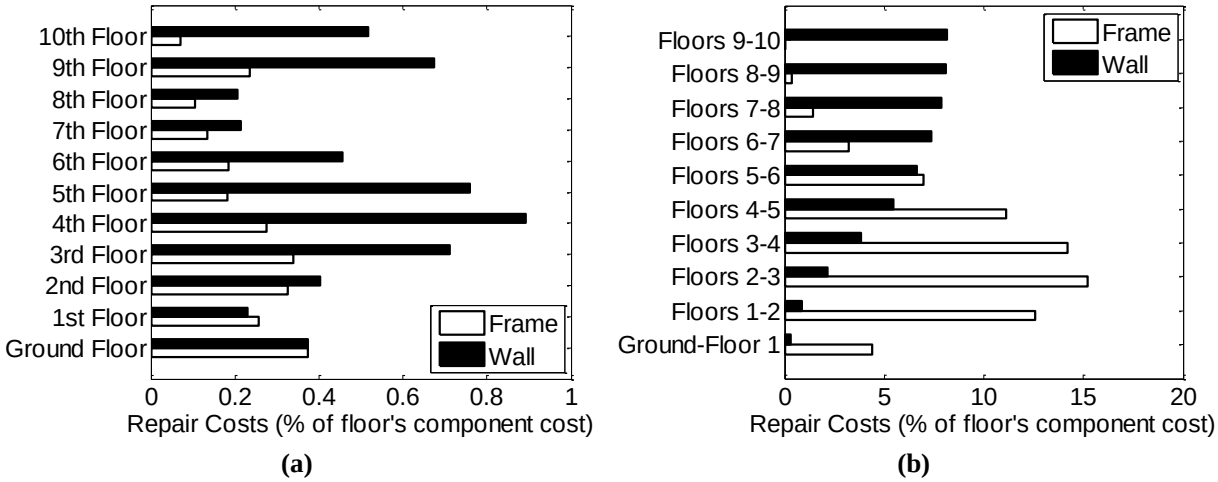

Figure 2.11. Expected loss by floor level in a 10% in 50 year event; (a) acceleration-related losses and (b) drift-related losses

Finally, losses can be deaggregated by component groups as shown in **Figure 2.12**. This information is useful to identify if certain components are incurring high losses and whether these can be replaced with an alternative type (e.g. replace heavy ceiling tiles with light-weight variants). Here, the wall building incurred higher losses for all acceleration-sensitive contents while the frame building had higher losses for all structural drift-sensitive components.

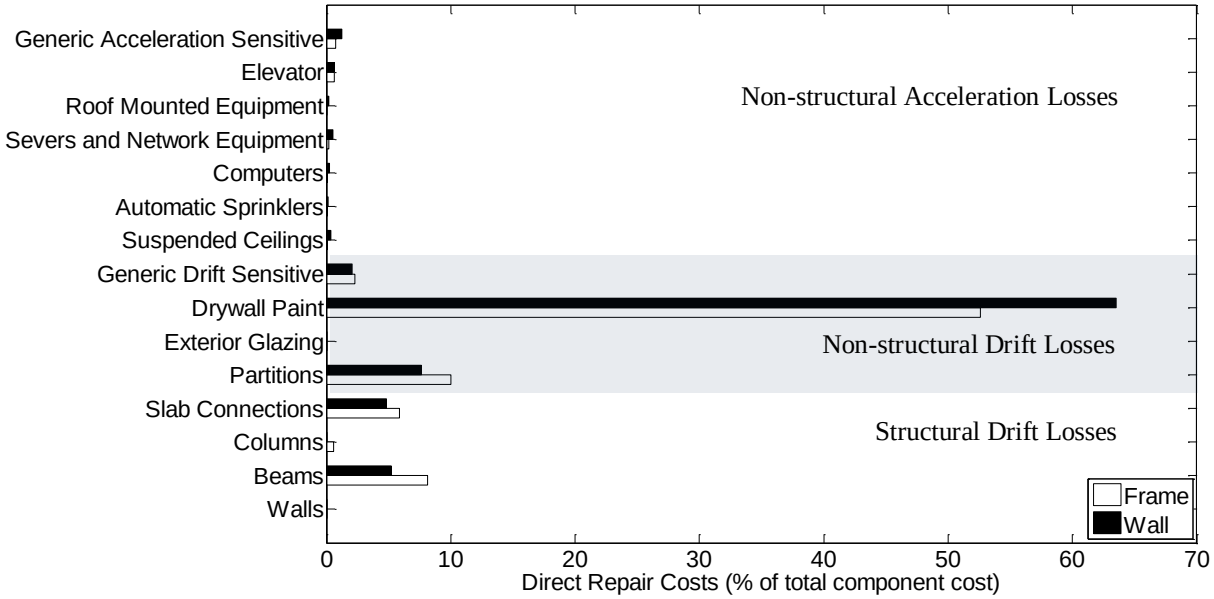

Figure 2.12. Expected loss by component in a 10% in 50 year event

Interestingly, the wall building incurred higher drywall paint damage-related losses. This was because the median interstorey drift which causes drywall paint damage is 0.39%,

which the 84th percentile *PID* response of the wall building exceeds on eight floors, compared to the frame building which exceeds this on just seven floors as shown in **Figure 2.5b**. Thus, it is possible for the wall structure to incur larger losses for some drift sensitive components despite the frame building experiencing the largest *PID* overall. Note that similar findings were not observed for the partition itself as the 0.39% median drift limit only corresponds to the first damage state for partitions which have a median repair cost of just 16.7% of its full-replacement cost. The second damage state which requires full-replacement has a median drift limit of 0.85%, which has a 2-5% probability of being exceeded on the bottom half of the frame building compared to less than 0.1% on all floors of the wall building. Therefore, despite more partitions being damaged in the wall building, the damage cost was higher in the frame building due to the increased damage to partitions.

2.7 TIME-BASED LOSS ASSESSMENT

2.7.1 Expected Annual Loss and Net Present Value Analysis

An alternate method for comparing the performance of the two buildings is to obtain the expected annual loss and calculate the life cycle costs for a specified duration which the buildings were in service. This is referred to as a "time-based loss assessment". The expected value and standard deviation of annual losses for both structures (*EAL* and σ_{LT} respectively) were calculated using **Eq. 2.8a** and **2.8b** respectively [17], while the expected annual loss and its dispersion are provided in **Table 2.4**.

$$EAL = \mu_{LT|IM}(im).\left|\frac{d\lambda_{IM}(im)}{dIM}\right|.dIM \quad \textbf{(2.8a)}$$

$$\sigma_{LT} = \sqrt{\int\left[\sigma^2_{LT|IM}(im) + \mu^2_{LT|IM}(im)\right]\left|\frac{d\lambda_{IM}(im)}{dIM}\right|.dIM - \mu^2_{LT}} \quad \textbf{(2.8b)}$$

Table 2.4. Frame and wall building annual loss comparisons

Case	Total Loss ($)	
	Expected	**Dispersion**
Frame	4,250	2.50
Wall	3,020	2.42

The most common method of conducting life cycle cost assessments is to calculate net-present-costs (*NPC*), which is the total cost (construction cost and seismic losses) that a building incurs over a duration of *N* years converted back to the present day's value for money. The calculation for this is shown in **Eq. 2.9**; where C_i is the initial construction cost, *r* is discount rate (taken as 6% here), and L_t is the loss incurred at year *t*. Since the contribution of C_i to *NPC* was not time dependent, the difference in initial construction cost was used instead of total cost (i.e. $C_{i,frame} = 0$, $C_{i,wall} = \$150{,}000$). This was done so that the *NPC* purely reflects the differences in cost.

$$NPC(r, N) = C_i + \sum_{t=1}^{N} \frac{L_t}{(1+r)^t} \quad \textbf{(2.9)}$$

Monte Carlo simulations were used to obtain a distribution of *NPC* by randomly selecting a value of L_t based on the values in **Table 2.4**. The results of this are shown in **Figure 2.13a**, which shows that the wall building was more expensive overall. This was because the wall building's savings from incurring lower losses was not sufficient to offset its higher initial construction costs. This would be true on average even if a discount rate of 0% was assumed as the difference in expected costs is only $1,250, and thus the wall building would need 120 years to offset the difference in initial costs.

The reason for the frame building having lower *NPC* was that the major contributions to annual losses were from low to moderate seismic events. This is shown by the deaggregation of *EAL* by *Sa*(1.5s) in **Figure 2.13b**, where the largest contributions were from events smaller than a 10% in 50 year event. This was also observed in past research [6, 17]. For these events, the additional loss incurred by the frame building was small relative to the

savings from having lower initial construction costs. As such, solely considering expected values may result in inadequate information regarding losses from low-occurrence but high-consequence events being conveyed to decision makers who may be risk-adverse (i.e. interested in minimizing losses in these rarer events).

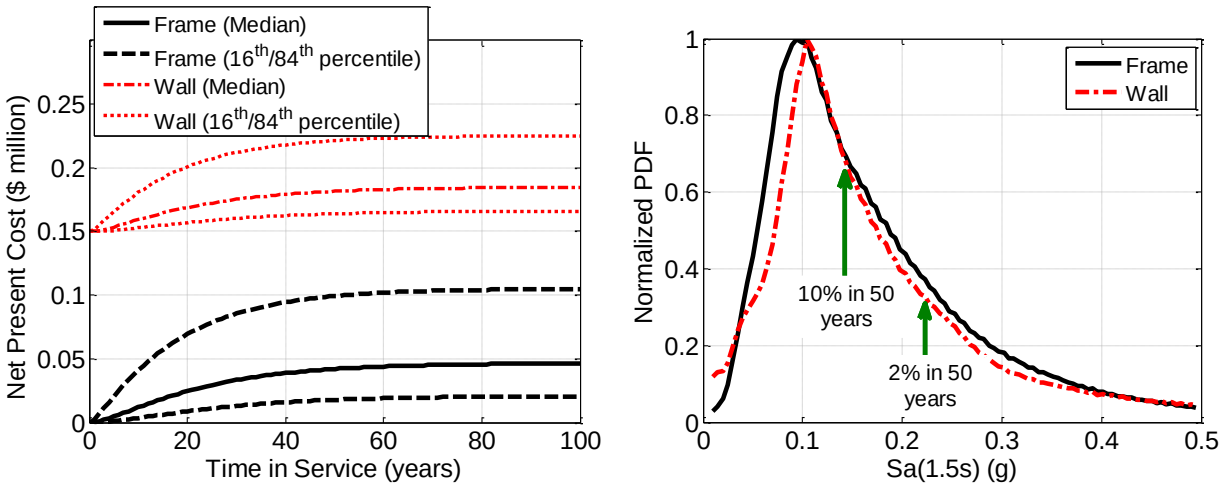

(a) **(b)**

Figure 2.13. Comparison considering annual loss; (a) *NPC* using expected value and dispersion of annual loss and difference in initial construction cost (r = 6%), (b) deaggregation of expected annual loss by *Sa*(1.5s)

2.7.2 Loss-Hazard and Effective Cost-Hazard Relationships

One method to account for other risk-appetites is to modify each building's loss-hazard curve. The generic loss-hazard curve, $\lambda_{LT}(l_t)$, was obtained following **Eq. 2.10** [17]. Here, $G_{LT|IM,NFR}(l_t|im)$ and $G_{LT|FR}(l_t)$ are conditional cumulative distribution functions of the total building loss for cases not requiring or requiring full-replacement, respectively. **Figure 2.14** compares the loss-hazard curves of the two buildings which show that the frame building incurs higher losses at all annual exceedance rates, *AER*.

$$\lambda_{LT}(l_t) = \int \left(G_{LT|IM,NFR}(l_t \mid im).P_{NFR}(im) + G_{LT|FR}(l_t).P_{FR|IM}(im) \right) \left| \frac{d\lambda_{IM}(im)}{dIM} \right| .dIM \qquad \textbf{(2.10)}$$

The simple modification made to the loss-hazard curve to account for other risk-appetites involved shifting it to the right by the difference in initial construction cost. This new curve is termed the "effective cost-hazard curve". This is useful for risk-adverse decision

makers as it contains information regarding losses at rare events. An example of this using the wall building loss-hazard curve is also shown in **Figure 2.14**. Here, the effective cost-hazard curve of the wall building crosses the frame building's loss-hazard curve at an *AER* of 0.0011 (return period of 910 years). As this is more frequent than a 'maximum credible' event (return period of 2,500 years), it is possible that risk-adverse decision makers may select the wall building over the frame building.

It should be noted here that the findings up to this point only considered direct repair costs. Consideration of fatalities and downtime would likely favour the wall building as it had a lower probability of requiring full-replacement compared to the frame structure. This may result in the *AER* at which the wall's effective cost-hazard crosses the frame's loss hazard increasing, which might make the wall building a more attractive option.

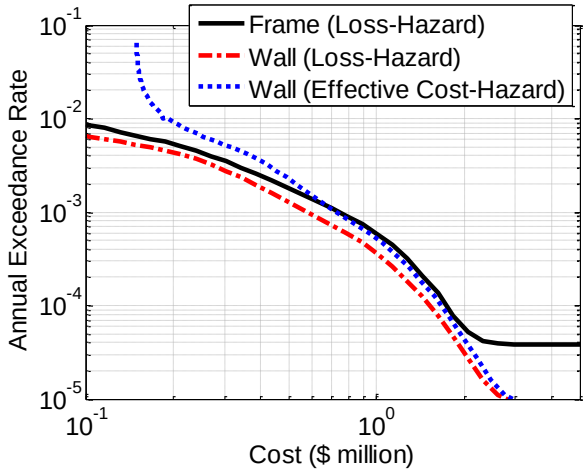

Figure 2.14. Comparison of loss-hazard and effective cost-hazard relationships

2.8 MITIGATION STRATEGIES AND BUILDING USAGE

The loss information discussed in previous sections was based on the buildings being used as offices with the inventory of contents listed in **Table 2.1**. However, there are other factors which may impact decisions, such as implication of mitigation strategies or potential changes in building usage.

One example of mitigation strategies would be to anchor acceleration-sensitive contents to prevent movement during earthquakes. While the acceleration demand was greater in the wall building, methods and cost to implement acceleration-related damage mitigation is likely to be similar in both cases. Hence it was assumed that the difference in initial construction cost remains the same. If acceleration-related damage was completely mitigated, then the effective cost-hazard curve for the wall building would cross that of the frame building at an *AER* of 0.00183 (return period of 550 years) as shown in **Figure 2.15a**, which makes the wall building more competitive if the mitigation strategy is to be implemented for both buildings.

A possible example for a change in building usage-type could be to use the case-study buildings as car-parking buildings instead. In this case, there would be significantly less non-structural contents, which will result in difference between the wall building's and the frame building's construction cost to increase to $200,000 as there were no longer savings from having reduced exterior glazing costs. Even though the wall building incurred even lower losses relative to the frame building as shown by the difference between the loss-hazard curves in **Figure 2.15b**, the effective cost-hazard curves only cross at an *AER* of 6.40×10^{-4} (return period of 1,560 years). In this case the frame building would quite likely be the preferred option.

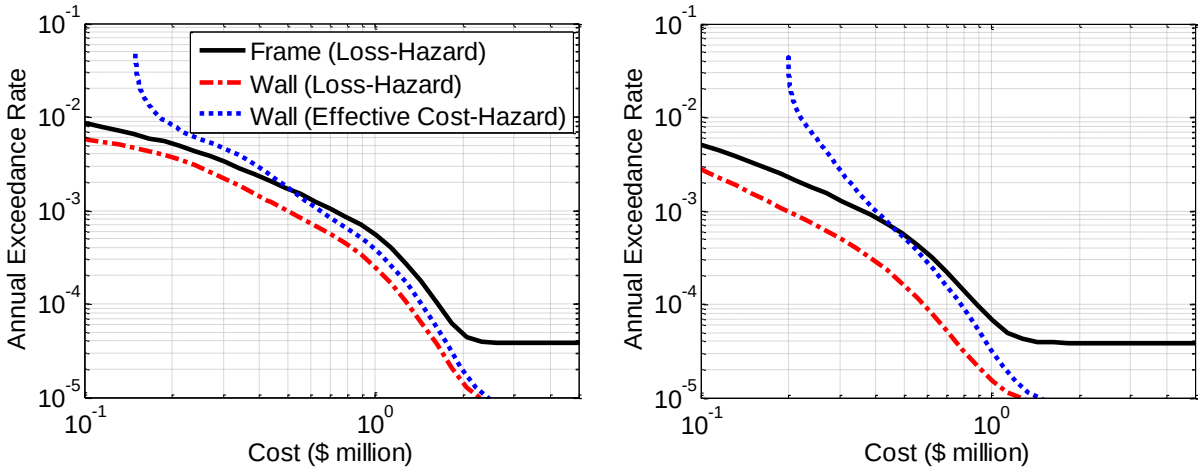

Figure 2.15. Effective cost-hazard assessments assessing effect of (a) limiting acceleration damage, and (b) changing building usage to a car-parking building

2.9 DISCUSSION

Much of the conclusions made in this chapter, and also in some of the following chapters, are based on the assumption that seismic losses and construction costs combined is the greatest driver behind deciding which building design is "optimal". In reality, this would not be the only deciding factor. Others such as (i) construction time (i.e. faster build allows for space to be rented out sooner), (ii) architectural features (i.e. less external walls and hence more open exterior space for views), and (iii) role of insurance (i.e. less affordable insurance may prompt owners to select more resilient buildings), might also be a factor. Nonetheless, seismic losses and construction costs are still one of the most important factors, and the conclusions reached still aids in decision-making.

Another assumption is that all stakeholders would be interested in all categories of damage-repair costs considered. This is not necessarily true, as building owners may not be concerned about their tenant's contents and may put more emphasis on the longevity of the building itself. In contrast, tenants might be more concerned with damage to components that may result in injuries, such as ceilings or furniture. While comparing damage losses to construction costs for the entire building is reasonable for some stakeholders, such as engineers to quantify the relative performance of various designs, this comparison may not be sensible for other types of stakeholders.

It should also be noted that statistical uncertainty had not been examined in detail in this study. In addition to the usual uncertainty arising from ground motion selection and structural analyses, several others are introduced through (i) selection of component fragility functions, (ii) assumptions in building inventory, and (iii) assumption of loss values incurred due to building collapse. These induced uncertainties may have an influence on seismic losses and expected annual losses. However, the qualitative conclusions, such as the reduced drift-related losses in wall buildings compared to frame buildings, still holds true. As such,

one should not treat the numerical outputs as definite, but rather as an indicator of the magnitude of likely losses.

2.10 CONCLUSIONS

Rigorous seismic loss assessments were performed on two 10 storey reinforced concrete buildings; one using a moment-resisting frame system and the other using cantilever walls. The specific findings from this study are that:

1. The wall building experienced higher peak total floor accelerations on all floors and higher peak interstorey drifts on the upper half of the building. However the frame building had the highest value of interstorey drift overall. This results in the wall building incurring higher acceleration-related losses but lower drift-related losses. The wall building also had a lower probability of requiring full-replacement, resulting in the wall building incurring lower total damage losses overall.
2. Cost-benefit assessments indicated that the frame structure was more cost-effective than the wall structure assuming a discount rate of 6% and up to 100 years in service. This was because the largest contribution to the annual losses, which were used to compute net-present-costs, arose from low to moderate seismic events where the reduced damage repair costs of wall buildings was insufficient to offset its initial construction costs.
3. In order to account for a range of risk-appetites, the loss-hazard curve was shifted to account for the difference in initial cost. This new curve was termed the “effective cost-hazard curve”. This approach was more beneficial for decision makers who were not risk-neutral, as it contained effective-cost information over a wide range of annual exceedance rates. Using the effective cost-hazard curve approach, the wall building was the more cost effective option at an annual exceedance rate corresponding to a

return period of 910 years or rarer. This return period was lower than that corresponding to a maximum credible event (2,500 years). As such, this may influence risk-adverse decision makers to select the wall building over the frame building instead.

4. Additional cases were considered where either (i) acceleration-related damage mitigation strategies (such as anchoring contents) were implemented, or (ii) the building's usage was converted to a car-parking building. It was found in the former that the wall building becomes the more cost effective option at an annual exceedance rate corresponding to a return period of 550 years or rarer, and hence the wall building becomes a more attractive option. If the building's usage was switched to a car-parking building however, the annual exceedance rate at which the curves cross corresponds to a return period of 1,620 years, which then makes the wall building a less attractive option.

2.11 REFERENCES

1. Wood, A., Noy, I., & Parker, M. (2015). The Canterbury rebuild five years on from the Christchurch earthquake. Bulletin of the Reserve Bank of New Zealand, 79(3), 3-16.
2. Cooper, M., Carter, R., & Fenwick, R. (2012). Volume 4 - Earthquake-prone buildings: Canterbury Earthquake Royal Commission.
3. Cornell, C. A., & Krawinkler, H. (2000). Progress and challenges in seismic performance assessment. PEER News, 3(2).
4. Krawinkler, H., & Miranda, E. (2004). Performance-based earthquake engineering. In Chapter 9 of Earthquake Engineering: From Engineering Seismology to Performance Based Engineering: CRC Press, Boca Raton, FL.
5. Porter, K. A., Kiremidjian, A. S., & LeGrus, J. S. (2001). Assembly-Based Vulnerability of Buildings and Its Use in Performance Evaluation. Earthquake Spectra, 17(2), 291-312.
6. Aslani, H., & Miranda, E. (2005). Probabilistic Earthquake Loss Estimation and Loss Disaggregation in Buildings: Department of Civil and Environmental Engineering, Stanford University.
7. Dhakal, R. P., & Mander, J. B. (2006). Financial Risk Assessment Methodology for Natural Hazards. Bulletin of the New Zealand Society of Earthquake Engineering, 39(2), 91-105.
8. Bradley, B. A., Lee, D. S., Broughton, R., & Price, C. (2009). Efficient Evaluation of Performance-based Earthquake Engineering Equations. Structural Safety, 31, 65-74.
9. Mitrani-Reiser, J. (2007). An Ounce of Prevention: Probabilistic Loss Estimation for Performance Based Earthquake Design. PhD Thesis, California Institute of Technology, Pasadena, California.
10. Baker, J. W., & Cornell, C. A. (2008). Uncertainty Propagation in Probabilistic Seismic Loss Estimation. Structural Safety, 30(3), 236-252.
11. Ramirez, C. M., & Miranda, E. (2009). Building-Specific Loss Estimation Methods and Tools for Simplified Performance-Based Earthquake Engineering. Department of Civil Engineering, Standford University.

12. Bradley, B. A. (2011). SLAT:Seismic Loss Assessment Tool (Version 1.16): Department of Civil and Natural Resources Engineering, University of Canterbury.
13. Naeim, F., & Hagie, S. (2012). PACT: Performance Assessment Calculation Tool. John A. Martin & Associates, INC. Los Angeles, California, US.
14. Wen, Y. K., & Kang, Y. J. (2001). Minimum Building Life-Cycle COst Design Criteria. II: Applications. Journal of Structural Engineering, 127(3), 338-346.
15. Ramirez, C. M., Liel, A. B., Mitrani-Reiser, J., Haselton, C. B., Spear, A. D., Steiner, J., Deierlein, G. G., & Miranda, E. (2012). Expected earthquake damage and repair costs in reinforced concrete frame buildings. Earthquake Engineering and Structural Dynamics, 41(11).
16. Moehle, J., Bozorgnia, Y., Jayaram, N., Jones, N. P., Rahnama, M., Shome, N., Tuna, Z., Wallace, J., Yang, T., & Zareian, F. (2011). Task 12 Report for the Tall Buildings Initiative: Case Studies of the Seismic Performance of Tall Buildings Designed by Alternative Means: Pacific Earthquake Engineering Research Center.
17. Bradley, B. A., Dhakal, R. P., Cubrinovski, M., MacRae, G. A., & Lee, D. S. (2009). Seismic Loss Estimation for Efficient Decision Making. Bulletin of the New Zealand Society of Earthquake Engineering, 42(2), 96-110.
18. Kleindorfer, P. R., & Kunreuthere, H. C. (1999). Challenges facing the insurance industry in managing catastrophic risks: The University of Chicago Press, Chicago.
19. Goda, K., & Hong, H. P. (2006). Optimal Seismic Design Considering Risk Attitude, Societal Tolerable Risk Level, and Life Quality Criterion. Journal of Structural Engineering, 132(12), 2027-2035.
20. von Neumann, J., & Morgenstern, O. (1994). Theory of games and economic behaviour. Princeton University Press, Princeton, N.J.
21. Levy, H. (1998). Stochastic dominance: Investment decision making under uncertainty: Kluwer Academic, Boston.
22. Bradley, B. A. (2010). A Generalized Conditional Intensity Measure Approach and Holistic Ground Motion Selection. Earthquake Engineering and Structural Dynamics, 39(12), 1324-1342.
23. Bradley, B. A. (2012). A ground motion selection algorithm based on the generalized conditional intensity measure approach. Soil Dynamics and Earthquake Engineering, 40, 48-61.
24. Bull, D. K., & Brunsdon, D. (2008). Examples of concrete structural design to New Zealand Standard 3010 (Red Book). Wellington, New Zealand: NZCS: Cement & Concrete Association of New Zealand.
25. Standards New Zealand. (2006). NZS 3101:2006, Concrete Structures Standard Part 1 - The Design of Concrete Structures: Standards New Zealand, Wellington, New Zealand.
26. Standards New Zealand. (2004). NZS 1170.5:2004, Structural Design Actions Part 5: Earthquake Actions New Zealand: Standards New Zealand, Wellington, New Zealand.
27. Soydas, O. (2009). Evaluation of Shear Wall Indexes for Reinforced Concrete Buildings. Masters Thesis, Middle East Technical University.
28. Burak, B., & Comlekoglu, H. (2013). Effect of Shear Wall Area to Floor Area Ratio on the Seismic Behavior of Reinforced Concrete Buildings. Journal of Structural Engineering, 13(11), 1928-1937.
29. Rawlinson & Co. (2012). Rawlinsons New Zealand construction handbook. Rawlhouse Publishing, Wellington, New Zealand.
30. Deierlein, G. G., Krawinkler, H., & Cornell, C. A. (2003). A Framework for Performance-based Earthquake Engineering. Paper presented at the 2003 Pacific Conference on Earthquake Engineering, Christchurch, New Zealand.
31. Jin, M., & Astaneh, A. (1998). Study of seismic resistance of desktop computers. ATC 29-1, Proceedings of seminar on seismic design, retrofit, and performance of nonstructural components, 379-392.
32. Porter, K. A. (2007). Fragility of hydraulic elevators for use in performance-based earthquake engineering. Earthquake Spectra, 23(2), 459-469.
33. Carr, A. J. (2004). Ruaumoko 2D - Inelastic dynamic analysis program. Department of Civil and Natural Resources Engineering, University of Canterbury, Christchurch.
34. Caughey, T. K. (1960). Calssical Normal Modes in Damped Linear Systems. Journal of Applied Mechanics, 27, 269-271.
35. Carr, A. J. (2008). Ruaumoko Manual (Vol. Volumne 2: User Manual for the 2:Dimensional Version Ruaumoko 2D). University of Canterbury, Christchurch, NZ.
36. Emori, K., & Schnobrich, W. C. (1981). Inelastic behaviour of concrete frame-wall structures. Journal of the Structural Division, ASCE, 107.
37. Saiidi, M., & Sozen, M. A. (1979). Simple and complex models for nonlinear seismic response of reinforced concrete structures. Illinois: University of Illinois.
38. Ghobarah, A., & Youssef, M. (1999). Modelling of reinforced concrete structural walls. Engineering Structures, 21(10), 912-923.

39. Elnashai, A. S., Pilakoutas, K., & Ambraseys, N. N. (1990). Experimental behaviour of reinforced concrete walls under earthquake loading. Earthquake Engineering and Structural Dynamics, 19(3), 389-407.
40. Thomsen, J. H., & Wallace, J. W. (2004). Displacement-based design of slender reinforced concrete structural walls - experimental verification. Journal of Structural Engineering, 130(4), 618-630.
41. Wallace, J. W. (2007). Modelling issues for tall reinforced concrete core wall buildings. The Structural Design of Tall and Special Buidlings, 16, 615-632.
42. Computers and Structures Inc. (2009). Sap2000 version 14.0.0. Computers and Structures, Inc. 1995 University Ave. Berkeley, CA.
43. Blakeley, R. W. G., Edmonds, F. D., Megget, L. M., & Wood, J. H. (1979). Cyclic Load Testing of Two Refined Reinforced Concrete Beam-Column Joints. Bulletin of the New Zealand Society of Earthquake Engineering, 12(3), 238-255.
44. Fenwick, R. C., & Fong, A. (1979). The Behaviour of Reinforced Concrete Beams under Cyclic Loading. Bulletin of the New Zealand Society of Earthquake Engineering, 12(3), 158-167.
45. Tagawa, H. (2005). Towards an understanding of seismic performance of 3D structures: stability & reliability. PhD Thesis, University of Washington, Seattle, USA.
46. Iwata, Y., Sugimoto, H., & Kuwamura, H. (2005). Reparability Limit of Steel Structural Buildings: Study on performance-based design of steel structural buildings Part2. Journal of Structural and Construction Engineering(588), 165-172. (in Japanese).
47. Kawashima, K., MacRae, G. A., Hoshikuma, J.-i., & Nagaya, K. (1998). Residual Displacement Response Spectrum. Journal of Structural Engineering, 124(5), 523-530.
48. Uma, S. R., Pampanin, S., & Christopoulos, C. (2010). Development of Probabilistic Framework for Performance-Based Seismic Assessment of Structures Considering Residual Deformations. Journal of Earthquake Engineering, 14(7), 1092-1111.
49. Ramirez, C. M., & Miranda, E. (2012). Significance of Residual Drifts in Building Earthquake Loss Estimation. Earthquake Engineering and Structural Dynamics, 41(11), 1477-1493.
50. Yazgan, U. (2009). The Use of Post-Earthquake Residual Displacements as a Performance Indicator in Seismic Assessment. PhD Thesis, Swiss Federal Institute of Technology (Eth Zurich), Switzerland.
51. King, A., Middleton, D., Brown, C., Johnston, D., & Johal, S. (2014). Insurance: Its Role in Recovery from the 2010-2011 Canterbury Earthquake Sequence. Earthquake Spectra, In-Press.
52. Cooper, M., Carter, R., & Fenwick, R. (2012). Volume 2 - The Performance of Christchurch CBD Buildings: Canterbury Earthquake Royal Commission.
53. ASCE. (2000). Prestandard and Commentary for the Seismic Rehabilitation of Buildings, FEMA 356. Federal Emergency Management Agency, Washington, D.C.
54. McGuire, R. K. (1995). Probabilistic Seismic Hazard Analysis and Design Earthquakes: Closing the Loop. Bulletin of the Seismological Society of America, 85(5), 1275-1284.
55. Bommer, J. J., Scott, S. G., & Sarma, S. K. (2000). Hazard-Consistent Earthquake Scenarios. Soil Dynamics and Earthquake Engineering, 19, 219-231.
56. Bradley, B. A. (2012). The Seismic Demand Hazard and Importance of the Conditioning Intensity Measure. Earthquake Engineering and Structural Dynamics, 41(11), 1417-1437.
57. Lin, T., Haselton, C. B., & Baker, J. W. (2013). Conditional spectrum-based ground motion selection. Part I: Hazard consistency for risk-based assessments. Earthquake Engineering and Structural Dynamics, 42(12), 1847-1865.
58. Stirling, M. W., McVerry, G. H., Gerstenberger, M. C., Litchfield, N. J., Van Dissen, R. J., Berryman, K. R., Barnes, P., Wallace, L. M., Villamor, P., Langridge, R. M., Lamarche, G., Nodder, S., Reyners, M. E., Bradley, B., Rhoades, D. A., Smith, W. D., Nicol, A., Pettinga, J., Clark, K. J., & Jacobs, K. (2012). National seismic hazard model for New Zealand : 2010 update. Bulletin of the Seismological Society of America, 102(4), 1514-1542.
59. Bradley, B. A. (2013). A New Zealand-Specific Pseudospectral Acceleration Ground-Motion Prediction Equation for Active Shallow Crustal Earthquakes Based on Foreign Models. Bulletin of the Seismological Society of America, 103(3), 1801-1822.
60. Field, E. H., Jordan, T. H., & Cornell, C. A. (2003). OpenSHA: A Developing Community-Modeling Environment for Seismic Hazard Analysis. Seismological Research Letters, 74(4), 406-419.
61. McVerry, G. H. (2003). From hazard maps to code spectra for New Zealand. Paper presented at the 2003 Pacific Conference on Earthquake Engineering, Christchurch, NZ.
62. Bommer, J. J., Stafford, P. J., & Alarcon, J. E. (2009). Empirical Equations for the Prediction of the Significant, Bracketed and Uniform Duration of Earthquake Ground Motion. Bulletin of the Seismological Society of America, 99(6), 3217-3233.

63. Campbell, K. W., & Bozorgnia, Y. (2010). A Ground Motion Prediction Equation for the Horizontal Component of Cumulative Absolute Velocity (CAV) Based on the PEER-NGA Strong Motion Database. Earthquake Spectra, 26(3), 635-650.
64. Ang, A. H. S., & Tang, W. H. (2007). Probability concepts in engineering: Emphasis on applications in civil and environmental engineering: John Wiley & Sons.
65. Paulay, T., & Priestley, M. J. N. (1992). Seismic Design of Reinforced Concrete and Masonry Buildings. John Wiley, New York.
66. Eurocode 8. (1994). Design Provisions for Earthquake Resistance of Structures. ENV 1998-2, Comite Europeen de Normalization, Brussels, 1994.
67. Birely, A. C. (2013). Seismic Performance of Slender Reinforced Concrete Structural Walls. PhD Thesis, University of Washington.

3. Wall Stiffness and Strength Effects on Earthquake Direct-Repair Losses

3.0 SUMMARY

Component-based probabilistic loss assessments of several 10-storey reinforced concrete wall buildings were conducted considering initial construction and direct repair costs to quantify the effect of varying stiffness and strength. The buildings were designed and analysed for Wellington subsoil class C conditions. It was found that increasing stiffness increases acceleration response, but reduces drifts and the need for full-replacement of the building; resulting in lower expected intensity-based damage losses by up to $1.52 million. In contrast, while increasing strength also results in increased total floor accelerations and lower probability of requiring full replacements, these buildings tend to incur higher peak interstorey drifts on upper floors; resulting higher losses during more frequent events but lower losses at rarer events. The stiffest and strongest buildings considered in this study have lower expected annual losses compared to most flexible and weakest buildings, but still incurred higher life-cycle costs overall considering initial construction and direct-repair losses only. Loss-hazard curve analyses considering initial construction costs showed the stiffest and strongest buildings considered in this study incurred lower losses in loss events more frequent than a 1 in 2,500 year event, and thus these buildings might still be favoured by risk-adverse decision makers.

3.1 INTRODUCTION

Seismic design guidelines require buildings to have sufficient stiffness, strength, and ductile detailing to limit non-structural damage in small shaking events, structural damage in moderate events, and collapse in severe events [1, 2]. However, there are diverging opinions

on whether stiffer and/or stronger buildings are more beneficial. One perception is that flexible and weaker buildings are cheaper overall due to their lower construction costs and the infrequent ***occurrence*** of strong earthquakes. Conversely, stiffer and stronger buildings are likely to incur less structural damage based on observations from historical events [3, 4], and hence reduce the ***consequence*** of an earthquake. It is difficult to reach a common consensus on which is superior as the outcome would depend on the decision makers' perception of risk. However, sufficient information to demonstrate the potential benefits or disadvantages of increasing stiffness and strength can be provided to aid decision-makers to select options based on their personal preference.

One such assessment is to estimate the building's losses associated with damage, injury, and downtime during earthquakes. A common methodology follows that popularized by the Pacific Earthquake Engineering Research (PEER) center [5, 6]. Several enhancements, such as the ability to conduct component-based assessments, have since been proposed [7-12]. Computer programs based on this methodology have been developed [10, 13, 14].

Past studies using loss estimation to quantify the influence of stiffness and strength exist. Wen and Kang [15] performed global building-based loss assessments of 9-storey steel moment resisting frame buildings with varying base shear coefficients (termed S_y in their study) located within Los Angeles. They found that S_y between 0.14 and 0.2 corresponded to the lowest seismic life-cycle cost (construction and damage repair). The life-cycle cost increases slightly for buildings designed for higher S_y due to higher initial costs, and drastically increases for lower S_y due to incurring greater damage. Elsewhere, Mitrani-Reiser [10] and C M Ramirez et al. [16] applied the PEER methodology to several reinforced concrete (RC) frame buildings. They compared the ratio of expected annual loss to the initial building cost and found that this was generally between 0.5-1.3%, indicating that expected losses are proportional to the initial construction costs.

A limitation of these studies is that the effects of varying stiffness or strength independently were not investigated. For example, none of the buildings considered by Wen and Kang [15] have the same S_y or fundamental period, T. It was also not clear if the force reduction factor, denoted as R in many countries (k_μ/S_p in New Zealand [17]), was varied. In actual practice, an engineer does not decide on a value of S_y for design, but rather obtains S_y through the selection of T and R. It is therefore important to identify the influence of these two parameters individually on the building's seismic performance. Note that while stiffness and strength are related [18], it is possible to vary one property while keeping the other constant for RC members by varying both reinforcing content and gross section geometry.

In this chapter, probabilistic component-based loss assessments of several 10-storey cantilever RC wall buildings were performed considering initial construction and direct-repair costs to quantify the importance of stiffness and strength individually. Note that injury and downtime losses were not considered due to their corresponding modelling approaches still being in its infancy as discussed in **Chapter 1**. These buildings are designed for conditions in Wellington, New Zealand. This chapter seeks to answer the following questions:

1. What is the effect of T and R on the acceleration response?
2. What is the effect of T and R on the drift response?
3. What is the effect of T and R on the need for full-replacements?
4. What is the effect of T and R on the incurred losses?
5. Is it more beneficial to increase T or R in design?

3.2 LOSS ESTIMATION OVERVIEW

3.2.1 General Framework

Seismic performance assessment frameworks, such as that by the Pacific Earthquake Engineering Research (PEER) center [5, 6], estimates losses in four steps: (i) predict the severity of ground shaking (measured using an intensity measure, *IM*), (ii) analyse the building's response (defined by an engineering demand parameter, *EDP*), (iii) assess the extent of damage (categorized by a damage measure, *DM*), and (iv) quantify resulting losses (referred to as decision variables, *DV*). Details of the methodology to link the different parameters are discussed in this section. While a number of studies had provided such details [5-8, 10], only those presented by Bradley et al. [19] are discussed as these were used in the Seismic Loss Assessment Tool (SLAT) program [13] which was utilized in this study.

3.2.2 Intensity Measure Hazard Calculation

The first step in probabilistic loss assessments is to estimate the rate of exceeding a given shaking intensity. This is done through probabilistic seismic hazard analyses (PSHA), and well-established procedures to perform this are available in literature (e.g. Kramer [20]).

3.2.3 Engineering Demand Parameter Response

One method of assessing *EDP* would be to relate it to *IM*. This can be conducted using **Eq. 3.1** [19], where $G_{EDP|IM}(edp|im)$ is the cumulative distribution of an *edp* being exceeded for a given *im*, and *C* and *NC* denote cases where collapse did or did not occur, respectively. Alternatively, the rarity of exceeding a given *edp* is another method of assessment. This can be calculated from **Eq. 3.2**, where $\lambda_{EDP}(edp)$ is the annual rate of exceeding a given *edp*, and $\lambda_{IM}(im)$ is the annual rate of exceeding a given *im*.

$$G_{EDP|IM}(edp \mid im) = G_{EDP|IM,NC}(edp \mid im)[1 - P_{C|IM}(im)] + P_{C|IM}(im) \quad \textbf{(3.1)}$$

$$\lambda_{EDP}(edp) = \int G_{EDP|IM}(edp \mid im)\left|\frac{d\lambda_{IM}(im)}{dIM}\right| dIM \quad \textbf{(3.2)}$$

3.2.4 Damage Measure and Loss Assessment Predictions

Damage to building components are linked to *EDP* using fragility functions. These estimate the probability of the i^{th} building component incurring the j^{th} damage state, DS_j, such as dislodging of ceiling tiles, for a given *EDP*, $P_{DSj|EDP}(ds_j|edp)$. Loss functions, which can be defined by the mean and standard deviation of repair costs for the i^{th} component incurring the j^{th} damage state, $\mu_{Li|DSj}(ds_j)$ and $\sigma_{Li|DSj}(ds_j)$, respectively, can be used to link damage to losses. Fragility and loss functions are available in literature [7, 8, 10, 13, 14, 21, 22], and can be combined together to compute the mean and standard deviation of the i^{th} component repair costs for a given *EDP* using **Eq. 3.3a** and **3.3b**, respectively. Here N_{DS} is the total number of damage states for the i^{th} building component.

$$\mu_{Li|EDP}(edp) = \sum_{j=1}^{N_{DS}} \mu_{Li|DSj}(ds_j).P_{DSj|EDP}(ds_j \mid edp) \quad \textbf{(3.3a)}$$

$$\sigma_{Li|EDP}(edp) = \sqrt{\sum_{j=1}^{N_{DS}} \left[\mu^2_{Li|DS}(ds_j) + \sigma^2_{Li|DS}(ds_j)\right] P_{DSj|EDP}(ds_j \mid edp) - \mu^2_{Li|EDP}(edp)} \quad \textbf{(3.3b)}$$

Loss distributions can be computed at various levels of ground motion shaking intensity, and is referred to as an "intensity-based loss assessment". At a component-level, the mean and standard deviation of the i^{th} component damage cost for a given *IM* ($\mu_{Li|IM}(im)$ and $\sigma_{Li|IM}(im)$, respectively) is calculated using **Eq. 3.4a** and **3.4b** [19], respectively. Here, the conditional probability density function of the *EDP-IM* relationship, $f_{EDP|IM}(edp|im)$, is calculated using **Eq. 3.4c**.

$$\mu_{Li|IM}(im) = \int \mu_{Li|EDP}(edp).f_{EDP|IM}(edp \mid im).dEDP \quad \textbf{(3.4a)}$$

$$\sigma_{Li|IM}(im) = \sqrt{\int \left[\mu^2_{Li|EDP}(edp) + \sigma^2_{Li|EDP}(edp)\right] f_{EDP|IM}(edp \mid im).dEDP - \mu^2_{Li|IM}(im)} \quad \textbf{(3.4b)}$$

$$f_{EDP|IM}(edp \mid im) = -\frac{dG_{EDP|IM,NFR}(edp \mid im)}{dEDP} \quad \textbf{(3.4c)}$$

At a global building level, the mean and standard deviation of total building damage loss for a given *IM* ($\mu_{LT|IM}(im)$ and $\sigma_{LT|IM}(im)$, respectively) is calculated using **Eq. 3.5a** and **3.5b**, respectively [19]. Here, *FR* and *NFR* refer to cases where full-replacement is or is not needed, respectively; $\mu_{LT|FR}$ and $\sigma_{LT|FR}$ are the mean and standard deviation of full-replacement cost, respectively; and *Nc* is the number of component groups present. Note that full-replacement means that the building either requires demolition or had collapsed.

$$\mu_{LT|IM}(im) = \left(\sum_{i=1}^{Nc} \mu_{Li|IM}(im)\right).P_{NFR|IM}(im) + \mu_{LT|FR}.P_{FR|IM}(im) \quad \textbf{(3.5a)}$$

$$\sigma^2_{LT|IM}(im) = \left(\sum_{i=1}^{Nc} \sigma^2_{Li|IM}(im)\right).P_{NFR|IM\,(im)} + \sigma^2_{LT|FR}.P_{FR|IM}(im) + \left[\left(\sum_{i=1}^{Nc} \mu_{Li|IM}(im)\right) - \mu_{LT|FR}\right]^2.P_{FR|IM}(im).P_{NFR|IM}(im) \quad \textbf{(3.5b)}$$

One common parameter used to compare between design options or mitigation strategies is to use annual losses. The expected value and standard deviation of this (*EAL* and σ_{LT}, respectively) are calculated using **Eq. 3.6a** and **3.6b**, respectively [19]. These are often used in net-present-cost cost-benefit assessments for assessing the relative benefits of implementing mitigation measures, or selecting between different building design options.

$$EAL = \mu_{LT|IM}(im).\left|\frac{d\lambda_{IM}(im)}{dIM}\right|.dIM \quad \textbf{(3.6a)}$$

$$\sigma_{LT} = \sqrt{\int\left[\sigma^2_{LT|IM}(im) + \mu^2_{LT|IM}(im)\right]\left|\frac{d\lambda_{IM}(im)}{dIM}\right|.dIM - \mu^2_{LT}} \quad \textbf{(3.6b)}$$

The loss-hazard curve, $\lambda_{LT}(l_t)$, which provides a measure of the rarity of incurring a certain value of loss, can be obtained following **Eq. 3.7** [19]. Here, $G_{LT|IM,NFR}(l_t|im)$ and $G_{LT|FR}(l_t)$ were conditional cumulative distribution functions of the total building loss for cases not requiring or requiring full-replacement, respectively.

$$\lambda_{LT}(l_t) = \int\left(G_{LT|IM,NFR}(l_t \mid im).P_{NFR}(im) + G_{LT|FR}(l_t).P_{FR|IM}(im)\right)\left|\frac{d\lambda_{IM}(im)}{dIM}\right|.dIM \quad \textbf{(3.7)}$$

3.2.5 Comparison Methods

The most common method of conducting life cycle costs uses *NPC* analysis, which involves calculating the total cost (construction cost and induced losses) that a building incurs over a duration of *N* years converted back to the present day's value for money. The calculation for this is shown in **Eq. 3.8** [19]; where C_i is the initial construction cost, *r* is annual discount rate, and *t* is the number of years that the building has been in service.

$$NPC(r,N) = C_i + \sum_{t=1}^{N} \frac{EAL}{(1+r)^t} \quad \textbf{(3.8)}$$

A limitation of *NPC* analysis is that by only considering annual losses, the findings are geared towards risk-neutral decision makers [23], particularly as majority of contributions to annual losses arises from low to moderate seismic events [8, 19]. To account for this, an alternate method was suggested in **Section 2.7.2**, where the difference in the buildings' initial construction costs were added to the losses in loss-hazard curves. This new curve is termed the "effective cost-hazard curve", and allows decision makers to select the optimal building based on their own risk appetite.

3.3 DESIGN AND ANALYSIS PROCEDURE

3.3.1 Building Properties and Design Parameters

The case study buildings are similar to the wall building exampled in **Chapter 2**. They are 10 stories high, with floor heights of 4.0 m on the ground and 3.6 m on other floors, and have floor masses of 700 tonnes. Four identical prismatic rectangular structural walls are designed to resist seismic action in each orthogonal direction. The base moment demand on each wall is obtained following the Equivalent Static Procedure from NZS1170.5:2004 [17], which provided more conservative base moment demands compared to modal analyses procedures. A 10% in 50 year uniform hazard spectra derived using probabilistic seismic

hazard analysis (PSHA) was used to obtain the design demands rather than the code spectra. This was to be consistent with the ground motion selection approach which required PSHA. More details are discussed in **Section 3.3.2**.

The *T* and *R* pairings considered are listed in **Table 3.1**. Buildings outside of this range either violated code limits (e.g. drifts, reinforcing content) or were unrealistic (e.g. large wall sizes). While *R* was kept constant for the first three cases, the absolute strength value varied as the elastic demand varied with *T*. This was acceptable since *T* and *R* are key parameters in engineering design, and thus 'strength' is hereby quantified as the provided capacity relative to its design elastic demand. An iterative procedure was adopted to detail the wall members' cross section so that the building's actual *T* and *R* matched the target values in **Table 3.1** while satisfying requirements in the New Zealand concrete standard, NZS3101:2006 [24]. This differed from common practice where iterations are rarely performed due to the computational effort required [18].

The inventory and density of building contents considered are mostly similar to the wall building considered in **Chapter 2** (**Table 2.1**), with the main difference being the size of the walls which affected the length of exterior beams and total area of glazing required. All non-structural element costs were assumed equal to its full-replacement cost specified in the SLAT's fragility database [13], while the Rawlinson Construction Handbook [25] was used to estimate the cost of the structural components. The total initial construction cost of the building is shown in **Table 3.1**, where 52-54% of the building cost comprises acceleration-sensitive contents, while structural components make up just 28-30%.

It can also be seen from **Table 3.1** that the initial construction cost of wall elements increases with stiffness and strength due to an increase in cross section size and/or reinforcing content. While the cost of other drift-sensitive components decreases with stiffness due to the increased size of structural walls, the opposite trend was observed with regards to strength.

This was because higher reinforcing content was required to increase strength, which caused the stiffness to also increase. Hence the cross section geometry must be decreased to keep stiffness constant, which leads to longer beams and more glazing being required.

Table 3.1. Description and initial construction cost of buildings

Case	R	Period (s)	Description	Costs ($ million)				
				Walls only	Other Structural	N-S Drift	N-S Acceleration	Total
Baseline	4	1.25	Baseline building	1.41	2.27	2.27	6.86	12.8
Stiffest	4	1.00	56% stiffness increase	1.66	2.13	2.23		12.9
Most flexible	4	1.50	31% stiffness decrease	1.24	2.36	2.28		12.7
Strongest	3	1.25	33% strength increase	1.53	2.36	2.28		13.0
Weakest	5	1.25	20% strength decrease	1.42	2.19	2.25		12.7

3.3.2 IM-Hazard and Ground Motion Selection

Probabilistic seismic hazard analyses (PSHA) was performed to: (i) obtain the 10% in 50 year uniform hazard spectra (UHS) for design, (ii) derive the seismic hazard curve for loss assessments, and (iii) select ground motion records. This was performed on OpenSHA [26] for Wellington (41.3^{o}S, 174.8^{o}E) on a site with a shear wave velocity, V_s30, of 400 m/s using New Zealand specific earthquake forecast models [27] and attenuation relationships [28]. The 10% in 50 year UHS used in design is shown in **Figure 3.1a**.

The ground motion selection methodology adopted was the General Conditioning Intensity Measure (GCIM) approach [29]. This approach first derives theoretical probabilistic distributions of various intensity measures, such as peak ground acceleration or duration measures, conditioned to the value of the selected conditioning intensity measure. The detailed methodology on deriving this distribution is provided by Bradley [29] and has been incorporated into OpenSHA [26]. The records are then selected such that the actual conditional distribution of various intensity measures for the entire record suite matches the theoretical distributions well. This approach is hazard-consistent and has been shown to remove bias in the building response-hazard regardless of the conditioning intensity measure

selected [30, 31]. This allows a single suite of records to be selected and used for all cases considered.

The spectral acceleration at 1.25 s, which is the mean fundamental period of the buildings considered, was selected as the conditioning intensity measure. The other intensity measures and the corresponding prediction equations considered in the selection process were: (i) 5% damped spectral acceleration values at periods ranging from 0.05 to 10.0 seconds, and peak ground acceleration, using Bradley [28], (ii) cumulative absolute velocity using Campbell and Bozorgnia [32], and (iii) significant duration parameters *Ds*575 and *Ds*595 using Bommer et al. [33].

Twenty records, each with two horizontal components, were selected at eleven shaking intensity levels ranging from 99% to 0.1% probability of exceedance in 50 years. Vertical ground shaking was not considered. The distribution of intensity measures from each set of twenty records matches theoretical probabilistic distributions closely. An example of this for the 10% in 50 year suite is shown in **Figures 3.1a** and **3.1b** for spectral acceleration and *Ds595* distributions, respectively. In the latter case, Kolmogorov-Smirnov (KS) tests [34] were performed to ensure that distribution of *Ds595* of the record-suite fits within the KS bounds. These bounds were derived assuming a 90% confidence level, and represent the maximum difference in probability allowed relative to the theoretical distribution. Similar checks were also performed for other types of intensity measures. Full details of the ground motion selection algorithm used, the selection of the weighting factors for the selected intensity measures, and intensity levels considered is described in Bradley [35]. The corresponding *Sa*(1.25s) hazard curve, which will be used in loss assessments later in this chapter, is shown in **Figure 3.1c**. The list of selected records and their scale factors are provided in **Appendix A Section A4.1**.

Note that attenuation equations used for the non-amplitude intensity measures are representative of active shallow faults, and may not be suitable for subduction zones which exist in the Wellington region. As there are no appropriate attenuation relationships for these cases, the equations used are still the best currently available [36]. For similar reasons, ground motion records were obtained from the PEER ground motion record database [37] despite the database only containing records representative of active shallow fault ruptures.

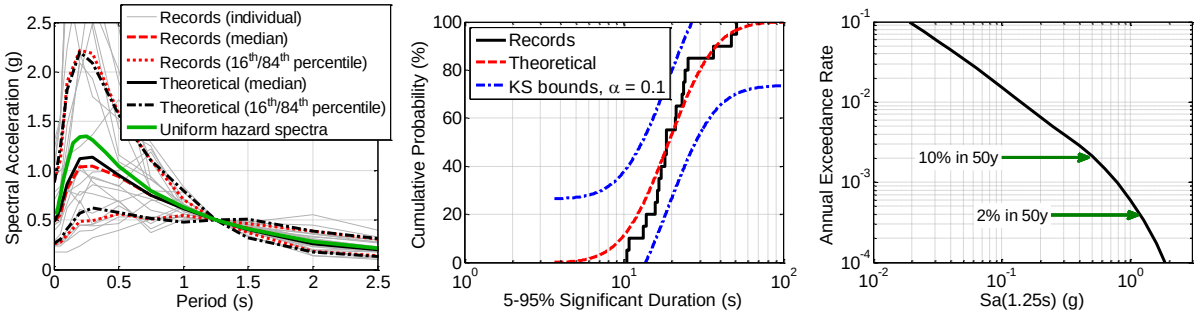

(a) **(b)** **(c)**

Figure 3.1. Seismic hazard and selected records; (a) spectral curves for 10% in 50 year record suite, (b) *Ds*595 conditional CDF for 10% in 50 year record suite, (c) *Sa*(1.25s) hazard

3.3.3 Structural Analysis Procedure

Dynamic inelastic response analyses were performed on Ruaumoko2D [38] using the simplified wall structural model shown in **Figure 3.2a**. Caughey damping [39] ratio of 5% was used for all elastic modes, and P-delta effects were modelled using large displacement analyses [40]. The walls were modelled allowing a plastic hinge of length L_p to form at the base only as shown in **Figure 3.2b**. As there is uncertainty regarding selection of L_p for analyses, a recommendation by Tagawa [41] shown in **Eq. 3.9** is followed. This differs from other expressions of plastic hinge length by explicitly considering the member's force-displacement post-elastic stiffness ratio, r_Δ, to ensure that the building's global response is realistic. Here, L is the member length, and r_ϕ is the post-elastic stiffness ratio of the moment-curvature relationship obtained from section analyses. The range of r_Δ for structural walls is within 2-5% based on past studies [42, 43], and a target r_Δ of 2% was assumed here.

$$L_p = \frac{r_\phi L}{3r_\Delta}(1 - r_\Delta) \tag{3.9}$$

The hysteretic behaviour of the structural walls was modelled using the SINA hysteresis rule [44] shown in **Figure 3.2c**, which closely matches the force-displacement behaviour observed in past experimental studies of multi-storey cantilever walls [42, 43]. The elastic stiffness, k_o, is assumed equal to the secant stiffness at first yield. Based on past research [42-44], (i) the crack closing force, F_{cr}, was taken as 0.3 times the yield force, F_y, and (ii) the crack closing displacement, Δ_{cr}, was taken as one third of the maximum displacement at zero force in the opposite direction, Δ_i.

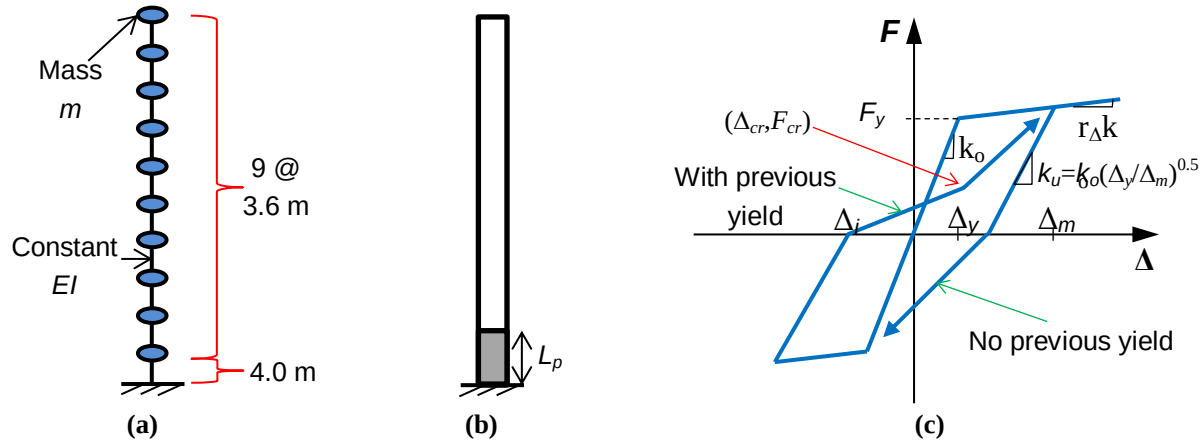

Figure 3.2. Illustration of structural and hysteretic model considered in study; (a) building model, (b) plastic hinge location, and (c) SINA hysteresis model

Limitations of this study are that (i) local failure modes such as wall buckling are not considered, (ii) plane sections were assumed to remain plane, and (iii) floor diaphragm effects are ignored. This was because models to properly account for these factors are complex and are still in development [45]. In addition, strength and stiffness degradation were not considered due to a lack of full-scale shake table experiments of walls for calibration. For simplicity, drift limits from FEMA 356 [46] were used to assess if a building requires 'full-replacement' or if it has collapsed. This is shown in **Table 3.2** where two criteria were considered. The first is related to failure of the structural walls, which is based on the maximum difference in drifts between floors since the walls respond as a cantilever,

and usually occurs between the ground and the 1st floor. The second relates to global building instability, and thus considers the maximum drift on any floor. If the building exceeds either condition, it was assumed that the building experiences the given damage state.

Table 3.2. Criteria to assess full-replacement and collapse damage states

Criteria	Building Damage State	
	Full-Replacement Drift Limits	**Collapse Drift Limits**
(1) Difference in inter-storey drift between subsequent floors	>1.0 %	>2.0%
(2) Maximum inter-storey drift on any floor	>2.0 %	>4.0%

3.3.4 Seismic Loss Estimation Procedure

The Seismic Loss Assessment Tool, SLAT [13], was used to perform the loss calculations. The peak total floor acceleration, peak inter-storey drift, and the number of full-replacement and collapse cases were extracted from the structural analyses and used as inputs into the computer program. Fragility and loss functions available in SLAT's fragility library were used for components where such data was available. Else, fragility and loss functions were adapted from the Performance Assessment Calculation Tool, PACT [14], or from Rawlinson's handbook [25]. Note that damage to wall members are assumed to be concentrated at its base due to its cantilever deformation pattern, and thus only the ground-1st floor inter-storey drift was considered in estimating losses to these elements. If a wall was damaged, it was assumed that only the bottom three floors would require repairs based on past damage observed during testing [47, 48].

The consequence of the demolition and collapse cases are assumed to be the same in regards to repair costs. In addition, the median replacement cost is assumed to be equal to the initial construction cost of the building. A dispersion of 0.35 was assumed to account for inherent variation in replacement costs charged by different service providers, and to allow for cases where (i) some building contents may be salvaged which reduces the loss, (ii) costs may be increased due to limitation of resources following an earthquake, and/or (iii) for other unforeseen cases.

3.4 STRUCTURAL RESPONSE ASSESSMENT

3.4.1 Peak Floor Acceleration and Inter-storey Drift Response

The building's peak total floor acceleration, A_{FT}, and peak inter-storey drift response, *PID*, which are *EDP*s used as component damage indicators in the loss assessment methodology, are examined in **Figure 3.3**. **Figure 3.3a** shows the median A_{FT} response using the 10% in 50 year set of ground motions (i.e. design-basis level shaking, DBE). Note that the x-axis does not begin at zero so that differences between the curves can be seen clearer. In all cases, A_{FT} increased from the ground to the 5th floor, decreased towards the 8th floor, and peaked at the roof. This differs from the response of ductile frame buildings, which generally experiences similar or decreasing A_{FT} with height [8, 19], due to (i) the difference in deformation patterns between the two structural system types, and (ii) differing contribution from higher order modes as discussed in **Section 2.5.2**.

The stiffest and strongest buildings considered in this study (see **Table 3.1**) have higher A_{FT} compared to more flexible and weaker cases due to (i) inertia forces, and hence accelerations, not being limited to the same extent in stronger buildings due to its higher capacity, and (ii) high frequency motion being filtered out in more flexible buildings. However, changing stiffness does not appear to have as great an effect as changing strength; particularly between the 3rd and 8th floor where a maximum increase of 5.8% in A_{FT} was observed between stiffest case and the baseline case, compared to a 13.8% increase for the strongest case relative to the baseline case. This was despite stiffness being increased by a higher percentage as shown in **Table 3.1**.

Figure 3.3b shows the median *PID* response of the buildings under DBE shaking, where *PID* increased with height due to the wall's cantilever deformation pattern. *PID* of the stiffest building was between 21-23% lower than that of the baseline case on all floors. Increasing strength also caused *PID* over the bottom few floors to decrease by up to 14.3%

compared to the baseline case. However, *PID* over the top few floors are similar. In fact, the *PID*-hazard response shown in **Figure 3.3c**, calculated using **Eq. 3.2**, showed that the strongest building does tend to incur the largest 9th floor to roof drift at an *EDP* annual exceedance rate, λ_{EDP}, lower than a 10% in 50 years event. This is in contrast to the drifts at the base, which decreases with strength as shown in **Figure 3.3d**. **Figures 3.3c** and **3.3d** however shows that the stiffest building generally incurred the lowest drifts overall. Observations from other shaking intensity levels matches the trends discussed, and thus other *EDP-IM* and *EDP*-hazard response curves are not shown or discussed.

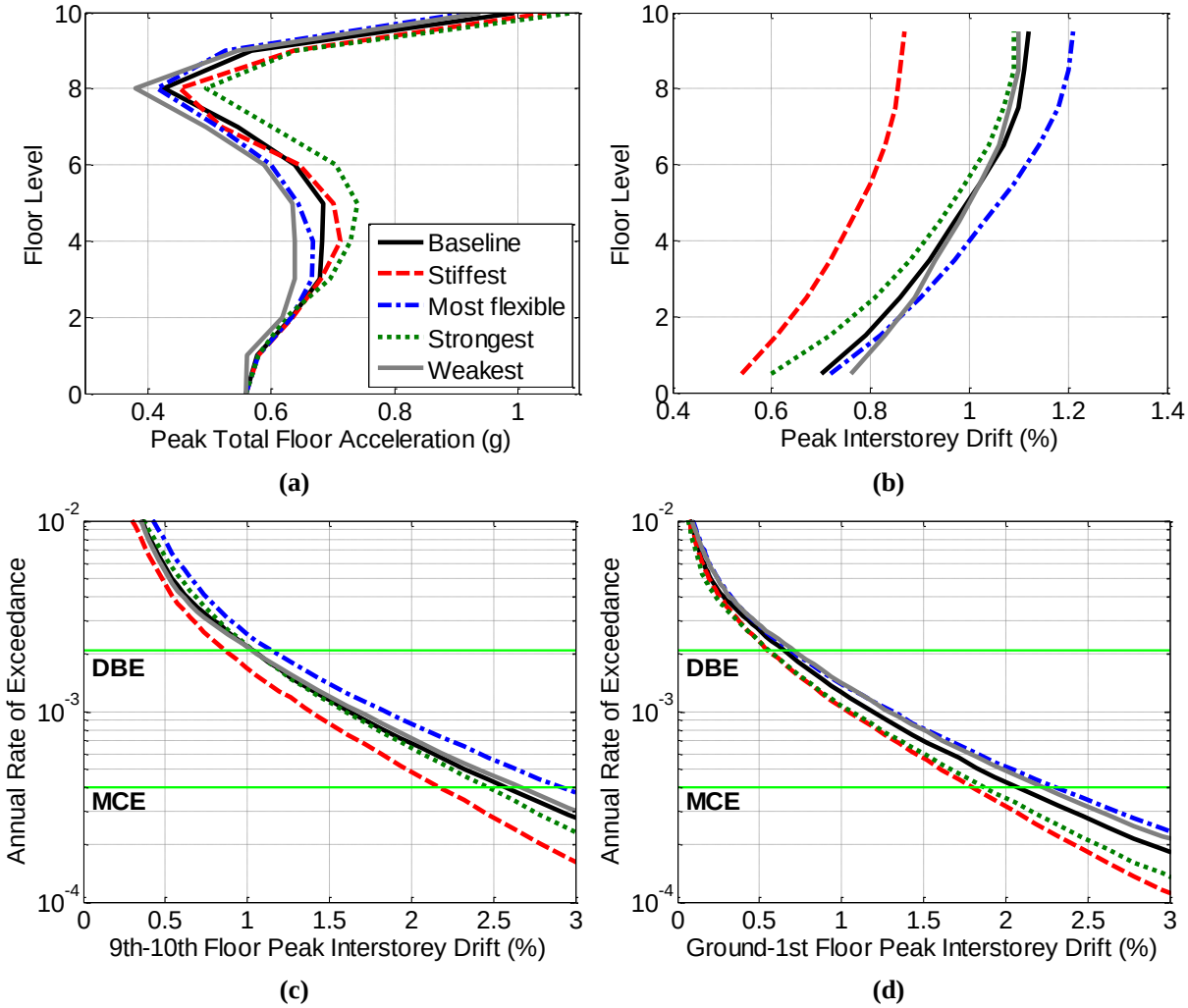

Figure 3.3. Building response; (a) DBE peak total floor acceleration, (b) DBE peak inter-storey drift, (c) 9th floor – roof drift hazard , and (d) Ground – 1st floor drift hazard

3.4.2 Investigation of Higher Drifts on Upper Floors of Stronger Buildings

There are several reasons why stronger buildings may experience higher interstorey drifts on upper floors. The first is that earlier yielding of weaker buildings in one direction might potentially lessen what could have possibly been an even more severe response in the opposite direction. An example of this is shown in **Figure 3.4** using one of the ground motion records from the 10% in 50 year suite. It can be seen from **Figure 3.4a** that the displacement response history at the weaker building's effective height has the largest positive response at 11.5 s, while the stronger building experiences the largest negative and absolute response at 12.2 s. Due to the weaker building's earlier yielding: (i) the weaker building has lesser potential energy in its system before unloading due to its lower capacity, and thus have lower velocities when unloading through the zero-force position, and (ii) it has to travel further in order to have greater response in the opposite direction compared to stronger buildings, as shown by the base moment versus the ground-1st floor interstorey drift response in **Figure 3.4b**. These factors resulted in the stronger building having the greatest negative and absolute peak response, both in terms of peak displacement at height of effective mass relative to the ground and interstorey drifts as shown in **Figures 3.4c** and **3.4d**, respectively.

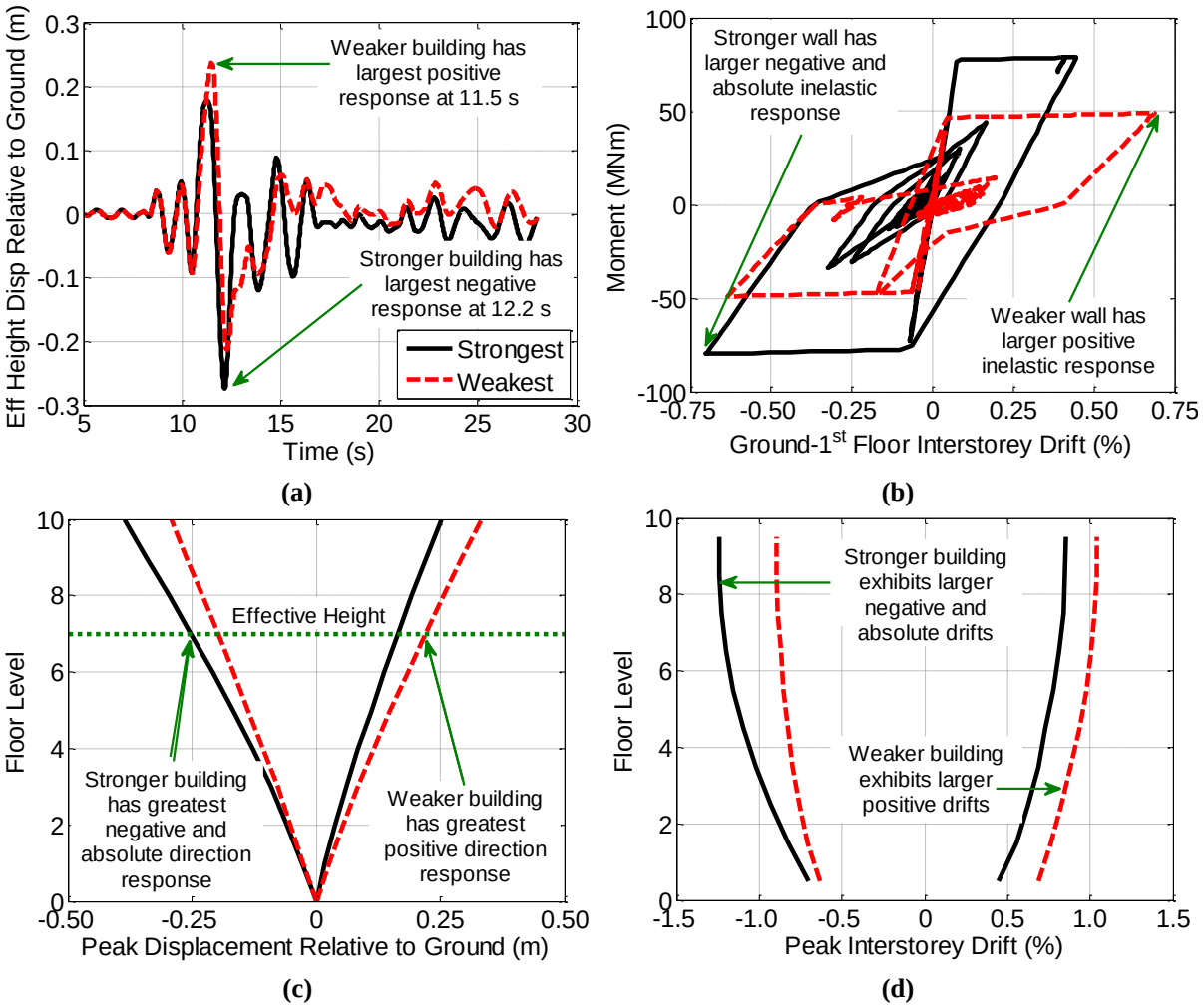

Figure 3.4. Prior yielding effects evaluation; (a) effective height displacement relative to ground response history, (b) base moment versus ground-1st floor interstorey drift response, (c) peak displacement relative to the ground, and (d) peak interstorey drift [NGA0795 N-S component record scaled by 5.0]

The second reason is due to resonance, which has a greater effect on stronger buildings. Consider the case shown in **Figure 3.5** using another ground motion record from the 10% in 50 year suite. It can be seen that from **Figure 3.5a** that there are three strong peaks in the total ground acceleration response history occurring approximately 1.25 s apart, which matches the fundamental period for the buildings of varying strength. This resulted in a few cycles of response exhibiting resonance behaviour in stronger buildings which starts at approximately the same time as the strong ground acceleration peaks, as shown in **Figure 3.5b**. Weaker buildings do not exhibit this to the same extent as: (i) the earlier yielding results in the period of the building elongating and taking it out of resonance, and (ii) there is less

potential energy in the system at the point of unloading, resulting in the response in the opposite direction to be less amplified. As such, the stronger building has greater peak displacements at height of effective mass relative to the ground and interstorey drifts in both directions on most floors, as shown in **Figures 3.5c** and **3.5d** respectively.

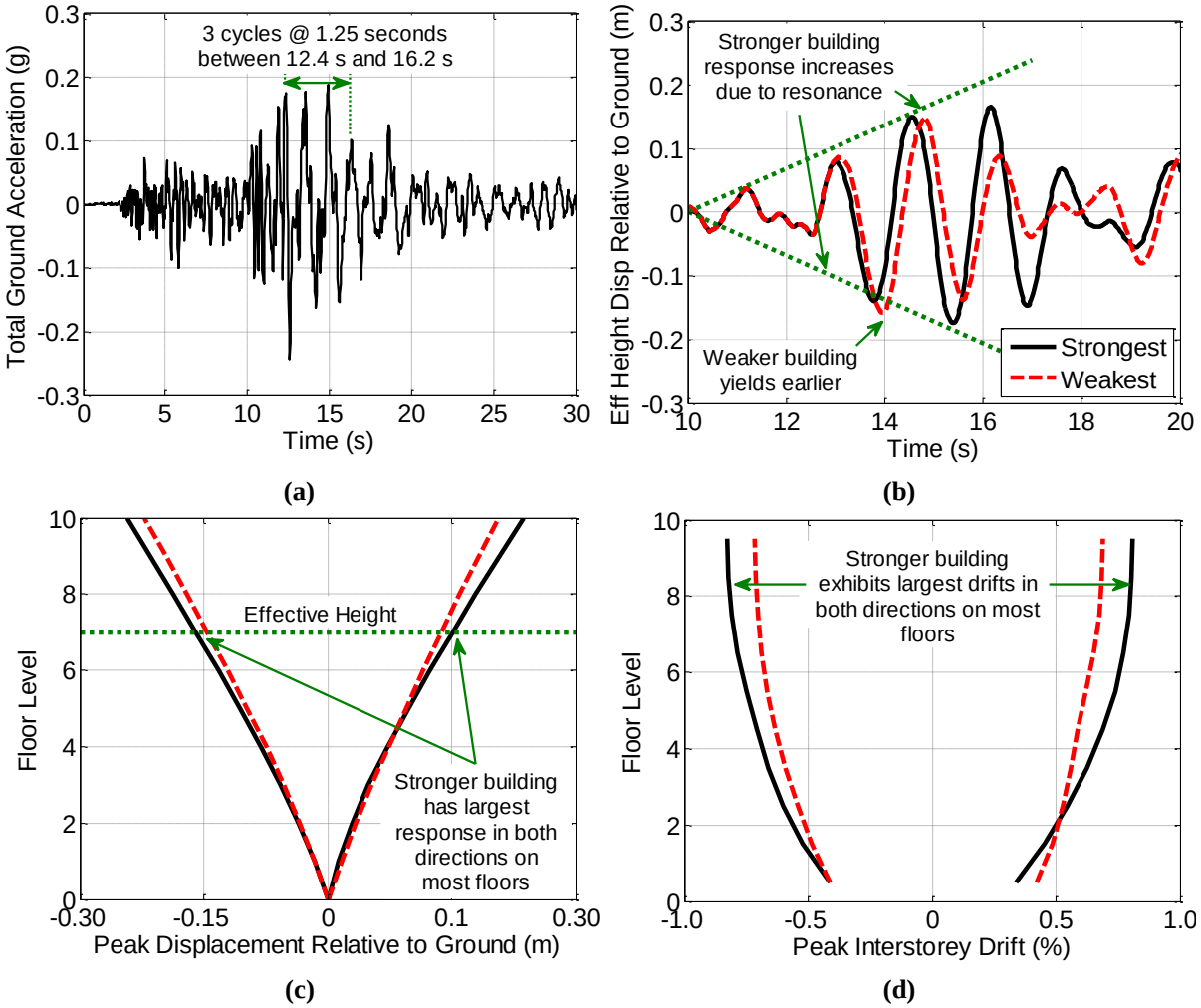

Figure 3.5. Building resonance evaluation; (a) total ground acceleration history, (b) effective height displacement relative to ground response history, (c) peak displacement relative to the ground, and (d) peak interstorey drift [NGA2221 N-S component record scaled by 11.2]

Finally, peak displacements at the height of effective mass are similar on average, as shown in **Figure 3.6a** using the average obtained from each of the 11 ground motion sets; which is similar to the equal-displacement assumption. An example of this is shown in **Figure 3.6b** using one of the records from the 10% in 50 year suite. Despite the similar displacements at the effective height, the stronger building has smaller drifts at its base in

both directions as shown in **Figure 3.6c** due to its lower inelastic response. However, due to its higher strength, the elastic first mode response on other floors in stronger buildings is larger. This resulted in stronger buildings having higher interstorey drifts on upper floors as shown in **Figure 3.6d**.

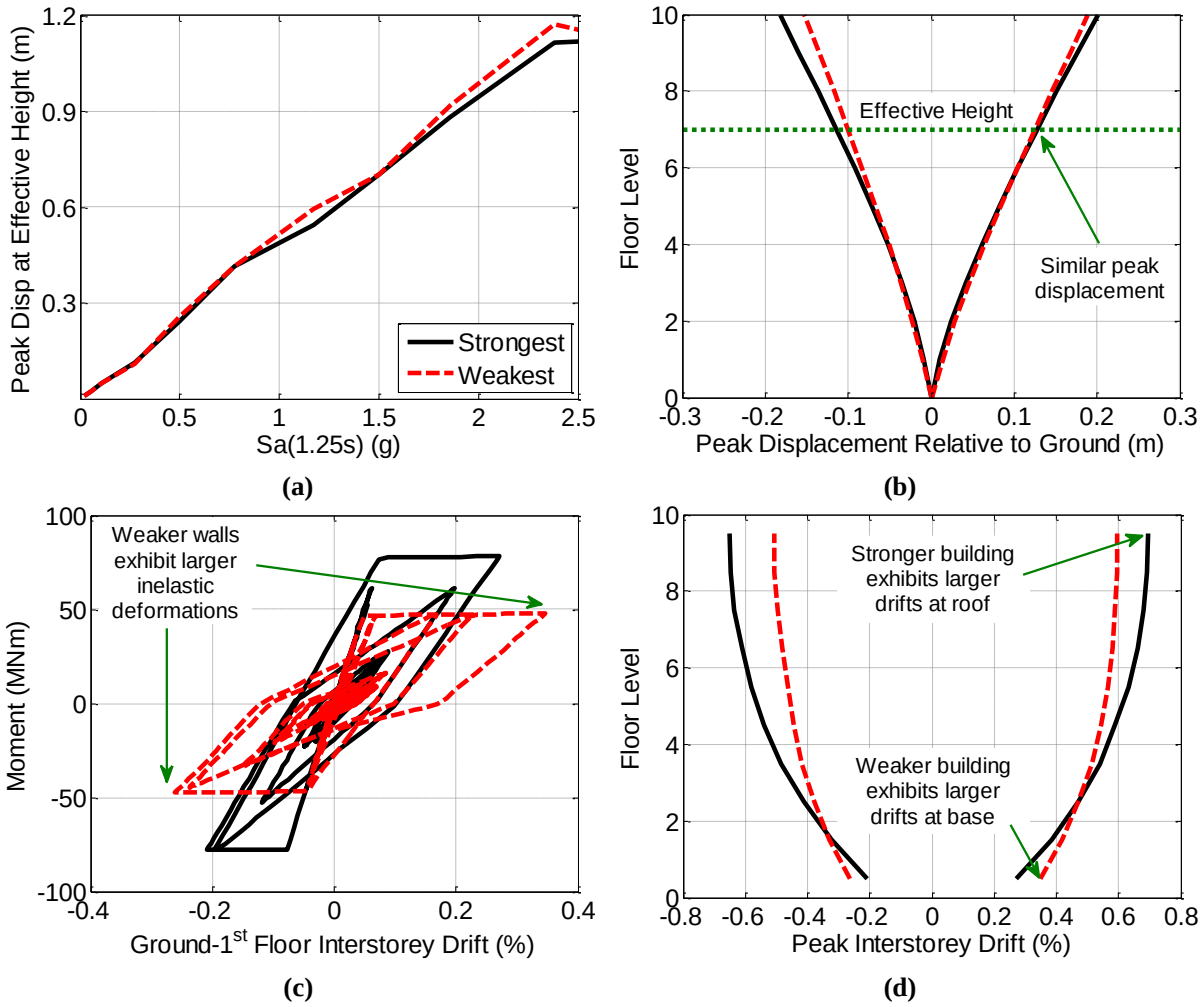

Figure 3.6. Equal displacement assumption evaluation; (a) average peak displacement at height of effective mass for each of the 11 ground motion sets, (b) peak displacement relative to the ground, (c) base moment versus ground-1st floor interstorey drift response, and (d) peak interstorey drift [(b)-(d) uses NGA3490 E-W component record scaled by 5.7]

While these observations explain the reason stronger buildings can have larger drifts on the building's upper floors, it should be noted that this is not always the case. At times, a weaker building may exhibit larger drifts overall due to experiencing significant inelastic response. Though not investigated, these observations are likely to also be applicable to other structural forms for the same reasons described here.

3.4.3 Full-Replacement and Collapse Assessment

The probability that full-replacement was required or collapse occurred versus *Sa*(1.25s) are shown in **Figures 3.7a** and **3.7b**, respectively. The stiffest building had the lowest probabilities overall. Stronger buildings also have a lower probability compared to weaker buildings when *Sa*(1.25s) < 0.8 g for full-replacement, and for all *Sa*(1.25s) considered for collapse cases. It does however have higher probability of requiring full-replacement at *Sa*(1.25s) > 0.8 g due to the larger drifts on upper floors, causing stronger buildings to fail the global stability criteria from **Table 3.2** more frequently.

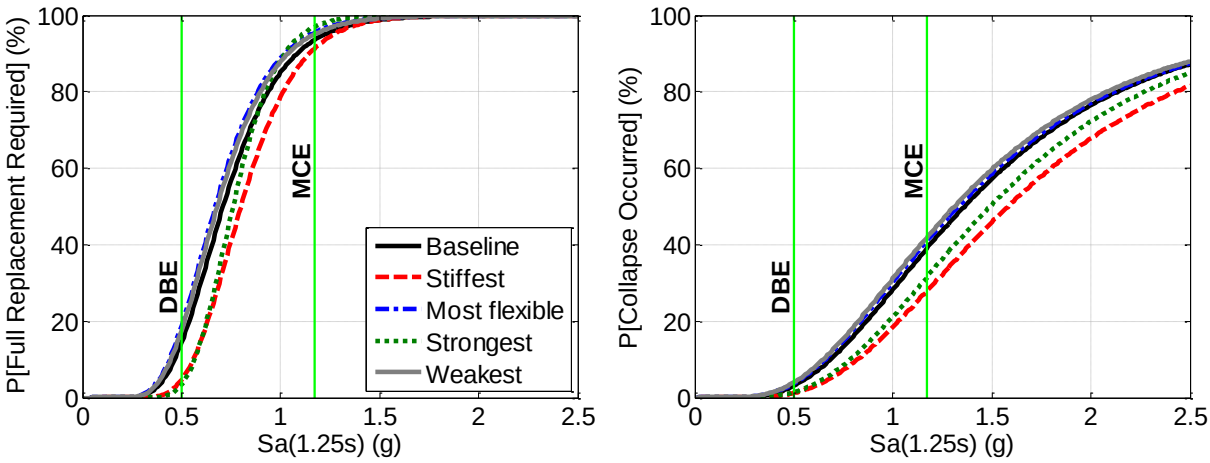

(a) **(b)**

Figure 3.7. Probability of (a) requiring full-replacement, or (b) experiencing structural collapse

3.4.4 Qualitative Summary of Stiffness and Strength Effect on Structural Response

Based on the observations made between **Sections 3.4.1** to **3.4.3**, the qualitative effect of increasing a building's stiffness or strength is as shown in **Table 3.3**.

Table 3.3. Qualitative summary of stiffness and strength effect on structural response

Response	Increasing stiffness	Increasing strength
Acceleration	Increase	Increase
Drift (lower half)	Decrease	Decrease
Drift (upper half)	Decrease	Increase/similar
Full replacement/collapse probability	Decrease	Decrease

3.5 INTENSITY-BASED LOSS ASSESSMENT

The expected total loss-*IM* curves, calculated using **Eq. 3.5a**, are shown in **Figure 3.8**; where the stiffest building had lower losses at all *IM* by up to \$1.52 million (or 11.8% of building cost) compared to the baseline building. The strongest buildings incur lower losses when *Sa*(1.25 s) > 0.3g by up to \$0.83 million (or 6.4% of building cost) compared to the baseline building, but incurs higher losses at more frequent events by up to \$0.17 million (or 1.3% of building cost). The latter observation was due to the stronger wall buildings having greater A_{FT} response on all floors and larger *PID* response on the top few floors.

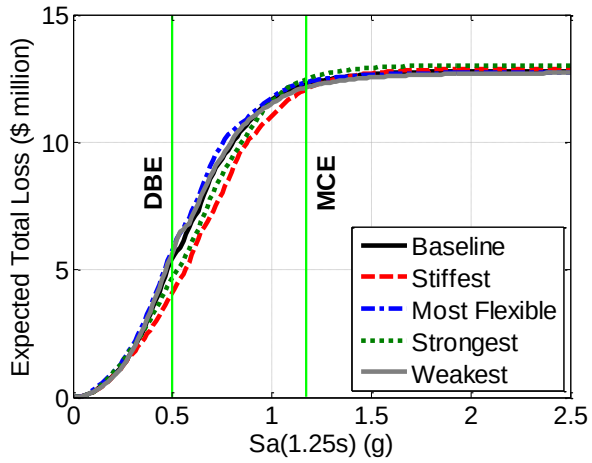

Figure 3.8. Expected total loss versus IM relationship considering direct-repair costs only

Figure 3.8 also shows that the expected total loss for all cases for a 2% in 50 year event (i.e. maximum credible event, MCE) or rarer is similar. This is because the probability of requiring full-replacement was high for all cases at events rarer than MCE as shown in **Figure 3.7a**, and that the cost of full-replacement is similar for all cases (within \$0.3 million as shown in **Table 3.1**).

In moderate events, the stiffest and the strongest buildings incurred lower losses. This is mainly due to flexible and/or weaker buildings having a higher probability of requiring full-replacement or of collapsing. This is shown in the breakdown of expected losses at DBE shaking levels by global damage state type in **Figure 3.9**, where approximately 50% of expected losses in flexible and weak buildings under DBE shaking were due to the need for

full-replacement or from collapse. This resulted in the expected absolute value of losses arising from full-replacement or collapse of flexible and weaker buildings to be four times that of stiffer and stronger buildings.

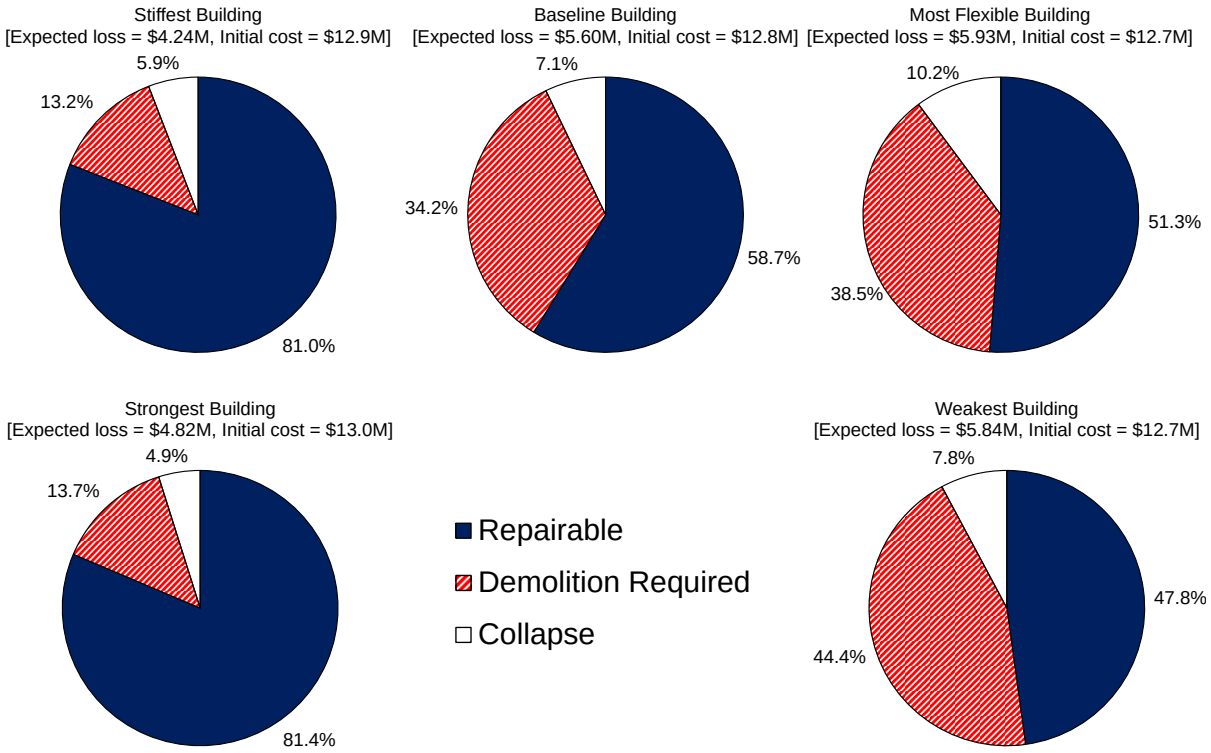

Figure 3.9. Deaggregation of expected losses in 10% in 50 year event by global damage states

It can be seen from **Figure 3.9** that the contribution of repairable damage losses was higher for the stiffest and the strongest buildings. This was mainly due to there being less cases where full-replacement was not needed in flexible and weaker buildings. To investigate the causes of repairable damage in more detail, the expected losses from damage to (i) structural, (ii) non-structural drift-sensitive, and (iii) non-structural acceleration-sensitive components in a DBE shaking event for non-collapse cases are shown in **Figure 3.10**. It can be seen that the cost of repairing structural components were less than 20% of its initial construction cost for that category alone, compared to over 30% for the non-structural elements. This was because the walls were only assumed to be damaged among the bottom three floors, and as a result the walls on the upper seven floors would not require significant repairs.

Figures 3.10a and **3.10b** shows that the stiffest building incurs a lower proportion of drift related losses compared to more flexible buildings due to its lower drift response as shown in **Figure 3.3b**. In contrast, the strongest building has slightly higher drift losses compared to weaker buildings due to incurring higher drifts on upper floors, which is the location of the largest drifts within the entire building overall. **Figure 3.10c** shows that both the stiffest and strongest building incurred the highest acceleration-related losses overall due to their higher A_{FT} response from **Figure 3.3c**. These factors resulted in the strongest building having the greatest repairable damage cost overall excluding full-replacement cases. It should be noted however that this finding is likely to be specific to cantilever buildings where the interstorey drift response and associated losses on the upper floors are the largest along the building's height. In other structural forms such as frame buildings, the largest drifts and associated losses occur on lower floors as shown previously in **Chapter 2** (**Section 2.5.1**), and therefore the increased drift response on upper floors for stronger frame buildings should have lesser impact on overall losses.

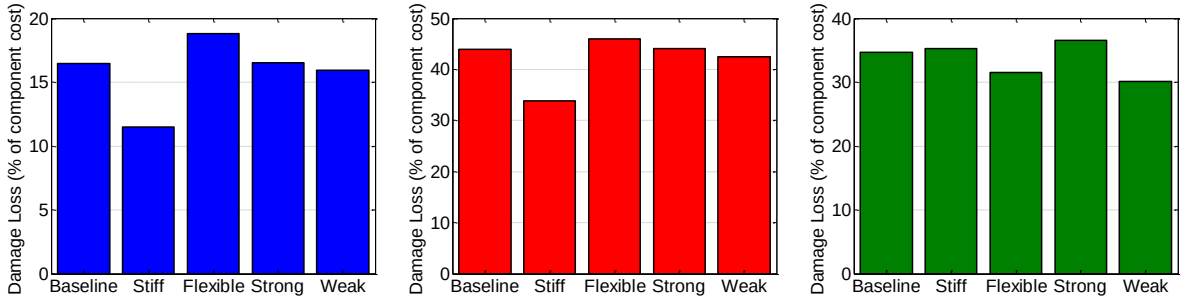

(a) **(b)** **(c)**

Figure 3.10. Damage loss as a percentage of construction cost of component group in 10% in 50 year event provided that full-replacement was not required; (a) structural, (b) non-structural drift, and (c) non-structural acceleration

Based on findings from **Figures 3.8** to **3.10**, it can be concluded that stiffer buildings would incur lower damage losses compared to more flexible buildings due to decreased drift-related losses, similar acceleration-related losses, and lower probability of requiring full-replacement. While stronger buildings incur lower expected damage losses compared to weaker buildings when full-replacement costs are included (**Figure 3.8**), the higher drift

response on upper floors meant that stronger buildings can in fact incur higher drift-related damage overall, particularly at smaller events.

3.6 COST-BENEFIT ASSESSMENT

3.6.1 Expected Annual Loss and Net-Present-Value Assessment

The expected annual losses, *EAL*, for each building, calculated using **Eq. 3.6**, are shown in **Table 3.4**. It can be seen that the *EAL* of the stiffest building was 17% lower compared to more flexible buildings, and was the lowest outright. In contrast, the difference between the strongest and weakest building was just 2% due to its poorer performance at more frequent events and larger drifts on upper floors. This shows that varying *T* has a greater effect on building performance compared to *R* for cantilever wall buildings.

Table 3.4. Wall buildings' annual loss

Annual Loss	Building Case				
	Baseline	**Stiffest**	**Most Flexible**	**Strongest**	**Weakest**
Expected ($)	36,000	32,400	39,000	35,300	36,100
Dispersion	2.32	2.31	2.31	2.33	2.34

Comparisons made using cost-benefit assessments following **Eq. 3.8** with a discount rate, *r*, of 6%, and using the difference in initial construction costs relative to the cheapest option as *IC*, is shown in **Figure 3.11**. It can be seen that after 50 years of being in service, the total cost of the stiffest building was almost equal to that of the baseline building, and was just $36,000 more than the most-flexible case despite costing over $160,000 more initially. There was however almost no decrease in the cost difference between the strongest and weakest building, with the former still costing almost $300,000 more after 50 years of being in service due to it having an annual expected loss just $800 less than the weakest building. Based on these findings, it is unlikely that the stiffest or strongest building would be selected due to their higher *NPC* if only construction and direct-repair costs were considered.

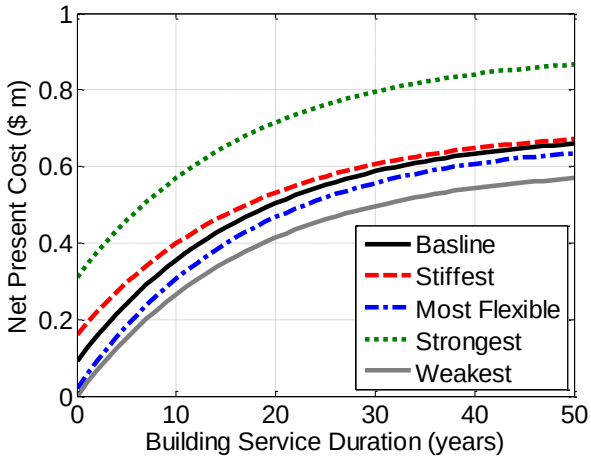

Figure 3.11. Cost-benefit assessment of buildings

3.6.2 Loss-Hazard Assessment

The loss-hazard curves for the buildings considered are calculated using **Eq. 3.7** as shown in **Figure 3.12a**, where the strongest and the most flexible buildings had higher losses up till an annual rate of exceeding total loss, λ_{LT}, of 0.002; corresponding to a 10% in 50 year loss event. This was due to (i) the flexible building having larger drifts and a greater chance of requiring full-replacement or of collapsing compared to stiffer buildings, and (ii) stronger buildings have higher accelerations on all floors, and higher drifts on upper floors during more frequent events, as shown by **Figure 3.12**. It can also be seen that the 2% in 50 year losses are similar in all cases due to all buildings having a high probability of requiring full-replacement at rare events.

The biggest difference between the various cases lies between the 10% and 2% in 50 year events. This is consistent with observations from **Figure 3.8** where the largest differences occurred between the DBE and MCE events, and is due to stronger and stiffer buildings having a lower probability of requiring full-replacement. While the stronger building incurred slightly higher losses at smaller events, it incurs up to $2.5 million less within this range.

The effective cost-hazard curves, which was computed by adding the difference in initial construction costs to loss values as discussed in **Section 3.2.5**, are shown in **Figure**

3.12b. Here, the stiffer building was the best option from an annual rate of exceeding a given effective-cost, λ_{EC}, of 0.003; or a 333 year return period loss event. As this is more frequent compared to a design-basis shaking event, stiffer buildings are likely to be favoured compared to more flexible buildings, particularly if the decision-maker is risk-adverse. Stronger buildings however are only more favourable compared to the weaker buildings from λ_{EC} of 0.0017, or a 588 year return period event, and thus might be less favourable. In general, stiffer buildings are more advantageous compared to stronger buildings due to (i) incurring lower drifts on all floors (**Figure 3.3b**), and (ii) generally having lower losses while costing less than the strongest building considered (**Figure 3.8**).

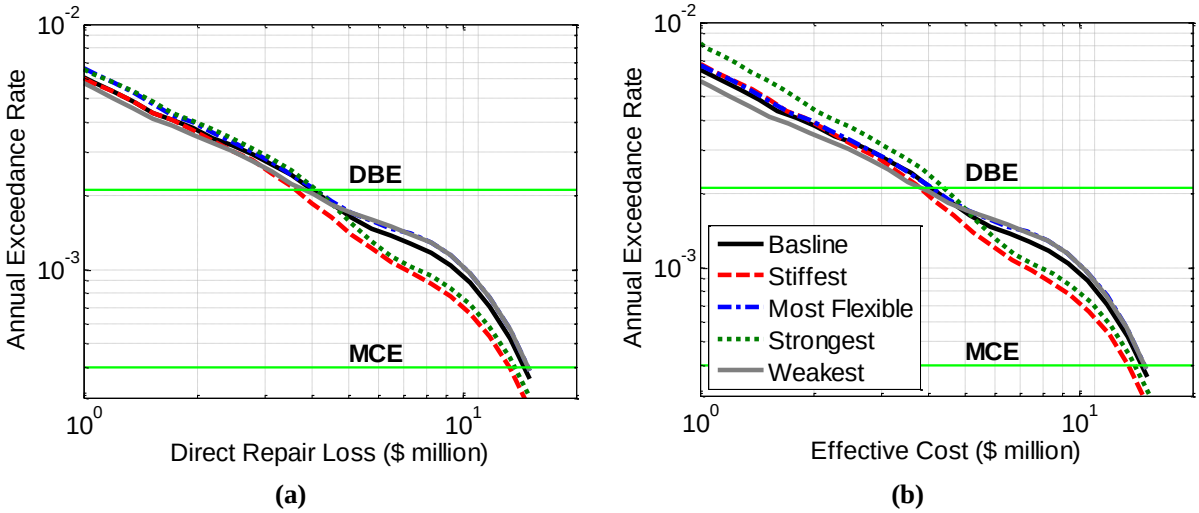

Figure 3.12. Cost-hazard curves: (a) total loss, (b) effective cost

3.7 CONCLUSIONS

This study quantifies the effect of changing T or R of a 10-storey RC wall building located on subsoil class C conditions in Wellington, New Zealand, in terms of initial construction costs and direct loss. It was found that:

1. Increasing stiffness and strength increases the building's total floor acceleration demands, though increasing strength appears to have greater influence than stiffness if both were increased by the same percentage.

2. Increasing stiffness reduces inter-storey drifts over all floors. Increasing strength also causes the inter-storey drifts over the bottom few floors to decrease. However, the drifts on upper floors may increase with strength at frequent events, which is due to (i) earlier yielding of weaker buildings diminishing what could have been a more severe response in the opposite direction, (ii) resonance, and (iii) higher elastic first-mode response of stronger buildings compared to weaker buildings. Weaker buildings tend to have higher drifts on all floors outright for a 10% in 50 year response or rarer.
3. Increasing stiffness and/or strength reduces the probability of requiring full-replacement or collapse occurring. Changing stiffness has a larger effect, as the higher drifts on upper floors in stronger buildings may cause global stability issues in stronger events.
4. Increasing stiffness reduces loss at all events considered, as the savings from reduced drift damage and need for full-replacement outweighs the increased acceleration-losses. This was despite over 50% of the building's initial costs being comprised of acceleration-sensitive non-structural contents. Increasing strength increases drift-related losses at more frequent events due to the higher drifts on the upper floors, and also results in large acceleration response and associated losses. However, the finding with regards to strength is likely to be specific to cantilever-type buildings where the largest drifts along the entire building are near the top.
5. Effective-cost hazard analysis showed that the stiffer building would be preferred from a return period of 333 years onwards, while the stronger building would be preferred over weaker buildings from a return period of 588 years onwards. Thus, increasing stiffness has a larger influence on the overall performance compared to stronger structures despite costing less.

3.8 REFERENCES

1. CEB. (1964). Recommendations for an International Code of Practice for Reinforced Concrete. Paris, France: Comité Européen du Beton (CEB).
2. Park, R., & Paulay, T. (1975). Reinforced Concrete Structures. New York, US: John Wiley & Sons.
3. Freeman, J. R. (1932). Earthquake Damage and Earthquake Insurance. New York, US: McGraw-Hill.
4. Berg, G. V. (1983). Seismic Design Codes and Procedures (Vol. 6). Berkeley, California, US: Earthquake Engineering Research Institute.
5. Cornell, C. A., & Krawinkler, H. (2000). Progress and challenges in seismic performance assessment. PEER News, 3(2).
6. Krawinkler, H., & Miranda, E. (2004). Performance-based earthquake engineering. In Chapter 9 of Earthquake Engineering: From Engineering Seismology to Performance Based Engineering: CRC Press, Boca Raton, FL.
7. Porter, K. A., Kiremidjian, A. S., & LeGrus, J. S. (2001). Assembly-Based Vulnerability of Buildings and Its Use in Performance Evaluation. Earthquake Spectra, 17(2), 291-312.
8. Aslani, H., & Miranda, E. (2005). Probabilistic Earthquake Loss Estimation and Loss Disaggregation in Buildings: Department of Civil and Environmental Engineering, Stanford University.
9. Bradley, B. A., Lee, D. S., Broughton, R., & Price, C. (2009). Efficient Evaluation of Performance-based Earthquake Engineering Equations. Structural Safety, 31, 65-74.
10. Mitrani-Reiser, J. (2007). An Ounce of Prevention: Probabilistic Loss Estimation for Performance Based Earthquake Design. PhD Thesis, California Institute of Technology, Pasadena, California.
11. Baker, J. W., & Cornell, C. A. (2008). Uncertainty Propagation in Probabilistic Seismic Loss Estimation. Structural Safety, 30(3), 236-252.
12. Ramirez, C. M., & Miranda, E. (2009). Building-Specific Loss Estimation Methods and Tools for Simplified Performance-Based Earthquake Engineering. Department of Civil Engineering, Standford University.
13. Bradley, B. A. (2011). SLAT:Seismic Loss Assessment Tool (Version 1.16): Department of Civil and Natural Resources Engineering, University of Canterbury.
14. Naeim, F., & Hagie, S. (2012). PACT: Performance Assessment Calculation Tool. John A. Martin & Associates, INC. Los Angeles, California, US.
15. Wen, Y. K., & Kang, Y. J. (2001). Minimum Building Life-Cycle COst Design Criteria. II: Applications. Journal of Structural Engineering, 127(3), 338-346.
16. Ramirez, C. M., Liel, A. B., Mitrani-Reiser, J., Haselton, C. B., Spear, A. D., Steiner, J., Deierlein, G. G., & Miranda, E. (2012). Expected earthquake damage and repair costs in reinforced concrete frame buildings. Earthquake Engineering and Structural Dynamics, 41(11).
17. Standards New Zealand. (2004). NZS 1170.5:2004, Structural Design Actions Part 5: Earthquake Actions New Zealand: Standards New Zealand, Wellington, New Zealand.
18. Priestley, M. J. N., & Kowalsky, M. J. (1998). Aspects of Drift and Ductility Capacity of Rectangular Cantilever Structural Walls. Bulletin of the New Zealand Society of Earthquake Engineering, 31(2), 73-85.
19. Bradley, B. A., Dhakal, R. P., Cubrinovski, M., MacRae, G. A., & Lee, D. S. (2009). Seismic Loss Estimation for Efficient Decision Making. Bulletin of the New Zealand Society of Earthquake Engineering, 42(2), 96-110.
20. Kramer, S. L. (1996). Geotechnical Earthquake Engineering: Prentice Hall, New Jersey.
21. Jin, M., & Astaneh, A. (1998). Study of seismic resistance of desktop computers. ATC 29-1, Proceedings of seminar on seismic design, retrofit, and performance of nonstructural components, 379-392.
22. Porter, K. A. (2007). Fragility of hydraulic elevators for use in performance-based earthquake engineering. Earthquake Spectra, 23(2), 459-469.
23. Goda, K., & Hong, H. P. (2006). Optimal Seismic Design Considering Risk Attitude, Societal Tolerable Risk Level, and Life Quality Criterion. Journal of Structural Engineering, 132(12), 2027-2035.
24. Standards New Zealand. (2006). NZS 3101:2006, Concrete Structures Standard Part 1 - The Design of Concrete Structures: Standards New Zealand, Wellington, New Zealand.
25. Rawlinson & Co. (2015). Rawlinsons New Zealand construction handbook. Rawlhouse Publishing, Wellington, New Zealand.
26. Field, E. H., Jordan, T. H., & Cornell, C. A. (2003). OpenSHA: A Developing Community-Modeling Environment for Seismic Hazard Analysis. Seismological Research Letters, 74(4), 406-419.
27. Stirling, M. W., McVerry, G. H., Gerstenberger, M. C., Litchfield, N. J., Van Dissen, R. J., Berryman, K. R., Barnes, P., Wallace, L. M., Villamor, P., Langridge, R. M., Lamarche, G., Nodder, S., Reyners, M. E., Bradley, B., Rhoades, D. A., Smith, W. D., Nicol, A., Pettinga, J., Clark, K. J., & Jacobs, K. (2012).

National seismic hazard model for New Zealand : 2010 update. Bulletin of the Seismological Society of America, 102(4), 1514-1542.
28. Bradley, B. A. (2010). NZ-Specific Pseudo-Spectral Acceleration Ground Motion Prediction Equations based on Foreign Models: Department of Civil and Natural Resources Engineering, University of Canterbury, Christchurch, New Zealand.
29. Bradley, B. A. (2010). A Generalized Conditional Intensity Measure Approach and Holistic Ground Motion Selection. Earthquake Engineering and Structural Dynamics, 39(12), 1324-1342.
30. Bradley, B. A. (2012). The Seismic Demand Hazard and Importance of the Conditioning Intensity Measure. Earthquake Engineering and Structural Dynamics, 41(11), 1417-1437.
31. Lin, T., Haselton, C. B., & Baker, J. W. (2013). Conditional spectrum-based ground motion selection. Part I: Hazard consistency for risk-based assessments. Earthquake Engineering and Structural Dynamics, 42(12), 1847-1865.
32. Campbell, K. W., & Bozorgnia, Y. (2010). A Ground Motion Prediction Equation for the Horizontal Component of Cumulative Absolute Velocity (CAV) Based on the PEER-NGA Strong Motion Database. Earthquake Spectra, 26(3), 635-650.
33. Bommer, J. J., Stafford, P. J., & Alarcon, J. E. (2009). Empirical Equations for the Prediction of the Significant, Bracketed and Uniform Duration of Earthquake Ground Motion. Bulletin of the Seismological Society of America, 99(6), 3217-3233.
34. Ang, A. H. S., & Tang, W. H. (2007). Probability concepts in engineering: Emphasis on applications in civil and environmental engineering: John Wiley & Sons.
35. Bradley, B. A. (2012). A Ground Motion Selection Algorithm Based on the Generalized Conditional Intensity Measure Approach. Soil Dynamics and Earthquake Engineering, 40, 48-61.
36. Tarbali, K., & Bradley, B. A. (2014). Representative ground-motion ensembles for several major earthquake scenarios in New Zealand, 2014 NZSEE Conference. Auckland, New Zealand.
37. Chiou, B. S. J., Darragh, R., Gregor, N., & Silva, W. (2008). NGA Project Strong-Motion Database. Earthquake Spectra, 24(1), 23-44.
38. Carr, A. J. (2004). Ruaumoko 2D - Inelastic dynamic analysis program. Department of Civil and Natural Resources Engineering, University of Canterbury, Christchurch.
39. Caughey, T. K. (1960). Calssical Normal Modes in Damped Linear Systems. Journal of Applied Mechanics, 27, 269-271.
40. Carr, A. J. (2008). Ruaumoko Manual (Vol. Volumne 2: User Manual for the 2:Dimensional Version Ruaumoko 2D). University of Canterbury, Christchurch, NZ.
41. Tagawa, H. (2005). Towards an understanding of seismic performance of 3D structures: stability & reliability. PhD Thesis, University of Washington, Seattle, USA.
42. Thomsen, J. H., & Wallace, J. W. (2004). Displacement-based design of slender reinforced concrete structural walls - experimental verification. Journal of Structural Engineering, 130(4), 618-630.
43. Wallace, J. W. (2007). Modelling issues for tall reinforced concrete core wall buildings. The Structural Design of Tall and Special Buidlings, 16, 615-632.
44. Saiidi, M., & Sozen, M. A. (1979). Simple and complex models for nonlinear seismic response of reinforced concrete structures. Illinois: University of Illinois.
45. Sedgh, R. E., Dhakal, R. P., & Carr, A. J. (2015). State of the Art: Challenges in analytical modelling of multi-storey shear wall buildings. Paper presented at the 2015 NZSEE Conference, Rotorua.
46. ASCE. (2000). Prestandard and Commentary for the Seismic Rehabilitation of Buildings, FEMA 356. Federal Emergency Management Agency, Washington, D.C.
47. Birely, A. C. (2013). Seismic Performance of Slender Reinforced Concrete Structural Walls. PhD Thesis, University of Washington.
48. Panagiotou, M., Restrepo, J. I., & Conte, J. P. (2011). Shake-Table Test of a Full-Scale 7-Story Building Slice. Phase 1: Rectangular Wall. Journal of Structural Engineering, 137(6), 691-704.

4. Validating the Sliding Mechanics of Office-Type Furniture using Shake-Table Experiments

4.0 SUMMARY

Pull-tests and shake-table tests of office-type furniture on carpet and vinyl flooring were performed to obtain friction coefficients and to validate the mechanics of content sliding and current modelling approaches. The static friction coefficient, μ_s, for furniture with and without wheels was between 0.13-0.30 and 0.36-0.45 on carpet flooring, respectively, and 0.07-0.13 and 0.39-0.45 on vinyl flooring, respectively. The kinetic friction coefficient, μ_k, was similar to μ_s for carpet flooring, but was up to 38% lower for vinyl flooring. Shake-table tests using sinusoidal floor excitations showed that: (i) the sliding force hysteresis loop was elasto-plastic on average, and (ii) peak total floor velocity significantly affected the extent of sliding. It was also found that the maximum sliding displacement obtained by numerical integration methods differed from experimental results by a factor between 0.3 and 3.0 on a case-by-case basis, but the average error was 5% when a suite of records was used. Preliminary sliding analyses of furniture within single-storey buildings of varying stiffness using a suite of ground motion records were performed. It was found that (i) the extent of sliding was not necessarily more severe in stiffer buildings despite the greater peak total floor acceleration demands, and (ii) considering only μ_k in content sliding analyses still produced reasonably accurate predictions.

4.1 INTRODUCTION

Building contents, such as hospital equipment or furniture, have the potential to slide over large distances as observed from past seismic events [1] and experimental shake-table studies [2, 3]. This potentially results in injuries, damage, and business/operational

disruptions [3, 4]. Due to this, there is a need to consider content movement in seismic risk assessments.

Many content sliding studies have been numerical in order to feasibly consider the wide range factors that affect content sliding. Examples of such studies includes (i) development of equations to predict the contents' maximum sliding displacement [5-7], (ii) investigating the influence of building response on the content sliding behaviour [8-10], and (iii) computing a content sliding spectrum [11]. Numerical approaches follows Amonton's and Coulomb's dry friction laws [12], which state that (i) friction force is independent of the contact area, (ii) friction force is proportional to the normal force, and (iii) kinetic friction is independent of sliding velocity. Based on this, the contents' total acceleration with time, $a_{CT}(t)$, can be defined using **Eq. 4.1** [13]; where $v_{CRF}(t)$ was the contents' velocity relative to the floor with time, and μ_s and μ_k were the static and kinetic friction coefficients, respectively.

$$a_{CT}(t) = \begin{cases} a_{FT}(t) & \text{when } |v_{CRF}(t)| = 0 \text{ and } |a_{FT}(t)| < \mu_s g \\ -\text{sgn}(v_{CRF}(t))\mu_k g & \text{when } |v_{CRF}(t)| > 0 \text{ or } |a_{FT}(t)| \geq \mu_s g \end{cases} \quad \textbf{(4.1)}$$

Despite the extensive use of **Eq. 4.1** in past studies, there exist few experimental studies which validated this for furniture subjected to seismic shaking. Those which did generally performed shake-table tests of rigid rectangular blocks, which may not be representative of typical office-type furniture, and/or had used on uncommon flooring materials (e.g. Teflon) [2, 14]. Typical values of μ_s and μ_k for office environments are thus not well-known.

It had also been observed in past experiment studies, both seismic and non-seismic related [15-18], that: (i) μ_k generally decreased with the velocity of the content relative to the floor, v_{CRF}, at low v_{CRF} for most materials, and (ii) μ_k may increase with v_{CRF} at higher v_{CRF} values and may exceed μ_s. The latter observation was attributed to the release of thermal energy during sliding, which is a fraction of v_{CRF} [18]. The v_{CRF} which triggered the change in μ_k-v_{CRF} trend was dependent on the contact surfaces' materials. Based on these findings,

Amonton's and Coulomb's dry friction laws may not be realistic. However, there is mixed opinion on the significance of this in seismic conditions [14, 15, 19]; though these studies have found that μ_k is generally lower than μ_s.

In addition to the potential issues regarding the applicability of Amonton's and Coulomb's dry friction laws, there also exists divided opinion on the importance of peak total floor acceleration, A_{FT}, on the extent of content sliding. Many studies assumed that the maximum sliding displacement of contents was solely dependent on A_{FT} [6, 20-23]. However, others had shown that shaking frequency was also important [8-10]; though no experimental studies have demonstrated this for pure sliding cases.

Based on these issues, there is a need for **Eq. 4.1** to be validated for seismic conditions so that content sliding analysis could be confidently used for seismic risk assessments. This study seeks to address these needs, and to better understand the mechanics of furniture sliding in office environments by performing: (i) static and kinetic friction tests; and (ii) shake-table tests using sinusoidal floor motion. Case studies were also examined to demonstrate the usefulness of numerical approaches. For the contents and flooring materials considered, answers to the following questions are sought:

1. What are typical values of μ_s, and do any parameters affect this?
2. What is the relation between μ_k and μ_s, and do any parameters affect this?
3. How accurate are numerical approaches in predicting the actual content's sliding response?
4. Is peak floor acceleration alone a good descriptor of the sliding response of contents subjected to sinusoidal floor motion? If not, which other parameters are important?
5. How important is the consideration of μ_s and μ_k in numerical approaches?

4.2 EXPERIMENTAL DETAILS

4.2.1 Furniture Properties

Several office-type items of furniture, herein termed ‘contents’ as to not confuse subscript notation with the floor response, were used in the experiments. These are shown in **Figure 4.1**, and consisted of: (i) a desk with rubber soles (D1); (ii) a desk with a metallic base (D2); (iii) a mobile drawer unit (MD); and (iv) a container (WC). These have masses of 24.5, 26.8, 31.3, and 2.2 kg, respectively. Both the drawer and the container are supported on wheels. The drawer’s wheels were able to also rotate 360^{o} in the horizontal plane, while the container’s wheels were fixed to only rotate in its longitudinal direction. Circular markers were attached to the sides of the contents to aid in motion tracking.

(a) (b) (c) (d)

Figure 4.1. Contents used in experiments; (a) Desk 1 (rubber soles), (b) Desk 2 (metallic base), (c) Drawer, (d) Container

4.2.2 Static and Kinetic Friction Tests Setup

Three types of tests were performed for each content and floor material pairing: (i) static pull-tests, (ii) kinetic pull-tests, and (iii) dynamic floor shaking. All tests were performed on the shake-table shown in **Figure 4.2a**. The shake-table has dimensions of 3.5 m by 2 m, and was displacement-controlled. Plywood was bolted onto the shake-table to protect the surface, and to allow the flooring materials to be glued on directly to prevent it from loosening. The flooring materials were ordered from The Flooring Centre, which is one of New Zealand’s largest independent floorcovering retailer. Two different types of flooring materials were tested: (i) a Pegasus solution dyed nylon carpet, and (ii) vinyl (from their $55.00 stock range as of 2013).

Static pull-tests were used to determine μ_s using the setup shown **Figure 4.2b**, where μ_s was the ratio between the total applied force which initiated sliding and the content's weight. This was performed five times in each direction to minimize directionality effects and to obtain an average of μ_s. The applied load height was initially varied, but was found to have no effect.

The kinetic friction coefficient, μ_k, was determined by connecting the content to a reaction frame using a steel rod as shown in **Figure 4.2c**. The shake-table was then displaced at rates of 3.0, 7.0 and 10.0 mm/s up to 100 mm from its initial position in each direction. A load cell, connected between the steel rod and the reaction frame, recorded the force required to keep the content stationary. The ratio of this force to the content's weight gives μ_k. This test could not be performed for the white container as its sloped sides made it difficult to connect the steel rod without causing uplifting effects. The test was performed twice for other contents; each starting in different directions. For both friction tests, additional weights were placed to observe if μ_s and μ_k had any dependencies on mass, the positioning of which did not appear to have an influence on the furniture's friction response from preliminary test results.

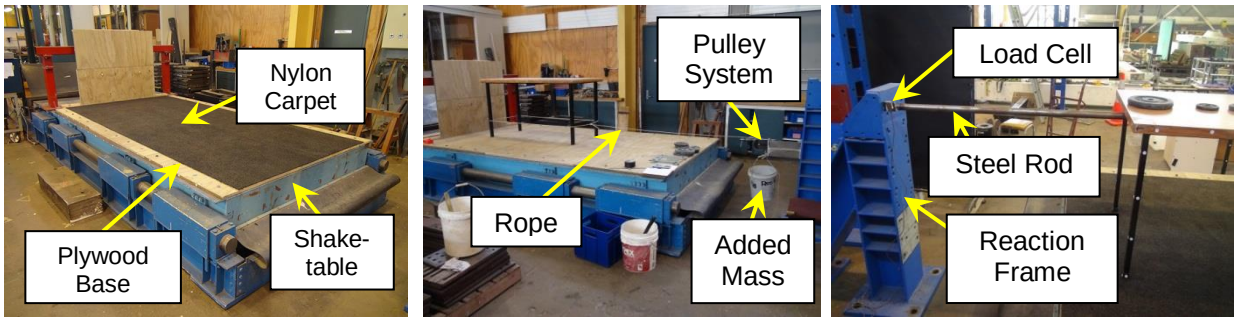

(a) Shake-table layout **(b) Static friction test** **(c) Kinetic friction test**

Figure 4.2. Testing configuration

4.2.3 Shake-table Test Input Motion and Measurements

Dynamic floor shaking tests was performed considering sinusoidal floor excitations to observe content sliding mechanics. As shown in **Figure 4.3a**, the excitation frequency was kept constant, while its amplitude was (i) increased linearly from zero over the first two

seconds, (ii) kept constant for a number of cycles, and (iii) reduced to zero over the final two seconds. The six amplitude and frequency pairings considered were listed in **Table 4.1**. Tests were performed twice, with each starting in a different direction to minimize directionality effects. The displacement amplitude was limited to 100 mm to avoid over-exerting the shake-table.

Table 4.1. Sinusoidal floor excitation patterns

Property	Case					
	1	**2**	**3**	**4**	**5**	**6**
Frequency, *f* (Hz)	1.0	1.5	1.5	2.0	2.0	2.5
Displacement amplitude, *D* (mm)	100	60	80	40	60	40

Accelerometers were placed on the top surface of the shake-table and contents, while video recordings were made at 200 frames per second using a Phantom high-speed camera (Miro M310 model) shown in **Figure 4.3b**. Software developed by the Hedrick Lab [24] was used to track the circular markers attached to the content to obtain the displacement response of both with time.

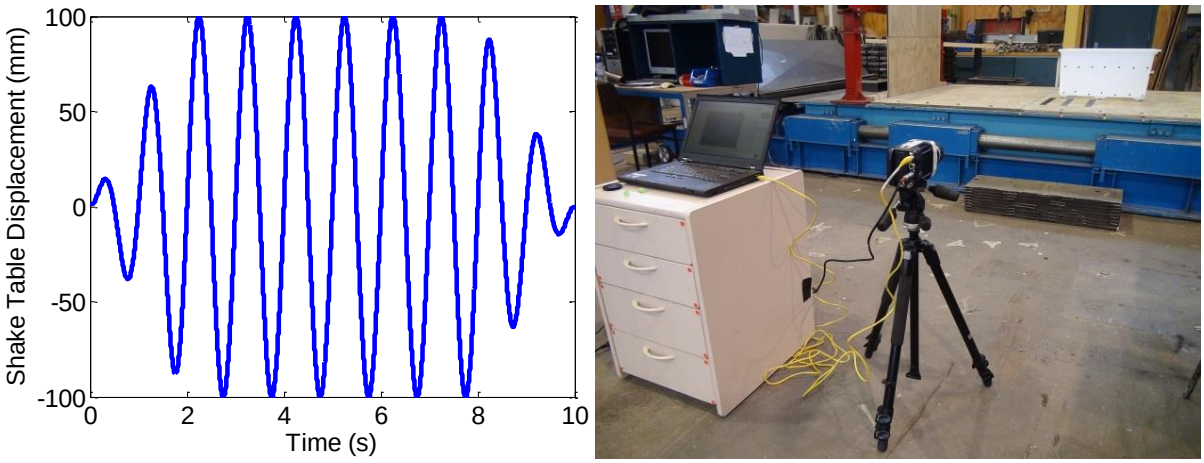

(a) **(b)**

Figure 4.3. Dynamic excitation tests; (a) Sample excitation (case 1), (b) camera setup

4.3 FRICTION COEFFICIENT TEST RESULTS

4.3.1 Static Friction Coefficients

The mean μ_s for each content, floor material, and applied mass considered are shown in **Table 4.2**. Note that an additional 10 kg was applied to the container as it was too light on its

own to obtain μ_s data. The ratio of the average μ_s between the vinyl and carpet flooring for the desks ranged from 0.96-1.25. This slight increase was due to the base of the desk tending to stick more to the vinyl surface, resulting in a similar or larger μ_s on vinyl flooring compared to carpet flooring.

The ratio of the average μ_s between the vinyl and carpet flooring for the contents on wheels ranged from 0.52-0.54. The difference between the response of these contents and the desks was that the friction resistance was from the wheels-axle interaction rather than the wheel-flooring surface. Thus, μ_s should theoretically be consistent as long as wheel rotation governs the sliding response. However, the compression of the carpet due to the contents' weight resulted in the contents digging into the carpet, resulting in additional forces being required to overcome this effect in order for the content to slide, causing the effective μ_s for contents with wheels on carpet flooring to be larger than that on vinyl. This effect also applied to the desks, but the "stickiness" of the vinyl surface had a greater effect.

It was also shown in **Table 4.2** that increasing the content mass by 10 kg (or an increase between 1.32 and 5.55 times) caused μ_s to decrease by 2- 6% on average. This difference was in the range of experimental variability and was likely not significant.

Table 4.2. Mean static friction coefficient

	Carpet		Vinyl	
Content	**+0 kg**	**+10 kg**	**+0 kg**	**+10 kg**
Desk 1 (D1)	0.41	0.40	0.40	0.38
Desk 2 (D2)	0.36	0.34	0.45	0.43
Drawer (MD)	0.13	0.13	0.07	0.07
Container (WC, +10 kg)	0.25	0.24	0.13	0.13

4.3.2 Kinetic Friction Coefficients

The average μ_k from kinetic pull-tests versus sliding displacement relationship is shown in **Figure 4.4** for contents on carpet flooring. It can be seen that the sliding response was largely elastoplastic in nature. In each case, μ_k increased until approximately μ_s (from **Table 4.2**) before decreasing slightly. μ_k tends to be marginally larger in one direction than the

other, which could be due to the difference between pushing and pulling of contents during this test.

The influence of additional mass on μ_k for both desks (37-41% increase for the 10kg case, and 74-82% for the 20 kg case), and the drawer (32% increase for the 10kg case, and 64% for the 20 kg case), are shown in **Figures 4.4a** to **4.4c**, respectively; while the influence of relative velocity on μ_k for both desks and the drawer are shown in **Figures 4.4d** to **4.4f**, respectively. It was observed that there was a slight decrease in μ_k with increasing mass, which was similar to the μ_s findings from **Table 4.2**. There was also an increase in μ_k with increasing relative velocity. However, both these effects were minor for the range of mass and relative velocity considered, and could potentially be due to experimental error.

The results using vinyl flooring are shown in **Figure 4.5**, where μ_k again increased with decreasing mass or increasing relative velocity. There were no distinct localized peaks in μ_k when reversal occurs for the desks, resulting in μ_s being a reasonable estimate of μ_k.

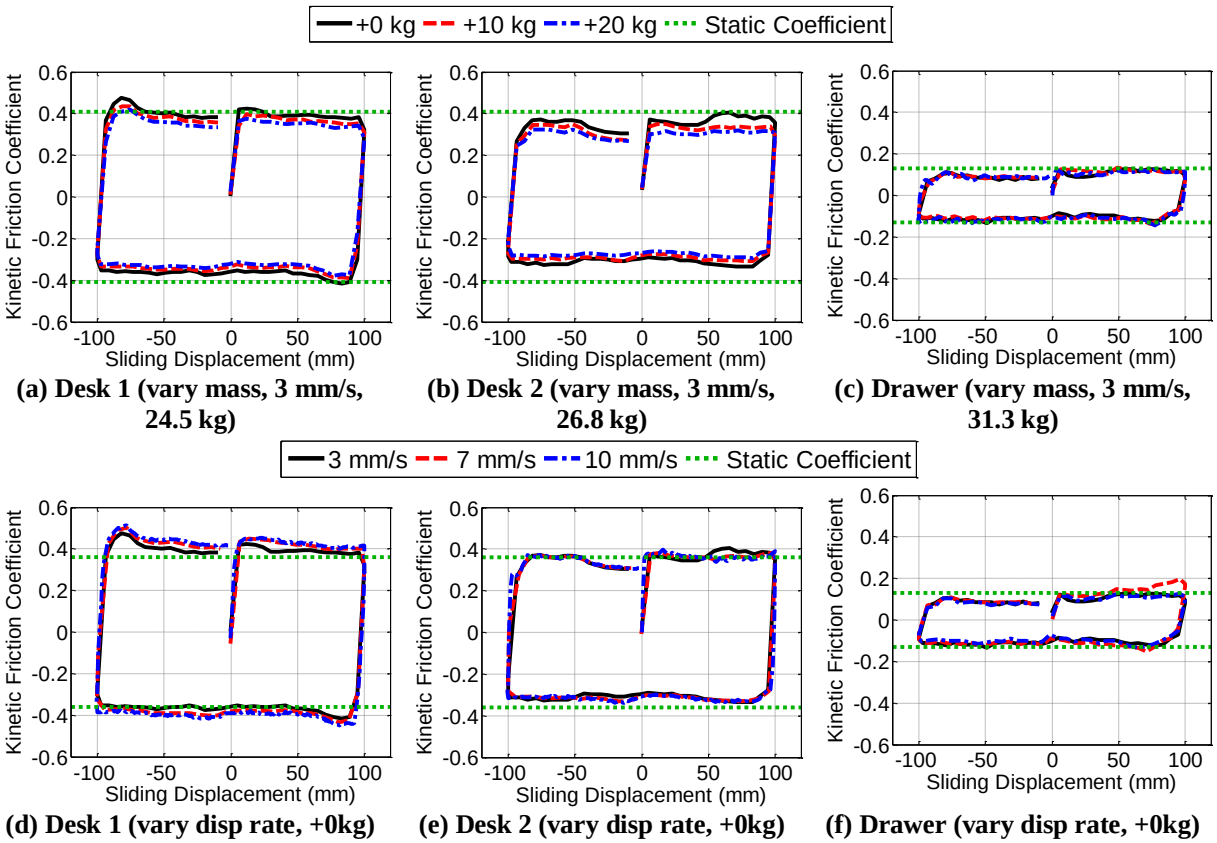

(a) Desk 1 (vary mass, 3 mm/s, 24.5 kg) **(b) Desk 2 (vary mass, 3 mm/s, 26.8 kg)** **(c) Drawer (vary mass, 3 mm/s, 31.3 kg)**

(d) Desk 1 (vary disp rate, +0kg) **(e) Desk 2 (vary disp rate, +0kg)** **(f) Drawer (vary disp rate, +0kg)**

Figure 4.4. Average kinetic friction coefficient versus sliding displacement relationship with varying content mass and floor displacement rates (carpet flooring)

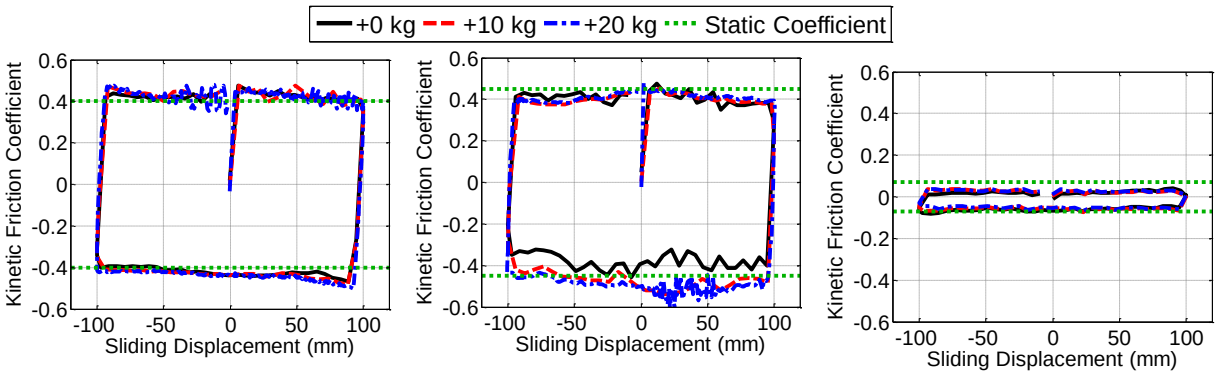

(a) Desk 1 (vary mass, 3 mm/s, 24.5 kg) **(b) Desk 2 (vary mass, 3 mm/s, 26.8 kg)** **(c) Drawer (vary mass, 3 mm/s, 31.3 kg)**

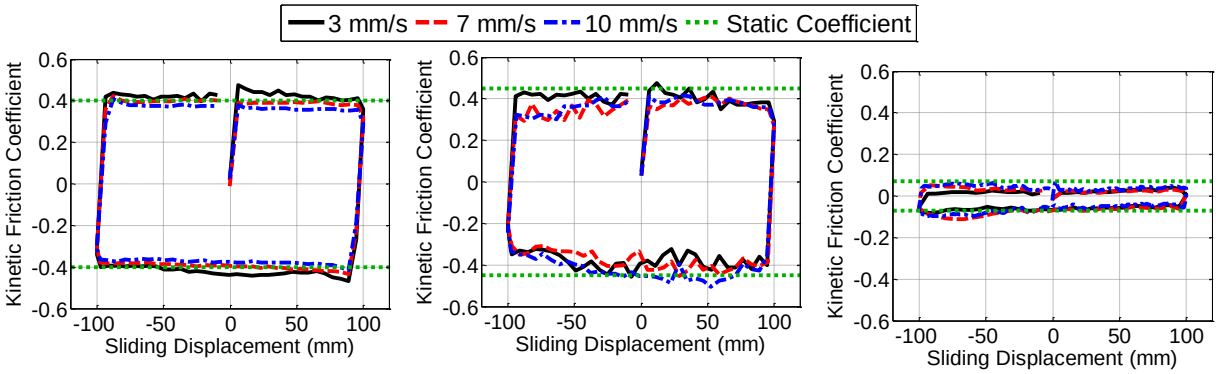

(d) Desk 1 (vary disp rate, +0kg) **(e) Desk 2 (vary disp rate, +0kg)** **(f) Drawer (vary disp rate, +0kg)**

Figure 4.5. Average kinetic friction coefficient versus sliding displacement relationship with varying content mass and floor displacement rates (vinyl flooring)

4.4 DYNAMIC RESPONSE OF SHAKE-TABLE AND CONTENTS

4.4.1 General Sliding Behaviour

This section examines the sliding behaviour of contents subjected to sinusoidal floor shaking. The response of Desk 2 on carpet flooring subjected to excitation Case 5 during the first four seconds of shaking is shown in **Figure 4.6**; where the total velocity response was obtained by differentiating the displacement response using a second order central difference approach. The contents' behaviour can be summarized as follows: (i) contents slid when the total floor acceleration at a given time, $a_{FT}(t)$, exceeded $\mu_s g$; (ii) the content's total velocity varied approximately linearly between peaks; and (iii) sliding terminated when the content and shake-tables' velocities matched. This was consistent with Amonton and Columb's laws [12]. Similar observations were made for the other tests performed.

It was also observed that contents predominantly slid in one direction more than the other initially, despite the shake-table's total acceleration response being approximately symmetric. This was because the duration between the time of separation and the time of reattachment differed in each sliding direction initially in cases where sliding immediately reverses when the relative velocity between the content and shake-table reaches zero. The sliding response does become more symmetric after several cycles as shown by the decreasing difference between the sliding displacement peaks.

Note that while the recorded shake-table displacement matched the input motions described in **Figure 4.3a**, the resulting shaking-table acceleration response was not sinusoidal in shape. This was due to stick-slip of the shake-table bearings which resulted in vibrations and high frequency accelerations. This can cause errors during: (i) estimation of the friction coefficients during sliding using the acceleration results from the dynamic tests, and (ii) validation of numerical approaches. This is further addressed later when discussing these findings in more detail.

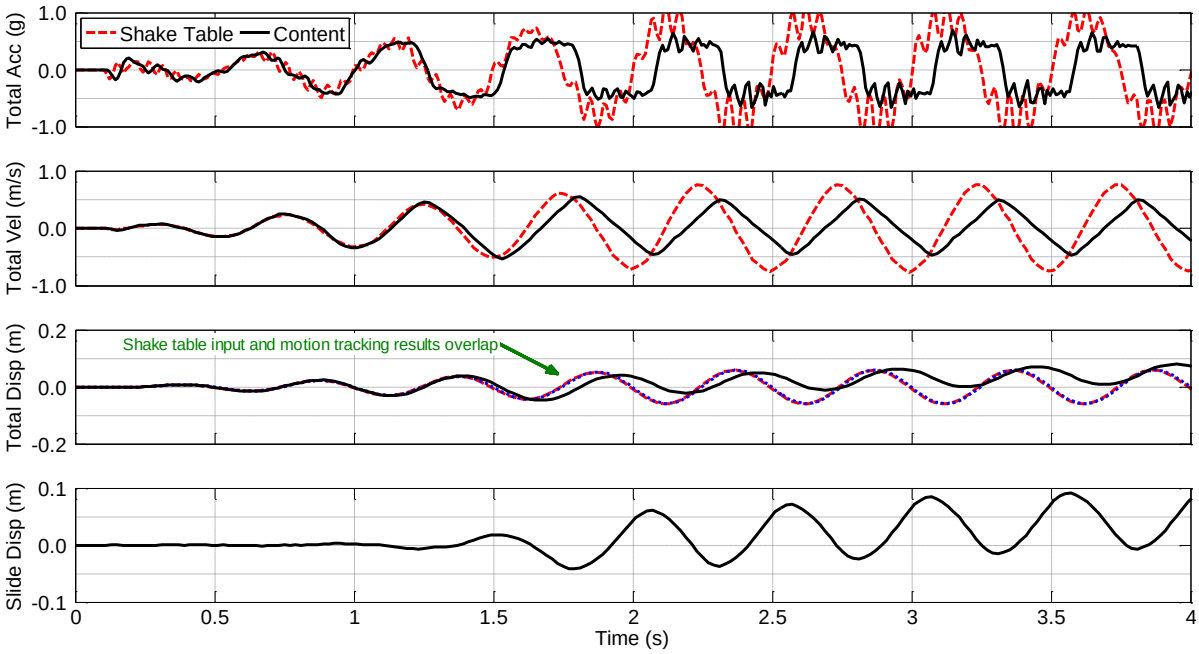

Figure 4.6. Shake-table and desk 2 response on carpet flooring (*f* = 2.0 Hz, *D* = 60 mm) – first 4 seconds

4.4.2 Estimation of the Kinetic Friction Coefficient from Dynamic Floor Excitations

The kinetic friction coefficient, μ_k, was estimated from the sinusoidal shake-table tests. The μ_k versus sliding displacement relationship for Desk 2 on carpet flooring using the Case 5 excitation is shown in **Figure 4.7a**. It may be seen that μ_k had significant variation with sliding displacement. In addition, μ_k was up to 71% larger than the value of μ_s obtained from pull-tests. This could be due to (i) vibration of Desk 2 alone, which was observed but difficult to measure, (ii) inherent variation in μ_k across the flooring and/or contact surface area, and (iii) the high frequency acceleration content of the shake-table due to its stick-slip. Due to this, reasonable μ_k-v_{CRF} relationships could not be obtained, and comparisons with past research [15-18] could not be made.

Given the variation in the accelerometer readings discussed previously, the average μ_k during each sliding excursion (i.e. a single sliding motion between peaks), $\mu_{k,avg}$, was computed instead. This was done by calculating the slope between each peak of the content's total velocity response and dividing it by acceleration due to gravity, g. Computed $\mu_{k,avg}$

values following this approach are shown in **Figure 4.7b**, where (i) $\mu_{k,avg}$ was reasonably consistent with each sliding excursion, and (ii) was well approximated by μ_s for this case.

The median $\mu_{k,avg}$ for all contents on carpet flooring are shown in **Figure 4.7c**, where apart from Desk 1, the median μ_k did not vary by more than 10% between the different sinusoidal cases. This indicated that while μ_k possibly varied with $v_{CRF}(t)$ based on results from **Figure 4.4**, its effect was not significant on average. The overall magnitude of $\mu_{k,avg}$ in both directions were similar; and any differences were likely due to experimental error, variability in the flooring material, or content support conditions. Similar findings were obtained for the vinyl flooring cases.

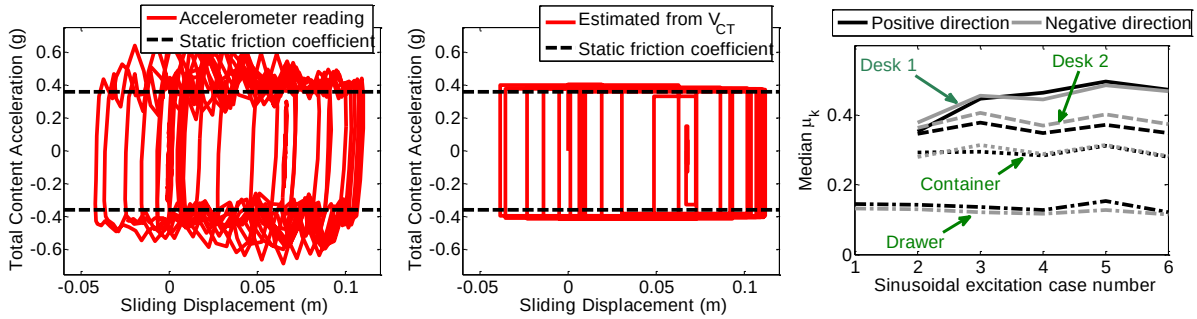

(a) **(b)** **(c)**

Figure 4.7. Kinetic friction coefficients from shake-table sinusoidal tests; (a) Variation using accelerometer reading (Desk 2 on carpet using Case 5), (b) average estimate (Desk 2 on carpet using Case 5), and (c) median of average estimate for differing cases on carpet

The median, x_m, and dispersion, ζ, of $\mu_{k,avg}$ are shown **Table 4.3**. The median $\mu_{k,avg}$ was between 0.98-1.17 times the median μ_s (+0 kg case) recorded in **Table 4.2** for contents on carpet flooring. These findings do contradict existing studies [14, 15, 19] which found that μ_k is generally lower than μ_s. This difference however could be attributed to the base of the content having to move through the carpet fibres rather than simply sliding on it, which causes additional drag forces to resist movement.

For vinyl flooring, the ratio between the median $\mu_{k,avg}$ and the median μ_s was between 0.57-1.08. These findings are more similar to those from existing studies [14, 15, 19] in that μ_k is lower than μ_s since there are no additional drag forces from the vinyl flooring material.

This resulted in contents on vinyl flooring having lower $\mu_{k,avg}$ compared to those on carpet flooring despite having a larger μ_s.

Note that the median $\mu_{k,avg}$ for the desks and drawer on vinyl flooring was 57-75% of μ_s obtained from the static friction test. This contrasted μ_k findings from kinetic friction tests in **Figure 4.5** where μ_s and μ_k were almost identical. This is likely due to the relative acceleration between the content and the flooring surface being zero in the kinetic friction tests as the flooring surface was displaced at constant velocity; whereas in the shake-table test and in reality the relative acceleration is unlikely to remain zero as shown in **Figure 4.6**. Therefore, the $\mu_{k,avg}$ values obtained from the dynamic test results were assumed to be more realistic, and were used for numerical validation in later sections.

Table 4.3. Kinetic friction coefficient results from shake-table tests (average during sliding)

	Carpet			Vinyl		
Content	x_m	ζ	**% of μ_s (+ 0kg)**	x_m	ζ	**% of μ_s (+ 0kg)**
Desk 1	0.45	0.108	1.10	0.30	0.110	0.75
Desk 2	0.37	0.063	1.03	0.30	0.197	0.67
Drawer	0.13	0.186	0.98	0.04	0.326	0.57
Container	0.29	0.125	1.17	0.14	0.057	1.08

4.4.3 Effect of Total Floor Acceleration Amplitude and Frequency

The response of Desk 2 subjected to sinusoidal excitation Cases 5 and 6 were compared to observe the influence of floor motion frequency. Both cases have nearly identical peak total floor (shake-table) accelerations, A_{FT}, which were 0.96 g and 1.01 g for Cases 5 and 6, respectively. Despite this, the maximum, residual, and individual sliding excursion displacements shown in **Figure 4.8a** were lower by 40% for Case 6 compared to Case 5; demonstrating that A_{FT} alone is not a good indicator of the extent of sliding displacement. This was further emphasized by the maximum sliding displacement versus A_{FT} plot in **Figure 4.8b** for all contents on both flooring materials, where there were no clear trends between the extent of sliding and A_{FT} alone. For example, the sliding response of the drawer (MD) on vinyl flooring was relatively constant despite A_{FT} ranging from 0.4 g to 1.0 g.

An alternate parameter proposed here for comparisons with the peak sliding displacement is the Modified Peak Total Floor Velocity, MV_{FT}, which was used to approximate the content's velocity relative to the floor. This accounts for the fact that the sliding displacement is dependent on the content's relative velocity to the floor. Assuming that the content and floor accelerations were constant with time, the expression for MV_{FT} is that shown in **Eq. 4.2**; where V_{FT} is the shake-table's peak total velocity. It can be seen from the maximum sliding displacement versus MV_{FT} plot in **Figure 4.8c** that there is a much clearer increasing trend for all cases considered compared to considering A_{FT} alone; indicating that V_{FT} is also important.

$$MV_{FT} = V_{FT}\left\langle 1 - \frac{\mu g}{A_{FT}} \right\rangle \qquad \textbf{(4.2)}$$

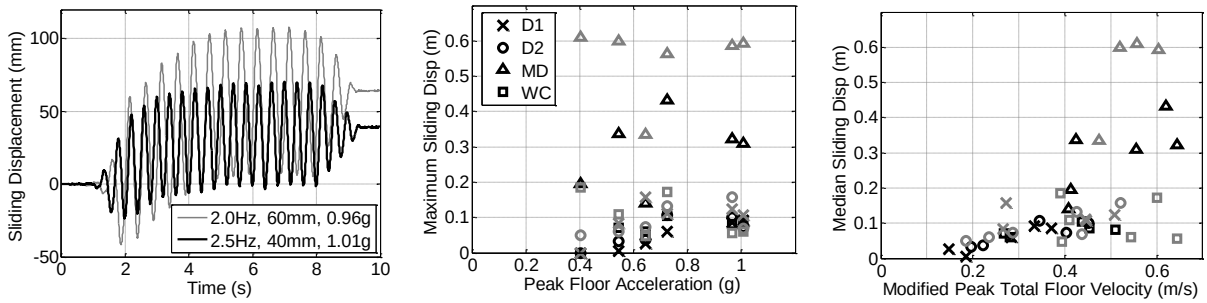

(a) **(b)** **(c)**

Figure 4.8. Influence of floor excitation frequency on median displacement of sliding excursions; (a) Case 5 versus Case 6 for Desk 2 on carpet flooring, (b) maximum sliding displacement-A_{FT}, (c) maximum sliding displacement-*MPTFV* [dark markers in (b) and (c) for carpet, light for vinyl]

To explain the limitations of considering A_{FT} alone, the generic content and floor total acceleration and total velocity curves in **Figures 4.9a** and **4.9b,** respectively, are examined. These curves were based on a single sinusoidal floor response cycle; where, ω_T is the total floor response frequency, and T_0 and T_e are the times at which the content separates and reattaches to the floor, respectively. The shaded area in **Figure 4.9b** equals the sliding excursion displacement. If A_{FT} and μ_k were kept constant but ω_T was decreased, this would result in (i) the content sliding for a longer duration, and (ii) the velocity amplitude increasing. Both of these would cause the sliding excursion displacement to increase. This

explains the reason behind Desk 2 on carpet flooring experiencing more severe response when subjected to sinusoidal excitation Case 5 in **Figure 4.8a**, and also demonstrates the importance of ω_T. However, ω_T would be difficult to obtain for more complex dynamic shaking inputs where there is no single unique frequency. Therefore, V_{FT} can be used as a substitute for ω_T instead since V_{FT} is dependent on both the total floor acceleration response and excitation frequency.

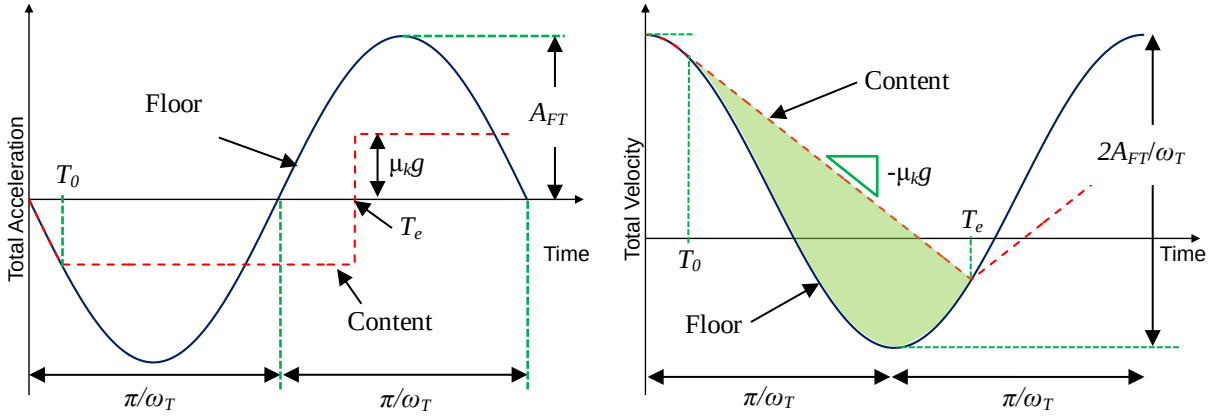

Figure 4.9. Effect of frequency on sliding excursion displacement for contents subjected to sinusoidal floor motion (a) total acceleration response, (b) total velocity response

While the importance of frequency is obvious for sinusoidal floor motions, there is practical significance for more realistic excitations. For example, stiffer buildings may also experience larger total floor accelerations compared to more flexible buildings, but would have a higher shaking frequency. Therefore, contents within stiffer buildings may not necessarily experience more severe sliding response. There is a limit to this as the decreased accelerations in very flexible buildings may prevent content sliding from occurring in the first place. The importance of stiffness is re-examined later in this study.

4.5 VALIDATION OF CONTENT SLIDING ANALYSES

The prior sections showed that the contents' overall sliding behaviour (**Figure 4.6**) and $\mu_{k,avg}$ (**Figure 4.7b**) were consistent with numerical modelling assumptions. It was however

evident from **Figure 4.7a** that variation in μ_k exist, which may cause numerical findings to differ from experimental findings. As such, validation of numerical models was required to observe the significance of this effect. Content sliding analyses were performed using Newmark integration scheme [25]; where $a_{CT}(t)$ was defined using **Eq. 4.1** [13], and the shake-table's total acceleration response history recorded from the dynamic tests was inputted as $a_{FT}(t)$.

The comparison between the recorded sliding displacement response from the shake-table test, and that from analyses for Desk 2 on carpet flooring subjected to Case 5 sinusoidal loading, is shown in **Figure 4.10a** using the median μ_s and $\mu_{k,avg}$ from **Tables 4.2** and **4.3**, respectively. It was shown that there was good agreement between the two cases before divergence occurred around the seventh cycle, resulting in the maximum and residual sliding displacements being over-predicted by 32% and 64%, respectively. While not shown here, divergence between experimental and numerical results also occurred for majority of cases considered; though the number of cycles at which this occurred, and the extent of divergence, varied.

In addition to ignoring the potential variation in μ_k along the flooring surface which was observed in **Figure 4.7a**, other reasons for the discrepancy between the numerical and experimental results could be due to the shake-table's stick-slip motion and vibrations. This meant that the total acceleration response inputted into the numerical models may not be the same as that felt by the content during testing.

It should also be noted that the numerical approach does not always over-predict the content's sliding response, as shown by the ratio between the maximum sliding displacement obtained from analysis against that from experiments in **Figures 4.10b** and **4.10c** for carpet and vinyl flooring, respectively. While errors on a case-by-case basis were between 0.3-3.0 times, the median ratios considering all furniture, which were calculated for each sinusoidal

excitation case, ranged between 0.58-1.35 for carpet flooring, and 0.95-1.32 for vinyl flooring. With the exception of Case 6 on carpet flooring, the average of all sinusoidal excitation cases were 1.05 and 1.06 for carpet and vinyl flooring, respectively. Based on these observations, the findings using numerical approaches are reasonable on average if multiple excitations were considered.

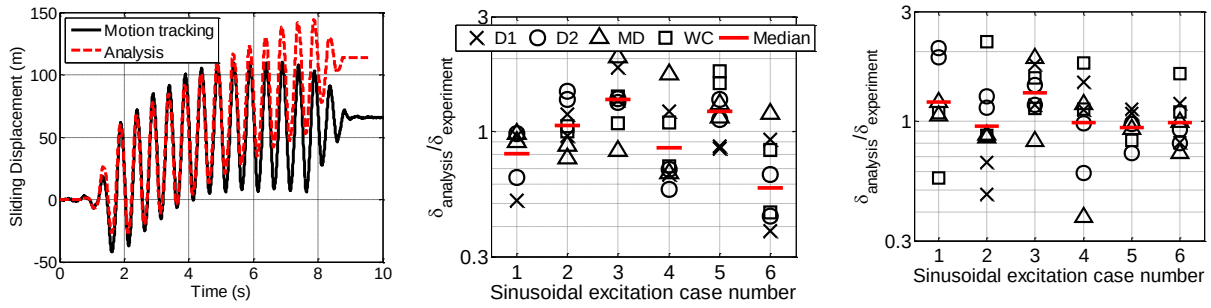

(a) **(b)** **(c)**

Figure 4.10. Comparison of experiment and numerical sliding displacement history; (a) f = 2.0 Hz, D = 60 mm carpet flooring, (b) maximum displacement ratio (numerical versus experimental) for carpet flooring, (c) maximum displacement ratio for vinyl flooring

4.6 NUMERICAL MODELLING APPLICATION EXAMPLES

4.6.1 Case Study Details

A preliminary numerical case-study examining the sliding response of contents resting on single-storey buildings was performed to observe (i) the effect of building stiffness on content sliding response, and (ii) the need to consider both μ_s and μ_k in analyses. The buildings have elastic fundamental periods ranging from 0.01 s to 1.50 s; and were designed for Wellington, New Zealand, subsoil class C conditions with a force reduction factor of 2.0.

The 10% probability of exceedance in 50 year uniform hazard spectra (UHS) used for design was obtained from OpenSHA [26] using New Zealand-specific rupture forecast models [27] and attenuation equations [28]. The ground motions used in the analyses were selected following the Generalized Conditioning Intensity Measure (GCIM) approach [29, 30], with the spectral acceleration at 0.50 s being selected as the conditioning intensity

measure. The other intensity measures selected, and their weighting factors, followed Bradley [30].

Only the drawer on vinyl flooring (μ_s = 0.066, $\mu_{k,avg}$ = 0.041) was analysed in this case study. The analyses were repeated three times considering (i) μ_s only, (ii) $\mu_{k,avg}$ only, and (iii) both μ_s and $\mu_{k,avg}$.

4.6.2 Effect of Building Stiffness

The building's median peak total floor acceleration response, A_{FT}, peaked at 0.25 s before decreasing with period, as shown by the A_{FT} spectral curves in **Figure 4.11a**. Despite the 0.25 s building having the largest median A_{FT} however, it did not have the largest maximum sliding displacement, δ_S, when both μ_s and $\mu_{k,avg}$ were considered in the analyses, as shown by the maximum sliding spectra in **Figure 4.11b**. Instead, the median, 16th, and 84th percentile δ_S peaked at 1.25 s.

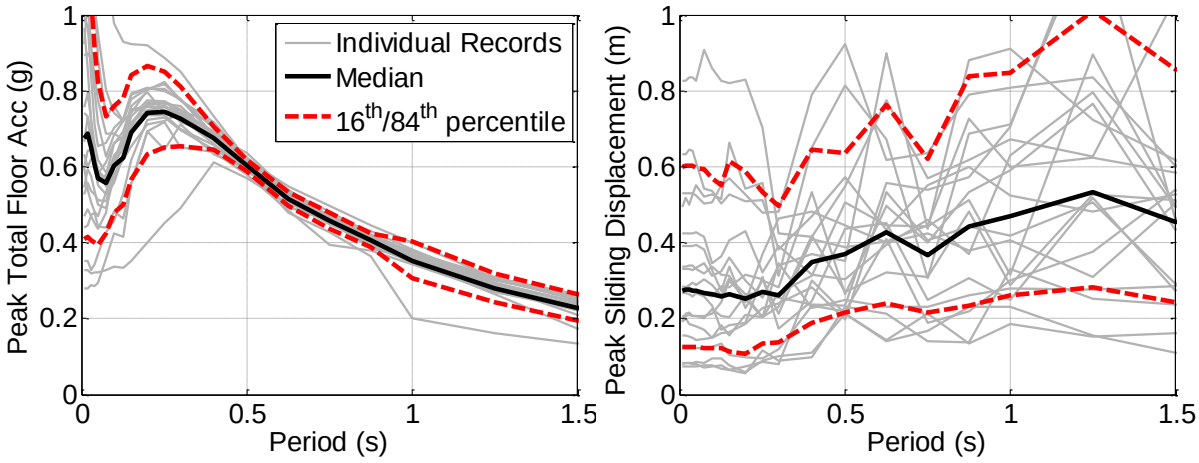

Figure 4.11. Effect of building stiffness case study; (a) Peak total floor acceleration response, and (b) peak sliding displacement response considering both μ_s and $\mu_{k,avg}$

The importance of shaking frequency was further illustrated using the total acceleration and sliding displacement response of contents within a building of a fundamental period, T, of 0.25 s and another of T = 1.25 s using one of the records from the selected suite as shown in **Figure 4.12**. While the A_{FT} recorded for the 0.25 s building (0.804 g) was much larger than

that of the 1.25 s building (0.282 g); the higher shaking frequency observed in the 0.25 s case in **Figure 4.12a** resulted in the duration of each acceleration peak being smaller than that of the 1.25 s case in **Figure 4.12b**. This resulted in the maximum sliding displacement for the 0.25 s case (0.205 m) to be 4.0 times smaller than that of the 1.25 s case in **Figure 4.12c**. This matched the discussions from **Figure 4.9**, and demonstrated the importance of shaking frequency.

These results highlighted that the sliding response of building contents may potentially be decreased by increasing a building's stiffness, despite its higher acceleration response. These findings may also apply to other non-brittle acceleration-sensitive components, such as unanchored rocking contents. However, brittle components such as fixed ceiling systems may still be severely affected by the higher accelerations in stiffer buildings.

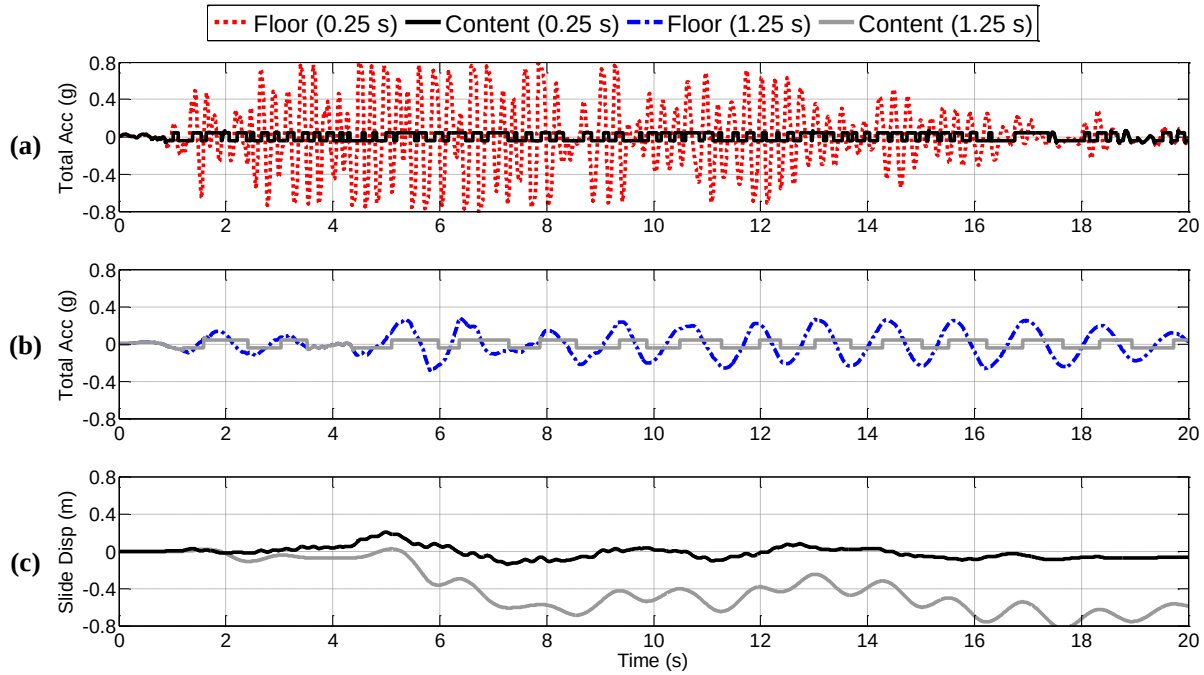

Figure 4.12. Effect of single-storey building stiffness on content sliding response; (a) content and floor acceleration response (0.25 s), (b) content and floor total acceleration response (1.25 s), and (c) content sliding displacement response for both 0.25 s and 1.25 s cases

4.6.3 Consideration of Friction Coefficients in Numerical Analysis

The ratio between the maximum sliding displacements considering (i) μ_s only, and (ii) $\mu_{k,avg}$ only, against that considering both μ_s and $\mu_{k,avg}$ using **Eq. 4.1**, are shown in **Figures**

4.13a and **4.13b**, respectively. It can be seen that the median ratio ranged from 0.56 to 0.92, while the 16th percentile ratio ranged from 0.33 to 0.76, when considering μ_s only. This demonstrated that considering μ_s only generally produced non-conservative predictions. In contrast, the median ratio considering μ_{kavg} only ranged from 0.96 to 1.00. As such, analysis considering only $\mu_{k,avg}$ may be performed in place of one considering both μ_s and $\mu_{k,avg}$ for simplicity.

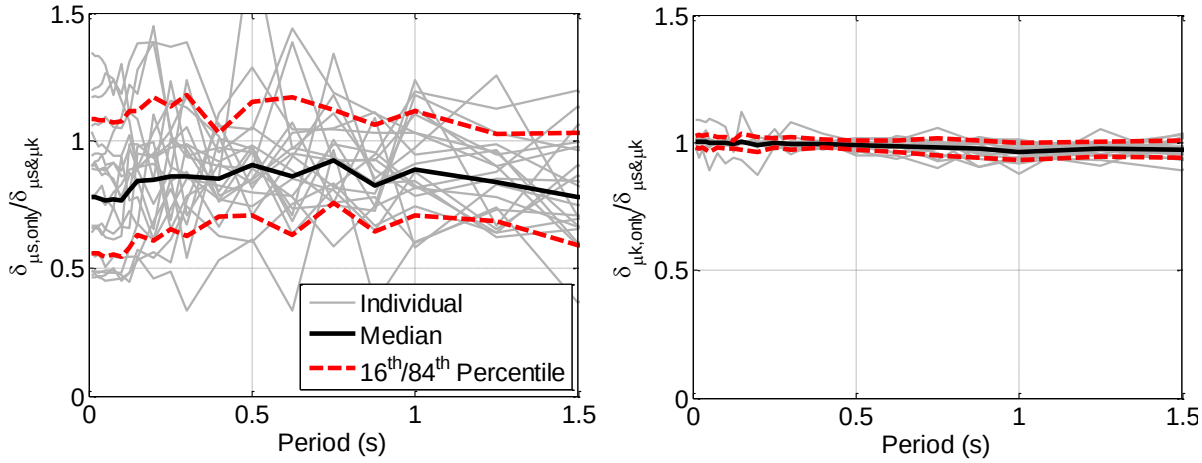

Figure 4.13. Ratio between maximum sliding displacement obtained from analyses considering (a) $\mu = \mu_s$, or (b) $\mu = \mu_k$, against that considering both μ_s and μ_k

4.7 CONCLUSIONS

Static and kinetic friction tests, and shake-table tests using sinusoidal floor motions, of office-type furniture on carpet and vinyl flooring were performed. It was found that:

1. The static coefficient of friction, μ_s, ranged between 0.13-0.30 and 0.07-0.13 for contents with wheels, and 0.36-0.45 and 0.39-0.45 for contents without wheels, on carpet and vinyl flooring, respectively. The contents' mass had negligible effect on μ_s.
2. The average kinetic coefficient of friction, $\mu_{k,avg}$, obtained from shake-table tests using sinusoidal motion was approximately equal to, or slightly larger than, μ_s for contents on carpet flooring; and was up to 38% lower on vinyl flooring. Kinetic friction tests showed varying mass and the content's velocity relative to the floor had marginal effect on μ_k.

3. Content sliding analyses matched shake-table test results with an average error of 5% considering all cases, though errors by up to a factor of 3 were observed on a case-by-case basis.
4. A_{FT} on its own was found to be an insufficient descriptor of the extent of content sliding. Consideration of peak total floor velocity, V_{FT}, together with peak total floor acceleration, A_{FT}, was more sufficient.
5. Using numerical approaches considering $\mu_{k,avg}$ on its own resulted in almost identical results to considering both μ_s and $\mu_{k,avg}$; indicating that μ_s may not need to be considered in analysis for simplicity.

4.8 REFERENCES

1. FEMA E-74. (2012). Reducing the Risks of Nonstructural Earthquake Damage - A Practical Guide.
2. Nagao, T., Kagano, H., & Hamaguchi, K. (2012). Full-Scale Shaking Table Test on Furnitures subjected to Long-Period Earthquake Motions. Paper presented at the 15th World Conference on Earthquake Engineering, Lisbon, Portugal.
3. Sato, E., Furukawa, S., Kakehi, A., & Nakashima, M. (2011). Full-scale shaking table test for examination of safety and functionality of base-isolated medical facilities. Earthquake Engineering and Structural Dynamics, 40(13), 1435-1453.
4. Dhakal, R. P. (2010). Damage to Non-Structural Components and Contents in 2010 Darfield Earthquake. Bulleting of the New Zealand Society for Earthquake Engineering, 43(4), 404-412.
5. Choi, B., & Tung, C. C. D. (2002). Estimating Sliding Displacement of an Unanchored Body Subjected to Earthquake Excitation. Earthquake Spectra, 18(4), 601-613.
6. Hutchinson, T. C., & Chaudhuri, S. R. (2006). Simplified Expression for Seismic Fragility Estimation of Sliding-Dominated Equipment and Contents. Earthquake Spectra, 22(3), 709-732.
7. Kaneko, M., Hayashi, Y., & Tamura, K. (1999). Evaluation of Sliding Displacement of Furniture during Earthquake - By using Revised Formula to Estimate Sliding Displacement of Furniture. Technical Papers of Annual Meeting of Architectural Institute of Japan, B-II, 537-538.
8. English, R., MacRae, G. A., & Dhakal, R. P. (2012). Hysteretic Influence on Earthquake Induced Sliding Damage of Contents. Paper presented at the 2012 NZSEE Conference, Christchurch, New Zealand.
9. Konstantinidis, D. A., & Nikfar, F. (2014). Seismic response of sliding equipment and contents in base-isolated buildings subjected to broadband ground motions. Earthquake Engineering and Structural Dynamics.
10. Lin, S. L., MacRae, G. A., Dhakal, R. P., & Yeow, T. Z. (2015). Building contents sliding demands in elastically responding structures. Engineering Structures, 86, 182-191.
11. Lin, S. L., MacRae, G. A., Dhakal, R. P., Yeow, T. Z., & English, R. (2012). Contents Sliding Response Spectra. Paper presented at the 2012 NZSEE Conference, Christchurch, NZ.
12. Meyer, E., Overney, R. M., Dransfeld, K., & Gyalog, T. (1998). Nanoscience - friction and rheology on the nanometer scale. Singapore: World Scientific Publishing.
13. Shenton III, H. W., & Jones, N. P. (1992). Base Excitation of Rigid Bodies. Part I: Formulation. Journal of Engineering Mechanics, 117(10), 2286-2306.
14. Aslam, M., Godden, W. G., & Scalise, D. T. (1975). Sliding Response of Rigid Bodies to Earthquake Motions: University of California, Berkeley.
15. Chaudhuri, S. R., & Hutchinson, T. C. (2005). Characterizing Frictional Behaviour for use in Predicting the Seismic Response of Unattached Equipment. Soil Dynamics and Earthquake Engineering, 25, 591-604.

16. Persson, B. N. J., Albohr, O., Mancosu, F., Peveri, V., Samoilov, V. N., & Sivebaek, I. M. (2003). On the nature of the static friction, kinetic friction, and creep. Wear, 254(7-8), 835-851.
17. Bureau, L., Baumberger, T., & Caroli, C. (2002). Rheological aging and rejuvenation in solid friction contacts. The European Physical Journal E, 8(3), 331-337.
18. Bar-Sinai, Y., Spatschek, R., Brener, E. A., & Bouchbinder, E. (2013). On the velocity-strengthening behaviour of dry friction. Journal of Geophysical Research: Solid Earth, 119.
19. Konstantinidis, D. A. (2008). Experimental and Analytical Studies on the Seismic Response of Freestanding and Anchored Building Contents. PhD Thesis, Civil and Environmental Engineering, University of California, Berkeley.
20. Chong, W. H., & Soong, T. T. (2000). Sliding Fragility of Unrestrained Equipment in Critical Facilities: Department of Civil, Structural and Environmental Engineering, University at Baffalo, New York, US.
21. Garcia, D. L., & Soong, T. T. (2003). Sliding Fragility of Block-Type Non-Structural Components. Part 1: Unrestrained Components. Earthquake Engineering and Structural Dynamics, 32, 111-129.
22. Chaudhuri, S. R., & Hutchinson, T. C. (2006). Fragility of Bench-Mounted Equipment Considering Uncertain Parameters. Journal of Structural Engineering 132(6), 884-898.
23. Cosenza, E., Di Sarno, L., Maddaloni, G., Magliulo, G., Petrone, C., & Prota, A. (2015). Shake table tests for the seismic fragility evaluation of hospital rooms. Earthquake Engineering and Structural Dynamics, 44(1), 23-40.
24. Hedrick, T. L. (2008). Software techniques for two- and three-dimensional kinematic measurements of biological and biomimetic systems. Bioinspiration & Biomimetics, 3(3).
25. Newmark, N. M. (1959). A Method of Computation for Structural Dynamics. Journal of Engineering Mechanics, 85(EM3), 67-94.
26. Field, E. H., Jordan, T. H., & Cornell, C. A. (2003). OpenSHA: A Developing Community-Modeling Environment for Seismic Hazard Analysis. Seismological Research Letters, 74(4), 406-419.
27. Stirling, M. W., McVerry, G. H., Gerstenberger, M. C., Litchfield, N. J., Van Dissen, R. J., Berryman, K. R., Barnes, P., Wallace, L. M., Villamor, P., Langridge, R. M., Lamarche, G., Nodder, S., Reyners, M. E., Bradley, B., Rhoades, D. A., Smith, W. D., Nicol, A., Pettinga, J., Clark, K. J., & Jacobs, K. (2012). National seismic hazard model for New Zealand : 2010 update. Bulletin of the Seismological Society of America, 102(4), 1514-1542.
28. Bradley, B. A. (2010). NZ-Specific Pseudo-Spectral Acceleration Ground Motion Prediction Equations based on Foreign Models: Department of Civil and Natural Resources Engineering, University of Canterbury, Christchurch, New Zealand.
29. Bradley, B. A. (2010). A Generalized Conditional Intensity Measure Approach and Holistic Ground Motion Selection. Earthquake Engineering and Structural Dynamics, 39(12), 1324-1342.
30. Bradley, B. A. (2012). A Ground Motion Selection Algorithm Based on the Generalized Conditional Intensity Measure Approach. Soil Dynamics and Earthquake Engineering, 40, 48-61.

5. Predicting the Maximum Sliding Displacement of Contents in Earthquakes

5.0 SUMMARY

Sliding of building contents in past earthquakes has caused injury, disruptions and damage. As such, equations to predict the content's maximum sliding displacement are required to include its effect in building performance assessments. This chapter examines six different prediction equations; including a new equation derived in this study based on the first sliding excursion of contents subjected to sinusoidal floor motion. The reliability of these equations was assessed by comparing the ratio of the maximum sliding displacement obtained from an numerical study to that using the prediction equations. The analytical study consists of modelling content sliding within three elastically responding five-storey buildings of varying periods subjected to the entire Pacific Earthquake Engineering Research center's ground motion database. It was found that the prediction equation derived in this study had the best fit out of all prediction equations considered, with its median sum of squared relative error being four to six times smaller than the next best prediction.

5.1 INTRODUCTION

Past observations from seismic events have shown that sliding of contents have potential to cause injuries, disruptions and damage; even on occasions where the primary structure suffered little or no damage [1-3]. This was further highlighted by shake table tests of multi-storey buildings fitted with office furnishings [4, 5], where large items such as copying machines slid several meters at high velocity. A study by Taghavi and Miranda [6] showed that damage losses due to content movement contributed to 17-20% of the total building direct damage-repair cost for office and hotel-type buildings, and around 44% for

hospitals; indicating the devastating effect which content sliding could have on seismic losses.

Based on this, content sliding should be considered in building seismic performance assessments. This had been done previously for rocking contents by Okada et al. [7], who developed a probabilistic framework to estimate injuries due to contents toppling. A similar approach can be used to assess the effects of content sliding, which would require fragility functions or prediction equations to estimate the extent of content sliding.

Several experimental studies have been conducted to develop fragility functions for content sliding [8-10]. However, these are often specific for the parameters considered. For example, Chong and Soong [8] developed fragility functions to estimate the probability of exceeding a target sliding displacement considering fixed values of friction coefficient, μ. It is not clear how these can be modified if considering other target displacements or μ. Another limitation is that these often use peak horizontal ground acceleration as the sole dependent parameter, while other parameters, such as frequency of floor response, have been shown to be important [5, 8, 10-12]. This was also observed from shake-table test results detailed in **Chapter 4** (**Section 4.4.3**).

In lieu of these limitations, prediction equations to estimate sliding displacement are more useful. Several prediction equations do exist [10, 13-16], and are discussed in detail in later sections. These existing prediction equations are generally either derived assuming a simplistic floor response or are empirical in nature. Additionally, a recent study by Lin et al. [17] has shown that the first sliding excursion (i.e. a single sliding motion from separation until the next reattachment) of a content subjected to sinusoidal floor motion, δ_{FE}, can be used to approximate the median response of contents subjected to realistic floor motions. However, a prediction equation based on this concept was not proposed.

While there are a number of prediction approaches, there have not been any comparisons made between these. Therefore, it is not immediately clear which of these equations is more reliable. Ideally, the best approach would be to compare the prediction equations against experimental results. However, there are few experimental test results present in literature, and those which are available do not have sufficient information to make comparisons. In addition, a large number of factors, such as different types of ground motion, building properties, and friction coefficients, need to be tested in order to account for a large range of scenarios. The number of experiments required to consider all these factors would be significant and is not feasible. A more robust approach would therefore be to compare the prediction equations against response history analysis (RHA) methods using numerical content sliding models, which had been validated in **Section 4.5**.

In this study, the concepts discussed by Lin et al. [17] will be used to derive a new prediction equation. The reliability of the newly proposed prediction equation, and those available in literature, were then assessed considering an analytical study on the sliding of contents located within elastic five-storey frame buildings using the entire suite of ground motion records available from the Pacific Earthquake Engineering Research (PEER) center's database [18]. In particular, answers are sought to the following questions:

1. Can a new prediction equation be derived based on findings by Lin et al. [17]?
2. How reliable are existing prediction equations in estimating the peak sliding displacement obtained from numerical modelling of contents movement?
3. Is the newly derived prediction equation the most reliable? If not, which is?

5.2 THE MECHANICS OF CONTENT SLIDING

Before discussing existing prediction equations, it is important to highlight the possible content movement states, conditions required to cause sliding, and sliding mechanics. Past

research [19, 20] has identified four states of content movement. These are (i) pure sliding, (ii) pure rocking, (iii) slide-rock, and (iv) at rest. This study considered the first and fourth states.

There are two conditions required to cause pure sliding. The first is that the maximum applied total floor acceleration, A_{FT}, must exceed the value required to trigger sliding, $\mu_s g$; where μ_s is the static friction coefficient, and g is the acceleration due to gravity. The second is that no uplift can occur. Consider the block shown in **Figure 5.1a**, which has a weight of W, and a centre of mass located a height of H and a horizontal distance of B to the closest base corner (point A). The maximum horizontal force which can act on the content is $\mu_s W$. Taking moments about point A, μ_s must be smaller than B/H so that the moment caused by the content's weight is greater than that caused by $\mu_s W$ to prevent uplift. The criteria for the different states of movement based on the conditions outlined here and other parameters discussed by Shenton III [19] is shown in **Figure 5.1b**.

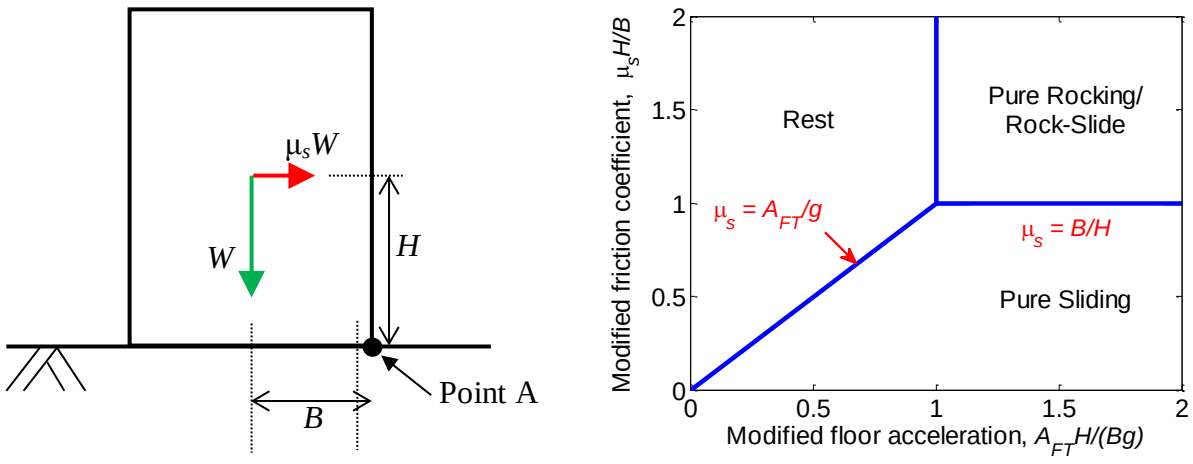

(a) **(b)**

Figure 5.1. Illustration of pure sliding criteria; (a) free body diagram of content, (b) visual representation of the conditions for various states of content movement

The mechanics of content sliding had been observed in detail in **Section 4.4.1**. In summary: (i) contents slid when the total floor acceleration at a given time, $a_{FT}(t)$, exceeded $\mu_s g$; (ii) the content's total velocity varied approximately linearly between peaks; and (iii) sliding terminated when the content and shake tables' velocities matched. This can be

observed from **Figure 5.2**, which shows the response of furniture and the shaking table from one of the tests performed in **Section 4.4.1**. This behaviour shows that floor acceleration dictates the initiation of sliding. However, **Section 4.4.3**, and other past experimental studies have documented that other factors, such as the relative velocity between the content and the structure, are also important [5, 8, 10-12]. It can also be seen from **Figure 5.2** that the content acceleration remains reasonably constant on average during sliding, which was also observed in **Section 4.4.2** and other experimental findings [5, 11, 12]. Therefore the dynamic friction coefficient, μ_k, can be assumed to be constant during sliding.

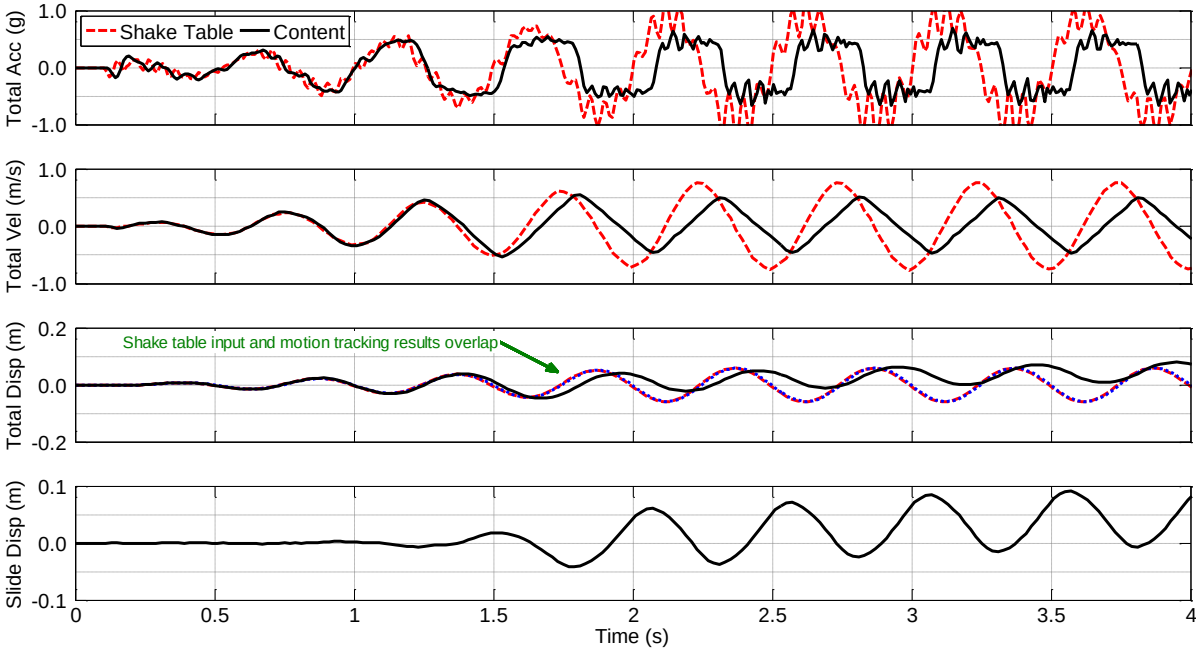

Figure 5.2. Floor (shake table) and content response on carpet flooring under sinusoidal loading – first 4 seconds

Based on the observations, **Eq. 5.1** can be used to obtain the content's total acceleration response at a point in time, $a_{CT}(t)$; where, $a_{FT}(t)$ is the floor acceleration with time, and $v_{CRF}(t)$ is the content's velocity relative to the floor with time. Similar equations have been stated by others [9-14, 21, 22]. **Eq. 5.1** matches experimental results well as previously observed in **Chapter 4** (**Section 4.5**). Numerical integration procedures, such as Newmark-beta methods [23], can be used together with the equations of motion to obtain the content's velocity and displacement response. This has been programmed into an algorithm on Matlab [24] and will

be used for comparing the reliability of the prediction equations. Note that μ_k was used instead of μ_s in the conditions during the analyses based on findings from **Section 4.6.3**, which showed that this simplification still resulted in reasonable predictions of the maximum sliding displacement. For the remainder of this chapter, the friction coefficient will be simply termed as μ.

$$a_{CT}(t) = \begin{cases} a_{FT}(t) & \text{when } |v_{CRF}(t)| = 0 \text{ and } |a_{FT}(t)| < \mu_s g \\ -\text{sgn}(v_{CRF}(t))\mu_k g & \text{when } |v_{CRF}(t)| > 0 \text{ or } |a_{FT}(t)| \geq \mu_s g \end{cases} \quad \textbf{(5.1)}$$

An alternative method used in past studies is to model the contact between the content and the floor using a spring with bilinear response to represent friction [25-28]. However, this method was not adopted in this study as: (i) there is difficulty specifying different damping to the content and building; and (ii) it is computationally demanding.

5.3 EXISTING PREDICTION STUDIES

Based on content sliding mechanics, Newmark [13] derived an equation for cases where the content is in direct contact with the ground, the latter of which was subjected to a rectangular pulse with acceleration A_g and duration of T_P. This results in the total velocity response observed in **Figure 5.3**, where T_R is the time of reattachment. The maximum total sliding displacement, δs, is the area between the ground and content total velocity response, and is calculated using **Eq. 5.2**, where V_g is the peak ground total velocity.

$$\delta_S = \frac{V_g^{\,2}}{2\mu g}\left(1 - \frac{\mu g}{A_g}\right) \quad \textbf{(5.2)}$$

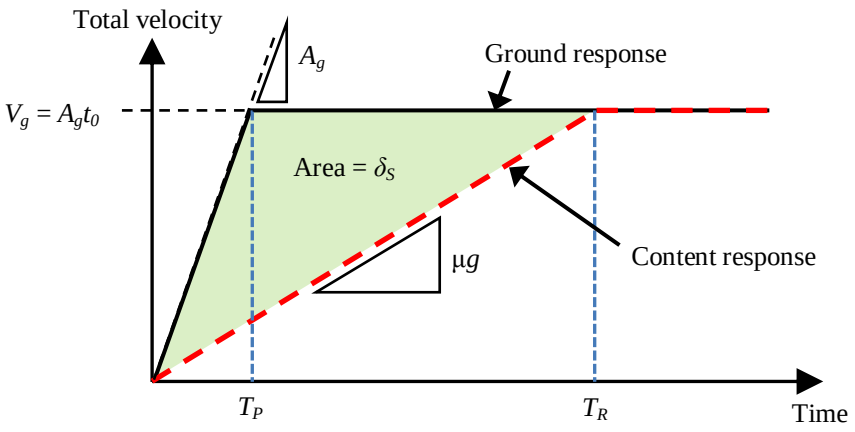

Figure 5.3. Ground and content response under pulse load applied to ground

Choi and Tung [14] suggested that total displacement should be used instead of total velocity, since total velocity is not readily available in design standards. They reformulated **Eq. 5.2** by considering the total area under the ground's velocity response curve to obtain the total displacement of the ground, D_g, at T_R. The end result is shown in **Eq. 5.3**. They suggested that the value corresponding to spectral displacement response at large periods can be used as D_g, since this is thought to be similar to the ground displacement [29]. While both **Eqs. 5.2** and **5.3** are based on the ground response in the prediction of content sliding, the floor response could be used instead for contents on other floors.

$$\delta_S = \frac{D_g\left(A_g / \mu g - 1\right)}{2\left(A_g / \mu g\right) - 1} \tag{5.3}$$

Choi and Tung [14] conducted a numerical study of content sliding within a multi-storey building subjected to 75 ground motion records to assess the reliability of **Eq. 5.3**. They used the mean value of peak total floor displacement, D_{FT}, and A_{FT} obtained from structural analysis into **Eq. 5.3** instead of the ground response parameters, and compared δ_s against the mean sliding displacement from analysis. They found that **Eq. 5.3** was conservative for lower ratios of A_{FT}/μ but non-conservative at higher ratios. They proposed the adjustment factor shown in **Eq. 5.4** be applied to **Eq. 5.4** to account for this. It is not clear if this is applicable to other cases apart from that used in their study.

$$Adj = 0.92\left[\left(\frac{A_{FT}}{\mu g}\right)^{3/8} - 1\right] \quad \textbf{(5.4)}$$

Kaneko et al. [15, 16] proposed two equations based on parametric studies using results from an numerical study. The first, detailed in Kaneko et al. [15], is shown in **Eq. 5.5**; where, V_{FT} is the total velocity of the floor. This empirical expression represents an envelope of the maximum sliding displacements and was shown to be very conservative. As such, this may not be suitable for use in building performance assessments. Note that V_{FT} must be in units of cm/s and δ_S will be in units of cm due to the empirical nature of this equation.

$$\delta_S = 0.0015\frac{{V_{FT}}^2}{\mu} \quad \textbf{(5.5)}$$

The second equation, detailed in Kaneko et al. [16], was formulated by parametric analysis of contents subjected to applied transient vibrations. A_{FT}, V_{FT} and δ_S are in units of cm/s^2, cm/s and cm respectively; while g is in units of cm/s^2. Saito et al. [28] used **Eq. 5.6** to compare against results from their shake-table tests investigating the effect of long period motion on sliding, and found that the trends exhibited are similar. A limitation of **Eq. 5.6** is that μ was limited to the range of 0.02 to 0.1 in the derivation.

$$\delta_S = 0.02\mu^{-0.3}\left(\frac{A_{FT}}{2\pi V_{FT}}\right)^{-0.5}\left(V_{FT}\left(1-\frac{\mu g}{A_{FT}}\right)\right)^{1.56} \quad \textbf{(5.6)}$$

Konstantinidis [10] conducted shake table tests to investigate the sliding behaviour of timber blocks, and is one of the few experimental studies which recommended equations to predict the median and dispersion of sliding response. The equation to predict the median sliding response is shown in **Eq. 5.7**.

$$\frac{\delta_S \omega^2}{A_{FT}} = 0.38\left(\frac{A_{FT}}{\mu g} - 1\right) \quad \textbf{(5.7)}$$

Lin et al. [17] followed a similar approach to Newmark [13], but included an elastic single-degree-of-freedom structure in between the ground and content. This resulted in the content being subjected to damped sinusoidal floor motion. Best-fit curves were generated to define (i) the first sliding excursion displacement, and (ii) the maximum sliding displacement. These were compared against results from an analytical study of contents located on an elastic single-degree-of-freedom structure subjected to the SAC ground motion record suite [30] which is representative of a 10% probability of exceedance in 50 year event in Los Angeles [31]. It was found that the first sliding excursion displacement, $\delta_{S,FE}$, obtained from the pulse motion analysis provided a reasonable estimate of the median sliding displacement using ground motion records. However, no prediction equation was provided for $\delta_{S,FE}$.

The prediction equations referenced, and the one which will be derived later in the study, are only used if $A_{FT} > \mu g$. Else, sliding would not have occurred and δ_S would be zero. In addition to the studies discussed, additional prediction equations have also been derived for periodic piecewise linear total floor velocity patterns or for more complex pulse shapes for near-fault ground motions [32-34]. A difficulty in using these is that the velocity or pulse pattern would have to be pre-defined based on the floor response history which is a complicated process. As such, these approaches were not considered in this study.

5.4 DERIVATION OF NEW PREDICTION EQUATION

In order to derive a simple prediction equation for $\delta_{S,FE}$, it will be assumed that a single velocity peak in an actual ground motion can be estimated using an equivalent undamped sinusoidal response cycle. The floor and contents' total acceleration and total velocity curves are shown in **Figures 5.4a** and **5.4b** respectively; where T_0 and T_e are the times at which content sliding initiates and ends in a single sliding excursion, respectively. The floor's total acceleration and velocity with time, $a_{FT}(t)$ and $v_{FT}(t)$, are described in **Eqs. 5.8** and **5.9**

respectively. Here v_{FTi} is the floor's initial total velocity, ω is the angular frequency of the floor response, and R_μ is defined as shown in **Eq. 5.10**.

$$a_{FT}(t) = -\frac{\mu g}{R_\mu}\sin(\omega t) \tag{5.8}$$

$$v_{FT}(t) = -\frac{\mu g}{R_\mu \omega}\cos(\omega t) + \left(v_{FTi} - \frac{\mu g}{R_\mu \omega}\right) \tag{5.9}$$

$$R_\mu = \mu g / A_{FT} \tag{5.10}$$

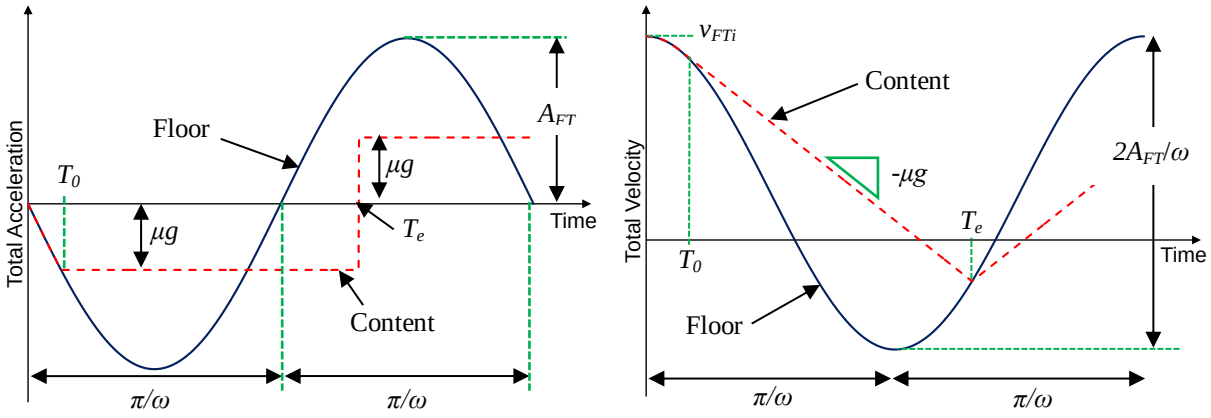

(a) **(b)**

Figure 5.4. Assumed sinusoidal floor response for derivation of maximum sliding displacement prediction equation; (a) total acceleration, and (b) total velocity

Based on **Figure 5.4a**, sliding will initiate at T_0 when the total floor acceleration exceeds μg in the negative direction. Therefore, $R_\mu = \sin(\omega T_0)$ at $t=T_0$ using **Eq. 5.8**. Based on this, the total floor velocity at T_0, $v_{FT}(T_0)$, is defined as that shown in **Eq. 5.11**.

$$v_{FT}(T_0) = \frac{\mu g}{R_\mu \omega}\sqrt{1 - R_\mu^{\,2}} + \left(v_{FTi} - \frac{\mu g}{R_\mu \omega}\right) \tag{5.11}$$

After T_0, the content's total velocity varies linearly until it matches that of the floor at T_e. The content's total velocity between T_0 and T_e with time, $v_{CT}(T_0<t<T_e)$, can be defined using **Eq. 5.12**. $\delta_{S,FE}$ can be obtained by taking the difference between **Eq. 5.12** and **Eq. 5.8** and integrating between T_0 and T_e. The calculation for $\delta_{S,FE}$ normalized by A_{FT}/ω^2 is shown in

Eq. 5.13, where T_Δ is the difference between T_e and T_0. Note that the initial velocity term is cancelled out.

$$v_{CT}(T_0 < t < T_e)) = \frac{\mu g}{R_\mu \omega}\sqrt{1-R_\mu{}^2} + \left(v_{Fi} - \frac{\mu g}{R_\mu \omega}\right) - \mu g(t - T_0) \quad \textbf{(5.12)}$$

$$\frac{\delta_{S,FE}\omega^2}{A_{FT}} = \omega T_\Delta \sqrt{1-R_\mu{}^2} - \frac{R_\mu \omega^2 T_\Delta{}^2}{2} - \sin\left(\omega T_\Delta + \sin^{-1}\left(R_\mu\right)\right) + R_\mu \quad \textbf{(5.13)}$$

T_Δ can be obtained by equating the content and floor total velocities together at T_e. A simplified version of this is shown in **Eq. 5.14**. While numerical methods are required to obtain T_Δ, this equation shows that T_Δ is only dependent on ω and R_μ, and hence parametric analysis can be used to derive an empirical equation to estimate T_Δ.

$$\cos\left(\omega T_\Delta + \sin^{-1}\left(R_\mu\right)\right) = \sqrt{1-R_\mu{}^2} - R_\mu \omega T_\Delta \quad \textbf{(5.14)}$$

The relationship between T_Δ and the inverse of ω is shown in **Figure 5.5a**. This relationship is linear, indicating that T_Δ is directly inversely proportional to ω. The relationship of T_Δ normalized by the natural period of floor response ($2\pi/\omega$) against R_μ is shown in **Figure 5.5b**. Using parametric analysis, this trend can be approximated by **Eq. 5.15**. Here, $R_{\mu,cr}$ corresponds to the critical value of R_μ; where if $R_\mu < R_{\mu,cr}$, separation would immediately occur after the content reattaches to the floor when subjected to undamped sinusoidal floor motion. A study by Younis and Tadjbakhsh [32] found that $R_{\mu,cr}$ was approximately 0.54, and this value will be adopted for $R_{\mu,cr}$. **Eq. 5.15** fits well with the numerical solution as shown in **Figure 5.5b**.

$$\frac{T_\Delta \omega}{2\pi} = \sqrt{1-R_\mu{}^{1-R_{\mu,cr}}} \quad \textbf{(5.15)}$$

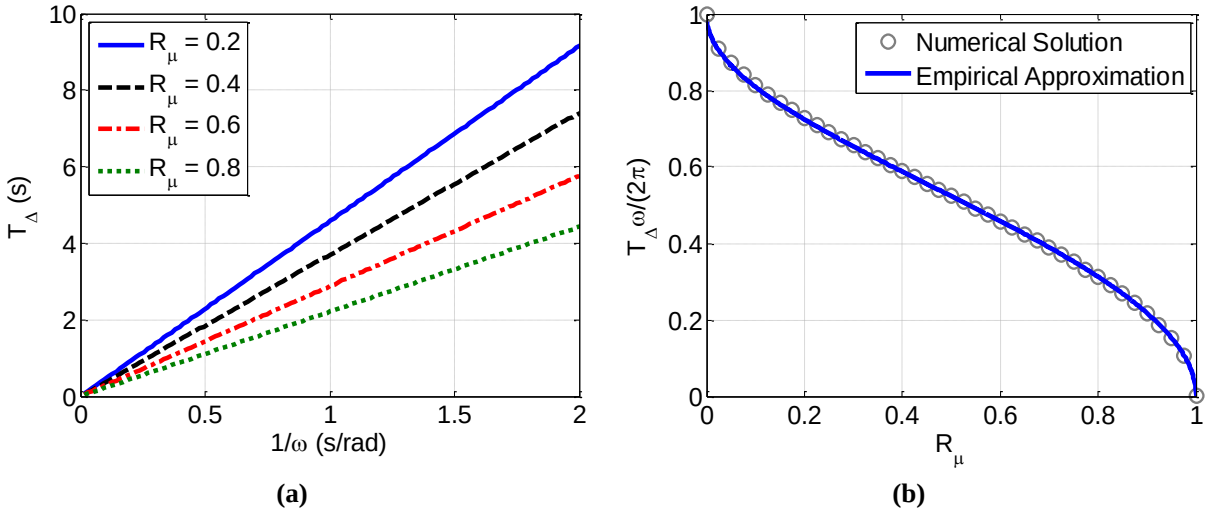

(a) **(b)**

Figure 5.5. Relationship between T_Δ to (a) inverse of ω and (b) R_μ

The final step in this derivation is to substitute **Eq. 5.15** into **Eq. 5.13**, the simplified form of which is shown in **Eq. 5.16**. Despite the length of the equation, it can be seen that the left hand term is just a function of R_μ. This can be provided in a chart or in tabulated form if to be used in design, an example of which is shown in **Figure 5.6a**. Note that **Figure 5.6a** matches that of Lin et al. [17] for an undamped floor motion. The ratio between the analytical and the predicted value of $\delta_{S,FE}$ is shown in **Figure 5.6b**. It can be seen that the difference between these values is negligible as the ratio is approximately 1.0 for all R values.

$$\frac{\delta_{S,FE}\omega^2}{A_{FT}} = 2\pi\sqrt{\left(1-R_\mu^{\,0.46}\right)\left(1-R_\mu^{\,2}\right)} - 2\pi^2 R_\mu\left(1-R_\mu^{\,0.46}\right) - \sin\left(2\pi\sqrt{1-R_\mu^{\,0.46}} + \sin^{-1}\left(R_\mu\right)\right) + R_\mu \quad \textbf{(5.16)}$$

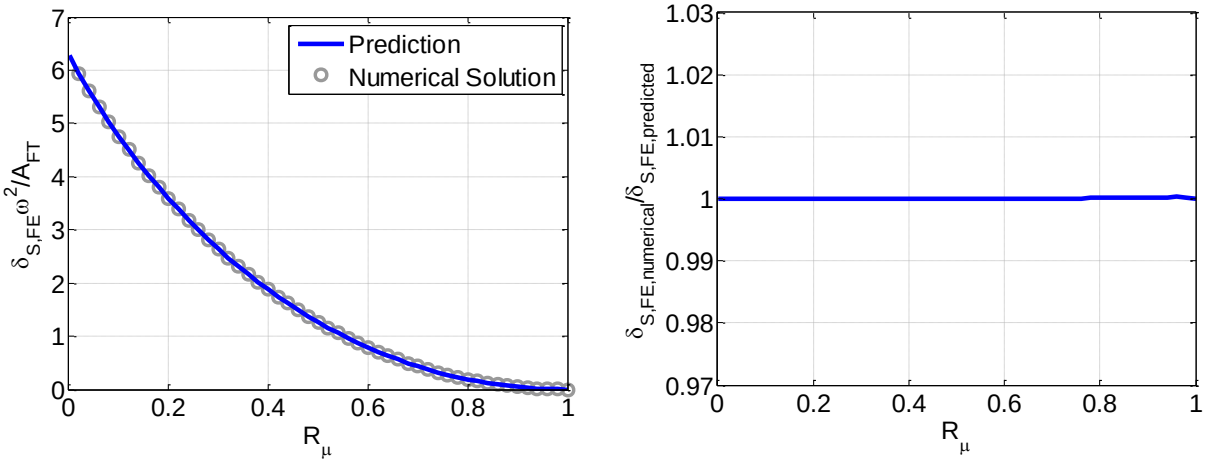

(a) **(b)**

Figure 5.6. Comparison of the first excursion sliding displacement obtained from predictions versus numerical modelling; (a) absolute values, (b) relative error

Thus far, $\delta_{S,FE}$ is the change in sliding displacement from T_0 to T_e. δ_S however depends on (i) the initial sliding displacement at T_0, and (ii) the occurrence of additional sliding excursions. Based on preliminary analyses, it was found that dividing $\delta_{S,FE}$ by two provided the best approximation of δ_S. Additionally, ω is not easily obtained for floors in multi-storey buildings, and thus it is assumed that $\omega \approx A_{FT}/V_{FT}$. Including these assumptions, the final form of the δ_S prediction is shown in **Eq. 5.17**. Note that the total floor velocity was used rather than the floor's velocity relative to the floor. This was because the ground has zero velocity relative to itself, which would imply that contents on the ground will not move if the latter was assumed which is obviously false. Both of these assumptions differ from Lin et al. [17], which uses relative displacement response and considers $\delta_S \approx \delta_{S,FE}$.

$$\frac{\delta_S A_{FT}}{V_{FT}^{\ 2}} = \frac{2\pi\sqrt{\left(1-R_\mu^{\ 0.46}\right)\left(1-R_\mu^{\ 2}\right)}-2\pi^2 R_\mu\left(1-R_\mu^{\ 0.46}\right)-\sin\left(2\pi\sqrt{1-R_\mu^{\ 0.46}}+\sin^{-1}\left(R_\mu\right)\right)+R_\mu}{2} \quad \textbf{(5.17)}$$

5.5 ANALYSES OF CONTENT MOVEMENT IN BUILDINGS

Analyses of content movement within three 5-storey elastically responding frame buildings were conducted to assess the reliability of each prediction equation. The general structural model is shown in **Figure 5.7**, and is based off a model used by Riley-Smith et al. [27]. It has a storey height of 4.0 m on the ground floor, and 3.6 m on other floors. It is assumed that the frame is prismatic and has the same mass on each floor. The fundamental period of the frame structure was taken as 0.5 s, 1.0 s and 1.5 s. Two dimensional elastic dynamic structural analyses were performed on OpenSees [35] using co-rotational transformation to consider P-delta effects [36] and assuming a Rayleigh damping ratio of 5% for the first and fourth elastic modes [37].

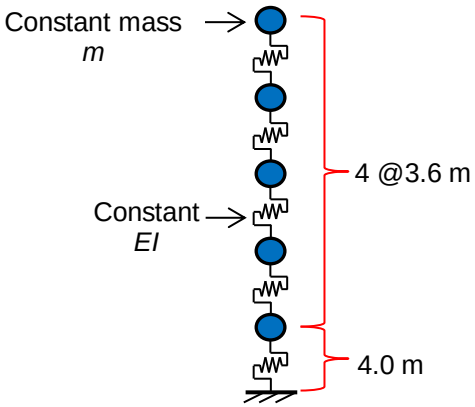

Figure 5.7. Structural model used in study

The ground motion record suite considered in this study comprises of all available ground motion records from the Pacific Earthquake Engineering Research database as of December 2012 [18]. At that time, the database contained 3,225 shallow crustal ground motions recorded worldwide, each containing two orthogonal horizontal components and one vertical component. Each horizontal component was applied to the structure individually and was not scaled, while vertical components were not considered.

After each analysis, the total acceleration response history, A_{FT}, V_{FT}, and D_{FT} of each floor were recorded. Content sliding analyses were then performed on Matlab [24] by solving **Eq. 5.1**, where the total acceleration response history was inputted as $a_{FT}(t)$ using Newmark's iterative scheme; while A_F, V_F, and D_F were used to predict the sliding response using the prediction models.

Three values of μ were considered; 0.1, 0.3, and 0.5. This covers the range of furniture considered in **Chapter 4**. Pull-test results by Aslam et al. [11], Chong and Soong [8], Chaudhuri and Hutchinson [12], Konstantinidis [10], and Nagao et al. [5] of rigid blocks mostly falls within this range as well.

5.6 COMPARISON OF PREDICTION EQUATIONS

In order to compare the reliability of each prediction, the ratio of the sliding displacement obtained from numerical analysis against that obtained from predictions, Δ_δ,

was calculated using **Eq. 5.18** for each case and ground motion record examined. If Δ_δ is less than 1.0, the prediction overestimates δ_S. The median of Δ_δ was then computed at every 0.05 steps of R_μ for a given building, floor level, and μ. The sum of squared relative error, *SSRE*, which is a measure of the difference between the median displacement ratio and the target (Δ_δ = 1.0), was then calculated using **Eq. 5.19**. Smaller *SSRE* indicates a better fit.

$$\Delta_\delta = \delta_{S,analytical} / \delta_{S,predicted} \quad \textbf{(5.18)}$$

$$SSRE = \sum_{i=1}^{n} \left[\ln(\Delta_\delta)_{median,i} \right]^2 \quad \textbf{(5.19)}$$

The predictions for contents located on the 3rd floor of a building with a period of 1.0s and μ of 0.1 is compared in **Figure 5.8**. It can be seen from **Figure 5.8a** that the prediction using Newmark [13] appears to match the analytical results well for R_μ between 0.15 and 0.65. Outside this range, the prediction overestimates the response; especially at higher values of R_μ where Δ_δ is in the range of 0.01. Despite being based off the same concept, the prediction using Choi and Tung [14] is non-conservative with the 16th percentile curve exceeding Δ_δ = 1.0 for most values of R_μ as shown by **Figure 5.8b**. This is likely due to the adjustment factor used by Choi and Tung [14] being specific for the case examined in their study. The *SSRE* for Newmark [13] and Choi and Tung [14] are the 3rd and 2nd highest considered, respectively.

The prediction using Kaneko et al. [15] is overly conservative as shown in **Figure 5.8c**, and it has the highest *SSRE* overall. This is because this method predicts the envelope of the maximum possible sliding displacement as discussed in **Section 5.3**. However, the prediction using Kaneko et al. [16] is a better fit as shown in **Figure 5.8d**. Like Newmark [13], the prediction matches the analytical results well for *R* between 0.15 and 0.65, but is conservative outside this range. However, the level of conservatism is lower, resulting in the *SSRE* being the 2nd lowest in this case.

The prediction using Konstantinidis [10] is non-conservative for R between 0.15 and 0.65 and conservative for values outside this range, as shown in **Figure 5.8e**. While Newmark [13] may have a better fit between 0.15 and 0.65, the relative error using Konstantinidis [10] is smaller overall, resulting in it having the 3rd lowest *SSRE*.

The new prediction equation proposed in this study provides the best fit, with the *SSRE* value being the lowest overall (about 3.6 times lower than that using Kaneko et al. [16]), as shown in **Figure 5.8f**. In addition, this was the only case where $\Delta_\delta = 1.0$ is within the 16th and 84th percentile lines for all R_μ values. The proposed prediction equation is therefore the best in the case examined.

The *SSRE* values obtained for μ = 0.1, 0.3 and 0.5 are shown in **Tables 5.1** to **5.3**, respectively. Of the existing prediction equations, **Table 5.1** shows that the prediction using Kaneko et al. [16] is the best for μ = 0.1, with a median *SSRE* 2.0 times lower than the next best case. However **Tables 5.2** and **5.3** show that the prediction by Konstantinidis [10] was the best for μ = 0.3 and 0.5, with a median SSRE between 1.1 and 1.2 times lower than the next best prediction. A reason for the increased error using Kaneko et al. [16] is that the equation was empirically derived for μ between 0.02 and 0.1 as discussed in **Section 5.3**, and thus the reliability may decrease for μ outside this range. The prediction using Kaneko et al. [15] remains the least reliable, with a median *SSRE* about 9.0 times that of the next worst case.

The prediction equation proposed in this study has the lowest SSRE of all predictions investigated in all but two cases. These cases are when the content was located on ground for μ = 0.3 and 0.5, though **Eq. 5.17** still provided the second-best prediction in these cases. A possible reason is that error was induced in the prediction equation from attempting to approximate the frequency of the ground response using A_{FT}/V_{FT}. Interestingly, Choi and Tung [14] was the most reliable in those two cases, despite having the second largest SSRE

in majority of other cases. The median *SSRE* for the newly proposed equation is between four to six times smaller than the next best prediction for all μ considered, indicating that this is the best prediction equation overall.

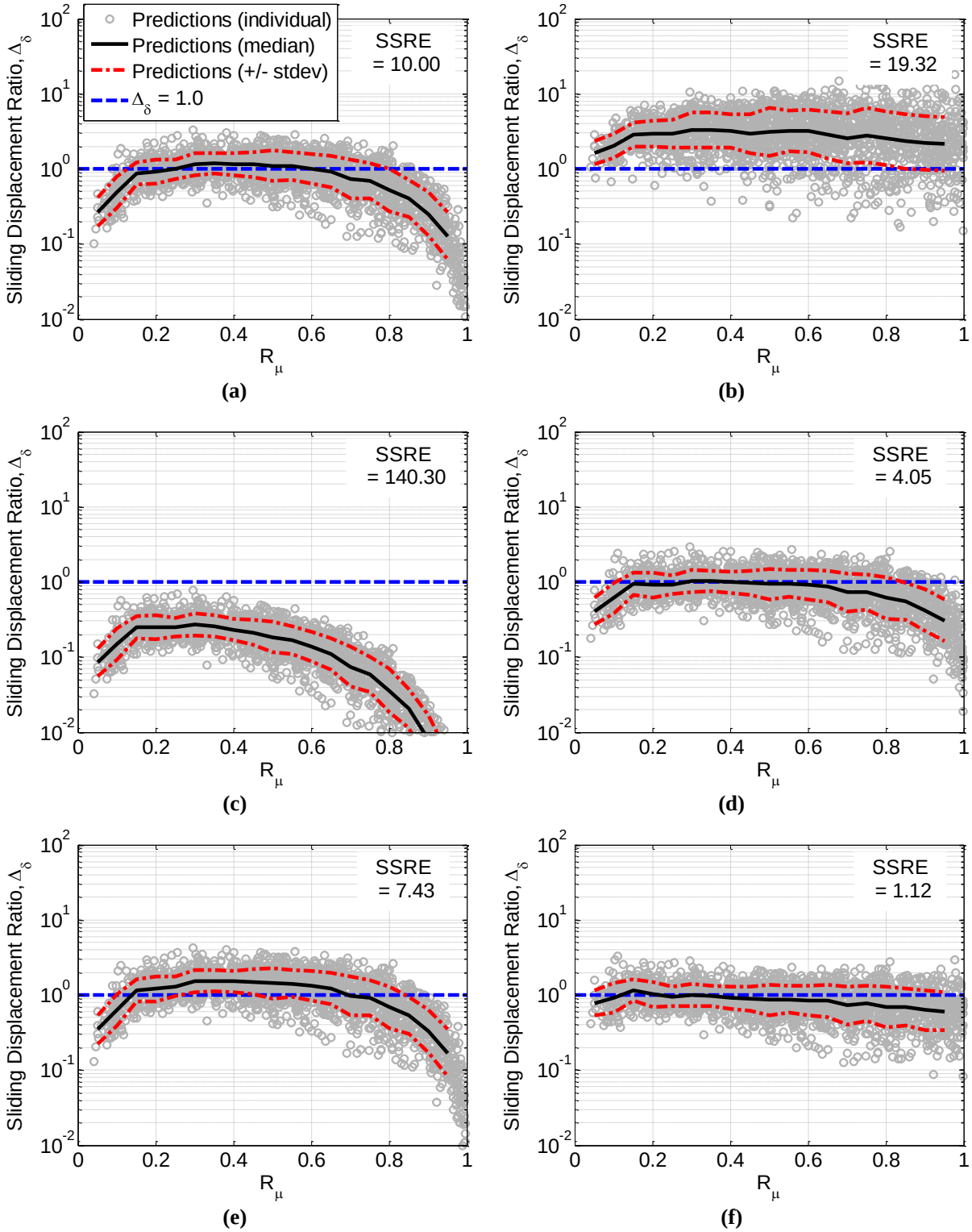

Figure 5.8. Comparison of prediction equations (*T* = 1.0 s, *μ* = 0.1, floor 3); (a) Newmark [13], (b) Choi and Tung [14], (c) Kaneko et al. [15], (d) Kaneko et al. [16], (e) Konstantinidis [10], and (f) Eq. 5.17

Table 5.1. *SSRE* values for μ = 0.1 (bold underlined font indicates best match for each case)

Structure	Floor	Newmark [13]	Choi and Tung [14]	Kaneko et al. [15]	Kaneko et al. [16]	Konstantinidis [10]	Eq. 5.17
Ground	0	15.66	6.02	163.70	8.18	11.68	**5.21**
0.5 s	1	12.78	8.83	149.80	5.64	9.36	**2.35**
	3	11.14	14.56	147.80	4.94	7.96	**1.94**
	5	8.76	22.67	131.11	2.95	7.26	**0.47**
1.0 s	1	10.73	9.43	147.05	4.42	7.87	**1.99**
	3	10.00	19.32	140.30	4.05	7.43	**1.12**
	5	7.74	27.75	124.40	2.45	6.68	**0.22**
1.5 s	1	9.76	10.52	142.83	3.91	7.12	**1.69**
	3	8.57	23.02	133.47	3.14	6.47	**0.57**
	5	7.58	31.08	121.59	2.39	6.75	**0.18**
Median *SSRE*		10.02	15.22	139.68	3.92	7.74	**0.99**

Table 5.2. *SSRE* values for μ = 0.3 (bold underlined font indicates best match for each case)

Structure	Floor	Newmark [13]	Choi and Tung [14]	Kaneko et al. [15]	Kaneko et al. [16]	Konstantinidis [10]	Eq. 5.17
Ground	0	19.56	**4.48**	171.84	18.96	14.65	8.53
0.5 s	1	8.14	7.46	133.39	7.35	5.86	**1.53**
	3	9.21	16.89	139.02	8.73	6.85	**1.90**
	5	6.48	25.61	122.25	4.92	5.78	**0.43**
1.0 s	1	8.22	8.82	135.29	7.55	6.08	**1.78**
	3	8.57	21.59	135.92	8.16	6.45	**1.33**
	5	6.46	28.8	121.43	4.83	5.81	**0.27**
1.5 s	1	8.7	9.24	135.63	8.1	6.51	**1.97**
	3	8.28	24.38	131.24	7.75	6.43	**1.1**
	5	6.2	31.62	118.13	4.55	5.79	**0.25**
Median *SSRE*		8.48	14.97	133.73	7.42	6.72	**1.14**

Table 5.3. *SSRE* values for μ = 0.5 (bold underlined font indicates best match for each case)

Structure	Floor	Newmark [13]	Choi and Tung [14]	Kaneko et al. [15]	Kaneko et al. [16]	Konstantinidis [10]	Eq. 5.17
Ground	0	23.99	**2.63**	183.8	28.01	17.39	12.12
0.5 s	1	9.38	6.31	129.4	9.75	7.19	**1.71**
	3	9.25	17.13	133.04	10.59	7.27	**1.81**
	5	6.53	25.78	119.08	6.78	6.01	**0.68**
1.0 s	1	10.67	7.51	136.43	11.10	8.40	**2.34**
	3	6.97	21.72	127.03	9.24	5.3	**1.05**
	5	5.6	31.32	115.98	6.34	5.27	**0.43**
1.5 s	1	9.54	9.29	131.59	11.3	7.19	**2.72**
	3	6.43	24.45	123.01	8.15	5.17	**0.69**
	5	5.48	33.64	112.07	5.97	5.42	**0.33**
Median *SSRE*		8.47	13.98	129.96	9.65	6.94	**1.33**

5.7 CONCLUSIONS

This chapter examines the reliability of six maximum content sliding displacement prediction equations, one of which is newly derived in this study, by comparing the predictions against results from an analytical study for elastic structures. In summary:

1. The new prediction equation derived in this study was based on concepts from Lin et al. [17], in that the first sliding excursion of a content subjected to undamped sinusoidal motion is related to the median sliding response of contents subjected to realistic ground motion records. The equation was derived using the equations of physical motion.
2. Of the five existing predictions, Kaneko et al. [16] was the most reliable for $\mu = 0.1$, with a median sum of squared relative error (*SSRE*) 2.0 times less than the next best prediction. However, Konstantinidis [10] was the most reliable for $\mu = 0.3$ and 0.5 with a median *SSRE* between 1.1 to 1.2 times less than the next best prediction. The least reliable was Kaneko et al. [15], whose median *SSRE* about 9.0 times larger than the next worse prediction, followed by Choi and Tung [14].
3. The newly derived equation has the best fit with the numerical results out of all prediction equations considered, with a median *SSRE* between four to six times lower than that of the next best prediction in almost all cases. Based on this, it is recommended that the newly derived equation be used in building performance assessments.

5.8 REFERENCES

1. Reitherman, B., Sabol, T., Bachman, R., Bellet, D., Bogen, R., Cheu, D., Coleman, P., Denny, J., Durkin, M., Fitch, C., Fleming, R., Gates, W., Goodno, B., Halling, M., Hess, R., Holmes, W., Jephcott, D., Kimmel, J., Kehrlein, D., Lizundia, B., Malley, J., Masek, J., Masri, S., McGavin, G., McKevitt, W., McMullen, J., Merz, K., Murry, J., Nisar, A., Norman, P., Patrucco, H., Peoples, D. R., Pierepiekarz, M., Rihal, S., Schiff, A., Selvaduray, G., Sullivan, R., Snyder, V., Turner, F., Vallabhan, C. V. G., & White, I. (1995). Nonstructural Damage. Earthquake Spectra, 11(S2), 453-514.

2. Dhakal, R. P. (2010). Damage to non-structural components and contents in 2010 Darfield Earthquake. Bulletin of the New Zealand Society of Earthquake Engineering, 43(3), 404-411.
3. FEMA E-74. (2012). Reducing the Risks of Nonstructural Earthquake Damage - A Practical Guide.
4. Takuya, N., Kajiwara, K., Fujitani, H., Fukuyama, K., Kawabe, H., Ohnishi, K., Kido, S., & Nakashima, M. (2008). Test on Seismic Response of High-Rise Building Focusing on Furniture and Non-Structural Components - Large Scale Test System based on E-defense Shaking Table. Journal of Structural and Construction Engineering, 73(628), 1007-1014.
5. Nagao, T., Kagano, H., & Hamaguchi, K. (2012). Full-Scale Shaking Table Test on Furnitures subjected to Long-Period Earthquake Motions. Paper presented at the 15th World Conference on Earthquake Engineering, Lisbon, Portugal.
6. Taghavi, S., & Miranda, E. (2003). Response Assessment of Nonstructural Building Contents: Pacific Earthquake Engineering Research Center, University of California Berkeley.
7. Okada, S., Nachi, N., & Endo, T. (2012). Seismic Assessment Method for Indoor Injury Risk and Its Application. Paper presented at the 15th World Conference on Earthquake Engineering, Lisbon, Portugal.
8. Chong, W. H., & Soong, T. T. (2000). Sliding Fragility of Unrestrained Equipment in Critical Facilities: Department of Civil, Structural and Environmental Engineering, University at Baffalo, New York, US.
9. Hutchinson, T. C., & Chaudhuri, S. R. (2006). Simplified Expression for Seismic Fragility Estimation of Sliding-Dominated Equipment and Contents. Earthquake Spectra, 22(3), 709-732.
10. Konstantinidis, D. A. (2008). Experimental and Analytical Studies on the Seismic Response of Freestanding and Anchored Building Contents. PhD Thesis, Civil and Environmental Engineering, University of California, Berkeley.
11. Aslam, M., Godden, W. G., & Scalise, D. T. (1975). Sliding Response of Rigid Bodies to Earthquake Motions: University of California, Berkeley.
12. Chaudhuri, S. R., & Hutchinson, T. C. (2005). Characterizing Frictional Behaviour for use in Predicting the Seismic Response of Unattached Equipment. Soil Dynamics and Earthquake Engineering, 25, 591-604.
13. Newmark, N. M. (1965). Effects of earthquakes on dams and embankments. Geotechnique, 15(2), 139-160.
14. Choi, B., & Tung, C. C. D. (2002). Estimating Sliding Displacement of an Unanchored Body Subjected to Earthquake Excitation. Earthquake Spectra, 18(4), 601-613.
15. Kaneko, M., Hayashi, Y., & Tamura, K. (1999). Evaluation of Sliding Displacement of Furniture During Earthquake. AIJ Journal of Technology and Design, 8, 73-78.
16. Kaneko, M., Hayashi, Y., & Tamura, K. (1999). Evaluation of Sliding Displacement of Furniture during Earthquake - By using Revised Formula to Estimate Sliding Displacement of Furniture. Technical Papers of Annual Meeting of Architectural Institute of Japan, B-II, 537-538.
17. Lin, S. L., MacRae, G. A., Dhakal, R. P., & Yeow, T. Z. (2015). Building contents sliding demands in elastically responding structures. Engineering Structures, 86, 182-191.
18. Chiou, B. S. J., Darragh, R., Gregor, N., & Silva, W. (2008). NGA Project Strong-Motion Database. Earthquake Spectra, 24(1), 23-44.
19. Shenton III, H. W. (1996). Criteria for Initiation of Slide, Rock and Slide-Rock Rigid-Body Modes. Journal of Engineering Mechanics, 122(7), 690-693.
20. Shao, Y., & Tung, C. C. (1999). Seismic Response of Unanchored Bodies. Earthquake Spectra, 15(3), 523-536.
21. Shenton III, H. W., & Jones, N. P. (1992). Base Excitation of Rigid Bodies. Part I: Formulation. Journal of Engineering Mechanics, 117(10), 2286-2306.
22. Garcia, D. L., & Soong, T. T. (2003). Sliding Fragility of Block-Type Non-Structural Components. Part 1: Unrestrained Components. Earthquake Engineering and Structural Dynamics, 32, 111-129.
23. Newmark, N. M. (1959). A Method of Computation for Structural Dynamics. Journal of Engineering Mechanics, 85(EM3), 67-94.
24. The MathsWorks Inc. (2012). MATLAB v 7.14 (R2012a). Natick, MA.
25. English, R., MacRae, G. A., & Dhakal, R. P. (2012). Hysteretic Influence on Earthquake Induced Sliding Damage of Contents. Paper presented at the 2012 NZSEE Conference, Christchurch, New Zealand.
26. Lin, S. L., MacRae, G. A., Dhakal, R. P., & Yeow, T. Z. (2013). Building Contents Sliding during Earthquakes. Paper presented at the 2013 NZSEE Conference, Wellington, NZ.
27. Riley-Smith, H., Cain, E. S., Yeow, T. Z., MacRae, G. A., & Dhakal, R. P. (2014). Building Content Sliding Demand - Analytical Studies of Contents in Elastic MDOF Structures. Paper presented at the 2014 NZSEE Conference, Auckland, NZ.
28. Saito, T., Takahashi, T., Hasegawa, R., Morita, K., Azuhata, T., & Noguchi, K. (2008). Shaking Table Test on Indoor Seismic Safety of Highrise Buildings (Part II. Movement of Furniture Under Long Period

Earthquake Ground Motion). Paper presented at the The 14th World Conference on Earthquake Engineering, Beijing, China.
29. Newmark, N. M., & Hall, W. J. (1982). Earthquake Spectra and Design: Earthquake Engineering Research Institute.
30. SEAOC. (1995). Vision 2000 - A Framework for Performance-based Design: Structural Engineers Association of California, Sacramento, California.
31. Somerville, P., Smith, N., Punyamurthula, S., & Sun, J. (1997). Development of Ground Motion Time Histories for Phase 2 of the FEMA/SAC Steel Project: CUREE.
32. Younis, C. J., & Tadjbakhsh, I. G. (1984). Response of Sliding Rigid Structure to Base Excitation. Journal of Engineering Mechanics, 110(3), 417-432.
33. Yegian, M. K., Marciano, E. A., & Ghahraman, V. G. (1991). Earthquake-Induced Permanent Deformations: Probabilistic Approach. Journal of Geotechnical Engineering, 117(1), 35-50.
34. Voyagaki, E., Mylonakis, G., & Psycharis, l. N. (2012). Rigid Block Sliding to Idealized Acceleration Pulses. Journal of Engineering Mechanics, 138(9), 1071-1083.
35. McKenna, F., Fenves, G. L., Scott, M. H., & Jeremic, B. (2000). Open System for Earthquake Engineering Simulation (OpenSees). Pacific Earthquake Engineering Research Center, University of California, Berkeley, CA.
36. Mazzoni, S., McKenna, F., Scott, M., & Fenves, G. (2009). Open system for engineering simulation user-command-language manual, version 2.0, Pacific Earthquake Engineering Research Center. University of California, Berkeley, Berkeley, CA.
37. Lord Rayleigh. (1877). Theory of Sound (two volumes): Dover Publications, New York.

6. Wall Building Stiffness and Strength Effect on Content Sliding in Wellington Seismic Conditions

6.0 SUMMARY

A numerical study of unobstructed content sliding within several low-to-midrise reinforced concrete cantilever wall buildings, designed to Wellington conditions in New Zealand, is performed to examine the influence of a building's strength and stiffness on contents' sliding response. It was shown that contents located in stronger buildings generally experienced larger sliding response. If the building was designed to be strong, the sliding response of contents with low friction coefficients was smaller in stiffer buildings compared to those in flexible buildings. This indicates that increasing a building's stiffness could have a beneficial effect on reducing content's sliding response despite its increased total floor accelerations; though this effect decreases with increasing building height or friction coefficient, or decreasing building strength. This study's findings were compared against a parametric equation for estimating the maximum sliding displacement. This equation, which was originally derived for contents located within elastic frame buildings, was found to be more efficient than considering total floor accelerations alone, but was under-conservative by a mean of 17%, for yielding multi-storey buildings. A design procedure considering content sliding using the parametric equation, and an example, is provided.

6.1 INTRODUCTION

Differing opinions on the "optimal" design stiffness of buildings in seismic regions exist (e.g. Freeman [1], Berg [2]). One view is that buildings should be flexible, as the increased period of vibration leads to a decrease in inertia forces. This encouraged the use of flexible buildings in Western countries, such as USA and New Zealand. Another view is that

stiffer buildings would experience lower drifts during shaking, and hence experience lesser structural damage. This was based on past observations, such as the superior performance of the stiff Japan Industrial Bank building compared to flexible buildings of similar age during the 1923 Great Kanto event [1]. Buildings in Japan are thus often designed and built to be stiff.

One method to assess the "optimal" design building stiffness is to consider the buildings' initial costs and performance. This study will primarily focus on the latter, though it should be noted that there are differing opinions on the former in literature [3, 4]. One method to judge a building's performance is to assess the likelihood of damage or injuries. Damage to building components are generally assumed to be caused by excessive drifts or accelerations. Drift-sensitive elements may include structural members, and vertical non-structural elements such as partitions. Acceleration-sensitive elements may include braced ceilings not fixed to walls, and general contents such as furniture and mechanical equipment.

Flexible buildings are likely to experience more drift-related damage and losses, and have a greater chance of pounding against other buildings. Furthermore, for buildings designed to the same force-reduction factor, *R*, a more flexible building would likely have greater residual displacement, even though the global ductility demands may be similar. Conversely, increasing stiffness may cause more acceleration-related damage.

A building's strength can also influence losses. If this was decreased without varying its elastic stiffness, the peak displacement at the height of effective mass should not change significantly based on the equal displacement assumption. However, the lower lateral force resistance in weaker buildings results in lower inertia forces and accelerations, which may decrease acceleration-related damage; though earlier and more significant yielding results in greater structural damage due to increased nonlinearity.

Sliding of contents, such as medical equipment and furniture, may lead to injuries, disruption, damage, and blockage of egress routes [5-7]. As such, this should be included in performance assessments. Sliding occurs when the total floor acceleration, $a_{FT}(t)$, exceeds μg; where μ is the friction coefficient and g is the acceleration due to gravity. The maximum sliding displacement, δ_S, is therefore often correlated with peak total floor acceleration, A_{FT}, alone [8-11]; implying that sliding is more severe in stiffer and/or stronger buildings.

Recent research however showed that while A_{FT} is a good indicator of the ***occurrence*** of sliding; it is insufficient on its own to describe the ***extent*** of sliding. Sato et al. [6] and Shi et al. [12] conducted shaking tests of full-scale four-storey hospital buildings fitted with contents, and found that δ_S was 0.7 m when A_{FT} was around 20 m/s^2 in one test, but was between 1.0 to 3.0 m when A_{FT} was around 2.4 m/s^2 in another; noting that this could be due to duration effects.

The shake-table tests of office furniture using sinusoidal excitations from **Chapter 4** also found that A_{FT} on its own was inadequate to describe the extent of content sliding. In particular, it was found that the shaking frequency, ω_T, has a strong influence on δ_S. This was explained considering the content and sinusoidal floor total acceleration and velocity response plots in **Figure 6.1**; where T_0 and T_e were the times when the content separates and reattaches to the floor, respectively. If A_{FT} and μ were constant but ω_T was decreased, the sliding duration (T_e-T_0) and the velocity amplitude increases, and thus so would the sliding displacement of a single excursion (back-and-forth movement, shaded area in **Figure 6.1b**).

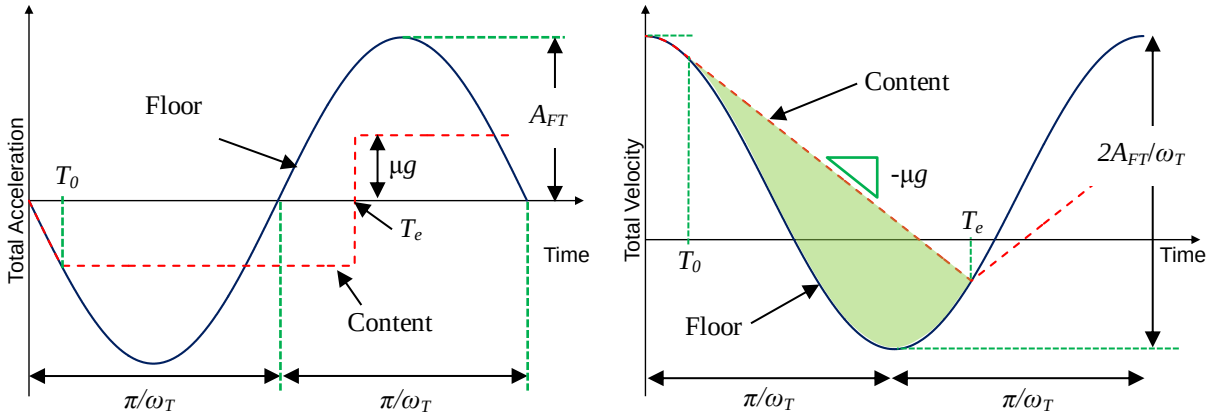

(a) Total acceleration **(b) Total velocity**

Figure 6.1. Typical response of contents under sinusoidal floor response

The importance of ω_T was also observed in an analytical study by Lin et al. [13] using sinusoidal floor motion with constant amplitude and frequency. They also found that δ_S for contents within elastic single-storey buildings subjected to realistic ground motions can be approximated by the first sliding excursion displacement of contents subjected to sinusoidal floor motion. A parametric estimate of δ_S, $\delta_{S,PARA}$, based on this was derived in **Chapter 5** (**Section 5.4**), where A_{FT}/V_{FT} was used to approximate ω_T. A simplified empirical version of this is shown in **Eq. 6.1**. The original form of the equation was compared this against other existing equations [14-17] in **Chapter 5** (**Section 5.6**) using an analytical study of contents within a five-storey elastic frame building subjected to the entire Pacific Earthquake Engineering Research (PEER) ground motion database (as of December 2012) [18], and was found to have the best-fit. However, buildings which yield or are sensitive to higher-order mode effects were not considered.

$$\delta_{S,PARA} = \begin{cases} \dfrac{V_{FT}^{\,2}}{A_{FT}}\left(\pi - 10.27\dfrac{\mu g}{A_{FT}} + 7.13\left(\dfrac{\mu g}{A_{FT}}\right)^{1.45}\right) & \text{if } \mu g < A_{FT} \\ 0 & \text{if } \mu g \geq A_{FT} \end{cases} \quad \textbf{(6.1)}$$

If both sides of **Eq. 6.1** were multiplied by $g/V_{FT}^{\,2}$, the relationship between the normalized sliding displacement, $\delta_S g/V_{FT}^{\,2}$, and A_{FT} can be approximated as shown in **Figure 6.2**. Here, $\delta_S g/V_{FT}^{\,2}$ increases initially regardless of μ. However, $\delta_S g/V_{FT}^{\,2}$ starts decreasing

once A_{FT} is larger than approximately 3.3μg, and tends towards a constant value at larger values of A_{FT}. This implies that δ_S may be more dependent on V_{FT} when A_{FT} is significantly larger than μ. If one assumes that V_{FT} is relatively constant regardless of the fundamental period of the building, then increasing the buildings' stiffness, and hence increasing A_{FT}, may potentially reduce δ_S, especially if A_{FT} is larger than 3.3μg. In reality, as (i) V_{FT} would be influenced by a building's strength and stiffness, and (ii) the sliding response is likely to be dependent on both A_{FT} and V_{FT}, it is not clear how δ_S may be influenced by a building's structural properties. As such, it is desirable to know if stiffer and/or stronger buildings are more beneficial to limit sliding-related damage or injury.

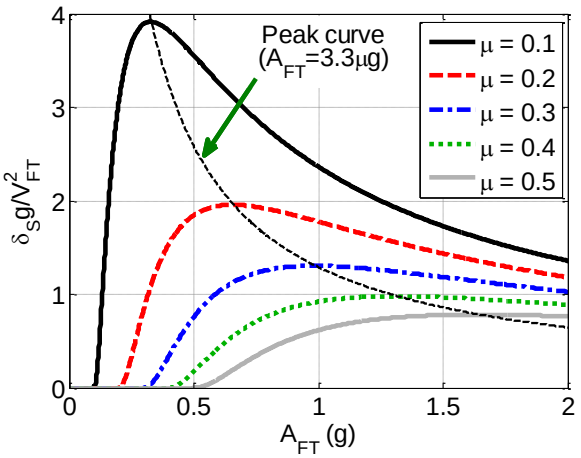

Figure 6.2. Relationship of normalized sliding displacement to peak total floor acceleration

This chapter addresses these needs by performing sliding analyses of contents located within several reinforced concrete wall buildings of varying stiffness, strength, and height. The site which the study focuses on is Wellington in New Zealand, and thus ground motion records were selected and buildings were designed to be specific to that region. Due to the infinite possible arrangement of contents (i.e. distance to walls or other obstacles), and variability of impact surface properties, the scope of this study is limited to unobstructed contents (i.e. free to move without impacting against obstacles) to understand the influence of stiffness and strength in its simplest case. Note that this study focuses solely on the influence of building properties on the extent of content sliding. The financial implications of designing

for stiffer and/or stronger buildings, or of the extent of content sliding, are not considered as a proper cost-benefit study should consider other building components not considered. This study seeks to answer the following questions:

1. How does δ_S change with building stiffness?
2. How does δ_S change with building strength?
3. Do the findings from (1) and (2) change if the building height was varied?
4. Is **Eq. 6.1** applicable to contents in yielding single-storey buildings?
5. Is **Eq. 6.1** applicable to contents in yielding multi-storey buildings?
6. How can δ_S be predicted for design?
7. Are stiffer and/or stronger structures better for reducing δ_S?

6.2 CASE STUDY DETAILS

6.2.1 Assessment Framework

The assessment framework used in this study is shown in **Figure 6.3**, and is based off the PEER loss assessment framework [19]. The main steps are to (i) predict the seismic shaking intensity (quantified by an intensity measure, *IM*), (ii) estimate the building's response (defined by a building engineering demand parameter, EDP_B), (iii) estimate the content response (defined by a content engineering demand parameter, EDP_C), and (iv) predict the damage and losses. As the focus in this study is on the content's response, the final step is not considered in this study. Note that this framework is general and may be applied to any region if appropriate design approaches and ground motion records are used.

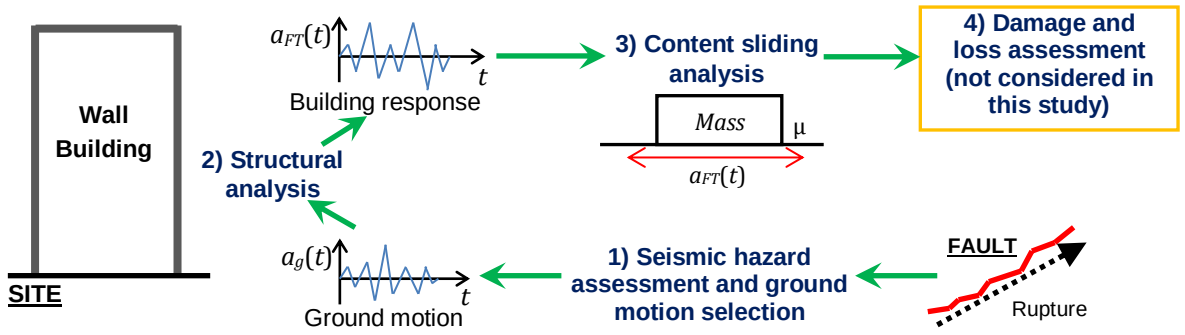

Figure 6.3. Integration of content sliding into PEER framework [19]

6.2.2 Wellington Seismic Conditions and Representative Ground Motions

Wellington (41.29^{o} S, 174.78^{o} E) is located within 20.0 km of numerous strike-slip faults, the three most notable of which (Wairarapa, Wellington, and Ohariu) are capable of rupturing with a magnitude over 7.0. It is also underlain by the Hikurangi subduction zone caused by the overlap of the Pacific Plate and the Australian Plate, which is capable of rupturing with a magnitude over 8.6. Both of these contribute to Wellington being located in amongst one of the highest seismicity regions in New Zealand [20]. Due to this, the region was selected for the case study investigation.

Probabilistic seismic hazard analysis (PSHA) for Wellington subsoil class C conditions was performed on OpenSHA [21], using New Zealand-specific rupture forecast models [22] and attenuation relationships [23], to obtain the annual rate of exceeding a given *IM* for the first step of the assessment in **Figure 6.3**. The conditioning intensity measure selected was spectral acceleration at 1.25 s, which corresponds to the mean period of the tallest building considered (as discussed later), *Sa*(1.25s). The *Sa*(1.25s)-hazard is shown in **Figure 6.4a**. PSHA was also used to obtain the 10% probability of exceedance in 50 years uniform hazard spectra (UHS) shown in **Figure 6.4b** for building design.

The Generalized Conditioning Intensity Measure (GCIM) approach was used to select records [24]. Using this method, selected record suites are consistent with site-specific seismic hazards, and thus *EDP*-hazard findings are also consistent regardless of the conditioning *IM* considered. The selection algorithm utilized follows Bradley [25]. Eleven

sets of 20 scaled records, each with two horizontal components, were selected; each set representing a given hazard level ranging from 99% to 0.1% probability of exceedance in 50 years. Thus, 440 individual record components were used in total. The 10% in 50 year set (*Sa*(1.25s) = 0.5g) is shown in **Figure 6.4b**. The advantage of this approach is that the conditional distributions of other intensity measures of the record suite are also consistent with site-specific conditions. An example of this is shown in **Figure 6.4c** for the 5-95% significant duration, *Ds595*; where the distribution of *Ds595* from the record suite was a good match to theory using Kolmogorov-Smirnov (KS) tests [26]. Note that only horizontal components of records were selected and used in analyses, as past studies had shown that vertical accelerations have negligible effect on contents on average [27-29].

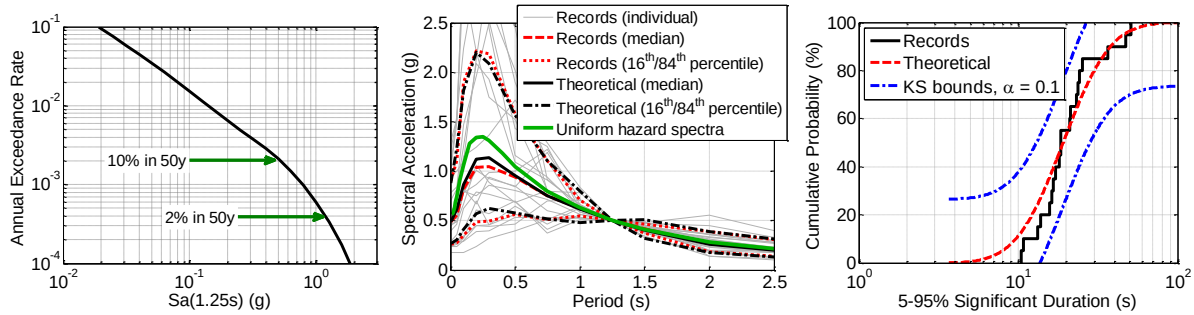

(a) **(b)** **(c)**

Figure 6.4. Seismic hazard and selected records; (a) Sa(1.25s) hazard, (b) Spectral curves for 10% in 50 year record suite, (c) *Ds*595 conditional CDF for 10% in 50 year record suite

6.2.3 Building Model and Structural Analysis

Single, 3, 6, and 10 storey reinforced concrete (RC) cantilever wall buildings were considered to observe if the effect of modifying strength and stiffness on content movement is consistent regardless of building height. Taller buildings were not considered, as a significant majority of the building stock in Wellington comprises of only low-to-midrise buildings. The buildings were designed using NZS1170.5's [30] equivalent static procedure using the UHS from **Figure 6.4b**.

The single-storey buildings' elastic period, *T*, was varied from 0.125 s to 2.0 s in steps of 0.125 s; while the force reduction factor, *R*, which is the ratio between the 10% in 50 year

elastic seismic demand and the provided capacity, was varied from 1.0 to 5.0 in steps of 1.0. This wide range of strength and stiffness was considered to obtain inelastic spectral curves for A_{FT}, V_{FT}, and δ_S for assessing if the results for the taller buildings were sensible.

All multi-storey buildings have 4.0 m ground floor height, and 3.6 m height for other floors. Three groups of buildings were considered for each building height as shown in **Table 6.1**: (i) varying strength for a fixed period; (ii) varying stiffness for stronger buildings (R = 1.0); and (iii) varying stiffness for weaker buildings (R = 5.0). Analyses for varying strength in stiffer or more flexible buildings were also performed, but had similar findings to Group 1 and were thus excluded. Note that: (i) the period range for the 10-storey building was selected based on drift limitations or design restrictions (i.e. allowable reinforcing ratio); (ii) the 3 and 6 storey building periods were selected to match drift demands of the 10-storey building under design loads; and (iii) some designs may be unrealistic due to failing design requirements, but were still considered regardless to include a wide range of T and R.

Table 6.1. Selected *T*-*R* pairings for wall building design

		3-storey building		**6-storey building**		**10-storey building**	
Group	**Vary**	***T* (seconds)**	***R***	***T* (seconds)**	***R***	***T* (seconds)**	***R***
1	*R*	0.57	1.0, 2.0, 3.0, 4.0, and 5.0	0.83	1.0, 2.0, 3.0, 4.0, and 5.0	1.25	1.0, 2.0, 3.0, 4.0, and 5.0
2	*T*	0.28, 0.49, 0.57, 0.65, and 0.77	5.0	0.37, 0.70, 0.83, 0.98, and 1.20	5.0	0.5, 1.00, 1.25, 1.50, and 2.00	5.0
3	*T*	0.28, 0.49, 0.57, 0.65, and 0.77	1.0	0.37, 0.70, 0.83, 0.98, and 1.20	1.0	0.5, 1.00, 1.25, 1.50, and 2.00	1.0

Inelastic structural response history analyses were performed using Ruaumoko2D [31] with a Caughey initial stiffness proportional damping ratio [32] of 5% across all modes. The model for the 10-storey building is shown in **Figure 6.5a**. P-delta effects were accounted for using large displacement analyses [33]. The walls were modelled allowing a plastic hinge of length L_p, defined using **Eq. 6.2** [34], to form at the base as shown in **Figure 6.5b**. Here, L is

the member length, and r_{Δ} and r_{ϕ} are the post-elastic ratios of the force-displacement and moment-curvature relationship respectively. The range of r_{Δ} is within 2-5% for structural walls based on past studies [35, 36], and thus a target r_{Δ} of 2% was assumed for this study.

$$L_p = \frac{r_{\phi} L}{3 r_{\Delta}} (1 - r_{\Delta}) \tag{6.2}$$

The hysteretic behaviour of the RC structural walls followed the SINA hysteresis rule [37] shown in **Figure 6.5c**, which matched the force-displacement behaviour of RC cantilever walls in past experimental research [35, 36]. The elastic stiffness, k_o, was assumed equal to the secant stiffness at first yield. Based on past research [35-37], the crack closing force, F_{cr}, was selected to be 0.3 times the yield force, F_y. The crack closing displacement, Δ_{cr}, was taken as one third of the maximum displacement at zero force in the opposite direction, Δ_i.

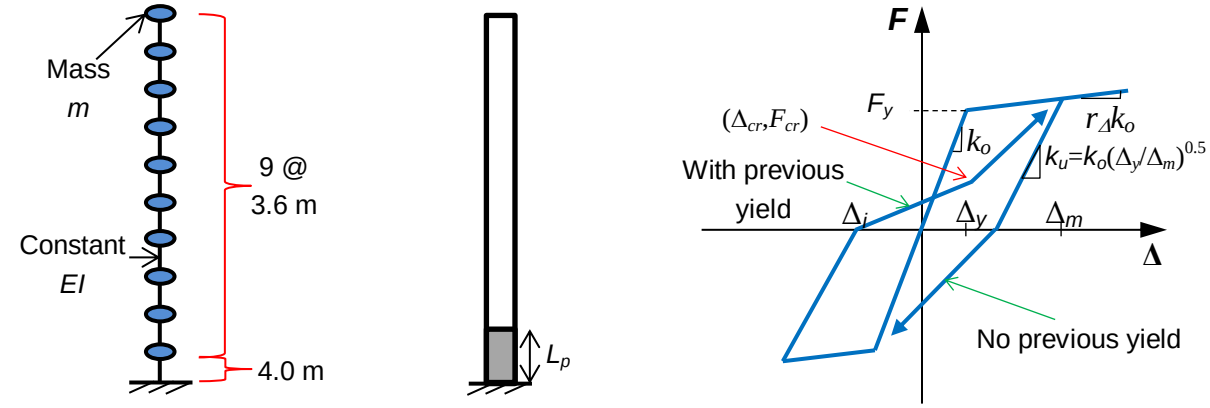

(a) MDOF building model **(b) Plastic hinge location** **(c) SINA hysteresis model**

Figure 6.5. Illustration of structural and hysteretic model considered in study

The suite of records selected earlier was used in the structural analysis for all buildings. The median and dispersion of EDP_B was obtained for each of the eleven sets of records. Linear interpolation was then performed to obtain the conditional probability distribution of $EDP_B > edp_B$ given $IM = im$, $G_{EDPB|IM}(edp_B|im)$, assuming a lognormal distribution.

6.2.4 Content Model and Sliding Analysis

Content sliding analysis was performed by: (i) extracting the total floor acceleration response history, $a_{FT}(t)$, from structural analysis, then (ii) obtaining the content's movement using Newmark integration schemes [38]. The content's total acceleration with time, $a_{CT}(t)$, was defined using **Eq. 6.3** [39]; where $v_{CRF}(t)$ is the content's velocity relative to the floor. This was advantageous over performing both simultaneously as: (i) it is easier to apply damping to the building only since the content response should be undamped; and (ii) performing the analyses separately allowed for different time steps to be used for each to decrease the overall computation time without sacrificing accuracy.

$$a_{CT}(t) = \begin{cases} a_{FT}(t) & \text{when } |v_{CRF}(t)| = 0 \text{ and } |a_{FT}(t)| < \mu g \\ -\text{sgn}(v_{CRF}(t))\mu g & \text{when } |v_{CRF}(t)| > 0 \text{ or } |a_{FT}(t)| \geq \mu g \end{cases} \quad \textbf{(6.3)}$$

In this study, μ was varied from 0.1 to 0.5 in steps of 0.1. The lower bound covers items on wheels [12] (i.e. a large proportion of hospital equipment), while the upper bound covers common items of furniture (i.e. desks) on carpet flooring as shown in **Chapter 4** (**Section 4.3.1**). Note that there are two types of friction coefficients; (i) static, μ_s, for when the content is stationary relative to the floor, and (ii) kinetic, μ_k, when the content is moving relative to the floor. It is assumed here that $\mu = \mu_s = \mu_k$, which is reasonable for numerical analyses based on findings from **Section 4.6.3**, and other existing literature [17, 29, 40, 41].

6.2.5 Computation of Response Hazard Curves

Traditionally, comparison of structural or content response was assessed using *EDP-IM* relationships. However, this is biased to the conditioning intensity measure used when selecting records. Instead, comparisons were made using the *EDP*-hazard (i.e. annual rate of exceeding a given *EDP*), $\lambda_{EDP}(edp)$, which is the same regardless of the selected conditioning intensity measure since the selected records were consistent with the Wellington site-specific

seismic hazard. **Eq. 6.4** was used to obtain the building's response-hazard curve, $\lambda_{EDPB}(edp_B)$ [42].

$$\lambda_{EDPB}(edp_B) = \int G_{EDPB|IM}(edp_B \mid im).\left|\frac{d\lambda_{IM}(im)}{dIM}\right|.dIM \quad \textbf{(6.4)}$$

For the content's response, the conditional EDP_C-IM relationship can only be obtained for cases where content sliding has initiated. As there are cases where A_{FT} was not sufficient to initiate sliding; the conditional probability that A_{FT} is larger than μg at a given IM, $G_{AFT|IM}[\mu g|im]$, needs to be included in calculating EDP_C-hazard. The full expression is shown in **Eq. 6.5**.

$$\lambda_{EDPC}(edp_C) = \int G_{EDPC|IM}(edp_C \mid \mu g < A_{FT}, im).G_{AFT|IM}[\mu g \mid im].\left|\frac{d\lambda_{IM}(im)}{dIM}\right|.dIM \quad \textbf{(6.5)}$$

6.3 CONTENT SLIDING IN SINGLE-STOREY BUILDINGS

6.3.1 Building Response

The 10% in 50 year A_{FT} and V_{FT} response curves for the single-storey buildings are shown in **Figure 6.6**, where the T = 0 response is that of the ground. These two EDP_B types are of particular interest as these are variables required for predicting $\delta_{S,PARA}$ using **Eq. 6.1**. It can be seen from **Figure 6.6a** that A_{FT} generally decreased with T (when T > 0.25 s) and R. This was because (i) higher frequency ground motion content is filtered out in more flexible buildings, and (ii) inertia forces and accelerations are limited by a building's strength capacity.

It was shown in **Figure 6.6b** that V_{FT} decreased with R for all values of T considered. However, the V_{FT}–T trends depended on R. For R = 1.0, V_{FT} increased with T initially until approximately 1.0 s, then decreased for the remainder of the period range considered. For weaker buildings, V_{FT} did not increase as significantly initially, and tends to start decreasing at a lower T. To explain these observations, consider two buildings being subjected to ground

shaking; one which is infinitely stiff and the other infinitely flexible. In the former case, V_{FT} will match the peak total ground velocity; while in the latter case V_{FT} would be zero. As such, V_{FT} should trend towards zero as T increases, which is consistent with the R = 5.0 case. The observed V_{FT} in between these two extremes would be dependent on the building's harmonic response, which is greater if the building had not yielded as observed for the R = 1.0 case.

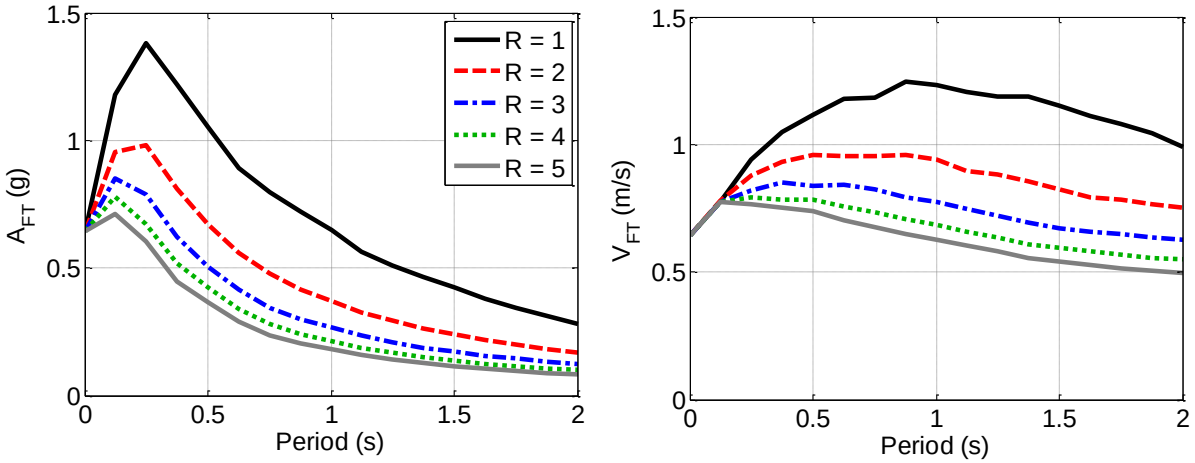

(a) Peak total floor acceleration (A_{FT}) **(b) Peak total floor velocity (V_{FT})**

Figure 6.6. 10% in 50 year single-storey buildings' response

6.3.2 Content Sliding Response

The 10% in 50 year δ_S curves from response history analysis, $\delta_{S,RHA}$, is shown in **Figure 6.7**, where T = 0 represents contents on the ground. Here, $\delta_{S,RHA}$ decreased with R at all T regardless of μ; indicating that contents exhibit greater response in stronger buildings. This was sensible as both A_{FT} and V_{FT} are larger in stronger buildings as shown in **Figure 6.6**.

The effect of stiffness on content sliding depended on R and μ. For R = 1.0, $\delta_{S,RHA}$ increased with T until around 0.75-1.00 s, and was 3-4 times that of contents on the ground, before remaining relatively constant or decreasing with T. As R and/or μ increases, T at which the peak $\delta_{S,RHA}$ occurs starts to decrease, and the rate at which $\delta_{S,RHA}$ decreases past this point increases. For large R and μ cases (i.e. R = 5.0 and μ = 0.3 in **Figure 6.7c**), $\delta_{S,RHA}$ generally decreased with T. This indicates that while $\delta_{S,RHA}$ is lower in stiffer buildings compared to

more flexible buildings if both are designed for low R and have low μ, the trends starts to reverse as R or μ increases.

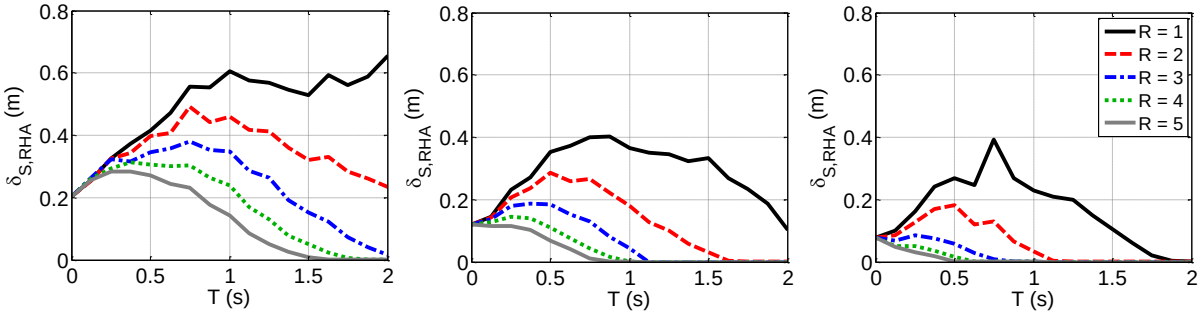

(a) μ = 0.1 **(b) μ = 0.2** **(c) μ = 0.3**

Figure 6.7. 10% in 50 year content sliding response for single-storey buildings

To further demonstrate that the observations from **Figure 6.7** are sensible, the detailed response of contents within two single-storey buildings designed for R = 1.0, one with T = 0.5 s and the other with T = 1.5 s, was examined. The ground motion used was recorded at the Calitri station during the 1980 Irpinia earthquake with a scale factor of 2.38. μ was taken as 0.1 for both cases. The resulting spectra matched the 10% in 50 year median target spectra and *Ds595* value in **Figure 6.4**. The total acceleration and sliding displacement response are shown in **Figure 6.8**. While A_{FT} for the 0.5 s building (1.00 g) was double that of the 1.50 s building (0.47 g), the higher shaking frequency of the total floor response observed in the 0.50 s case resulted in shorter duration of each acceleration peak. This resulted in $\delta_{S,RHA}$ for the 0.5 s case (0.20 m) being half that of the 1.50 s case. This is consistent with findings from **Chapter 4** (**Sections 4.4.3** and **4.6.3**), and highlights that A_{FT} on its own is an insufficient descriptor of $\delta_{S,RHA}$.

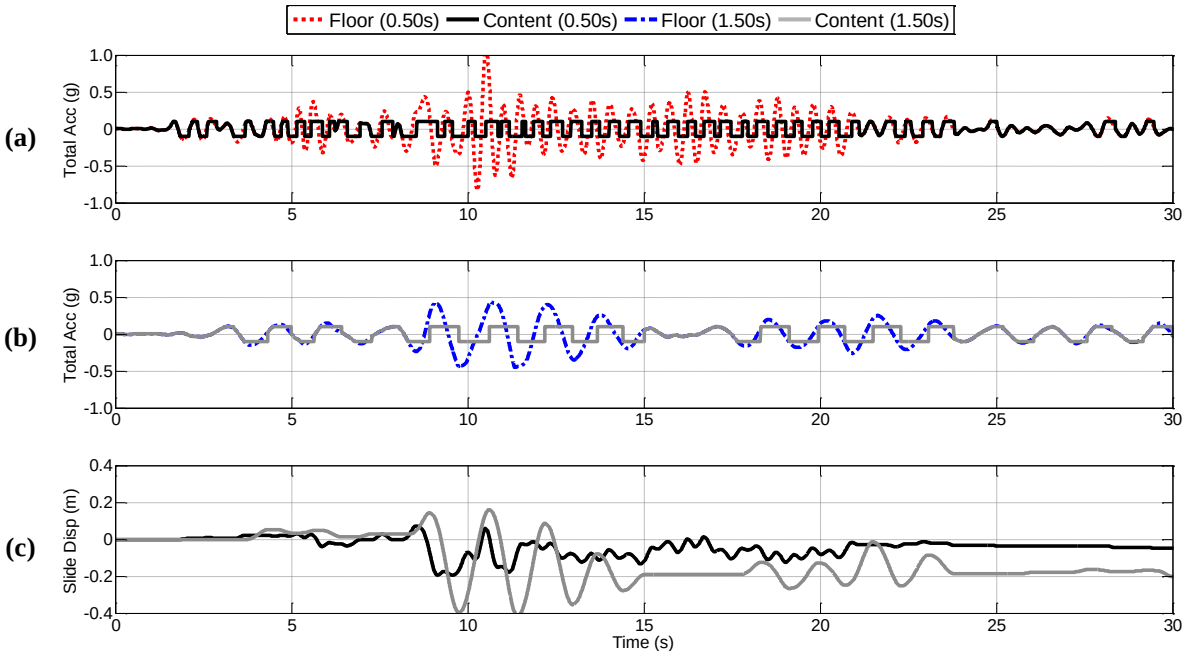

Figure 6.8. Example of shaking frequency influence on content sliding response; (a) 0.50 s building and content total acceleration response, (b) 1.50 s building and content total acceleration response, and (c) content sliding displacement response for both 0.50 s and 1.50 s cases

6.3.3 Relationship between Content and Building Response

The median $\delta_{S,RHA}$-$\mu g/A_{FT}$ relationship using analytical results from all 440 individual ground motion component records is shown in **Figures 6.9a** to **6.9c**. Here, $\delta_{S,RHA}$ decreased with $\mu g/A_{FT}$, but increased with T, R and μ at a given $\mu g/A_{FT}$. However, this does not imply that $\delta_{S,RHA}$ increases with T, R and μ directly. For example, while $\delta_{S,RHA}$ was 0.1 m when μ = 0.1 and $\mu g/A_{FT}$ = 0.34, the equivalent $\mu g/A_{FT}$ at μ = 0.2 is 0.68 which corresponded to $\delta_{S,RHA}$ of 0.02 m; demonstrating that $\delta_{S,RHA}$ decreases with μ which is sensible. The clear difference in the trends for all cases showed that $\mu g/A_{FT}$ alone is an insufficient parameter for describing $\delta_{S,RHA}$ due to shaking frequency and velocity effects not being properly considered.

If $\delta_{S,RHA}$ is compared against $\delta_{S,PARA}$ from **Eq. 6.1** instead, the relationships are consistent regardless of T, R, and μ as shown in **Figures 6.9d** to **6.9f** respectively. In addition, the lognormal distribution dispersion, ζ, is significantly reduced using **Eq. 6.1** (mean ζ of 0.37) compared to considering $\mu g/A_{FT}$ alone (mean ζ of 0.62), indicating that **Eq. 6.1** is more efficient at predicting δ_S for yielding single-storey buildings.

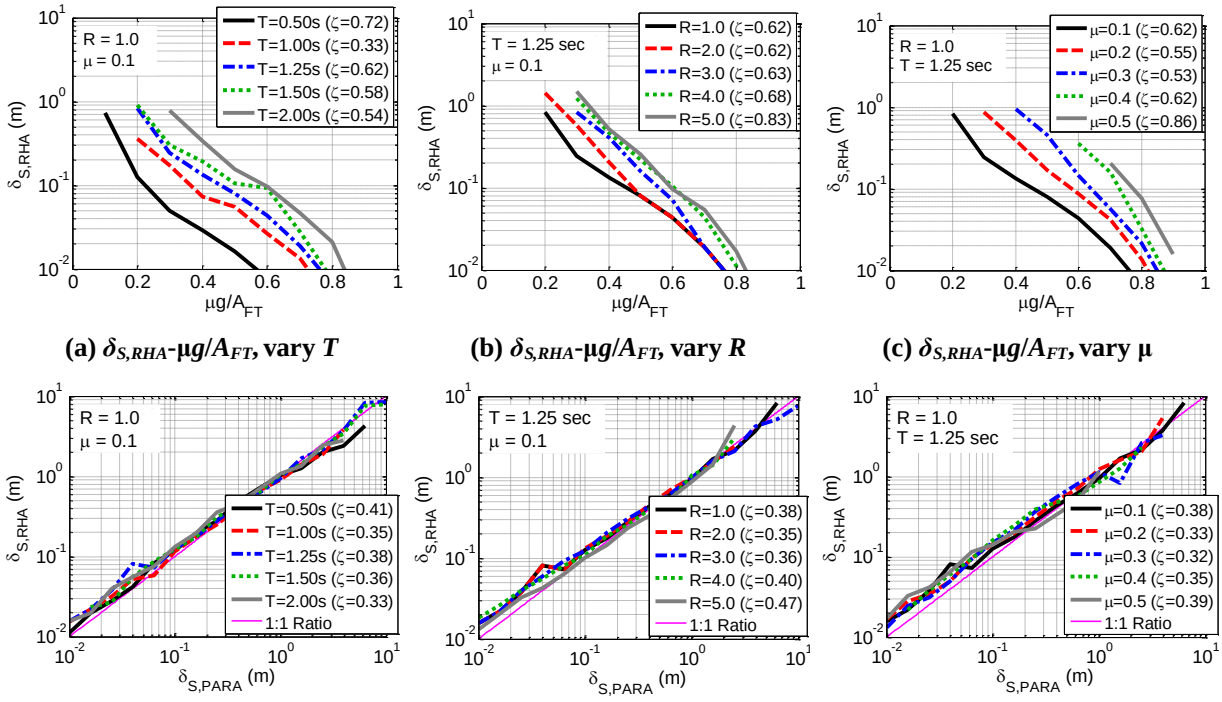

(a) $\delta_{S,RHA}$-μg/A_{FT}, vary T **(b) $\delta_{S,RHA}$-μg/A_{FT}, vary R** **(c) $\delta_{S,RHA}$-μg/A_{FT}, vary μ**

(d) $\delta_{S,RHA}$- $\delta_{S,PARA}$, vary T **(e) $\delta_{S,RHA}$- $\delta_{S,PARA}$, vary R** **(f) $\delta_{S,RHA}$- $\delta_{S,PARA}$, vary μ**

Figure 6.9. Median δ_S-EDP_B relationship for single-storey buildings (dispersion, ζ, in legend)

6.4. CONTENT SLIDING IN MULTI-STOREY BUILDINGS

6.4.1 Building Response

The 10% in 50 year A_{FT} and V_{FT} response of the multi-storey buildings are shown in **Figures 6.10** and **6.11**, respectively. It can be seen from **Figures 6.10a-6.10c** that the A_{FT} response of the multi-storey buildings decreased with R (i.e. increases with strength) on all floors for a given T for the 3, 6, and 10 storey buildings, respectively. A_{FT} also decreases with T (i.e. increases with stiffness) over the top few floors of the building, regardless if the building was designed to be strong (i.e. R = 1.0 in **Figures 6.10d-6.10f**), or weak (i.e. R = 5.0 in **Figures 6.10g-6.10i**). These are consistent with the single-storey building response in **Figure 6.6a**, and was again due to: (i) filtering of high frequency ground motion content in flexible buildings, and (ii) capping of inertia forces and accelerations in weaker buildings.

Interestingly, A_{FT} increases with T over the lower floors of the building; particularly for taller structures. This was due to the increasing contribution of the building's second mode in taller buildings, which for the 10 storey building: (i) peaks around the 4th floor, and (ii) has a

period 0.17 times that of the first mode period. In particular, the second mode period of an elastic 0.5 s and a 2.0 s building are 0.085 s and 0.34 s, respectively; and the equivalent spectral accelerations at these periods are 0.79 g and 1.10 g, respectively, using the median GCIM curve from **Figure 6.4b**. Thus, the second mode total acceleration response of a more flexible building may be greater than that of a stiffer building, despite the first mode response being lower (0.95 g and 0.40 g for T = 0.5 s and 2.0s building, respectively). This shows that A_{FT} is not necessarily larger in stiffer buildings on all floors.

The 10% in 50 year V_{FT} response of the multi-storey buildings also decreased with R on all floors for a given T, as shown in **Figures 6.11a-6.11c** for the 3, 6, and 10 storey buildings, respectively. However, V_{FT} generally increases with T within strong buildings (R = 1.0), particularly for the 3 and 6 storey buildings in **Figures 6.11d-6.11e**, respectively. Interestingly, the 10 storey building trends in **Figure 6.11f** was different as the T = 2.00 s building had a lower V_{FT} compared to the T = 1.00, 1.25, and 1.50 s buildings. These findings were consistent with the R = 1.0 single-storey buildings' in **Figure 6.6b**, where V_{FT} increased with T until approximately 1.00s, which was the period range of the 3 and 6 storey buildings considered and explains the V_{FT} rends observed in those cases. V_{FT} then decreased afterwards which matched the T = 2.00 s 10-storey building findings.

The V_{FT} response in weaker buildings (R = 5.0) from **Figures 6.11g-6.11i** decreases with T, though this effect was more pronounced in the 10-storey building. This was also consistent with single-storey buildings' findings in **Figure 6.6b**, where V_{FT} decreased with T for R = 5.0. As the difference in fundamental building periods was smaller for shorter buildings, the difference in V_{FT} would also be smaller compared to those from taller buildings.

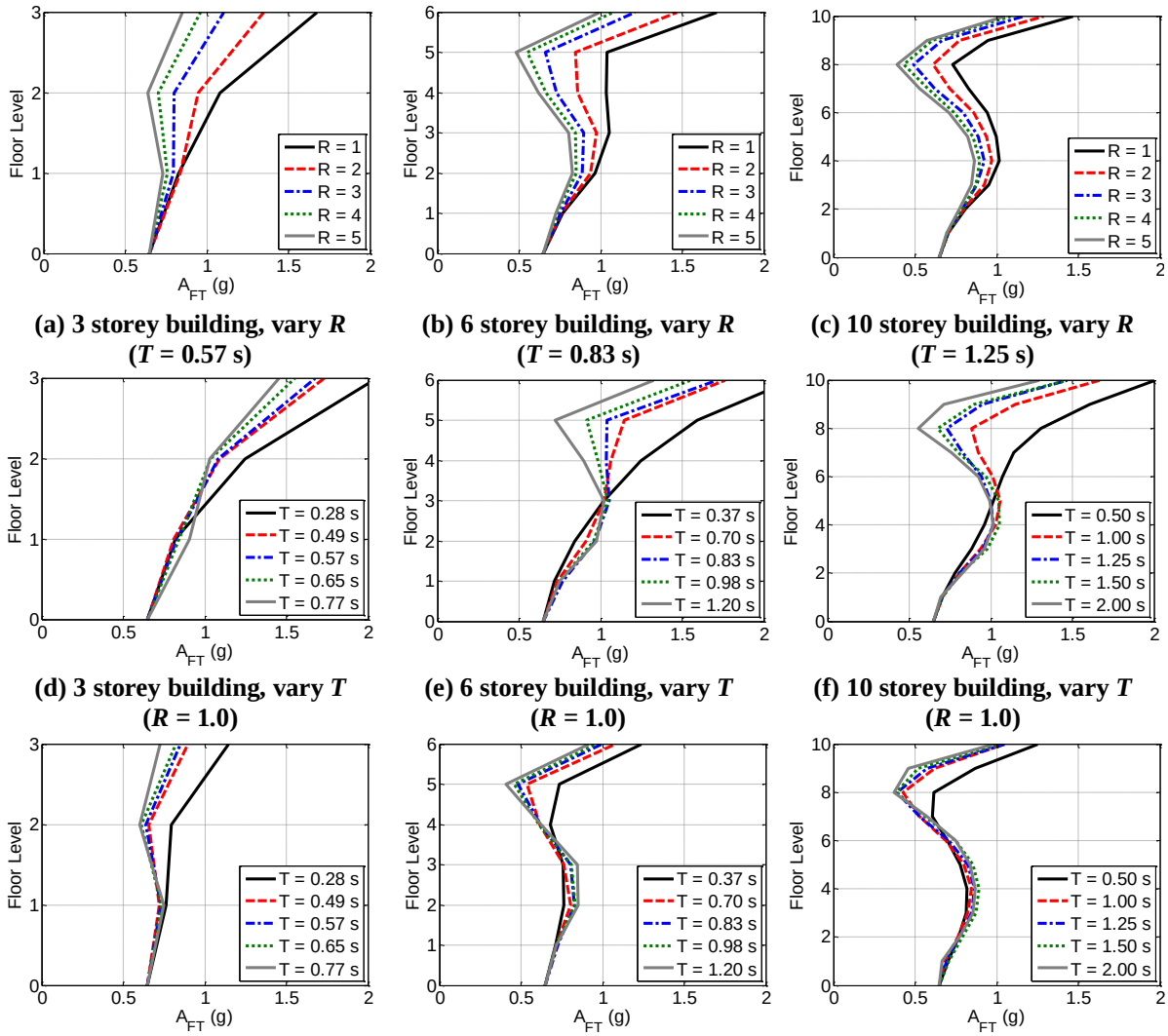

(a) 3 storey building, vary *R* (*T* = 0.57 s) **(b) 6 storey building, vary *R* (*T* = 0.83 s)** **(c) 10 storey building, vary *R* (*T* = 1.25 s)**

(d) 3 storey building, vary *T* (*R* = 1.0) **(e) 6 storey building, vary *T* (*R* = 1.0)** **(f) 10 storey building, vary *T* (*R* = 1.0)**

(g) 3 storey building, vary *T* (*R* = 5.0) **(h) 6 storey building, vary *T* (*R* = 5.0)** **(i) 10 storey building, vary *T* (*R* = 5.0)**

Figure 6.10. 10% probability of exceedance in 50 years peak total floor acceleration response for multi-storey building cases

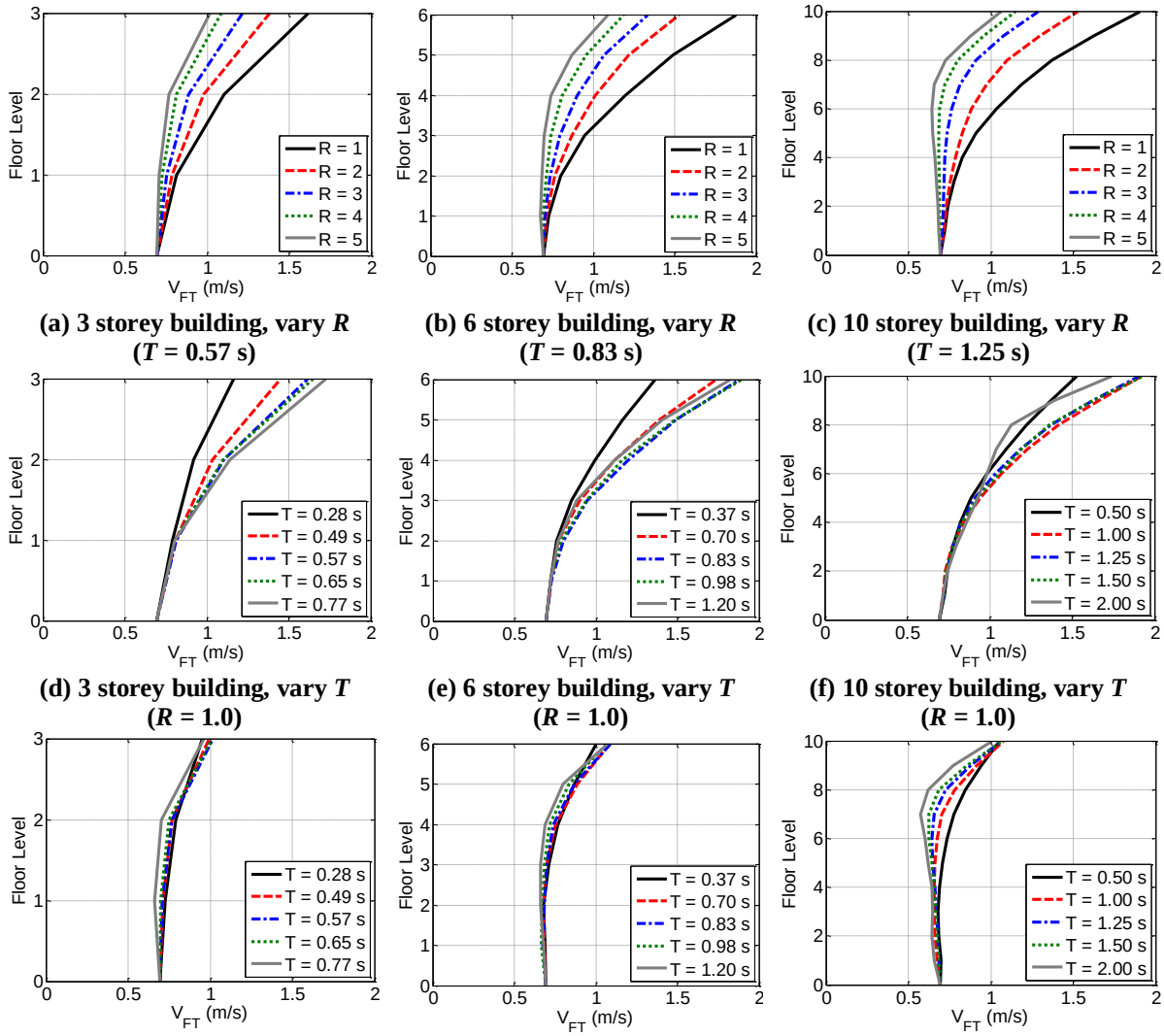

(a) 3 storey building, vary *R* (*T* = 0.57 s) **(b) 6 storey building, vary *R* (*T* = 0.83 s)** **(c) 10 storey building, vary *R* (*T* = 1.25 s)**

(d) 3 storey building, vary *T* (*R* = 1.0) **(e) 6 storey building, vary *T* (*R* = 1.0)** **(f) 10 storey building, vary *T* (*R* = 1.0)**

(g) 3 storey building, vary *T* (*R* = 5.0) **(h) 6 storey building, vary *T* (*R* = 5.0)** **(i) 10 storey building, vary *T* (*R* = 5.0)**

Figure 6.11. 10% probability of exceedance in 50 years peak total floor velocity response for multi-storey buildings

6.4.2 Content Response

The 10% in 50 year $\delta_{S,RHA}$ response for μ = 0.1 is shown in **Figure 6.12**. It can be seen from **Figures 6.12a** to **6.12c** for the 3, 6, and 10-storey building, respectively, that $\delta_{S,RHA}$ decreases with R regardless of building height. This was due to the greater A_{FT} and V_{FT} response as observed previously for the single-storey buildings.

For strong buildings (i.e. R = 1.0) and μ = 0.1, increasing stiffness results in (i) similar $\delta_{S,RHA}$ over the bottom half of the building, and (ii) $\delta_{S,RHA}$ increasing with T on upper floors in most cases, as observed in **Figures 6.12d** to **6.12f** for the 3, 6, and 10-storey building, respectively. The former observation was due to A_{FT} and V_{FT} being similar over the bottom

half of the building, as observed in **Figures 6.10** and **6.11**, respectively. Over the top half of the building however, A_{FT} of stiffer buildings is considerably higher than 3.3μ*g*. As such, the normalized peak sliding displacement would be considerably smaller. In addition, V_{FT} is generally lower for stiffer buildings when R = 1.0. Both of these factors combined resulted in $\delta_{S,RHA}$ being lower for stiffer buildings in this case.

Building height appears to have an effect on $\delta_{S,RHA}$ when varying stiffness in weak buildings (i.e. R = 5.0) for μ = 0.1. The $\delta_{S,RHA}$ response is similar among all cases for the 3-storey building in **Figure 6.12g**. However, stiffer buildings tend to have the largest $\delta_{S,RHA}$ as the building height increases as shown in **Figure 6.12i**. This was because while V_{FT} decreases with T in weaker buildings, the difference between V_{FT} for the 10-storey building was greater due to the larger range of T considered as observed in **Figure 6.11i**; resulting in a greater difference in $\delta_{S,RHA}$ for taller buildings.

The 10% in 50 year $\delta_{S,RHA}$ response for μ = 0.3 is shown in **Figure 6.13**. As with the μ = 0.1 case, $\delta_{S,RHA}$ decreases with R regardless of building height as observed from **Figures 6.13a** to **6.13c**. In addition, $\delta_{S,RHA}$ still tends to increase with T for the 3 and 6-storey R = 1.0 buildings as observed in **Figures 6.13d** and **6.13e**, respectively. For the 10-storey R = 1.0 building case in **Figure 6.13f** however, it can be seen that the most flexible building has the lowest $\delta_{S,RHA}$ overall. This was because (i) A_{FT} is less than 3.3μ*g* on most floors as observed in **Figure 6.10f**, resulting in the normalized peak sliding displacement decreasing with T, and (ii) a lower V_{FT} response as discussed previously from **Figure 6.11f**.

For the R = 5.0 buildings considering μ = 0.3 in **Figures 6.13g** to **6.13i**, it can be seen that $\delta_{S,RHA}$ decreases with T, though the size and difference in $\delta_{S,RHA}$ between the various cases was small. The former observation was due to A_{FT} and V_{FT} being larger for stiffer buildings on upper floors, resulting in larger $\delta_{S,RHA}$. The latter was due to A_{FT} being much

lesser than 3.3μ*g* on most floors as observed in **Figures 6.10g** to **6.10i** for the 3, 6, and 10-storey building, respectively, resulting in smaller normalized peak sliding displacements.

Based on these observations, the content's response are consistent with background theory discussed previously (see **Figure 6.2**), and are therefore reasonable.

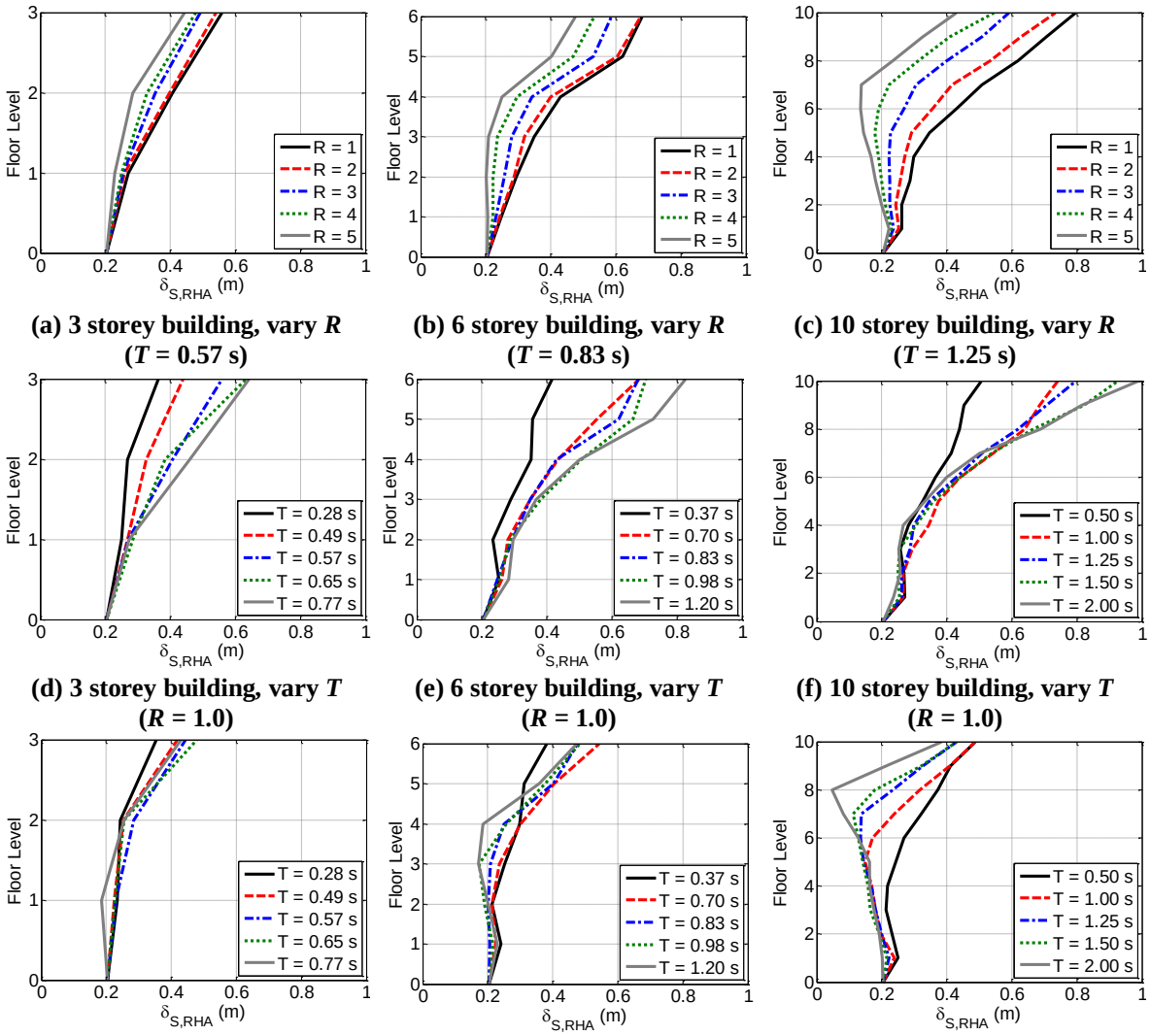

(a) 3 storey building, vary *R* (*T* = 0.57 s) **(b) 6 storey building, vary *R* (*T* = 0.83 s)** **(c) 10 storey building, vary *R* (*T* = 1.25 s)**

(d) 3 storey building, vary *T* (*R* = 1.0) **(e) 6 storey building, vary *T* (*R* = 1.0)** **(f) 10 storey building, vary *T* (*R* = 1.0)**

(g) 3 storey building, vary *T* (*R* = 5.0) **(h) 6 storey building, vary *T* (*R* = 5.0)** **(i) 10 storey building, vary *T* (*R* = 5.0)**

Figure 6.12. 10% probability of exceedance in 50 years peak sliding displacement for multi-storey buildings (μ = 0.1)

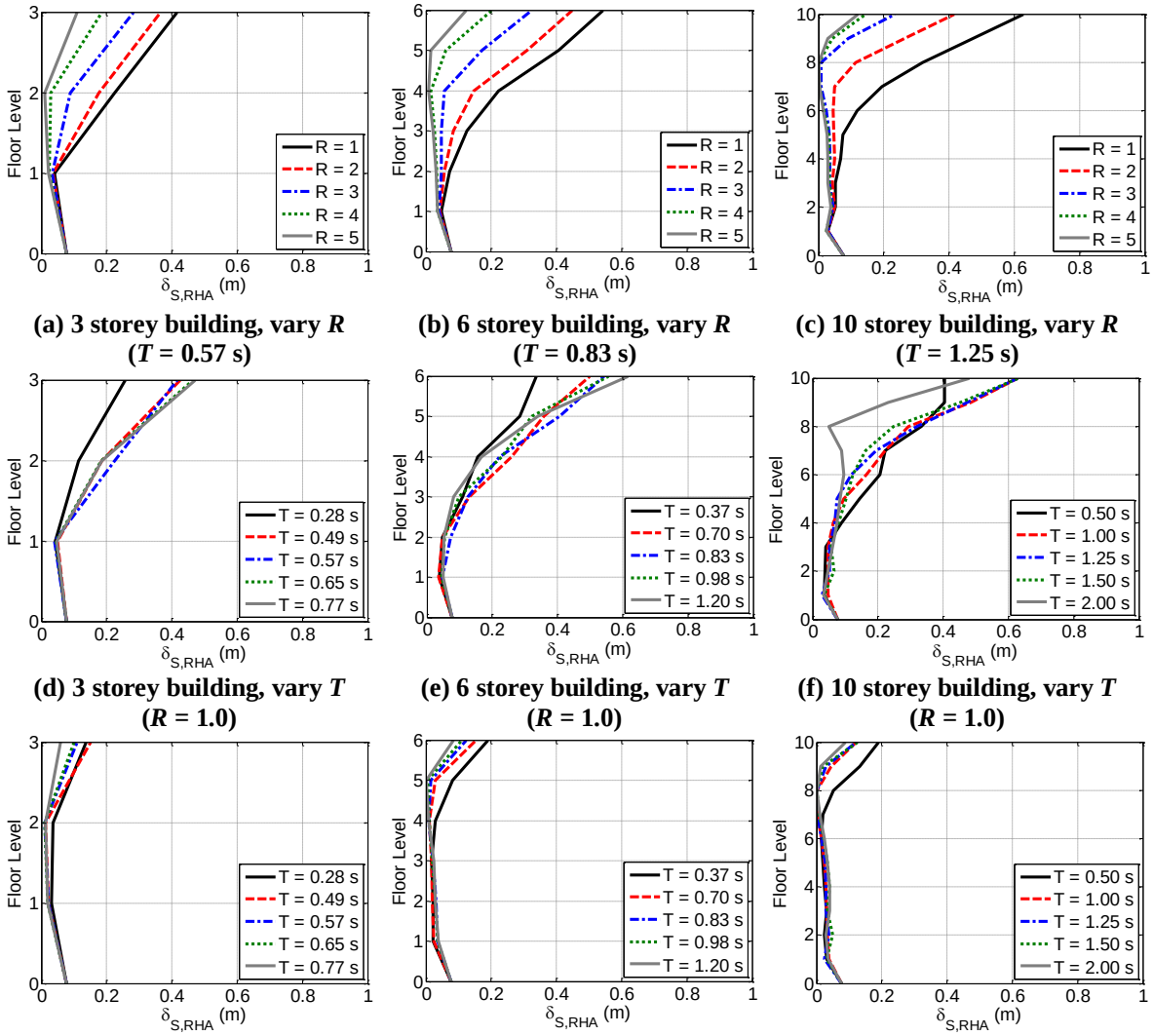

(a) 3 storey building, vary *R* (*T* = 0.57 s) **(b) 6 storey building, vary *R* (*T* = 0.83 s)** **(c) 10 storey building, vary *R* (*T* = 1.25 s)**

(d) 3 storey building, vary *T* (*R* = 1.0) **(e) 6 storey building, vary *T* (*R* = 1.0)** **(f) 10 storey building, vary *T* (*R* = 1.0)**

(g) 3 storey building, vary *T* (*R* = 5.0) **(h) 6 storey building, vary *T* (*R* = 5.0)** **(i) 10 storey building, vary *T* (*R* = 5.0)**

Figure 6.13. 10% probability of exceedance in 50 years peak sliding displacement for multi-storey buildings (μ = 0.3)

6.4.3 Relationship between Content and Building Response

The median $\delta_{S,RHA}$-μ/A_{FT} relationship for varying R, T, μ, and floor level using analytical findings from all 440 ground motion record components are shown in **Figure 6.14**. It can be seen from **Figures 6.14a** to **6.14c** that $\delta_{S,RHA}$-μ/A_{FT} was consistent regardless of R when μ/A_{FT} was greater than 0.4 for the 3, 6, and 10 storey building, respectively. This was because the building and content response is identical in buildings of the same period until yielding occurs. In contrast, the $\delta_{S,RHA}$-μ/A_{FT} relationship was vastly different for varying T (**Figures 6.14d** to **6.14f**) and μ (**Figures 6.14g** to **6.14i**). The $\delta_{S,RHA}$-μ/A_{FT} relationship for different floors of the building appear to be consistent within the 3 and 6 storey buildings, as

shown in **Figures 6.14j-6.14k**, respectively; but has greater variation in the 10-storey building.

In contrast, the $\delta_{S,RHA}$-$\delta_{S,PARA}$ relationship was consistent regardless of R, T, μ, and floor level as shown in **Figure 6.15**. However, the estimate of $\delta_{S,PARA}$ from **Eq. 6.1** is slightly under-conservative by an average of 14% for the 3 and 6 storey building, and 17% for the 10 storey building. This could be due to the assumption made in the derivation of **Eq. 6.1** of A_{FT}/V_{FT} being a reasonable substitute for the dominant frequency of total floor excitation, ω_T; which may not be applicable to buildings sensitive to higher-order mode effects.

It should also be noted that the mean ζ of the $\delta_{S,RHA}$-μ/A_{FT} and the $\delta_{S,RHA}$-$\delta_{S,PARA}$ relationships were 0.80 and 0.43, respectively; and that the number of floors in the building does not appear to have noticeable effects on the latter. This again showed $\delta_{S,PARA}$ from **Eq. 6.1** is more sufficient and efficient compared to considering A_{FT} alone, and that **Eq. 6.1** should be used instead to predict the content's sliding response.

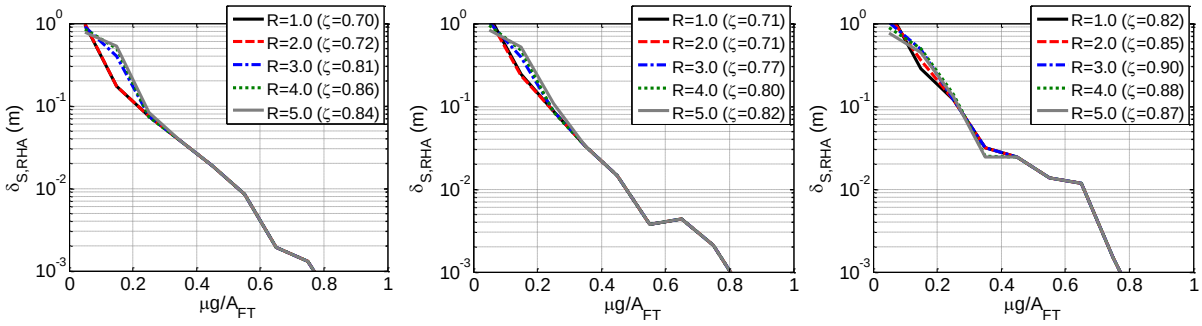

(a) 3 storey building, vary *R* (*T* = 0.57 s, μ = 0.1, Floor 3) **(b) 6 storey building, vary *R* (*T* = 0.83 s, μ = 0.1, Floor 6)** **(c) 10 storey building, vary *R* (*T* = 1.25 s, μ = 0.1, Floor 10)**

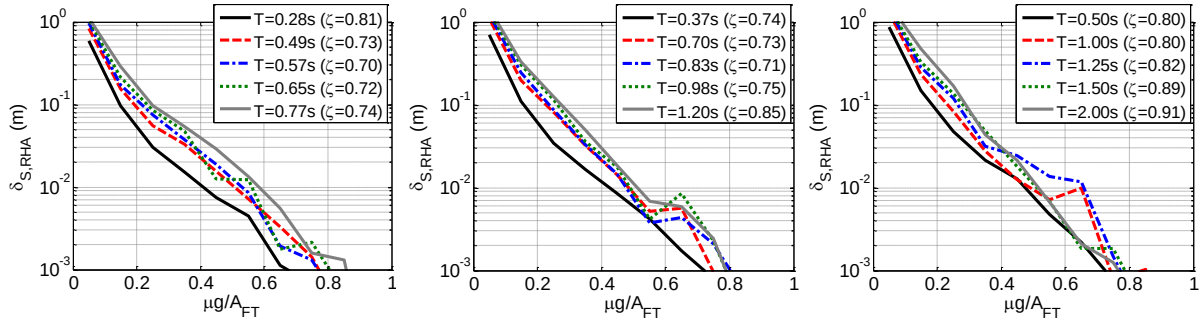

(d) 3 storey building, vary *T* (*R* = 1.0, μ = 0.1, Floor 3) **(e) 6 storey building, vary *T* (*R* = 1.0, μ = 0.1, Floor 6)** **(f) 10 storey building, vary *T* (*R* = 1.0, μ = 0.1, Floor 10)**

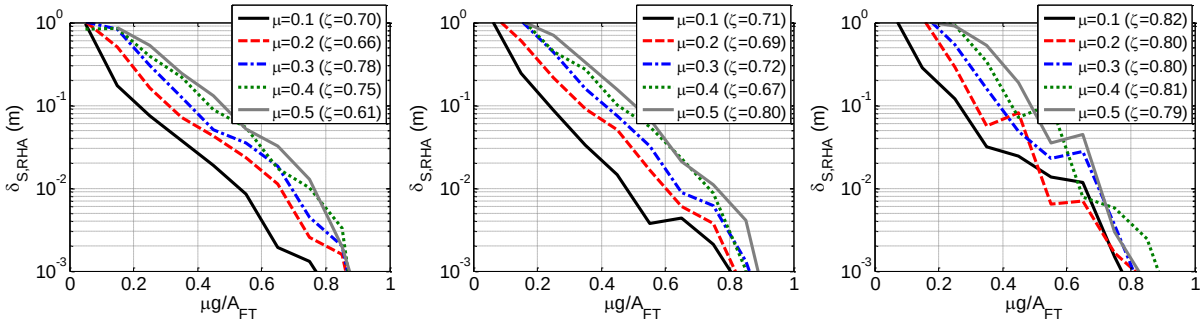

(g) 3 storey building, vary μ (*T* = 0.57 s, *R* = 1.0, Floor 3) **(h) 6 storey building, vary μ (*T* = 0.83 s, *R* = 1.0, Floor 6)** **(i) 10 storey building, vary μ (*T* = 1.25 s, *R* = 1.0, Floor 10)**

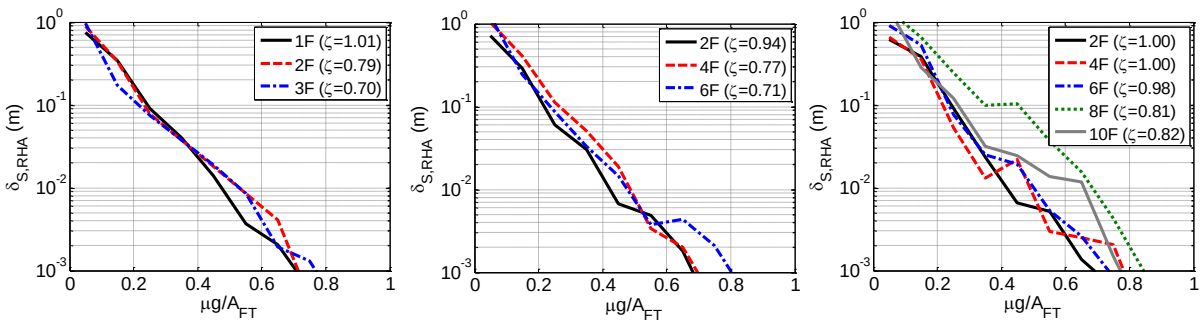

(j) 3 storey building, vary floor (*T* = 0.57 s, *R* = 3.0, μ = 0.1) **(k) 6 storey building, vary floor (*T* = 0.83 s, *R* = 1.0, μ = 0.1)** **(l) 10 storey building, vary floor (*T* = 1.25 s, *R* = 1.0, μ = 0.1)**

Figure 6.14. Median $\delta_{S,RHA}$ -$\mu g/A_{FT}$ relationship for multi-storey buildings (dispersion given in legend)

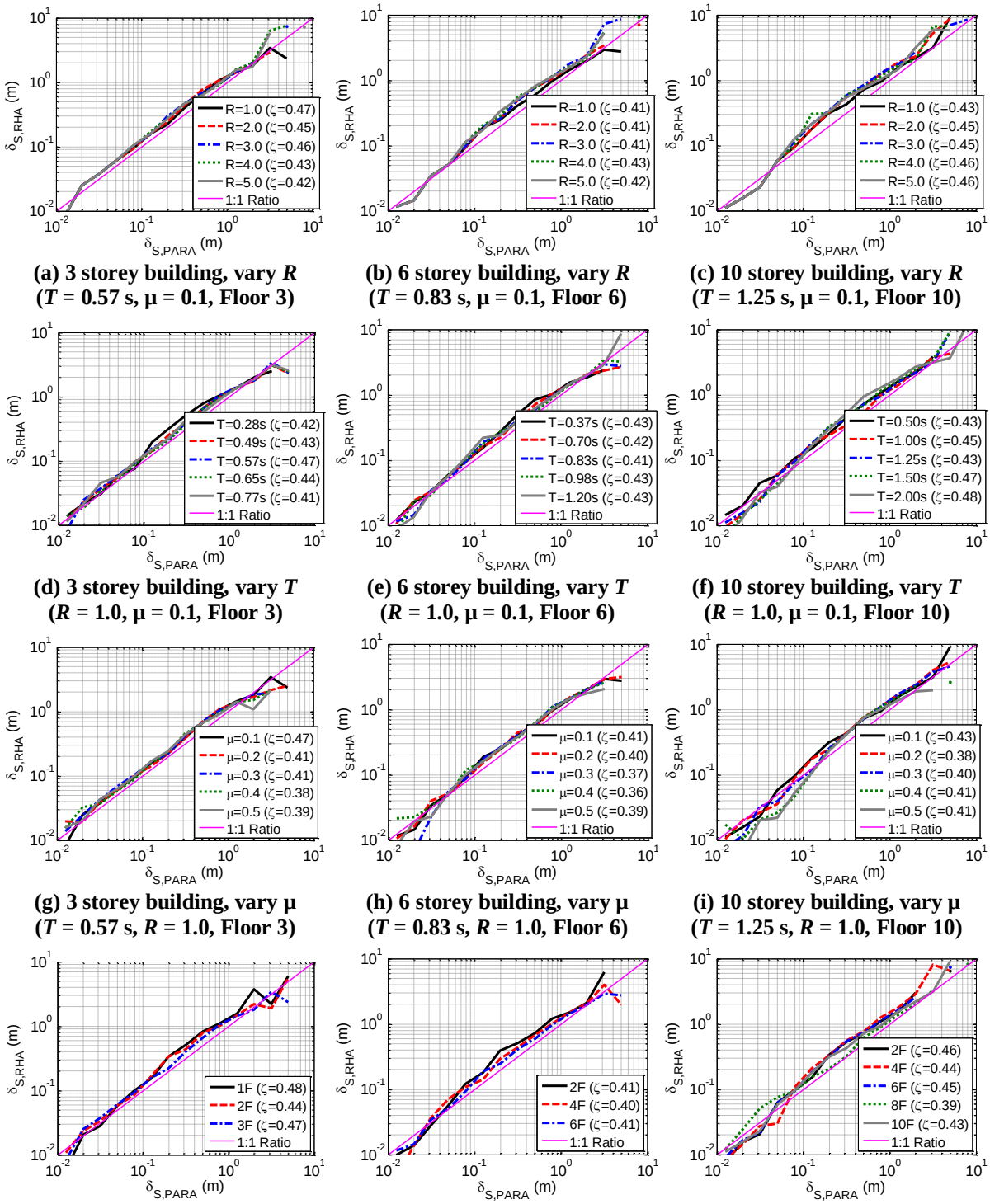

(a) 3 storey building, vary *R* (*T* = 0.57 s, μ = 0.1, Floor 3)

(b) 6 storey building, vary *R* (*T* = 0.83 s, μ = 0.1, Floor 6)

(c) 10 storey building, vary *R* (*T* = 1.25 s, μ = 0.1, Floor 10)

(d) 3 storey building, vary *T* (*R* = 1.0, μ = 0.1, Floor 3)

(e) 6 storey building, vary *T* (*R* = 1.0, μ = 0.1, Floor 6)

(f) 10 storey building, vary *T* (*R* = 1.0, μ = 0.1, Floor 10)

(g) 3 storey building, vary μ (*T* = 0.57 s, *R* = 1.0, Floor 3)

(h) 6 storey building, vary μ (*T* = 0.83 s, *R* = 1.0, Floor 6)

(i) 10 storey building, vary μ (*T* = 1.25 s, *R* = 1.0, Floor 10)

(j) 3 storey building, vary floor (*T* = 0.57 s, *R* = 3.0, μ = 0.1)

(k) 6 storey building, vary floor (*T* = 0.83 s, *R* = 1.0, μ = 0.1)

(l) 10 storey building, vary floor (*T* = 1.25 s, *R* = 1.0, μ = 0.1)

Figure 6.15. Median $\delta_{S,RHA}$- $\delta_{S,PARA}$ relationship for multi-storey buildings (dispersion given in legend)

6.5 APPLICATION TO BUILDING USAGE TYPES

The discussions up to this point had been on the effect of building structural properties on content sliding. Knowing this information, the concepts can be applied to several building usage types to qualify the best design approach to reduce content sliding.

Buildings of high importance, such as hospital buildings, are generally designed to be stronger to limit yielding and damage to structural elements. Furthermore, the building may be significantly stronger than designed due to conservatism as observed in steel buildings during the 2011 February earthquake in Canterbury, New Zealand. In hospitals, much of the contents are on casters which are usually left unlocked for mobility reasons [12], resulting in μ being approximately 0.1 or less [6]. Hence, designing the building to be as stiff as possible would reduce the content sliding response (see **Figures 6.12d** to **6.12f**). Even if μ is greater than 0.1 in strong buildings, such as that due to the possibility of the content's wheels changing direction during shaking, $\delta_{S,RHA}$ in stiffer buildings should still be lower than that of more flexible buildings (see **Figures 6.13d** to **6.13f**) in most cases. The exception to this would be for the most flexible 10-storey in **Figure 6.13f**, which indicates that the benefits of increasing the building's stiffness may diminish with increasing building height.

Buildings of lower importance, such as office buildings, are generally designed to be weaker. These buildings have a larger proportion of contents without casters, such as desks, where μ is between 0.3 to 0.5 as observed in **Chapter 4** (**Section 4.4.2**). For cases where μ is greater than 0.3, δ_S was similar on most floors as shown in **Figures 6.13g** to **6.13i**, but was up to 0.10 m greater over the top few floors in stiffer buildings. If the contents are on casters, increasing the building's stiffness would not cause δs to increase for most floors, and δs may even be lower towards the top of the building as shown in **Figures 6.12g** to **6.12i**. As such, increasing stiffness will not result in significantly more severe content sliding in most cases for buildings of lower importance.

Note that while this study shows that stronger buildings are likely to incur higher content response, this does not vindicate that weaker buildings should be designed for in general on its own. Other factors, such as the extent of drift-related damage, the need for demolition after strong shaking, and the potential for collapse should also be considered. It should also be noted that the higher A_{FT} response of stiffer buildings may lead to greater damage of brittle acceleration-sensitive components, such as some ceiling systems; and thus a balancing act is required to limit acceleration-related damage and the movement of building contents.

6.6 DESIGN APPLICATIONS

Consideration of content sliding in design is important as these can impact against occupants, and/or block egress paths which hinder the ability of occupants to safely leave a building following major shaking. To limit these consequences, contents can either be sufficiently restrained, or be provided with sufficient room to slide without hindering others. For the latter approach, a minimum safe distance between large building contents and egress routes can be estimated in the following three steps:

1. Estimate the building's A_{FT} and V_{FT} response.
2. Use **Eq. 6.1** to predict the median sliding displacement, $\delta_{S,PARA}$.
3. Obtain the design sliding displacement, $\delta_{S,DES}$, by considering the dispersion in the parametric equation and selecting a target percentile value. Note that a factor of 1.17 was included to account for possible under-conservatism as observed in **Figure 6.15**.

A dispersion of 0.43 was assumed for the final step. This was based on the average dispersion from **Figure 6.15**. $\delta_{S,DES}$ can then be calculated using **Eq. 6.6**, where Z denotes the number of standard deviations $\delta_{S,DES}$ is from $\delta_{S,PARA}$ on a natural log scale. Z can be read from probability tables to obtain the target percentile (e.g. $Z = 1.65$ for the 95^{th} percentile).

$$\delta_{S,DES} = \exp(\ln(1.17\delta_{S,PARA}) + 0.43Z) \quad \textbf{(6.6)}$$

A design example considering a 10-storey wall building designed for post-2011 earthquake Christchurch, New Zealand, subsoil class D conditions with R = 4 and T = 1.25 s is discussed here. If a single content with μ = 0.1 in the building should have an 84% chance of not blocking any escape paths in an event similar to the 2011 February earthquake in Christchurch, the design checks would be as follows:

Step 1: Response history analysis of the building was performed to predict A_{FT} and V_{FT} using the four recordings from the 2011 February earthquake closest to the central business district; the Christchurch Botanic Gardens (CBGS), Christchurch Cathedral College (CCCC), Christchurch Hospital (CHHC), and Christchurch Resthaven (REHS) records [43]. The mean A_{FT} and V_{FT} response on the 10th floor of the building, where the movement of contents was most severe based on **Figure 6.13**, was 0.83g and 1.29 m/s respectively. Note that an alternate method to predict A_{FT} would be to use recommendations available in seismic codes, and simple approaches to predict V_{FT} can be developed for similar usage.

Step 2: $\delta_{S,PARA}$ would be 0.46 m using **Eq. 6.1** based on A_{FT} and V_{FT} from the first step.

Step 3: Based on **Eq. 6.6**, along with Z = 1.0 to obtain an 84th percentile value, $\delta_{S,DES}$ would be 0.83 m, which implies that larger building contents should be placed at least 0.83 m away from egress routes. If content sliding analysis is performed using the four ground motion records, the mean sliding displacement would be 0.58 m, which shows that this design approach is conservative.

6.7 CONCLUSION

Response history analyses of content sliding in inelastic reinforced-concrete wall buildings were performed for subsoil class C conditions in Wellington, New Zealand, to assess the influence of building properties on the response of contents. It was found that:

1. Increasing the building's stiffness causes $\delta_{S,RHA}$ to decrease in strong buildings with low friction coefficients, μ. However, the effectiveness of increasing stiffness to minimize $\delta_{S,RHA}$ decreases with increasing building height, *T*, *R*, and μ. While $\delta_{S,RHA}$ may increase if the building's stiffness was increased in the latter cases, the size of $\delta_{S,RHA}$ was small, and the difference between different stiffness cases were minor.
2. Increasing the building's strength by decreasing the force reduction factor, *R*, caused an increase in $\delta_{S,RHA}$. This was true for all cases considered, and showed that contents in stronger buildings will likely experience more severe sliding response.
3. The findings were similar regardless of the number of floors in the building, though the benefit of increasing stiffness in strong buildings diminishes with increasing building height. In addition, the content's response in taller buildings tends to be slightly influenced by higher-order mode effects.
4. **Eq. 6.1**, which was developed for elastic single-degree-of-freedom buildings, was efficient and sufficient to estimate the maximum sliding displacement of contents within yielding single-storey buildings.
5. **Eq. 6.1** provided a slightly under-conservative (by up to 17%) estimate of the median analytical response of yielding multi-storey buildings. The error appears to increase slightly with building height. Nonetheless, the equation was still more efficient compared to considering A_{FT} alone.

6. A three step design procedure was proposed to estimate the maximum content sliding displacement. An example using the 2011 February Canterbury earthquakes was provided.
7. Increasing the stiffness of buildings of high importance results in decreased content sliding response in most cases, particularly for shorter buildings and contents with low friction coefficients. In weaker buildings of lower importance and contents with higher friction coefficients, contents within stiffer buildings do incur higher sliding response. However, the differences in the peak sliding displacements across the different cases for weaker buildings are generally small. As such, designing for stiffer buildings have the potential to limit content sliding response for buildings of high importance, and does not result in more severe response for buildings of lower importance.

6.8 REFERENCES

1. Freeman, J. R. (1932). Earthquake Damage and Earthquake Insurance. New York, US: McGraw-Hill.
2. Berg, G. V. (1983). Seismic Design Codes and Procedures (Vol. 6). Berkeley, California, US: Earthquake Engineering Research Institute.
3. Bull, D. K. (1991). Evaluation of a 10-storey building using alternative structural systems. Journal of the Cement and Concrete Association of New Zealand, 35, 2-16.
4. Yeow, T. Z., MacRae, G. A., Dhakal, R. P., & Bradley, B. A. (2012). Seismic Sustainability Assessment of Structural Systems: Frame or Wall Structures? Paper presented at the 15th World Conference on Earthquake Engineering, Lisbon, Portugal.
5. Nagao, T., Kagano, H., & Hamaguchi, K. (2012). Full-Scale Shaking Table Test on Furnitures subjected to Long-Period Earthquake Motions. Paper presented at the 15th World Conference on Earthquake Engineering, Lisbon, Portugal.
6. Sato, E., Furukawa, S., Kakehi, A., & Nakashima, M. (2011). Full-scale shaking table test for examination of safety and functionality of base-isolated medical facilities. Earthquake Engineering and Structural Dynamics, 40(13), 1435-1453.
7. FEMA E-74. (2012). Reducing the Risks of Nonstructural Earthquake Damage - A Practical Guide.
8. Chong, W. H., & Soong, T. T. (2000). Sliding Fragility of Unrestrained Equipment in Critical Facilities: Department of Civil, Structural and Environmental Engineering, University at Baffalo, New York, US.
9. Hutchinson, T. C., & Chaudhuri, S. R. (2006). Simplified Expression for Seismic Fragility Estimation of Sliding-Dominated Equipment and Contents. Earthquake Spectra, 22(3), 709-732.
10. Garcia, D. L., & Soong, T. T. (2003). Sliding Fragility of Block-Type Non-Structural Components. Part 1: Unrestrained Components. Earthquake Engineering and Structural Dynamics, 32, 111-129.
11. Shao, Y., & Tung, C. C. (1999). Seismic Response of Unanchored Bodies. Earthquake Spectra, 15(3), 523-536.
12. Shi, Y., Kurata, M., & Nakashima, M. (2014). Disorder and damage of base-isolated medical facilities when subjected to near-fault and long-period ground motions. Earthquake Engineering and Structural Dynamics, 43(11), 1683-1701.

13. Lin, S. L., MacRae, G. A., Dhakal, R. P., & Yeow, T. Z. (2015). Building contents sliding demands in elastically responding structures. Engineering Structures, 86, 182-191.
14. Newmark, N. M. (1965). Effects of earthquakes on dams and embankments. Geotechnique, 15(2), 139-160.
15. Choi, B., & Tung, C. C. D. (2002). Estimating Sliding Displacement of an Unanchored Body Subjected to Earthquake Excitation. Earthquake Spectra, 18(4), 601-613.
16. Kaneko, M., Hayashi, Y., & Tamura, K. (1999). Evaluation of Sliding Displacement of Furniture during Earthquake - By using Revised Formula to Estimate Sliding Displacement of Furniture. Technical Papers of Annual Meeting of Architectural Institute of Japan, B-II, 537-538.
17. Konstantinidis, D. A. (2008). Experimental and Analytical Studies on the Seismic Response of Freestanding and Anchored Building Contents. PhD Thesis, Civil and Environmental Engineering, University of California, Berkeley.
18. Chiou, B. S. J., Darragh, R., Gregor, N., & Silva, W. (2008). NGA Project Strong-Motion Database. Earthquake Spectra, 24(1), 23-44.
19. Cornell, C. A., & Krawinkler, H. (2000). Progress and challenges in seismic performance assessment. PEER News, 3(2).
20. Tarbali, K., & Bradley, B. A. (2015). Representative Ground-Motion Ensembles for Several Major Earthquake Scenarios in New Zealand. Bulletin of the New Zealand Society for Earthquake Engineering, 47(4), 231-252.
21. Field, E. H., Jordan, T. H., & Cornell, C. A. (2003). OpenSHA: A Developing Community-Modeling Environment for Seismic Hazard Analysis. Seismological Research Letters, 74(4), 406-419.
22. Stirling, M. W., McVerry, G. H., Gerstenberger, M. C., Litchfield, N. J., Van Dissen, R. J., Berryman, K. R., Barnes, P., Wallace, L. M., Villamor, P., Langridge, R. M., Lamarche, G., Nodder, S., Reyners, M. E., Bradley, B., Rhoades, D. A., Smith, W. D., Nicol, A., Pettinga, J., Clark, K. J., & Jacobs, K. (2012). National seismic hazard model for New Zealand : 2010 update. Bulletin of the Seismological Society of America, 102(4), 1514-1542.
23. Bradley, B. A. (2010). NZ-Specific Pseudo-Spectral Acceleration Ground Motion Prediction Equations based on Foreign Models: Department of Civil and Natural Resources Engineering, University of Canterbury, Christchurch, New Zealand.
24. Bradley, B. A. (2010). A Generalized Conditional Intensity Measure Approach and Holistic Ground Motion Selection. Earthquake Engineering and Structural Dynamics, 39(12), 1324-1342.
25. Bradley, B. A. (2012). A Ground Motion Selection Algorithm Based on the Generalized Conditional Intensity Measure Approach. Soil Dynamics and Earthquake Engineering, 40, 48-61.
26. Ang, A. H. S., & Tang, W. H. (2007). Probability concepts in engineering: Emphasis on applications in civil and environmental engineering: John Wiley & Sons.
27. Gazetas, G., Garini, E., Berrill, J. B., & Apostolou, M. (2012). Sliding and Overturning Potential of Christchurch 2011 Earthquake Records. Earthquake Engineering and Structural Dynamics, 41(14), 1921-1944.
28. Aslam, M., Godden, W. G., & Scalise, D. T. (1975). Sliding Response of Rigid Bodies to Earthquake Motions: University of California, Berkeley.
29. Konstantinidis, D. A., & Nikfar, F. (2014). Seismic response of sliding equipment and contents in base-isolated buildings subjected to broadband ground motions. Earthquake Engineering and Structural Dynamics.
30. Standards New Zealand. (2004). NZS 1170.5:2004, Structural Design Actions Part 5: Earthquake Actions New Zealand: Standards New Zealand, Wellington, New Zealand.
31. Carr, A. J. (2004). Ruaumoko 2D - Inelastic dynamic analysis program. Department of Civil and Natural Resources Engineering, University of Canterbury, Christchurch.
32. Caughey, T. K. (1960). Calssical Normal Modes in Damped Linear Systems. Journal of Applied Mechanics, 27, 269-271.
33. Carr, A. J. (2008). Ruaumoko Manual (Vol. Volumne 2: User Manual for the 2:Dimensional Version Ruaumoko 2D). University of Canterbury, Christchurch, NZ.
34. Tagawa, H. (2005). Towards an understanding of seismic performance of 3D structures: stability & reliability. PhD Thesis, University of Washington, Seattle, USA.
35. Thomsen, J. H., & Wallace, J. W. (2004). Displacement-based design of slender reinforced concrete structural walls - experimental verification. Journal of Structural Engineering, 130(4), 618-630.
36. Wallace, J. W. (2007). Modelling issues for tall reinforced concrete core wall buildings. The Structural Design of Tall and Special Buidlings, 16, 615-632.
37. Saiidi, M., & Sozen, M. A. (1979). Simple and complex models for nonlinear seismic response of reinforced concrete structures. Illinois: University of Illinois.

38. Newmark, N. M. (1959). A Method of Computation for Structural Dynamics. Journal of Engineering Mechanics, 85(EM3), 67-94.
39. Shenton III, H. W., & Jones, N. P. (1992). Base Excitation of Rigid Bodies. Part I: Formulation. Journal of Engineering Mechanics, 117(10), 2286-2306.
40. Chaudhuri, S. R., & Hutchinson, T. C. (2005). Characterizing Frictional Behaviour for use in Predicting the Seismic Response of Unattached Equipment. Soil Dynamics and Earthquake Engineering, 25, 591-604.
41. Chaudhuri, S. R., & Hutchinson, T. C. (2006). Fragility of Bench-Mounted Equipment Considering Uncertain Parameters. Journal of Structural Engineering, 132(6), 884-898.
42. Bradley, B. A., Dhakal, R. P., Cubrinovski, M., MacRae, G. A., & Lee, D. S. (2009). Seismic Loss Estimation for Efficient Decision Making. Bulletin of the New Zealand Society of Earthquake Engineering, 42(2), 96-110.
43. Bradley, B. A., & Cubrinovski, M. (2011). Near-source Strong Ground Motions Observed in the 22 February 2011 Christchurch Earthquake. Seismological Research Letters, 82(6), 853-865.

7. Development of a Building-Specific Injury Prediction Framework

7.0 SUMMARY

A building-specific seismic injury prediction framework which considers injuries due to people falling and movement of building contents (i.e. furniture) is proposed. The framework implements: (i) a weighting system to spatially distribute occupants; (ii) methods to quantify impact velocity on occupants arising from people falling or being stuck by contents; and (iii) injury severity and costs models. The framework is applied to a 10-storey office building considering various office room layouts to demonstrate its usage. Based on the assumptions made, the findings with regards to injury severity and cause were consistent with injury data collected from the 1994 Northridge and 2011 Canterbury events in terms of breakdown of injuries by severity and cause. Application of the framework for (i) deriving injury rates for use in less sophisticated injury models such as that used in HAZUS®, and (ii) assessing the feasibility of injury mitigation strategies, are demonstrated.

7.1 INTRODUCTION

Injuries and deaths, damage repair costs, and downtime, are often considered to be the major sources of loss in earthquake-related loss estimations [1]. For injuries and deaths, the potential socioeconomic impact includes treatment and rehabilitation costs, loss of productivity and efficiency, and the decreased quality of life for serious injury survivors [2].

Causes and severity of indoor injuries occurring due to building damage (excluding secondary hazards and other causes) may be summarized by the event tree shown in **Figure 7.1**, where the building's global damage state has an influence on the resultant injuries. For example, occupants may be trapped under rubble during building collapse, which may result

in instant deaths or delays in receiving medical treatment. In cases where the building did not collapse, injuries may be caused by the occupant being hit by objects (i.e. building contents, spalling concrete, ceiling tiles), loss of balance resulting in people falling, or from action-related injuries (i.e. injuries resulting from people taking evasive action during shaking). These sources may result in injuries of varying severity from minor (i.e. self-aid treatment) to fatal. Building-related injuries may also occur to those outside the building, such as the threat of exterior bricks falling onto passersby.

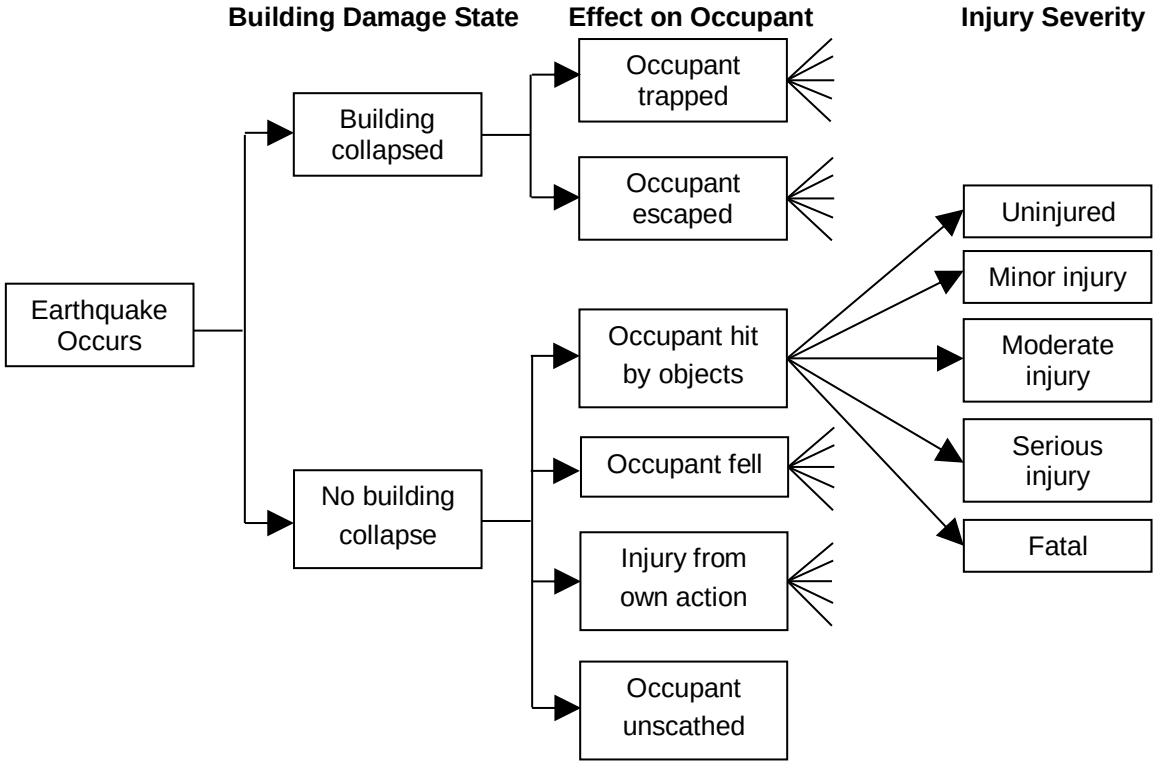

Figure 7.1. Event diagram for indoor injuries directly caused by building damage occurring during earthquakes and excludes secondary factors and other causes [3, 4]

Models to predict the number of fatalities during earthquakes exist. However, the majority of earthquake-related injuries in structures designed to modern seismic codes are non-fatal [5]. This is due to improving engineering practice which results in increasing rarity of building collapse, which is historically the major cause of fatalities [6, 7]. Non-fatal injuries may therefore have a larger contribution to the total injury-related losses. For example, Porter et al. [8] estimated that non-fatal injuries accounted for 96% of the total

injury costs during the 1994 Northridge earthquake; including medical treatment cost, decrease in quality of life, among others.

Majority of non-fatal injuries result from people (i) losing balance and falling over, or (ii) being struck by moving building contents (i.e. furniture) [9-15]. These sources should therefore be explicitly considered for better estimates of injury-related losses. However, few injury prediction methods considers these sources, and/or did not consider injury severity or cost. To address these needs, an injury prediction framework considering these factors is developed in this chapter, and then applied to a 10-storey reinforced concrete cantilever wall office building to demonstrate its usage. Answers to the following are sought:

1. What has been done to address non-fatal injuries in the past?
2. How does the new injury prediction framework improve upon existing methods?
3. How do the framework outputs compare against historical injury data and less advanced models?
4. What are the applications of the model?

7.2 LITERATURE REVIEW

7.2.1 Existing Injury Prediction Methods ignoring Room Interior

One of the more widely used approaches for predicting injury is the Cambridge University Casualty Model [7] for regional-scale modelling. In its original form, the model estimates the number of deaths resulting from building collapse for a particular building class *b*, K_{Sb}, using **Eq. 7.1**. Here, D_b is the number of buildings of class *b* that collapsed during a shaking event, $M1_b$ is the population occupying building class *b* assuming full occupation, $M2_b$ is the percentage of full occupancy at time of shaking, $M3_b$ is the percentage of present occupants trapped by collapse, $M4_b$ is the percentage of occupants killed outright at time of collapse, and $M5_b$ is the percentage of occupants who later died. Similar regional-level

models exists [16-21], and a building-specific version had been proposed by Mitrani-Reiser [22].

$$Ks_b = D_b\left[M1_b \times M2_b \times M3_b \times (M4_b + M5_b)\right] \quad \textbf{(7.1)}$$

More recent approaches however use datasets which consider other levels of injury severity. Examples of such databases includes those from ATC-13 [23], Seligson et al. [24], Cambridge University Earthquake Damage Database [25], and HAZUS® [4]. These were provided for various levels of global building damage, ranging from slight (i.e. superficial cracks) to complete-collapse (i.e. loss of gravity load carrying capacity). An example of pre-defined injury rates is shown in **Table 7.1** for reinforced-concrete wall buildings from HAZUS® [4]. Note that the drift limits listed in **Table 7.1** were obtained from FEMA 356 [26] rather than HAZUS® [4], as the latter assumed that structural walls can exhibit the same drift response as frame members. This is despite the tension reinforcing within wall members exhibiting larger strains at the same level of drift compared to frame members, leading to earlier failure.

Table 7.1. Injury probability for reinforced concrete wall and frame buildings [4]

	Drift limits		**Injury severity level**			
Global damage state	**Walls (%)**	**Frames (%)**	**Minor (%)**	**Moderate (%)**	**Serious (%)**	**Fatal (%)**
Slight	0.25	0.50	0.05	0	0	0
Moderate	0.50	1.00	0.25	0.03	0	0
Extensive	1.00	2.00	1	0.1	0.001	0.001
Complete-no collapse	2.00	4.00	5	1	0.01	0.01
Complete-collapse			40	20	5	10

A limitation of these datasets are that they are derived based on scarce regional-level historical data, such as the ratio of non-hospitalized to hospitalized injury numbers over a region [4]. The variation in injury rates at a building-specific level would likely be larger, especially for non-collapse cases as conditions specific to the building, such as density and layout of building contents, will have an effect on injury rates.

7.2.2 Existing Injury Prediction Methods considering Room Interior

Two approaches exists which consider the interior of the building during shaking. The first, by Yeo and Cornell [27], predicts fatalities caused by falling floor slabs due to failure of support beams. The first step is to spatially distribute occupants by splitting the floor area into smaller grids based on the floor slab arrangement, then assigning a number of people to each grid based on a given population density. Everyone within the grid is assumed to suffer fatal injuries if the slab above the grid falls.

A second approach by Okada et al. [28] predicts furniture toppling onto people. This involves calculating the clear floor area (i.e. the area not taken up by upright furniture), $Area_N$, and that taken up by furniture which would topple, $Area_T$. Assuming that occupants have uniform probability of being located anywhere within the clear floor area, the probability of toppling furniture impacting an occupant is $Area_T/Area_N$.

There are several limitations of both approaches. Firstly, no information on modelling the number and density of occupants was provided. Secondly, variation in the injury severity resulting from impact with objects, and their associated treatment costs, were not considered. Finally, injuries due to people losing balance and falling over or from content sliding were not included.

7.2.3 Transient Occupancy Rate Models

The Cambridge Model's [7] transient occupancy rates are commonly used to predict the number of occupants present at the time of shaking. Their office-type occupancy rates increase from and decrease to zero at the start and end of working hours, respectively, and are relatively constant in between. However, building energy conservation research found that rates generally dropped at lunchtime [29-32]. This is considered in a model proposed by Wong and Mui [32]; which also includes time-based variance and allows for modification of working hours. An example for 09:00-17:30 working hours is shown in **Figure 7.2**. The

percentage of full occupancy is however only calibrated for office conditions in Hong Kong and may not be fully applicable to other regions due to regional behavioural differences, such as whether people are likely to spend their break time in their office

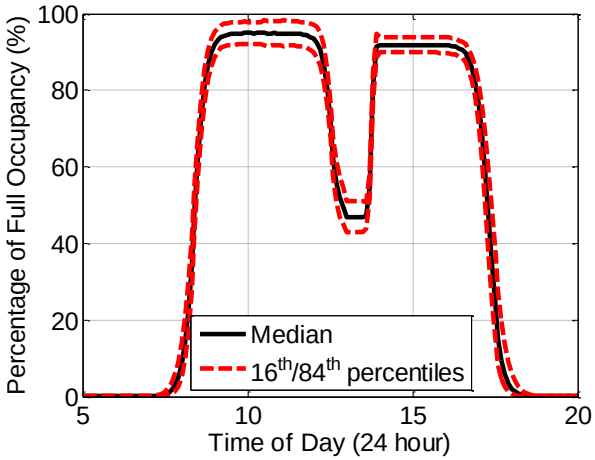

Figure 7.2. Occupancy rate (09:00-17:30 working hours) [32]

7.2.4 Occurrence of Occupants Falling

Fragility functions have been proposed by Jongkees and Groen [33] and De Graaf and Weperen [34] to predict the total floor acceleration which cases loss of balance. However, Abu-Faraj et al. [35] found that people are often able to recover their balance initially, and may be able to withstand accelerations up to five times higher than those reported by Jongkees and Groen [33] and De Graaf and Weperen [34] before actually falling. Abu-Faraj et al. [35] however did not propose any fragility functions, and no methodologies are available for predicting the severity of injuries due to occupants falling.

7.2.5 Content Movement Response

The response of contents has traditionally been correlated to total floor accelerations only. However, rocking (e.g. Kaneko et al. [36]) and sliding (e.g. **Chapters 4** to **6**) studies have shown that shaking frequency is also important. Parametric approaches have been developed to account for this effect ([36], **Chapter 5**), but these do not consider energy loss from impact against interior walls and other obstacles.

Energy loss may be considered when performing numerical content movement analyses using a coefficient of restitution. The coefficient of restitution for rocking cases, e_r, which is the ratio of angular velocity after and before impact, can be obtained using **Eq. 7.2** [37]. The sliding coefficient of restitution, e_s, which is the ratio of the content's velocity relative to the floor, v_{CRF}, after and before impact, may be obtained from: (i) rock fall data [38] ($e_s \approx 0.5$); or (ii) findings from an experimental study by Jankowski [39] where several solid balls made of varying materials were dropped onto rigid surfaces ($0.6 < e_s < 0.8$).

$$e_r = \left(1 - \frac{3}{2}\sin^2\left[\tan^{-1}\left(\frac{B}{H}\right)\right]\right)^2 \left(1 - \frac{3}{2}\cos^2\left[\tan^{-1}\left(\frac{B}{H}\right)\right]\right) \quad \textbf{(7.2)}$$

Rocking is the predominant response mode for rigid block-like contents if the static friction coefficient was higher than its width (B) to height (H) ratio; while the opposite is true for sliding [40]. A typical equation for the angular acceleration response of rigid rectangular blocks, $\ddot{\theta}_C$, is given in **Eq. 7.3** (e.g. Konstantinidis [41]). Here, θ_C is the block's rotation relative to vertical; a_{FT} is the floor's total acceleration; g is the acceleration due to gravity; and θ^* is given by **Eq. 7.4**. $\ddot{\theta}_C$ is zero if neither condition for **Eq. 7.3** is satisfied. Note that if $\theta_C(t)$ exceeds θ^*, the furniture is assumed to have toppled over.

$$\ddot{\theta}_C(t) = -\frac{3g}{\sqrt{B^2 + H^2}}\left[\text{sgn}[\theta_C(t)].\sin\left(\theta^*(t)\right) + \frac{a_{FT}(t)}{g}\cos\left(\theta^*(t)\right)\right] \quad \begin{matrix}\text{when } |\theta_C(t)| > 0 \\ \text{and/or } |a_{FT}(t)| > Bg/H\end{matrix} \quad \textbf{(7.3)}$$

$$\theta^*(t) = \tan^{-1}\left(\frac{B}{H}\right) - |\theta_C(t)| \quad \textbf{(7.4)}$$

The generic equation for the total acceleration response of sliding contents, a_{CT} (e.g. Shenton III and Jones [42]) is given in **Eq. 7.5**. Here, μ_s and μ_k are the static and kinetic friction coefficients, respectively.

$$a_{CT}(t) = \begin{cases} a_{FT}(t) & \text{when } |v_{CRF}(t)| = 0 \text{ and } |a_{FT}(t)| < \mu_s g \\ -\text{sgn}(v_{CRF}(t))\mu_k g & \text{when } |v_{CRF}(t)| > 0 \text{ or } |a_{FT}(t)| \geq \mu_s g \end{cases} \quad \textbf{(7.5)}$$

7.2.6 Injury Severity Assessment

A rating system for quantifying injury severity commonly used in automotive safety and sports injury research is the Abbreviated Injury Scale [43], *AIS*. The scale ranges from 0 for no injuries, to 6 for fatal injuries, and is assigned to each body region individually.

Injury indices exists which can be linked to an *AIS* rating. Examples include the maximum chest compression, C_{max}, and the viscous criterion, *VC* [44, 45], for skeletal and soft issue chest injuries, respectively. *VC* can be calculated following **Eq. 7.6**; where t is the time from start of impact, $C(t)$ is the chest compression with time, and B is the width of the chest. Others exist for head, arm, and leg injuries [46-50]. Indices may be obtained from numerical models, such as the Lobdell model [51] in **Figure 7.3** for obtaining the compression response of a person's chest subjected to an impact mass, m_1, with a given velocity. Here, m_2, and m_3 represent the sternum and spinal masses, respectively; and the springs and dashpots represent the soft tissue, bone structure, and organs. Typical parameter values are shown in **Table 7.2**. Models for other body parts exist, but are more computationally complex to use.

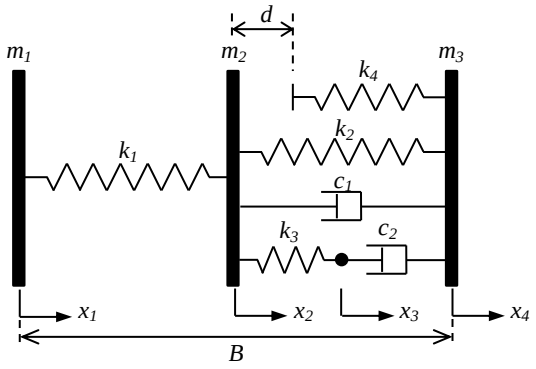

Figure 7.3. Thorax model [51]

$$VC = \max\left[\frac{dC(t)}{dt} \times \frac{C(t)}{B}\right] \quad \textbf{(7.6)}$$

Table 7.2. Thorax model parameters [51]

Masses (kg)		Distances (mm)	
m_2	0.45	d	38
m_3	27.2	B	222
Springs (kN/m)		**Dashpots (kN/m/s)**	
k_1	281	$c_{1,tension}$	0.525
k_2	26.3	$c_{1,compression}$	0.230
k_3	13.2	c_2	0.180
k_4	52.6		

Payne and Patel [52] provided impact velocity values that corresponded to a given injury index or an *AIS* rating. However, these do not consider impact mass, and were based on expert opinion. Nonetheless, fragility functions based off Payne and Patel's [52] recommendations, and those from other studies [44-50], are shown in **Figure 7.4**.

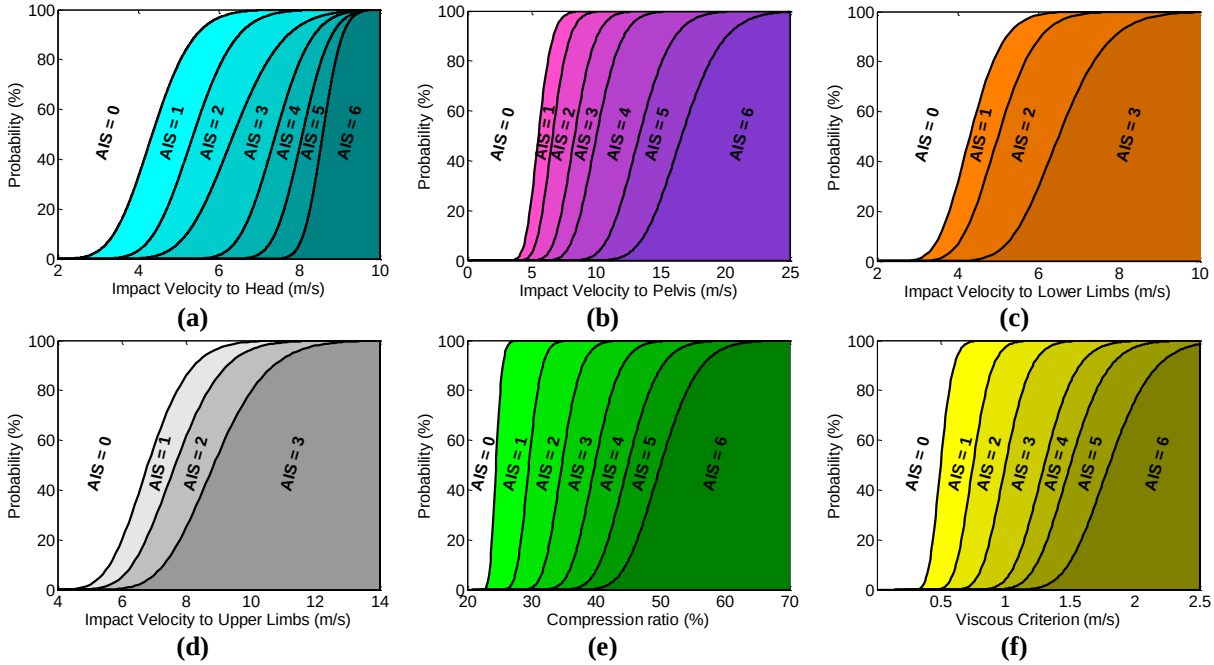

Figure 7.4. Injury fragility functions for (a) head, (b) pelvis, (c) lower limbs, (d) upper limbs, (e) chest – skeletal structure, and (f) chest – soft tissue [44-50, 52]

7.2.7 Injury Cost Assessment

The maximum *AIS* rating a person received across all body parts may be used to predict costs based on values provided by regional transport agencies, such as the Federal Highway Administration (FHA) [53] or the New Zealand Ministry of Transport [54]. However, treatment and recovery costs are dependent on the body region affected which is not

considered by these sources, nor do these necessarily provide costs at an *AIS* level. More rigorous datasets including this information have been provided by Miller [2] and Zaloshnja et al. [55]. This was derived by grouping car accident-related data from the US based on which body region incurred the highest *AIS* rating. If multiple body parts had the highest *AIS*, the data was assigned to the group with the higher hierarchy; the order of which was (i) spine, (ii) head, (iii) lower extremities (legs, hip), (iv) upper extremities (arm, shoulder), (v) trunk, (vi) face, and (vii) minor injuries. The median injury cost for some of the body parts are shown in **Table 7.3**; which accounts for medical treatment costs, decrease in quality of life, among others. It should be noted that while the general losses are similar to those by the FHA, these are almost double of those suggested by the New Zealand Ministry of Transport. This is due to the global variation in a regional economy and healthcare situations (i.e. a person's income, or cost of healthcare).

Table 7.3. Median injury cost ($ million in 2015 USD) [2, 55]

	AIS rating					
Dominant body part hierarchy	1	2	3	4	5	6
Head	0.10	0.50	1.10	2.80	6.30	6.13
Lower extremity (pelvis and lower limbs)	0.01	0.18	0.90	1.20	2.14	6.13
Upper extremity (arms)	0.02	0.20	0.64	N/A		
Chest	0.02	0.15	0.64	1.18	1.32	6.13
General (i.e. ignoring affected body parts)	0.02	0.25	0.93	2.36	4.90	6.13

7.3 PROPOSED INJURY PREDICTION FRAMEWORK

7.3.1 Framework Overview

This chapter's proposed injury prediction framework is shown in **Figure 7.5**. Several inputs are required for the framework, such as building and room properties. Structural analysis is performed for each ground motion record to assess if the building had collapsed based on the drifts in **Table 7.1**. If collapse did not occur, further content response analyses are performed prior to performing Monte Carlo simulations to predict injuries.

The first step in each Monte Carlo simulated trial is to determine the number of people present during shaking using occupancy models. If the building did not collapse, the next steps are to (i) predict each occupant's location and height, (ii) quantify the effect of people falling or being struck by contents, and (iii) assess injury severity using **Figure 7.4**. If collapse occurred, the HAZUS® [4] injury rates are used instead due to a range of complexities involved with collapse; such the collapse mechanism, the interaction of contents with the collapsed structure, and identifying which object impacted against occupants during collapse. The final step is to assign injury costs assuming a lognormal dispersion using the median values from **Table 7.3**. A dispersion of 0.1 was assumed for injury costs, and only injuries to the head, chest, extremities (arms and legs), and hips are considered due to fragility functions not being redily available for other body regions.

Note that behavioural factors during shaking events (i.e. "drop-cover- hold"), and secondary hazards (i.e. fire) are not considered. In addition, failure of other types of non-structural elements were not considered as (i) furniture movement and people falling caused most non-fatal injuries [9-15], and (ii) models to identify the exact failure location of other elements, such as ceilings or air conditioning systems, is not well developed. The framework can however be easily modified to incorporate occupant behaviour and failure of other non-structural elements once methods to consider these have been developed.

Methodologies to predict (i) the time when the event occurred, which is required to use **Figure 7.4**, (ii) the location of occupants, and (iii) properties of impact against occupants falling or being struck by moving contents, are proposed in the following subsections.

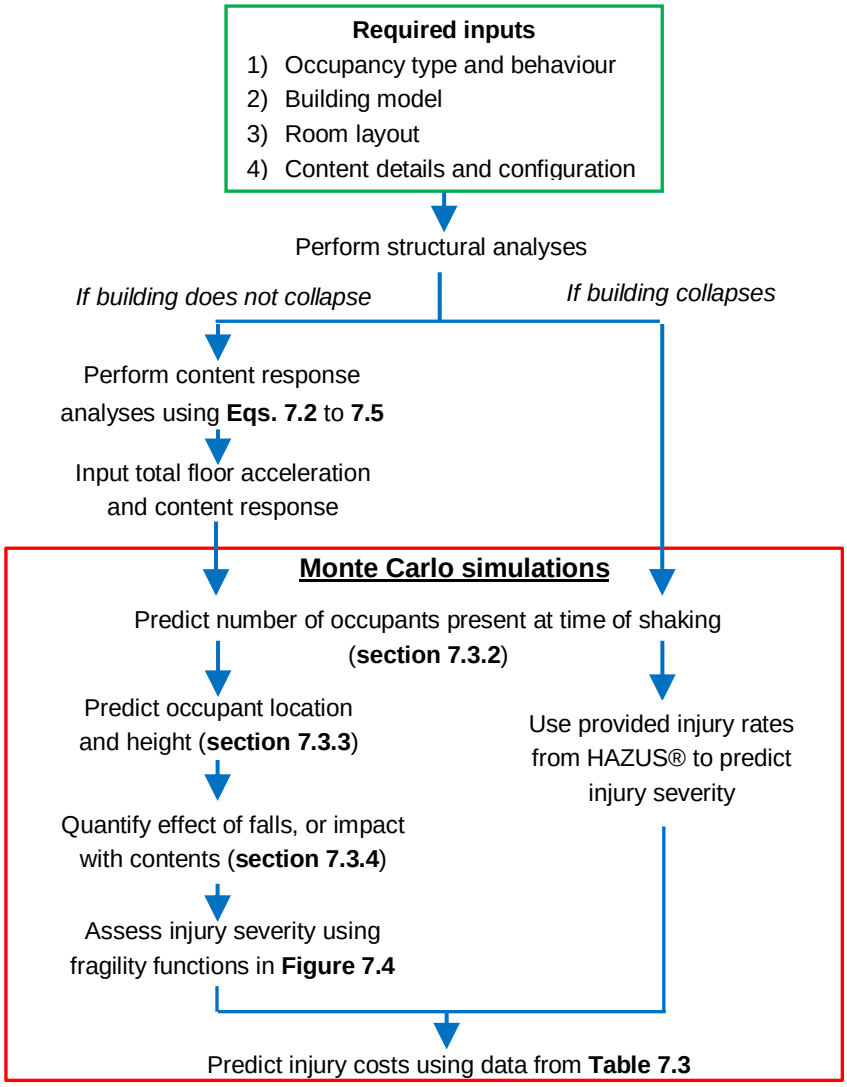

Figure 7.5. Proposed building-specific indoor injury prediction framework

7.3.2 Predicting Time of Event

In order to use existing transient occupancy models, the time of earthquake occurrence must first be predicted. For office buildings using Wong and Mui's [32] model in **Figure 7.2**, this is done by predicting: (i) if it was a working day, and (ii) the time of day. For the first part, it is assumed that the general population worked 240 days in a year. A random number between 0 and 1 was then generated. If this number is greater than 0.658 (i.e. 240 working days out of 365 days a year), the event occurs on a non-working day, and no one is assumed to be present at the time of shaking. Else, an additional random number between 0 and 1 is multiplied by 24 hours to obtain the time of the event for use with the model in **Figure 7.2**.

7.3.3 Determining Occupant Location

Occupant spatial distribution is performed by: (i) splitting the clear floor area into grids; (ii) assigning each occupant to a specific grid, some of which may be occupied by multiple people; and (iii) obtaining occupants' coordinates. The grid layout is defined by: (i) seat locations to consider the occupants' body position; and (ii) splitting irregularly-shaped floor areas into regular shapes. Each grid is assigned to be for sitting-only or standing-only.

In order to assign occupants to grids, the maximum occupancy is defined based on: (i) the number of seats available; and (ii) the maximum number of standing occupants allowed based on judgement. Weighting factors based on engineering judgement are then applied to each sitting or standing vacancy to reflect the likelihood of it being occupied. The cumulative weights are then calculated and normalized by the maximum cumulative weight to give a cumulative probabilistic distribution, which is then used with random number generators to assign an occupant to a given vacancy. The weighting factor for that vacancy is then reset to zero to prevent the next occupant from being assigned to the same location. Occupants assigned to seats are assigned to its corresponding grid, while standing occupants are assumed to have uniform probability of being located anywhere within the standing-only floor area.

Occupant coordinates are obtained by assuming uniform probability of the occupant being located anywhere within their assigned grid, as per Okada et al.'s [28] approach. The occupant's *x* coordinate, C_x, is obtained from **Eq. 7.7**; where C_W and $L_{W\text{-}E}$ are the grid's west-most coordinate and west-east length, respectively; and *rand* is a random number between 0 and 1. The *y* coordinate is obtained using a similar approach.

$$C_x = C_W + L_{W-E} \times rand \quad \textbf{(7.7)}$$

7.3.4 Occupant Injury Mechanisms

Two types of injury mechanisms are considered if the building did not collapse; (i) people losing balance and falling over, or (ii) people being hit by moving contents. The first step is to assess the time at which falling occurs to determine the sequence of events. The fragility function to predict the total floor acceleration that caused falling, A_{fall}, follows a lognormal distribution with a median of 0.17 g and a dispersion of 0.69. This assumes that the median accelerations causing loss of balance [33, 34] represent the 5th percentile, while Abu-Faraj et al.'s [35] findings represent the 95th percentile. A_{fall} for each occupant in each trial can thus be obtained using **Eq. 7.8**. The time which an occupant falls is when the floor's total acceleration combining both horizontal components, $a_{FTC}(t)$, first exceed A_{fall}. If occupants fell before being struck by contents, fall analysis should be performed first, and vice versa.

$$A_{fall} = \exp\left[\ln(0.17) + 0.69.\Phi^{-1}(rand)\right] \quad \textbf{(7.8)}$$

If the occupant falls, he or she is assumed to have uniform probability of falling in any direction. Note that in reality the fall direction might be linked to the direction of strong shaking, though no studies had investigated this. The angle at which the person falls in a clockwise direction relative to north is predicted using a generated random number multiplied by 360^{o}. If the occupant landed on contents, trigonometry is used to identify the body part that bore the brunt of impact considering typical body proportions (i.e. Loomis [56]).

Occupants falling onto the floor are assumed to either land on their arms or hips for simplicity, and the occupant's fall response is assumed to mimic an inverted pendulum system initially at rest. **Eq. 7.9** can therefore be derived to obtain the impact velocity, V_i, based on existing closed-form solutions for inverted pendulum systems [57]; where θ_{body} is the body's angle relative to vertical, H is the occupant's height, and H_{IO} is the distance

between point of impact and the occupant's feet position. This equation assumes that a person's center of mass is located just above their hips at approximately 60% of their height.

$$V_i = H_{IO}\sqrt{\frac{16g(1-\cos(\theta_{body})}{4.7H}} \quad \textbf{(7.9)}$$

Three scenarios are possible if occupants are struck by contents. The first is "pre-fall rocking"**,** where contents toppled onto upright occupants as shown in **Figure 7.6a**. Here, V_i is the content's angular velocity at the time of impact multiplied by the distance between the contact and pivot. Further fall analysis is not performed if this occurred as occupants are assumed to be pinned by the toppled content.

The second type is "post-fall rocking", where contents toppled onto fallen occupants as shown in **Figure 7.6b**. Here, V_i and the impact location on the occupant's body are recorded at each end of the impact. The mean V_i is then calculated for each affected body part.

The final type is "sliding" as shown in **Figure 7.6c**, where V_i is the content's velocity relative to the floor at impact. The possibility of this impact causing upright occupants to fall was not considered for simplicity, and hence further fall analysis is required in this case if the occupant was stuck before falling. If any body part except for the chest was subjected to multiple impacts from a range of sources, the largest V_i obtained overall is considered in injury severity and cost assessment.

The impact mass is required to obtain damage indices for chest injuries. For rocking cases, this is determined by using a simply-supported beam analogy; where the mean contact axis location and the pivot were the "supports" location. The reaction force at the contact point is thus equal to the impact weight. The impact mass for sliding contents is taken as the contents' mass. Impact masses are then distributed to the affected body parts proportionately to their affected length. The impact mass caused by falling is assumed to be zero. If the chest

area was subjected to multiple impacts from a range of sources, each impact's mass-V_i pairing needs to be evaluated to determine the highest injury severity level.

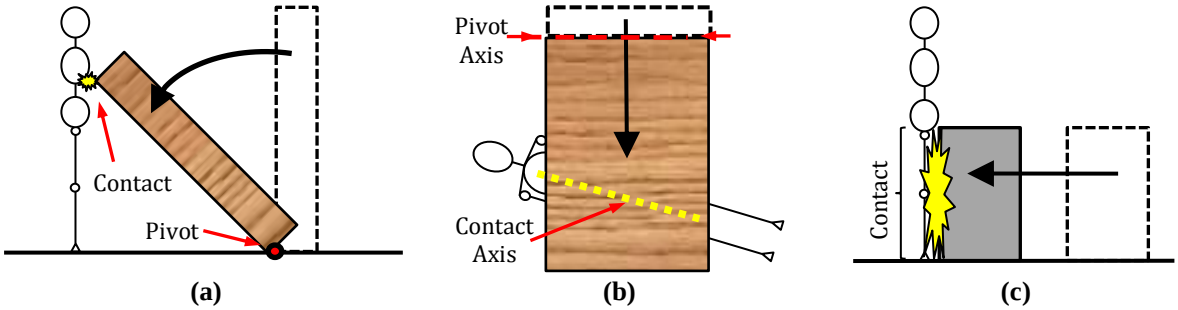

Figure 7.6. Content movement injury mechanisms; (a) Content falling onto standing occupant (side elevation), (b) content falling onto fallen occupant (top view), and (c) sliding impact

7.4 CASE-STUDY DETAILS

7.4.1 Building Details

The proposed framework was applied to a case-study 10-storey reinforced concrete wall office building to demonstrate its usage. The building has floor heights of 4.0 m on the ground floor, 3.6 m on other floors, and a fundamental period of 1.25 s. It was designed for conditions representative of a shear wave velocity (*Vs30*) of 400 m/s (subsoil class C conditions [58]) in Wellington, New Zealand, with a strength reduction factor of 4.0. The building's strength and stiffness are similar in each orthogonal direction. This building is akin to the "baseline" building adopted in **Chapter 3**.

7.4.2 Room, Content, and Floor Grid Details

Three office-room layouts were considered in this study, and were based on typical room layouts found at the University of Canterbury. These are labelled Layout A, Layout B, and Layout C, and are shown in **Figures 7.7a** to **7.7c**, respectively. The framework was applied for all three layouts individually. For each case, it is assumed that each floor of the building contains 24 rooms in total; 12 with the orientations shown in **Figure 7.7**, and another 12 with the layout flipped horizontally. Other areas such as stairwells were not

considered. The details of the contents present in each of the three room layouts are provided in **Table 7.4**.

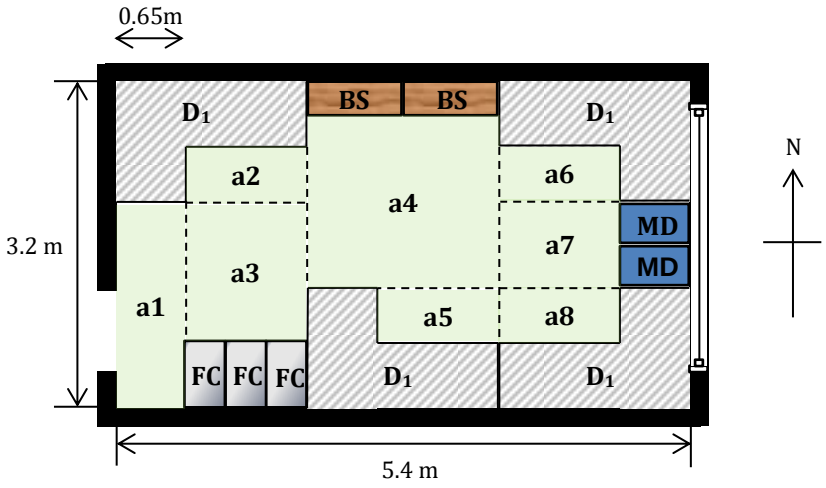

(a)

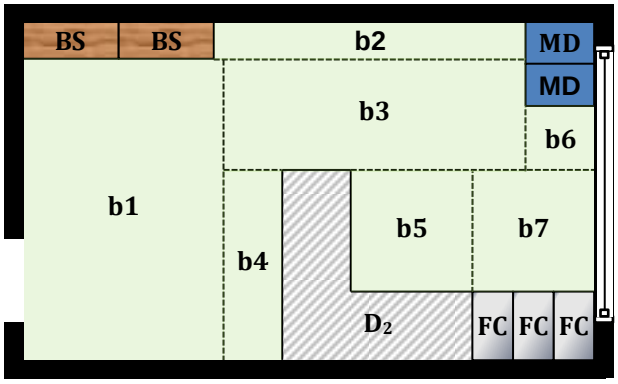

(b)

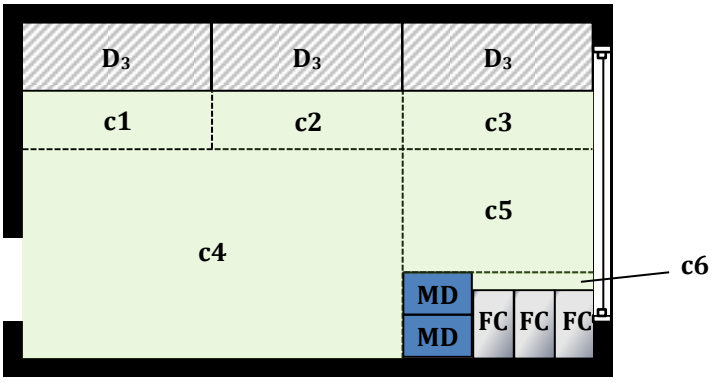

(c)

Figure 7.7. Case study room layouts; (a) Layout A, (b) Layout B, and (c) Layout C

Table 7.4. Content properties

Content	Rooms	Outer E-W (m)	Outer N-S (m)	Height (m)	μ
Mobile drawers (MD)	A, B, and C	0.65	0.40	0.55	0.1 in E-W 0.45 in N-S
Filing Cabinets (FC)		0.39	0.65	1.65	0.45
Bookshelves (BS)	A and B	0.9	0.2	1.75	
Office desk 1 (D1) [0.65 m depth]	A only	1.80	1.20	0.75	
Office desk 2 (D1) [0.65 m depth]	B only	1.80	1.80	0.75	
Office desk 3 (D3)	C only	1.8	0.65	0.75	

For each layout in **Figure 7.7**, the occupiable floor areas were subdivided into grids (i.e. a1, a2, a3, etc). Grids a2, a5, a6, a7, b5, c1, c2, and c3 are where the occupants sit while working, and thus contained one seat each. Grid b4 contains two extra seats for visitors. The remaining grids are for standing-only. It was assumed that a maximum of three occupants may be standing in any of the rooms at any one time, in addition to those already sitting. The probability of a standing occupant being located in any of the remaining grids was assumed proportional to its area. An example of this for Layout A is shown in **Table 7.5**.

Table 7.5. Probability of a standing person occupying each of the standing-only grids

Grid	Floor area (m^2)	Cumulative floor area (m^2)	Cumulative probability
a1	1.30	1.30	0.187
a3	1.55	2.85	0.412
a4	3.15	6.00	0.867
a7	0.92	6.92	1.000

Weights of 1.0 and 0.2 were assumed for each seat and standing vacancy, respectively, due to the higher likelihood that occupants would be sitting while working. The exception was for seats in grid b4, where a weight of 0.25 was assumed instead since these are less likely to be occupied. An example of the individual and normalized cumulative weighting factors for an empty floor with Layout A rooms is shown in **Table 7.6**. Once the first occupant has been assigned a location, the individual weighting for that location would be reset to zero, and the process repeats.

Table 7.6. Weightings for an empty floor

	Individual Weighting					Normalized Cumulative Weighting				
	Sitting-only Grid				Standing	Sitting -only Grid				Standing
Room	*2*	*5*	*6*	*8*	(up to 3 spaces)	*2*	*5*	*6*	*8*	(up to 3 spaces)
1	1	1	1	1	0.6	0.0091	0.0181	0.0272	0.0362	0.0417
2	1	1	1	1	0.6	0.0507	0.0598	0.0688	0.0779	0.0833
…	…	…	…	…	…	…	…	…	…	…
24	1	1	1	1	0.6	0.968	0.976	0.986	0.995	1.000

7.4.3 Occupancy Details

The transient occupancy model implemented for each floor was that by Wong and Mui [32]. Full occupancy was assumed to be 96 occupants per floor in Layout A (four full-time occupants assigned to each room), 36 occupants per floor in Layout B (assuming 1.5 occupants in each room on average), and 72 occupants per floor in Layout C (three full-time occupants assigned to each room). The standing height distribution for adult New Zealanders has a median of 1.71 m (from the OECD database [59]). A lognormal dispersion of 0.07 was assumed for this study. The effective height of sitting occupants' was assumed to be 75% of their standing height.

7.4.4 Ground Motion Selection

Ground motion suites were selected using the Generalized Conditioning Intensity Measure approach [60, 61] for Wellington City (41.3^{o}S, 174.8^{o}E) using New Zealand-specific rupture forecast [62] and attenuation models [63]. The spectral acceleration at the building's fundamental period, *Sa*(1.25s), was chosen as the conditioning intensity measure. Suites of twenty records sets were selected at eleven hazard levels between 99% and 0.1% probability of exceedance in 50 years. The design-basis event (DBE) suite is shown in **Figure 7.8a**, while the seismic hazard curve is shown in **Figure 7.8b**. Note that *Sa*(1.25s) corresponding to the serviceability level event (SLE), DBE, and maximum credible event (MCE) are annotated in **Figure 7.8b** for future reference in latter sections of this chapter.

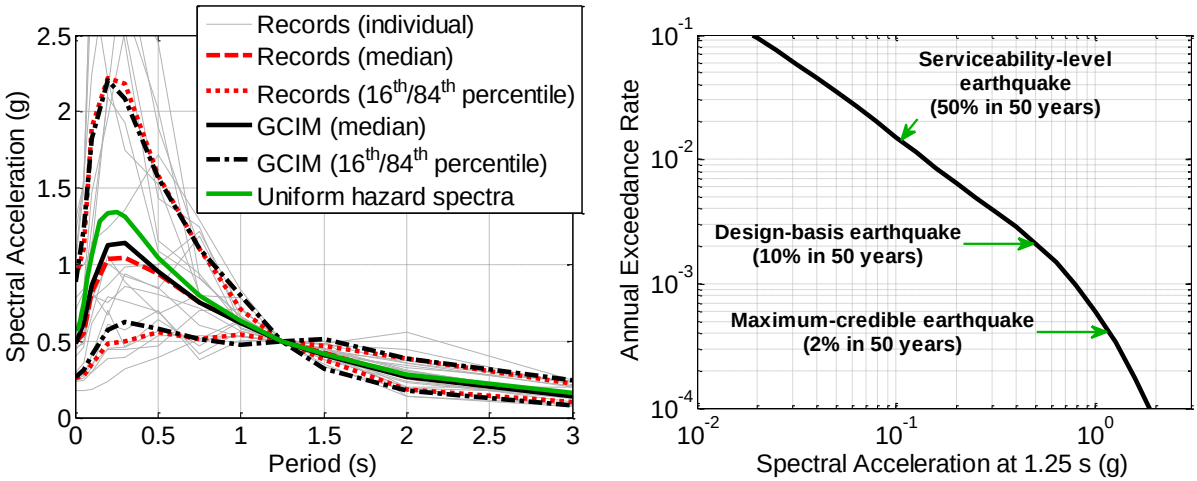

Figure 7.8. Seismic hazard and selected records; (a) *Sa*(1.25s) hazard, and (b) comparison of selected records and theoretical spectral curves at DBE

7.4.5 Structural Response Analysis Details

Inelastic structural response history analyses were performed on Ruaumoko2D [64] using (i) large displacement analyses [65] to consider second-order effects, (ii) the SINA hysteresis rule [66] for modelling the wall's response, and (iii) a Caughey [67] initial stiffness proportional damping ratio of 5% across all modes. Strength and stiffness degradation were not considered due to a lack of full-scale shake table experiments of walls for calibration. Instead, drift limits from **Table 7.1** were used to assess if a building had collapsed, which was assumed to occur if the first storey's peak inter-storey drift exceeded 2% (significant wall damage), or if the inter-storey drift on any floor exceeded 4% (global instability).

7.4.6 Content Response Analysis Details

Based on the content's properties in **Table 7.4**, the bookshelves (BS) and filing cabinets (FC) would exhibit rocking response, while others exhibit sliding response. The content's response was modelled using **Eqs. 7.2** to **7.5**. For sliding cases, it was assumed that the kinetic friction coefficient, μ_k, may also be used as the static friction coefficient, μ_s, as this still produces reasonably accurate findings as discussed in **Chapter 4** (**Section 4.6.3**).

7.5 DEMONSTRATION OF INJURY PREDICTION FRAMEWORK

7.5.1 Step 1 – Predicting Number of Occupants

To demonstrate the usage of the injury prediction framework from **Figure 7.5**, an example considering a single trial using Layout A is examined. Three random numbers were generated to predict the number of people present on a single floor during the event: 0.423, 0.392, and 0.122. Following **Section 7.3.2**, the first number indicates that the event occurred on a working day since this is less than 0.658; while the second number was multiplied by 24 hours to predict that the event occurred at 9:24 am. The distribution of full occupancy percentage from **Figure 7.2** at this time has a median of 94.6% and a dispersion of 0.03. This distribution and the third random number generated are used in a similar approach to **Eq. 7.8** to predict that 91.3% of full occupancy, or 88 people (rounded to the nearest whole number), were present on that floor during the event. As the time and day of the event is the same regardless of the building's floor level, only the last part was repeated for the remaining floors within the building for the same trial.

7.5.2 Step 2 – Predicting Location and Height of Occupants

Assuming that the building had not collapsed, the second step in the framework is to predict each occupant's location and height. Five random numbers were generated: 0.081, 0.952, 0.174, 0.500, and 0.768. Following the approach outlined in **Section 7.3.3**, the first number is used with **Table 7.6** to determine that the occupant was standing in Room 2, the second number is used to identify that the occupant was located in a7 based on **Table 7.5**. The third and fourth numbers are used to determine that occupant was located at (3.8 m, 1.6 m) using **Eq. 7.7**. The final is used to predict an occupant height of 1.80 m following a similar approach to **Eq. 7.8** based on the assumed height distribution described in **Section 7.4.3**. The individual weighting for standing in Room 2 is decreased by 0.2 before considering the next occupant as the location is now occupied.

7.5.3 Step 3 – Injury Mechanism Analysis

The next step in the framework is to predict the effect of occupants falling or being struck by moving contents following **Section 7.3.4**. Two random numbers were generated: 0.905 and 0.694. The first is used to determine that A_{fall} = 0.42 g using **Eq. 7.8**. The second is used to predict that, if the occupant were to fall, the direction would be 250^o (360^o × 0.694) clockwise of North.

Based on the fall direction and room layout in **Figure 7.9a**, the occupant would interact with the right-most bookshelf by either falling onto it, or being struck by it after having fallen. If the floor and bookshelf response obtained from analyses is as shown in **Figures 7.9b** and **7.9c**, respectively, the occupant would fall at 9 s while the bookshelf toppled at 21 s. Therefore, fall analysis should be performed first. Note that neither mobile drawer slid far enough to hit the occupant, and thus was not considered in this case.

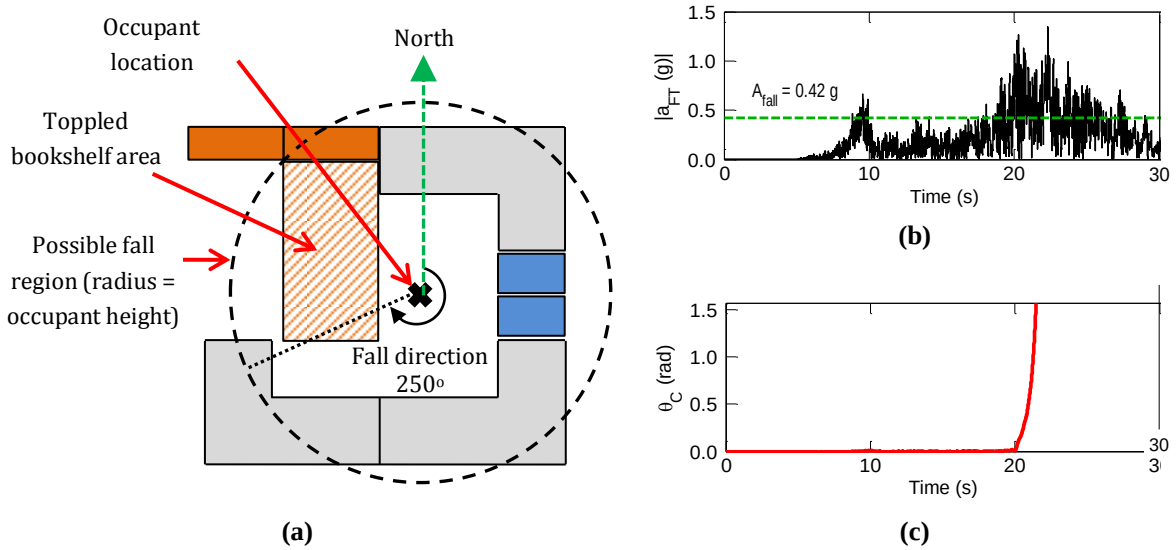

Figure 7.9. Sequence of events; (a) fall direction and radius, (b) total floor acceleration response history, (c) bookshelf rotation response

It can also be seen from **Figure 7.9a** that the occupant will fall onto the south-western-most desk based on the fall direction and occupant height. Assuming the desk has little movement due to its larger μ, the horizontal distance between the occupant and the desk is 1.44 m using geometry. As the desk's height is 0.75 m, the impact location on the occupant relative to their feet, H_{IO}, would be 1.62 m as shown in **Figure 7.10a**. This corresponds to the

head area based on generic body proportions in **Figure 7.10b** [56]. V_i is therefore 5.12 m/s using **Eq. 7.9**. It is assumed that the occupant's body is flat on the ground after falling with an effective body length of 1.44 m for the content-impact assessments.

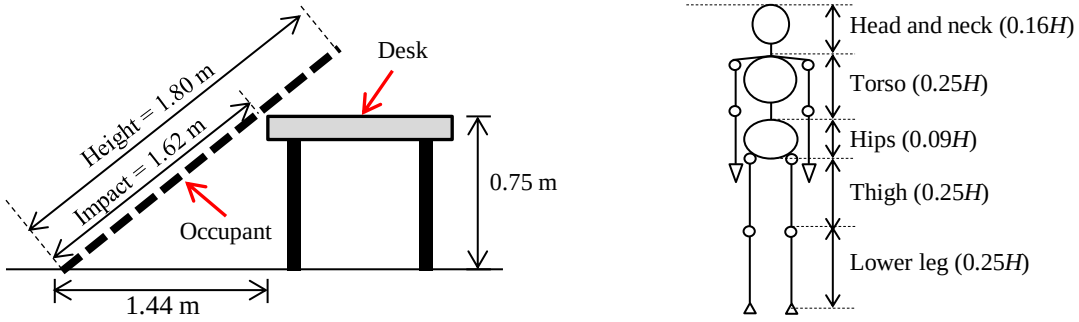

Figure 7.10. Fall injury assessment; (a) Location of impact, (b) typical body proportions [56]

The bookshelf impact type in this case is "post-fall rocking". The left-most and right-most impact points are 1.15 m and 0.21 m from the occupant's feet, and 1.75 m and 1.42 m from the bookshelf's pivot axis, respectively. If the bookshelf's angular velocity obtained from furniture response analysis at impact is 3 rad/s, for example, then V_i at each end would be 5.25 m/s and 4.26 m/s. The impact mass is 41 kg using the simply-supported beam analogy. V_i and cumulative impact mass at body part boundaries are equal to those shown in **Table 7.7** where the occupant's effective body length of 1.44 m was considered. The mean V_i on the legs, hip, and chest are 4.52 m/s, 4.87 m/s, and 5.09 m/s, respectively; while the impact masses acting on each body part are 22.2 kg, 5.7 kg, and 13.1 kg, respectively.

Table 7.7. Interpolated impact velocity and cumulative mass

Location	Lower impact point (0.21 m)	Lower limb/hip boundary (0.5 *H* = 0.72 m)	Hip/Chest boundary (0.59 *H* = 0.85 m)	Upper impact point (1.15 m)
Impact Velocity (m/s)	4.26	4.78	4.93	5.25
Cumulative mass (kg)	0	22.2	27.9	41.0

7.5.4 Step 4 – Injury Severity and Cost Evaluation

The final two steps in the framework are to predict each occupant's injury severity, and the associated costs. Firstly, the mean V_i and impact mass to the chest from **Table 7.7** was inputted into the Lobdell model [51], where m_3 was fixed as the occupant was flat on the

floor. This resulted in C_{max} and *VC* being 20.8% and 0.49 m/s, respectively. Five random numbers were generated to predict the injury severity to the head, pelvis, lower limbs, the chest's skeletal structure, and the chest's soft tissue, respectively: 0.644, 0.815, 0.127, 0.537 and 0.913. Using the fragility functions from **Figure 7.4**, the head and lower limbs incur an *AIS* of 1.0 and 3.0, respectively, while other body parts are uninjured.

As the lower extremity is the most severely injured, the median injury cost will therefore be $0.90 million from **Table 7.3**. If a random number of 0.435 was generated, the incurred injury cost would be $0.885 million using a similar approach to **Eq. 7.8** assuming a dispersion of 0.1 as discussed in **Section 7.3.1**.

7.5.5 Application of Framework to Entire Building

The example up to this point only considered a single occupant. The overall process would need to be repeated for every occupant present, and further trials are required to obtain a distribution of injury severity and injury-related costs. It was found from sensitivity analysis that 5,000 trials per record are sufficient to provide consistent probabilistic outputs.

7.6 CASE-STUDY FINDINGS

7.6.1 Structural and Content Response

The probability of building collapse with *Sa*(1.25s) is shown in **Figure 7.11a**; where the 'raw data' is the percentage of ground motion records within each suite that resulted in building collapse, and the 'lognormal fit' is the best-fit lognormal distribution. The probability of collapse increased with *Sa*(1.25s) as expected; and was approximately 0%, 3.0%, and 38.7% at SLE, DBE, and MCE events, respectively.

The 16th and 84th percentile A_{FTC} response at SLE, DBE, and MCE events are shown in **Figure 7.11b**, where the A_{FTC} response increased with shaking intensity as expected. The peak response tends to occur around the 4th floor, and was at a minimum around the 8th floor.

The former observation is due to the effect of the second mode; which (i) is not be limited by inelastic behavior to the same extent as the first mode, (ii) has a peak around half the height of the building, and (iii) has a spectral acceleration value larger than that for the first mode (i.e. 1.30 g versus 0.50 g for the first and second mode, respectively, using the 10% in 50 year UHS from **Figure 7.8a)**. In the latter case, the second mode response is near zero at the 8th floor, explaining the lower A_{FTC} response.

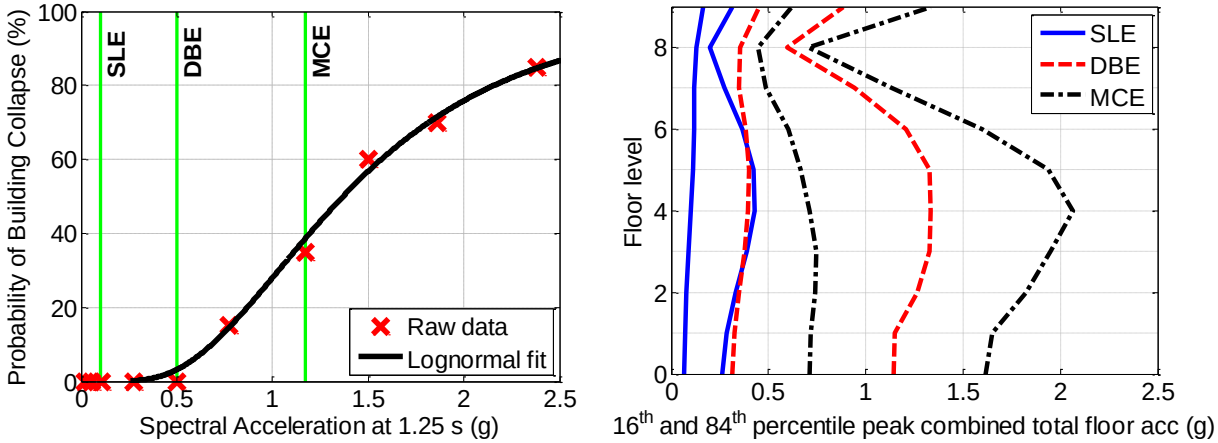

Figure 7.11. Building response; (a) collapse probability, (b) peak total floor acceleration

7.6.2 Content Response

The probability of contents overturning with floor level is shown in **Figure 7.12a**. None of the filing cabinets overturned, and bookshelves had minimal response around the 7th and 8th floor. Interestingly, the highest overturning probability occurred around the 2nd and 3rd floor, which does not correspond to the location of peak A_{FTC} response in **Figure 7.11b**. This indicates that content movement response and related injuries are not proportional to A_{FTC}. This is likely due to shaking frequency effects in a similar fashion to sliding contents as discussed in **Chapters 4** and **6**.

It can be seen from the content sliding probability in **Figure 7.12b** that mobile drawers (MD) slid for all cases, while the desks slid in most cases. The drawers however had an 84th percentile peak sliding displacement greater than 0.30 m on all floors, compared to the desks which slid less than 0.25 m, as shown in **Figure 7.12c**. The sliding response trends with floor

level also differed from the A_{FTC} response, which is again consistent with **Chapters 4** and **6** findings. Due to the minimal response of the filing cabinets and desks, these were not considered further in the injury analyses to decrease computation time.

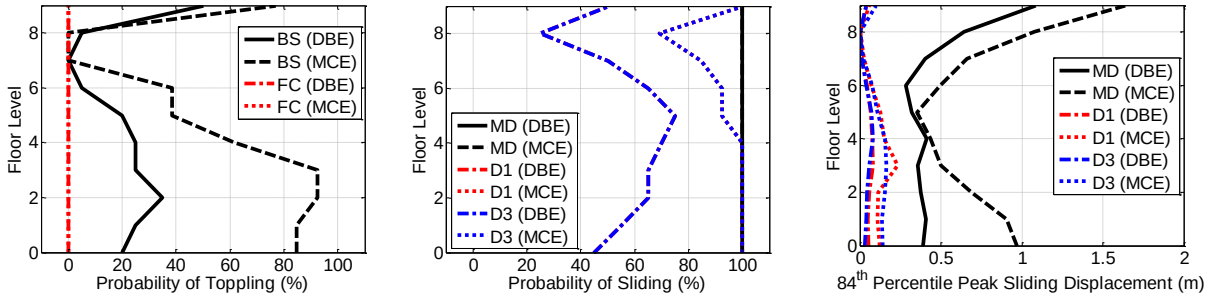

(a) **(b)** **(c)**

Figure 7.12. Content's response for non-building collapse; (a) toppling probability, (b) sliding probability, (c) 84th percentile peak sliding displacement given that sliding had occurred

7.6.3 Injury Severity Rates

Injury rates obtained using the SLE suite of records are shown for Layout A (**Figures 7.13a** to **7.13c**), Layout B (**Figures 7.13d** to **7.13f**), and Layout C (**Figures 7.13g** to **7.13i**) for minor (*AIS* = 1), moderate (*AIS* = 2 and 3), and serious or fatal injuries (*AIS* > 4), respectively. At this shaking level, virtually all injuries were caused by occupants falling, as significant content movement and building collapse are rare during SLE shaking The variation of injury probability with floor level has similar trends to the variation of A_{FT} shown in **Figure 7.11** due to the use of A_{FT} as the sole *EDP* in the implemented falling occurrence fragility function. It can also be seen that the probability of a minor injury occurring due to falls was approximately double of that for moderate injuries.

Interestingly, the SLE injury rates in **Figure 7.13** were larger than those by HAZUS® [4] for "extensive" building damage in **Table 7.1**, despite the case-study building only having minor damage at SLE level shaking. There are two possible reasons for this. Firstly, "drop-cover-hold" evasion measures were not considered, and hence the estimates in **Figure 7.13** are on the conservative side. Secondly, the region's seismicity was not considered in the HAZUS® [4] rates. In reality, a building located in a higher seismicity zone would (i) be

designed with a higher strength, and (ii) be subjected to stronger events; resulting in higher floor accelerations. For example, a building in Auckland designed with T = 1.25 s and R = 4.0 for DBE level shaking (Sa(1.25s) = 0.13g from NZS1170.5:2004 [58]) would experience lower floor accelerations compared to a building with the same T and R but designed for Wellington DBE level shaking (Sa(1.25s) = 0.50g from **Figure 7.8a**) due to yielding earlier. Thus, more fall and content movement-related injuries would occur for the Building in Wellington, even though both would likely have similar peak displacements assuming equal displacement. As such, future provided injury rates should factor in a site's seismicity for more realistic predictions.

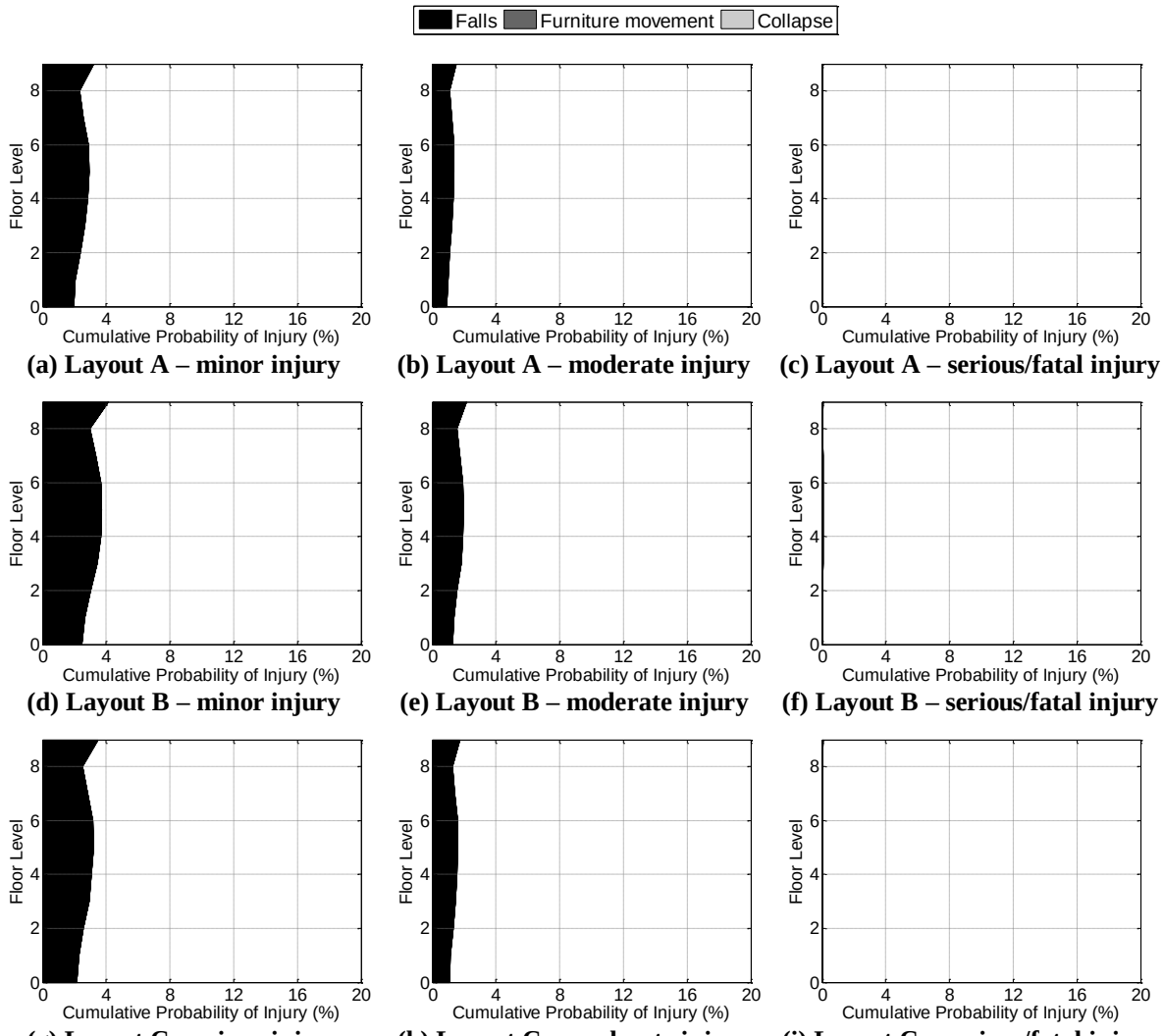

(a) Layout A – minor injury **(b) Layout A – moderate injury** **(c) Layout A – serious/fatal injury**

(d) Layout B – minor injury **(e) Layout B – moderate injury** **(f) Layout B – serious/fatal injury**

(g) Layout C – minor injury **(h) Layout C – moderate injury** **(i) Layout C – serious/fatal injury**

Figure 7.13. Case study injury severity rates per floor under SLE shaking

Similar figures were obtained for DBE level shaking, and are shown in **Figure 7.14**. A higher percentage of occupants were injured compared to the SLE event, which is expected since the DBE event is more severe. Falls still accounts for most injuries and still results in twice as many minor injuries compared to major injuries. However, the probability of injury due to occupants falling does not vary much with floor level. This was because the 16th percentile A_{FTC} values from **Figure 7.11b** exceeded the 84th percentile A_{fall} value (0.34 g) on all floors for these events, resulting in a similar probability of occupants falling with floor level.

Injuries caused by content movement in DBE events varied with floor level, and its trend was consistent with the content's response in **Figure 7.12**. These also usually resulted in moderate injuries. Content movement was the main cause of moderate injuries in Layout A as shown in **Figure 7.14b**. This however was not as significant in Layout B (**Figure 7.14e**), and had no effect in Layout C (**Figure 7.14h**). This was because the bookshelves in Layout A were located close to most sitting-only grids, where there were more likely to be occupants. People within these grids may potentially fall onto the path of toppling bookshelves, resulting in injuries. The bookshelves in Layout B however were located further away from areas where occupants were most likely to be present, while Layout C had no toppling furniture. This shows the sensitivity of furniture layout in injury modelling, and that smart placement of furniture may in itself reduce the chance of injuries occurring. It should also be noted that the number of moderate injuries were higher than minor injuries on certain floors in Layout A due to the higher probability of people being impacted by furniture, though such observations did not exist for Layout B and Layout C rooms.

The probability of occupants being injured due to building collapse was consistent regardless of the room layout. This was because the injury rates from HAZUS® [4] were

applied to all cases in the event of building collapse, and thus the room's interior was not considered for this case.

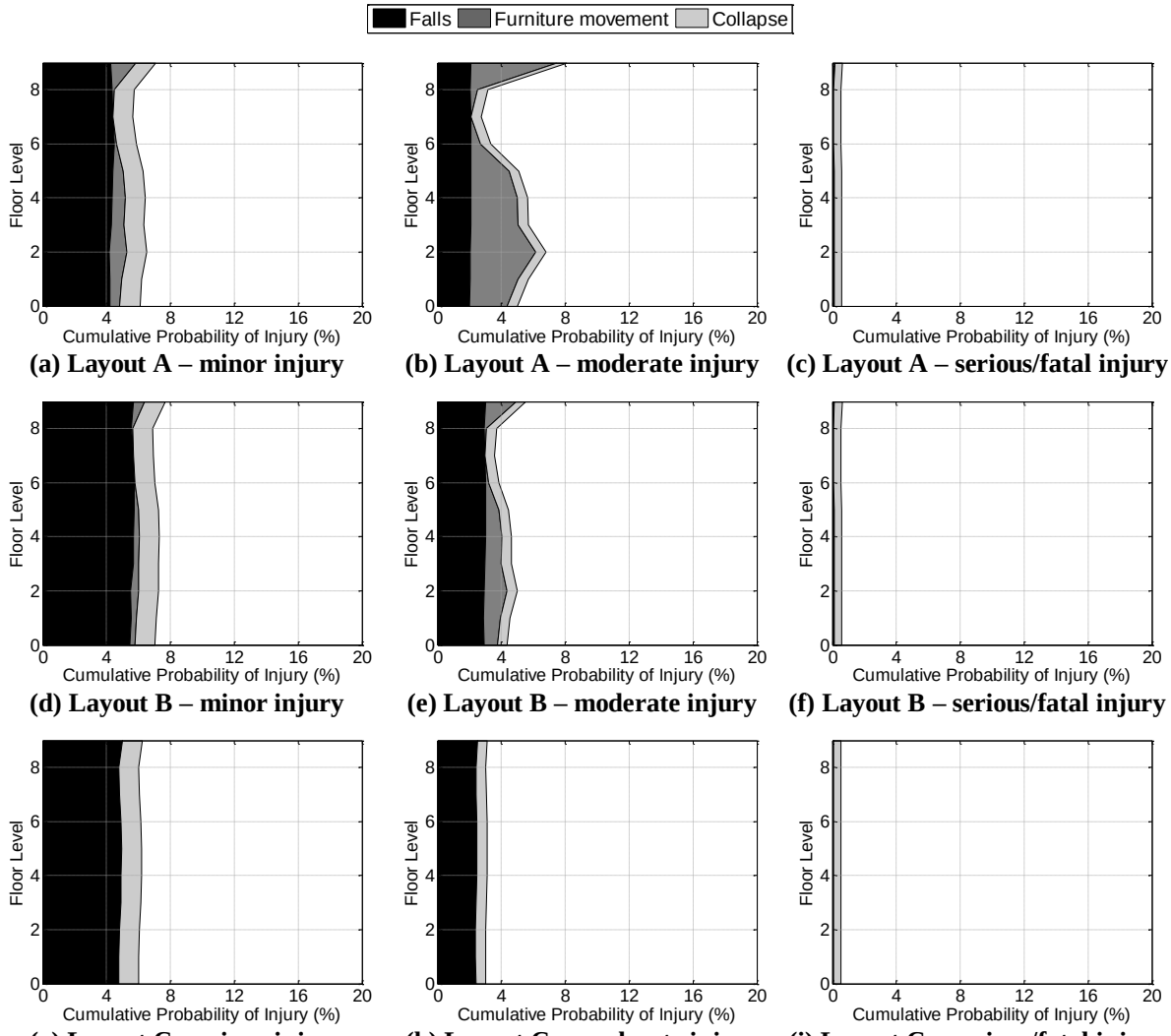

(a) Layout A – minor injury **(b) Layout A – moderate injury** **(c) Layout A – serious/fatal injury**

(d) Layout B – minor injury **(e) Layout B – moderate injury** **(f) Layout B – serious/fatal injury**

(g) Layout C – minor injury **(h) Layout C – moderate injury** **(i) Layout C – serious/fatal injury**

Figure 7.14. Case study injury severity rates per floor under DBE shaking

The MCE injury rate data is shown in **Figure 7.15**, where majority of injuries were caused by building collapse despite the probability of this occurring being 38.9%. This was due to the usage of the HAZUS® [4] injury rates from **Table 7.1** for the event of collapse, which is significantly larger than the non-collapse-related injury rates observed thus far. Note that lesser falling-related injuries occurred in the MCE event compared to the DBE event due to the decrease in non-collapse cases, resulting in the left branch of the framework in **Figure 7.5** being used less often. The increased shaking severity does not necessarily result in more falls either for non-collapse cases as there already is a high probability of people tripping and

falling in DBE shaking due to A_{FT} usually being larger than A_{fall} on all floors. This resulted in the occurrence of fall-related injuries being almost constant with height. Collapse-related injury rates was also generally constant with height since its effect was the same on all floors. The main difference is due to content-related injuries, of which there are none in Layout C due to no furniture toppling occurring.

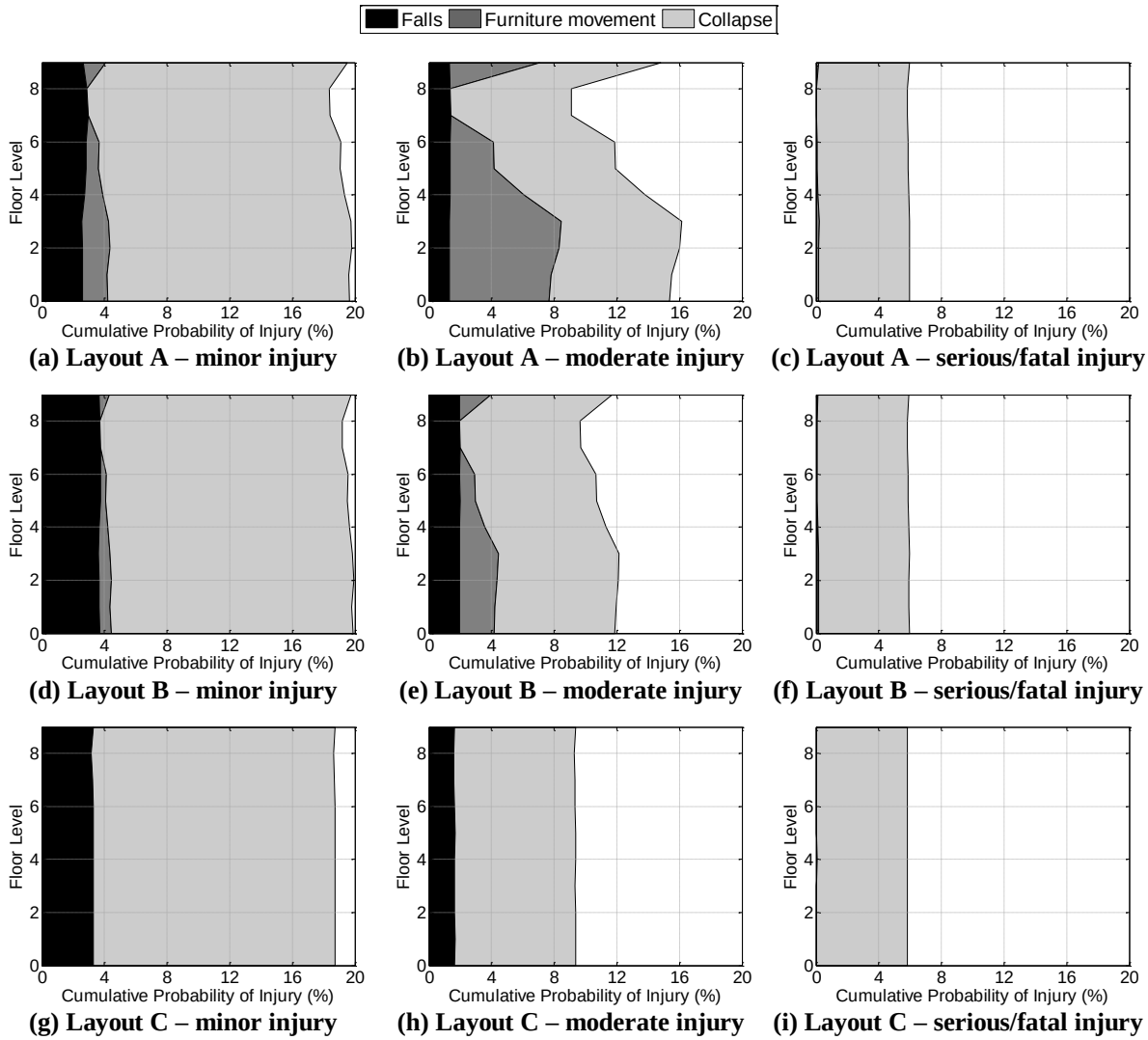

(a) Layout A – minor injury **(b) Layout A – moderate injury** **(c) Layout A – serious/fatal injury**

(d) Layout B – minor injury **(e) Layout B – moderate injury** **(f) Layout B – serious/fatal injury**

(g) Layout C – minor injury **(h) Layout C – moderate injury** **(i) Layout C – serious/fatal injury**

Figure 7.15. Case study injury severity rates per floor under MCE shaking

7.6.4 Case Study Injury Cost

The 84th percentile costs on each floor during SLE, DBE, and MCE events are shown in **Figures 7.16a to 7.16c** for Layout A, B, and C, respectively. The cost trends with floor level are consistent with **Figures 7.13** to **7.15** as for all cases: (i) injury costs increased with shaking severity, and (ii) the DBE and MCE curve peaked at the 2nd floor similarly to the

content overturning response in **Figure 7.12a**. This assessment allows for identifying floors more prone to incurring higher injury costs.

Expected intensity-based loss, $E_{Li|IM}(im)$, is another method of assessment. $E_{Li|IM}(im)$ is calculated using **Eq. 7.10** [22]; where L_i is the total injury cost within the building; $E_{LiOF|IM,NC}(im)$, $E_{LiFM|IM,NC}(im)$, and $E_{Li|IM,C}(im)$ are the expected losses from occupants falling, content movement, and collapse, respectively, at a given intensity measure, $IM = im$; and $P_C(im)$ is the probability of collapse. The contribution of costs by injury source was calculated by only using one of $E_{LiOF|IM,NC}(im)$, $E_{LiFM|IM,NC}(im)$, or $E_{Li|IM,C}(im)$ in **Eq. 7.10**, and setting the other two to zero. Deaggregation of findings by injury source is shown in **Figures 7.16d to 7.16f** for Layouts A, B, and C, respectively; where (i) falling injuries was the major contributor when $Sa(1.25s) < 0.25$ g, (ii) content movement-related costs were larger than that of falling injuries at DBE level in Layout A, MCE level in Layout B, but never in Layout C; and (iii) collapse-related injuries had the highest contribution at more severe events. This information is useful to identify the best approach to meet performance objectives at specific shaking intensities; such as anchoring contents to reduce content movement-related injury costs during DBE shaking ($Sa(1.25s) = 0.50$ g).

$$E_{Li|IM}(im) = \left[E_{LiOF|IM,NC}(im) + E_{LiFM|IM,NC}(im)\right]\left[1 - P_C(im)\right] + E_{Li|IM,C}(im).P_C(im) \quad \textbf{(7.10)}$$

The annual rate of exceeding a given cost, $\lambda_{Li}(l_i)$, is another assessment method. This can be calculated using **Eq. 7.11** [68]; where $G_{Li|IM,NC}(l_i|im)$, and $G_{Li|IM,C}(l_i|im)$ are cost exceedance probabilities for non-collapse and collapse-related injuries, respectively. Note here that $G_{Li|IM,NC}(l_i|im)$ combines both fall and content movement-related injuries as these are not necessarily mutually exclusive events (i.e. a person falling may then be injured by toppling content). $\lambda_{Li}(l_i)$ curves are shown in **Figures 7.16g to 7.16i**; where non-collapse-related injuries dominate at frequent events where $\lambda_{Li}(l_i) > 6\times10^{-4}$ (return period lower than 1,670 years), while collapse dominates at rarer events where $\lambda_{Li}(l_i) < 1.8\times10^{-4}$ (return period

greater than 5,560 years). While the rarity of incurring collapse-related losses appear to contrast the large expected collapse-related losses observed at more frequent events in **Figures 7.16d to 7.16f**, it should be noted that the consequence of collapse is significant (almost $1 billion), and as such the expected loss is large despite the rarity of collapse for frequent events. As risk is a function of both occurrence and consequence, **Figures 7.16g to 7.16i** is more useful in conveying risk.

$$\lambda_{Li}(l_i) = \int \left(G_{Li|IM,NC}(l_i \mid im, NC).P_{NC}(im) + G_{Li|IM,C}(l_i \mid im).P_{C|IM}(im) \right) \left| \frac{d\lambda_{IM}(im)}{dIM} \right| .dIM \quad \textbf{(7.11)}$$

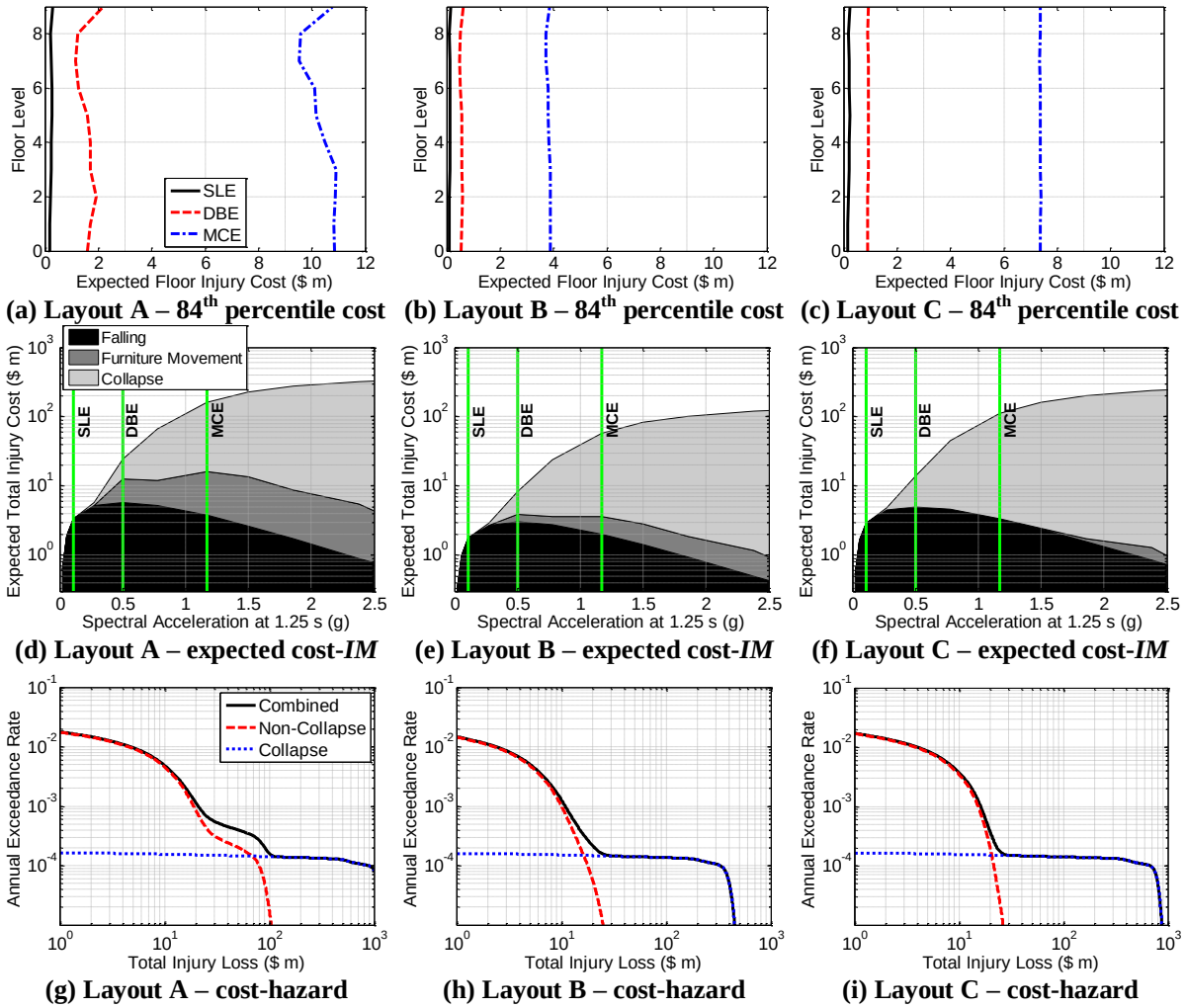

(a) Layout A – 84th percentile cost **(b) Layout B – 84th percentile cost** **(c) Layout C – 84th percentile cost**

(d) Layout A – expected cost-*IM* **(e) Layout B – expected cost-*IM*** **(f) Layout C – expected cost-*IM***

(g) Layout A – cost-hazard **(h) Layout B – cost-hazard** **(i) Layout C – cost-hazard**

Figure 7.16. Case study injury cost results

7.7 COMPARISON WITH HISTORICAL DATA SETS

Historical datasets collected by Seligson and Shoaf [12] detailing the severity of injuries during the 1994 Northridge earthquake, and by Shoaf et al. [10] and Johnston et al. [15] investigating the cause of injuries and the affected body region during the 1994 Northridge and 2011 Canterbury events, respectively, were compared against the framework's outputs to observe if the latter were reasonable. To approximate the relative severity of the Northridge and Canterbury earthquakes in relation to the case study shaking intensity, the distribution of *Sa*(1.25 s) obtained from all ground motions recorded during each event are shown in **Figures 7.17a** and **7.17b**, respectively, and the case study's SLE, DBE, and MCE shaking intensities are annotated. Here, around 60% of recordings made during the 1994 Northridge earthquake was smaller than the case-study SLE, and around 67% of those from the 2011 Canterbury event was smaller than the case-study DBE. This does not imply that the two events are minor, as some sites during the Northridge earthquake recorded shaking intensities close to the case-study's MCE level. Rather, it is the smeared seismicity which is low due to recordings being made over a wider region.

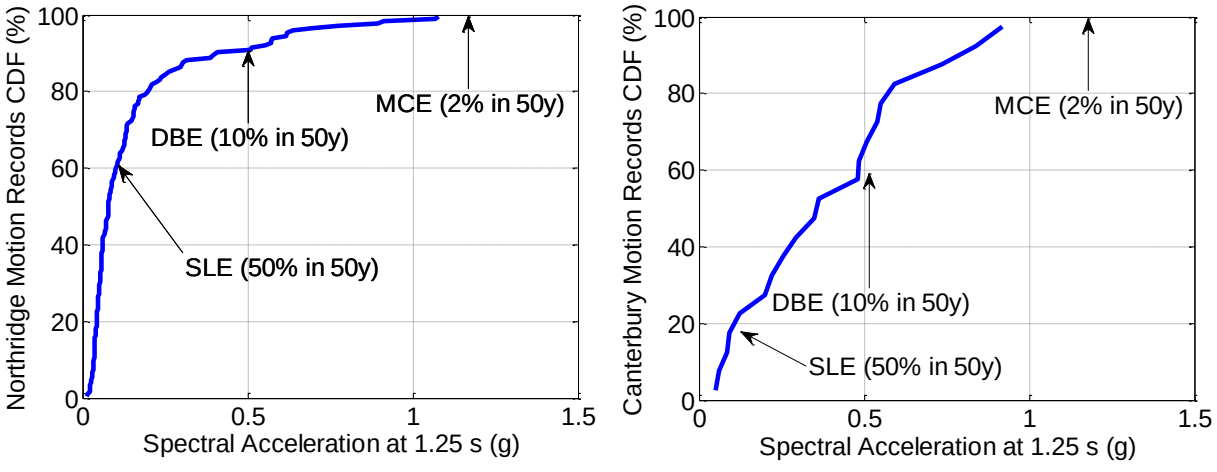

Figure 7.17. Severity of (a) 1994 Northridge and (b) 2011 Canterbury earthquakes against equivalent case-study shaking intensity

Deaggregation of injuries by severity, cause, and affected body part are shown in **Figures 7.18a** to **7.18c**, respectively. The percentage of population who were injured, P_{injury},

for each case is shown in the legend. Note that the SLE, DBE, and MCE case-study findings represent the mean deaggregation considering all three room layouts. It can be seen from **Figure 7.18a** that the breakdown of SLE injuries by injury severity is similar to that of the Northridge data by Seligson and Shoaf [12]. This is reasonable as the 60th percentile of the recorded shaking intensity during the Northridge earthquake was similar to the case-study's SLE as shown in **Figure 7.17a**. The similarity between the case-study SLE findings and the Northridge data therefore shows that the injury framework outputs were reasonable. Note that comparisons cannot be made with the Canterbury earthquake data as details on injury severity were not available.

Figure 7.18b shows that the DBE results closely matched the Canterbury data reported by Johnston et al. [15] with regards to the proportion of injuries which were fall-related, which is reasonable as the case-study's DBE shaking severity is equivalent to the 67th percentile *Sa*(1.25s) value as discussed in **Figure 7.17b**. However, contents had a smaller contribution to injuries. This could be due to Layout C where there were virtually no content-related injuries at DBE shaking level, or that Johnston et al. [15] included types of contents not considered in the framework. In addition, it can be seen that collapse has a large contribution to injuries using the framework despite its rarity, which is due to the significantly higher injury rates for collapse cases provided by HAZUS® [4] in comparison to the non-collapse rates obtained from the framework. In contrast to the framework outputs and the Canterbury data, the Northridge data collected by Shoaf et al. [10] had found that most injuries were content-related. However, the sample size by Shoaf et al. [10] is small (149 out of 24,000 medically-treated injuries being documented) compared to Canterbury (4,900 out of 7,170), and thus may not be as representative. Based these observations and the reasons behind them, the framework injury source outputs appear reasonable.

Figure 7.18b shows that the framework predicted that most injuries were to the head, which contrasts existing data by Shoaf et al. [10] and Johnston et al. [15] where most occurred at the extremities (i.e. arms and legs). This contrast could be due to the possibility that occupants may use their arms to protect themselves when falling, which is not considered in the framework. In addition, 50% of injuries documented by Johnston et al [15] occurred in regions other than those included in the framework; such as face, spine, and dental injuries, among others. Fragility functions to estimate injury severity for these other regions could not be found and hence were not considered at this time. Other possible reasons for differences between the framework's outputs and anecdotal data include: (i) the limited amount of historical data available for comparisons; (ii) complexity in practice for identifying the most critically injured body part; (iii) use of regional-scale data for comparisons with the building-specific findings; and (iv) the buildings considered were designed specifically for the case-study conditions, and may not be applicable to the Northridge and Canterbury regions.

Finally, it can also be seen from the legend that the percentage of occupants injured using the framework is much larger than those observed from Northridge and Canterbury. This could be due to the case-study building being stronger than those in Northridge and Canterbury as it is located in an area with greater seismicity. In addition, occupant behavioral tendencies to mitigate injuries, such as "drop-cover-hold", were not explicitly considered in the model. Based on this, and the findings related to body-parts, the framework gives more conservative estimates of injury costs. This can be improved by incorporating occupant behaviour into the framework, or by using more advanced models for assessing injuries to body parts such as incorporating the effect of impact mass on all body regions.

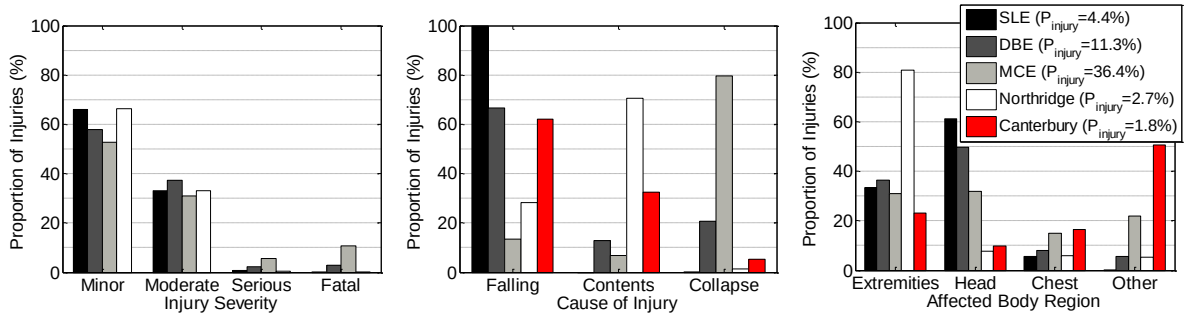

Figure 7.18. Deaggregation of injuries considering average of all three room layouts by (a) severity, (b) cause, and (c) affected body part

7.8 APPLICATION OF FRAMEWORK

7.8.1 Derivation of Sample Values for Simplified Injury Assessment

The proposed framework can be applied to a range of different buildings of varying room layout configurations to obtain sample injury rates for use in less sophisticated injury models such as that by HAZUS® [4]. An example of obtaining these rates are provided in this section for different building global damage states as commonly assumed in past models. Note however that this methodology should be repeated considering other seismic regions to obtain region-specific injury rates, the importance of which was discussed previously in **Section 7.6.3**.

The first step for each individual ground motion used in the framework is to calculate the building's damage ratio, *BDR*, which is a measure of how close the building is to collapse. *BDR* for wall buildings is defined using **Eq. 7.12**, where ID_{bot} and ID_{top} are the interstorey drift between the ground and 1st floor, and between the 9th floor and the roof, respectively. The 2% and 4% are based on the drift limits for collapse caused by extensive wall damage and global building instability, respectively, as discussed previously in **Section 7.4.5**. Based on this definition, *BRD* of 0.125, 0.25, and 0.5, and 1.0 corresponds to slight, moderate, extensive, and collapse damage, respectively.

$$BDR = \max\begin{pmatrix} ID_{bot} / 2\% \\ ID_{top} / 4\% \end{pmatrix} \quad \textbf{(7.12)}$$

Injury rates for Layout A versus *BDR* are shown in **Figures 7.19a** to **7.19c** for minor, moderate, and serious/fatal injuries, respectively. It can be seen that the rates are approximately linear initially when fall response, and hence A_{FT}, governs injuries. Once A_{FT} is large enough, the injuries due to people falling over starts to level off as shown in **Figure 7.19a**, as the probability of occupants falling would not change much. Content movement-related injuries however starts to occur when *BDR* is greater than 0.2, and causes a wider dispersion of injury rates. The mean trends in **Figure 7.19**, and for the other two layouts, were approximated using a bilinear curve. The values on the bilinear curve at the various global building damage states of interest were then recorded and are as shown in **Table 7.8**.

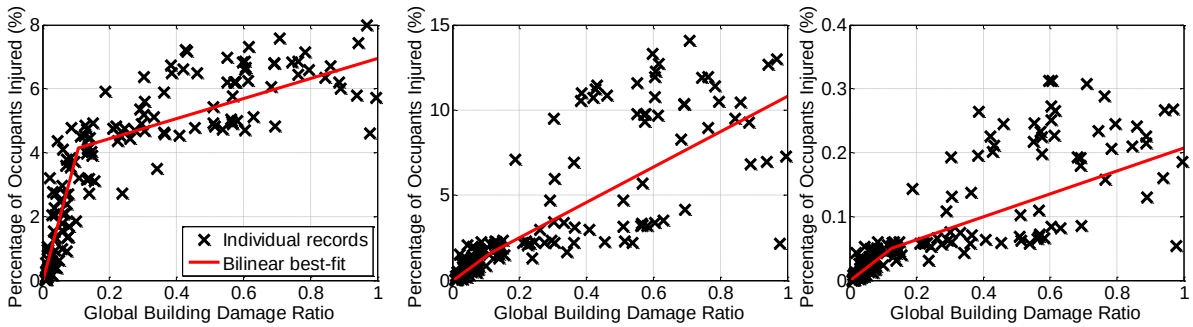

Figure 7.19. Proportion of occupants who incurred an injury with a given severity versus global building damage for room Layout A; (a) minor, (b) moderate, (c) serious/fatal

Table 7.8. Sample injury rates from case study

		Global Building Damage Level			
Injury Severity	**Layout**	**Slight (*BDR* = 0.125)**	**Moderate (*BDR* = 0.25)**	**Extensive (*BDR* = 0.50)**	**Complete – no collapse (*BDR* = 1.0)**
Minor (%)	A	4.2	4.6	5.4	7.0
	B	5.6	5.8	6.4	7.4
	C	4.8	4.9	5.1	5.7
	Average	**4.9**	**5.1**	**5.6**	**6.7**
Moderate (%)	A	1.7	3.0	5.6	0.8
	B	2.5	3.4	4.4	6.5
	C	2.3	2.4	2.6	2.9
	Average	**2.2**	**2.9**	**4.2**	**6.7**
Serious (%)	A	0.05	0.07	0.12	0.21
	B	0.07	0.09	0.12	0.20
	C	0.05	0.06	0.06	0.07
	Average	**0.06**	**0.07**	**0.10**	**0.16**
Fatal (%)	A	0.004	0.005	0.008	0.015
	B	0.006	0.007	0.009	0.013
	C	0.005	0.005	0.005	0.006
	Average	**0.005**	**0.006**	**0.007**	**0.011**

It can be seen that the values reported in **Table 7.8** are generally higher than those provided by HAZUS® [4]. This could again be due to (i) the high seismicity of the case-study scenario, resulting in a large proportion of minor and moderate injuries even for slight building damage, and (ii) the exclusion of behavioural factors in the framework which may reduce the number of injuries which occur.

7.8.2 Feasibility of Mitigation Approaches

Another use of the injury framework is to assess the feasibility of implementing mitigation strategies. A brief case-study evaluating the effectiveness of fixing toppling-sensitive furniture for Layouts A and B was examined to demonstrate its usefulness. It was estimated here that it costs \$17 to fix a single item of furniture, or \$20,200 in total if all toppling-sensitive furniture (i.e. bookshelves and filing cabinets) within the building was fixed. This was based on the assumption that: (i) a labourer's hourly rate was \$25 [69]; (ii) toppling furniture required two labourers and ten minutes to fix each; (iii) other furniture did

not require fixing; and (iv) the material cost for fixing each furniture was $8.50 based on the New Zealand Earthquake Commission's furniture-fixing guide [70] and local hardware store prices.

The framework was applied to the case-study building assuming that no furniture toppling occurred. Cost-benefit analysis between this case, and that assuming furniture did topple, was performed using net-present-cost (*NPC* analysis based on **Eq. 7.13**, where *IC* is the initial mitigation cost, *N* is the duration in years, *r* is the discount rate, and *EAL* is the expected annual injury loss calculated using **Eq. 7.14**. *EAL* was $0.279 and $0.257 million for cases with unfixed and fixed toppling furniture for Layout A, respectively, and was $0.119 and $0.117 million for Layout B, respectively. The former indicates that the expected savings made in a single year ($0.022 million) already equaled the cost of fixing contents. The *NPC* curves assuming *r* of 6% from fixing furniture was therefore constantly lower than that if the furniture was unfixed for Layout A as shown in **Figure 7.20a**; with the total expected savings reaching around $0.45 million after 50 years. The difference for Layout B was smaller as shown in **Figure 7.20b** due to the smaller contribution of furniture toppling to injuries. However, anchoring toppling-sensitive furniture still proved to be a cost-effective solution as it results in lower *NPC* after 12 years of the building being in service.

$$NPC(r,N) = IC + \sum_{t=1}^{N} \frac{EAL}{(1+r)^t} \quad \textbf{(7.13)}$$

$$EAL = E_{Li|IM}(im).\left|\frac{d\lambda_{IM}(im)}{dIM}\right|.dIM \quad \textbf{(7.14)}$$

A limitation of this assessment method was that the use of expected values only suited risk-neutral decision makers [71]. An "effective injury cost-hazard curve", which consisted of shifting the $\lambda_{Li}(l_i)$ curves in **Figure 7.16c** to the right by *IC*, could be used for varying risk-appetites instead. The effective hazard curves for Layout A and B are shown in **Figures 7.20c** and **7.20d**, respectively, where the benefits from fixing contents only affected events with an

annual exceedance rate between 2.0×10^{-3} and 1.3×10^{-4} (or a 500 to 7,690 year return period). However, the negligible difference at other exceedance rates illustrated that there were minimal downsides in investing $20,200 to secure contents. Based on both assessment methods, the decision should still be to fix toppling contents.

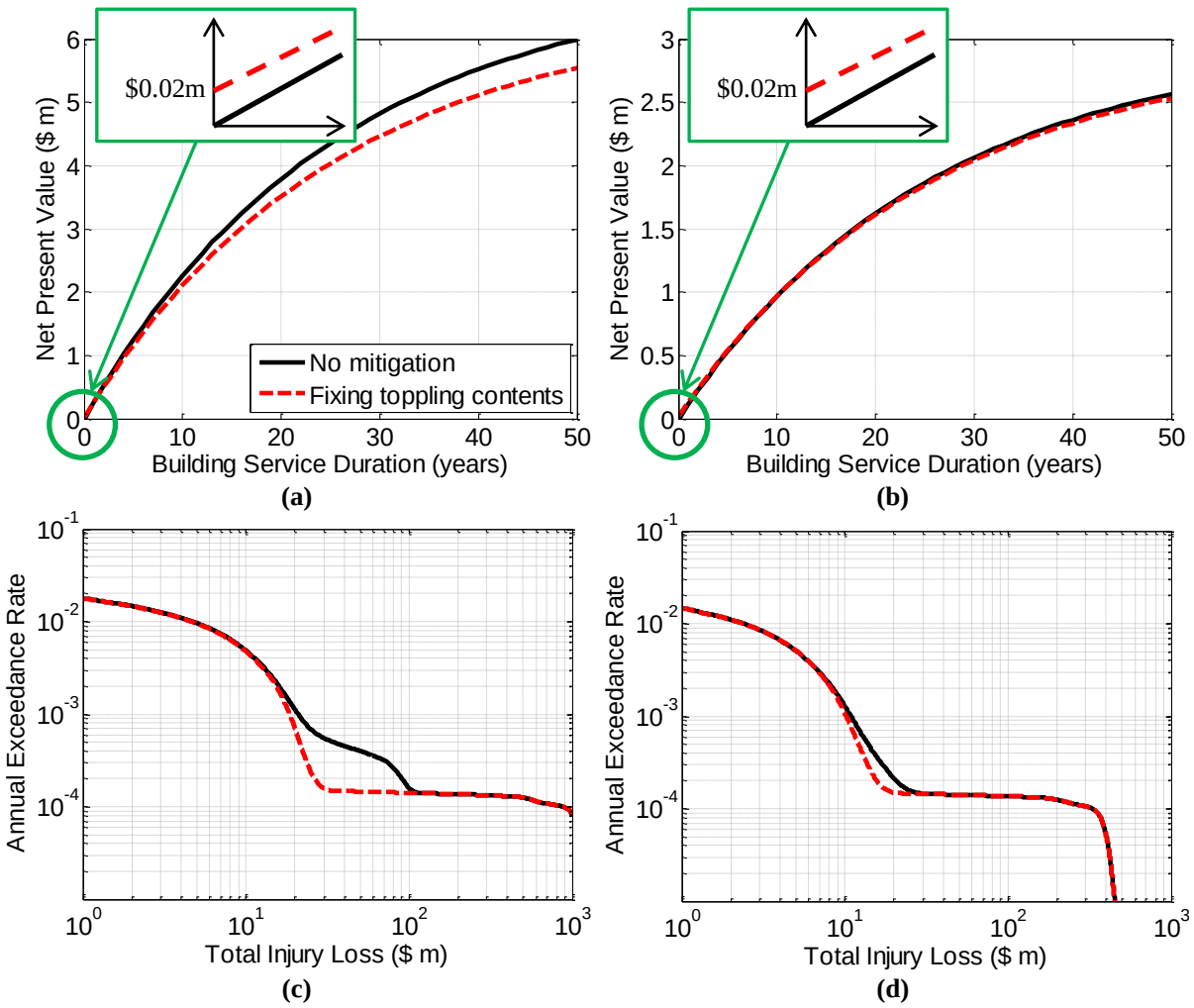

Figure 7.20. Cost-benefit assessment of mitigation strategies; (a) Net-present-value, (b) effective loss hazard curve

7.9 CONCLUSIONS

A seismic indoor injury prediction framework with consideration of injuries due to (i) occupants losing balance and falling over, and (ii) content movement is proposed. The framework was applied to a case-study building to demonstrate its application. The conclusions are as follows:

1. Current injury prediction methods which consider non-fatal injuries either use predefined injury rates, or predict the occurrence of toppling contents hitting occupants without considering its consequence. Models exist to predict the occurrence of falling, the severity of injuries for a given impact velocity, and injury costs for a given severity; but they had not been incorporated together into a usable framework.
2. The framework proposed in this study describes methods to incorporate existing models for use in seismic risk assessments. In addition, methodologies to spatially distribute occupants to account for non-uniform occupant densities, and to predict impact velocity and mass acting on occupants from various sources, are proposed to link the occurrence of impacts against the occupant to injury severity.
3. The case-study injury rates using the proposed model are consistent with injury data from the 1994 Northridge and 2011 Canterbury events for injury severity and cause information. There were notable differences between the case-study injury rates and the recorded anecdotal data however in identifying the most critically injured body part, and the percentage of occupants who were injured. The rates were also more conservative than those proposed by HAZUS® [4]. The contrasts are likely due to (i) exclusion of occupant behaviour when attempting to avoid injuries, such as "drop-cover-hold", and (ii) the case-study buildings were designed for a region with higher seismicity and thus experience higher peak total floor accelerations, and hence fall-related injuries, compared to buildings in zones of lower seismicity designed with the same force reduction factor.
4. The framework can be used for several purposes. This includes (i) deriving sample injury rates for use with more basic injury models, such as those by HAZUS® [4], or (ii) for assessing the feasibility of implementing mitigation strategies. Examples demonstrating the application of the framework for these purposes were provided.

7.10 REFERENCES

1. Deierlein, G. G., Krawinkler, H., & Cornell, C. A. (2003). A Framework for Performance-based Earthquake Engineering. Paper presented at the 2003 Pacific Conference on Earthquake Engineering, Christchurch, New Zealand.
2. Miller, T. R. (1993). Costs and Functional Consequences of U.S. Roadway Crashes. Accident Analysis and Prevention, 25(5), 593-607.
3. So, E. K. M., & Spence, R. (2006). Factors Determining Human Casualties in Earthquakes: A Revised Loss Modelling Approach. Paper presented at the 8th US National Conference on Earthquake Engineering, San Francisco, California, US.
4. FEMA. (2015). Hazus(R) - MH 2.1 Technical Manual - Earthquake Model: Department of Homeland Security, Mitigation Division, Washington, D.C.
5. Allen, T. I., Marano, K. D., Earle, P. S., & Wald, D. J. (2009). PAGER-CAT: A Composite Earthquake Catalog for Calibrating Global Fatality Models. Seismological Research Letters, 80(1), 57-62.
6. Osaki, Y., & Minowa, M. (2001). Factors Associated with Earthquake Deaths in the great Hanshin-Awaji Earthquake, 1995. American Journal of Epidemiology, 153(2), 153-156.
7. Coburn, A. W., Spence, R. J. S., & Pomonis, A. (1992). Factors determining human casualty levels in earthquakes: Mortality prediction in building collapse. Paper presented at the Tenth World Conference in Earthquake Engineering, Madrid, Spain.
8. Porter, K. A., Shoaf, K. I., & Seligson, H. A. (2006). Value of Injuries in the Northridge Earthquake. Earthquake Spectra, 22(2), 555-563.
9. Murakami, H. (1996). Chances of Occupant Survival and SAR Operation in the Buildings Collapsed by the 1995 Great Hanshin Earthquake, Japan. Paper presented at the Eleventh World Conference on Earthquake Engineering, Acapulco, Mexico.
10. Shoaf, K. I., Sareen, H., Nguyen, L. H., & Bourque, L. B. (1998). Injuries as a result of California Earthquakes in the Past Decade. Disasters, 22(3), 218-235.
11. Peek-Asa, C., Kraus, J. F., Bourque, L. B., Vimalachandra, D., Yu, J., & Abrams, J. (1998). Fatal and hospitalized injuries resulting from the 1994 Northridge earthquake. International Journal of Epidemiology, 27(3), 459-465.
12. Seligson, H. A., & Shoaf, K. I. (2003). Human impacts of earthquakes. In Earthquake Engineering Handbook. CRC Press, Boca Raton, FL: W F Chen, C R Scawthorn.
13. Petal, M. A. (2004). Urban Disaster Mitigation and Preparedness: The 1999 Kocaeli Earthquake. PhD Thesis, Department of Urban Planning, University of California, LA.
14. Spence, R., & So, E. K. M. (2009). Estimating Shaking-Induced Casualties and Building Damage for Global Earthquake Events: Cambridge Architectural Research Ltd, Cambridge, UK.
15. Johnston, D., Standring, S., Ronan, K., Lindell, M., Wilson, T., Cousins, J., Aldridge, E., Ardagh, M. W., Deely, J. M., Kirsch, S. J. T., & Bissell, R. (2014). The 2010/2011 Canterbury earthquakes: context and cause of injury. Natural Hazards, 73(2), 627-637.
16. Ohta, Y., Ohashi, H., & Kagami, H. (1986). A Semi Empirical Equation for Estimating Occupant Casulty in an Earthquake. Paper presented at the 8th European Conference on Earthquake Engineering, Lisbon, Portugal.
17. Murakami, H. O. (1992). A Simulation Model to Estimate Human Loss for Occupants of Collapsed Buildings in an Earthquake. Paper presented at the 10th WCEE, Madrid, Spain.
18. Shiono, K., Krimgold, F., & Ohta, Y. (1991). Post-Event Rapid Estimation of Earthquake Fatalities for the Management of Rescue Activity. Comprehensive Urban Studies, 44, 61-105.
19. Stojanovski, P., & Dong, W. (1994). Simulation Model for Earthquake Casualty Estimation. Paper presented at the Fifth U.S. National Conference on Earthquake Engineering, Chicago, Illinois, US.
20. Nichols, J. M., & Beavers, J. E. (2003). Development and Calibration of an Earthquake Fatality Function. Earthquake Spectra, 19(3), 605-633.
21. So, E. K. M., & Spence, R. (2013). Estimating shaking-induced casualties and building damage for global earthquake events: a proposed modelling approach. Bulletin of Earthquake Engineering, 11(1), 347-363.
22. Mitrani-Reiser, J. (2007). An Ounce of Prevention: Probabilistic Loss Estimation for Performance Based Earthquake Design. PhD Thesis, California Institute of Technology, Pasadena, California.
23. Applied Technology Council. (2002). Commentary on the use of ATC-13 EQ Damage Evaluation data for Probable Maximum Loss Studies of California Buildings. Redwood City, CA.
24. Seligson, H. A., Shoaf, K. I., & Kano, M. (2006). Development of Casualty Models for Non-Ductile Concrete Frame Structures for use in PEER's Performance-Based Earthquake Engineering Framework.

Paper presented at the 8th US National Conference on Earthquake Engineering, San Francisco, California, US.
25. CUEDD. (2009). Cambridge University Earthquake Damage Database. from http://www.arct.cam.ac.uk/eq/
26. ASCE. (2000). Prestandard and Commentary for the Seismic Rehabilitation of Buildings, FEMA 356. Federal Emergency Management Agency, Washington, D.C.
27. Yeo, G. L., & Cornell, C. A. (2003). Building-Specific Seismic Fatality Estimation Methodology. Paper presented at the 9th International Conference on Applications of Statistics and Probability in Civil Engineering (ICASP9), San Francisco, California, USA.
28. Okada, S., Nachi, N., & Endo, T. (2012). Seismic Assessment Method for Indoor Injury Risk and Its Application. Paper presented at the 15th World Conference on Earthquake Engineering, Lisbon, Portugal.
29. Keith, D. (1997). Use of Peak Occupancy Data to Model the Effects of Occupancy-Sensing Lighting Controls. Masters Thesis, Faculty of the Graduate School of the University of Colorado.
30. Abushakra, B., & Claridge, D. (2001). Accounting for the Occupancy Variable in Inverse Building Energy Baselining Models. Paper presented at the First International Conference for Enchance Building Operations, Austin, Texas.
31. Mahdavi, A. (2009). Patterns and Implications of User Control Actions in Buildings. Indoor and Built Environment, 18(5), 440-446.
32. Wong, L. T., & Mui, K. W. (2011). Modelling Transient Occupant Loads for Offices. Architectural Science Review, 49(1), 53-58.
33. Jongkees, L. B. W., & Groen, J. J. (1942). The Stability of the Human Body [Dutch]. Nederlands Tiidschrift voor Geneeskunde, 86, 1401-1407.
34. De Graaf, B., & Weperen, W. V. (1997). The Retention of Balance: An Exploratory Study into the Limits of Acceleration the Human Body Can Withstand Without Losing Equilibrium. Human Factors, 39(1), 111-118.
35. Abu-Faraj, Z. O., Akar, H. A., & Al-Qadiri, M. N. (2010). Evaluation of Fall and Fall Recovery in a Simulated Seismic Environment: A Pilot Study, 32nd Annual International Conference of the IEEE EMBS. Buenos Aires, Argentina.
36. Kaneko, M., & Hayashi, Y. (2004). A Proposal for Simple Equations to Express a Relation between Overutrning Ratios of Rigid Bodies and Input Excitations. Paper presented at the 13th World Conference on Earthquake Engineering, Vancouver, Canada.
37. Sorrentino, L., AlShawa, O., & Decanini, L. D. (2011). The relevance of energy damping in unreinforced masonry rocking mechanisms. Experimental and analytic investigations. Bulletin of Earthquake Engineering, 9(5), 1617-1642.
38. Rocscience. (2015). RocFall - Statistical Analysis of Rockfalls.
39. Jankowski, R. (2010). Experimental study on earthquake-induced pounding between structural elements made of different building materials. Earthquake Engineering and Structural Dynamics, 39(3), 343-354.
40. Shenton III, H. W. (1996). Criteria for Initiation of Slide, Rock and Slide-Rock Rigid-Body Modes. Journal of Engineering Mechanics, 122(7), 690-693.
41. Konstantinidis, D. A. (2008). Experimental and Analytical Studies on the Seismic Response of Freestanding and Anchored Building Contents. PhD Thesis, Civil and Environmental Engineering, University of California, Berkeley.
42. Shenton III, H. W., & Jones, N. P. (1992). Base Excitation of Rigid Bodies. Part I: Formulation. Journal of Engineering Mechanics, 117(10), 2286-2306.
43. States, J. D. (1969). The Abbreviated and the Comprehensive Research Injury Scales. Paper presented at the 13th STAPP Car Crash Conference, Boston, MA.
44. Viano, D. C., & Lau, I. V. (1988). A Viscous Tolerance Criterion for Soft Tissue Injury Assessment. Journal of Biomechanics, 21(5), 387-399.
45. Viano, D. C., & King, A. I. (2006). Biomechanics of Chest and Abdomen Impact, Fourth Edition. In J. D. Bronzino (Ed.), Biomedical Engineering Fundamentals: CRC Press.
46. Kroell, C. K., Schneider, D. C., & Nahum, A. M. (1971). Impact Tolerance and Response to the Human Thorax. Paper presented at the 15th Stapp Car Crash Conference, Coronado, CA.
47. Kroell, C. K., Schneider, D. C., & Nahum, A. M. (1974). Impact tolerance and response to the human thorax II. Paper presented at the 18th Stapp Car Crash Conference, Ann Arbor, MI.
48. Automotive Engineers of Japan. (2006). Impact Biomechanics for Engineers and Medical Staff: Automotive Engineers of Japan.
49. Prasad, P., & Mertz, H. J. (1985). The position of the United States delegation to the ISO working group 6 on the Use of HIC in the automotive environment. Washington DC.

50. MacKay, M. (2007). The Increasing Importance of the Biomechanics of Impact Trauma. Sadhana, 32(4), 397-408.
51. Lobdell, T. E., Kroell, C. K., Schneider, D. C., Hering, W. E., & Nahum, A. M. (1973). Impact Response of the Human Thorax. In W. F. King & H. J. Mertz (Eds.), Human Impace Response Measurement and Simulation (pp. 201-245): Plenum Press, New York.
52. Payne, A. R., & Patel, S. (2001). Occupant Protection and Egress in Rail Systems: MIRA.
53. Federal Highway Administration. (1994). Technical Advisory: Motor Vehicle Accident Costs, Technical Advisory #7570.2: U.S. Department of Transportation, Washington, D.C.
54. Ministry of Transport. (2016). Social Cost of Road Crashes and Injuries 2015 Update. New Zealand.
55. Zaloshnja, E., Miller, T. R., Romano, E., & Spicer, R. (2004). Crash costs by body part injured, fracture involvement, and threat-to-life severity, United States, 2000. Accident Analysis and Prevention, 36(3), 415-427.
56. Loomis, A. (1949). Figure Drawing for All It's Worth: The Viking Press.
57. Belendez, A., Pascual, C., Mendez, D. I., Belendez, T., & Neipp, C. (2007). Exact Solution for the Nonlinear Pendulum. Revista Brasileira de Ensino de Fisica, 29(4), 645-648.
58. Standards New Zealand. (2004). NZS 1170.5:2004, Structural Design Actions Part 5: Earthquake Actions New Zealand: Standards New Zealand, Wellington, New Zealand.
59. OECD. (2009). Society at a Glance 2009: OECD Social Indicators. OECD Publishing, Paris.
60. Bradley, B. A. (2010). A Generalized Conditional Intensity Measure Approach and Holistic Ground Motion Selection. Earthquake Engineering and Structural Dynamics, 39(12), 1324-1342.
61. Bradley, B. A. (2012). A Ground Motion Selection Algorithm Based on the Generalized Conditional Intensity Measure Approach. Soil Dynamics and Earthquake Engineering, 40, 48-61.
62. Stirling, M. W., McVerry, G. H., Gerstenberger, M. C., Litchfield, N. J., Van Dissen, R. J., Berryman, K. R., Barnes, P., Wallace, L. M., Villamor, P., Langridge, R. M., Lamarche, G., Nodder, S., Reyners, M. E., Bradley, B., Rhoades, D. A., Smith, W. D., Nicol, A., Pettinga, J., Clark, K. J., & Jacobs, K. (2012). National seismic hazard model for New Zealand : 2010 update. Bulletin of the Seismological Society of America, 102(4), 1514-1542.
63. Bradley, B. A. (2010). NZ-Specific Pseudo-Spectral Acceleration Ground Motion Prediction Equations based on Foreign Models: Department of Civil and Natural Resources Engineering, University of Canterbury, Christchurch, New Zealand.
64. Carr, A. J. (2004). Ruaumoko 2D - Inelastic dynamic analysis program. Department of Civil and Natural Resources Engineering, University of Canterbury, Christchurch.
65. Carr, A. J. (2008). Ruaumoko Manual (Vol. Volumne 2: User Manual for the 2:Dimensional Version Ruaumoko 2D). University of Canterbury, Christchurch, NZ.
66. Saiidi, M., & Sozen, M. A. (1979). Simple and complex models for nonlinear seismic response of reinforced concrete structures. Illinois: University of Illinois.
67. Caughey, T. K. (1960). Calssical Normal Modes in Damped Linear Systems. Journal of Applied Mechanics, 27, 269-271.
68. Aslani, H., & Miranda, E. (2005). Probabilistic Earthquake Loss Estimation and Loss Disaggregation in Buildings: Department of Civil and Environmental Engineering, Stanford University.
69. Rawlinson & Co. (2015). Rawlinsons New Zealand construction handbook. Rawlhouse Publishing, Wellington, New Zealand.
70. The New Zealand Earthquake Comission (EQC). (2015). Easy Ways to Quake Safe Your Home.
71. Goda, K., & Hong, H. P. (2006). Optimal Seismic Design Considering Risk Attitude, Societal Tolerable Risk Level, and Life Quality Criterion. Journal of Structural Engineering, 132(12), 2027-2035.

8. Wall Stiffness and Strength Effect on Injuries and Damage Repair Cost in Seismic Events

8.0 SUMMARY

A case-study applying the newly derived injury prediction framework from **Chapter 7** to several 10-storey cantilever wall buildings of various stiffness and strength was examined to quantify the effect of these building properties on injuries. It was found that buildings with greater stiffness or strength had lower occurrences of building collapse and related injuries. However, there was an increase in peak total floor accelerations, A_{FT}, which is correlated to more fall-related injuries occurring. Building content movement-related injuries occurred more in the strongest building compared to the weakest building due having higher A_{FT} yet similar floor shaking frequency. In contrast, content movement-related injuries occurred less in the stiffest building compared to the most flexible building on most floors due to its higher floor shaking frequency despite also experiencing higher A_{FT}. Based on these findings, and the building damage repair costs investigated previously in **Chapter 3** which excluded the effect of downtime, it was found that (i) stiffer buildings incur lower total losses (i.e. injury and damage) compared to more flexible buildings, and (ii) varying strength had minimal effect on total losses. Cost-benefit assessment showed that increasing stiffness is a financially viable option to improve the building's seismic resilience. Sample injury rates based on this study's findings are proposed for use in less sophistical injury modelling approaches.

8.1 INTRODUCTION

Existing literature (e.g. Freeman [1], Berg [2]) examined conflicting viewpoints on the optimal stiffness of a building in regards to improving earthquake resilience. For example, flexible buildings, which are generally cheaper to construct than stiffer buildings, are also

likely to have lower inertia forces and total floor accelerations under typical earthquake records where spectral accelerations decrease with increasing period. However, flexible buildings experience larger drifts which result in greater damage to drift-sensitive non-structural elements such as partitions, and greater plastic displacement or rotation demands. As such, it is not clear whether increasing a building's stiffness would improve its overall performance or reduce earthquake related losses. Likewise, increasing strength is likely to reduce structural damage but would likely increase total accelerations, and hence it is also not clear if increasing strength is better overall.

The influence of stiffness and strength on direct damage-repair costs of several 10-storey reinforced concrete cantilever wall buildings was examined in **Chapter 3**. It was found that the stiffest building and the strongest building considered both incurred lower damage losses for events equivalent to a design-level earthquake or rarer compared to the weakest building and the most flexible building. However, cost-benefit assessments using expected annual loss, *EAL*, showed that the expected savings over a 50 year lifespan for these two buildings were not sufficient to offset their increased initial construction costs. A limitation of this study was that injury and downtime losses were not included.

The influence of a building's stiffness and strength on the sliding response of building contents (i.e. furniture, machinery) was examined in **Chapter 6** considering a wider range of buildings with a varying number of floors. It was shown that contents in stiffer buildings often have a less severe displacement response compared to those in more flexible buildings despite experiencing larger total floor accelerations, A_{FT}. This was due to the higher floor shaking frequency of stiffer buildings, resulting in lower floor velocities relative to the content and smaller back-and-forth sliding motion excursions. Contents in stronger buildings however tended to have larger response due to them having a larger A_{FT} yet similar shaking frequency compared to weaker buildings. A limitation of **Chapter 6** is that the effect of

content movement on damage loss and injuries were not considered. However, the indoor injury prediction framework developed in **Chapter 7** is capable of estimating injuries caused by contents sliding and rocking; in addition to those from occupants falling and building collapse.

In this chapter, the newly developed injury prediction framework, room layouts, and content detailsfrom **Chapter 7** is applied to the case-study buildings from **Chapter 3** to assess the influence of a building's stiffness and strength on predicted injuries, and the impact of injuries on decision-making outcomes. Answers to the following are sought:

1. What are the major sources of injury for each shaking intensity level?
2. How does the building's stiffness and strength affect injuries from the various sources?
3. How significant are cost associated with injury (i.e. medical treatment, decrease in quality of life) in relation to those for damage direct-repairs(i.e. replacing damaged components within a building)?
4. Which building is best considering losses over the design life?
5. Do the conclusions from (4) change using a loss-hazard assessment?
6. How can the findings be used to derive sample injury rates for use in less sophisticated prediction approaches?

8.2 CASE STUDY DETAILS

8.2.1 Building Properties

Five 10-storey reinforced concrete cantilever wall buildings with floor heights of 4.0 m on the ground floor and 3.6 m on other floors were considered for this study. These buildings were designed using a 10% probability of exceedance in 50 years uniform hazard acceleration spectra (UHS) derived from probabilistic seismic hazard analyses (described in

Section 8.3.2) for subsoil class C conditions [3] in Wellington, New Zealand. Their fundamental periods, *T*, and design force reduction factors, *R*, are listed in **Table 8.1**. Further details on the design procedure are described in **Section 3.3.1**. Note that for the remainder of this chapter, "strength" is quantified as the wall's base moment capacity relative to that required for an $R = 1.0$ design, rather than its absolute value.

Table 8.1. Description and initial construction cost of buildings

Case	R	Period (s)	Description	Costs ($ million)				
				Walls only	Other Structural	N-S Drift	N-S Acceleration	Total
Baseline	4	1.25	Baseline building	1.41	2.27	2.27	6.86	12.8
Stiffest	4	1.00	56% stiffness increase	1.66	2.13	2.23		12.9
Most flexible	4	1.50	31% stiffness decrease	1.24	2.36	2.28		12.7
Strongest	3	1.25	33% strength increase	1.53	2.36	2.28		13.0
Weakest	5	1.25	20% strength decrease	1.42	2.19	2.25		12.7

The building components considered within each building were identical to that from **Section 2.2.2**, with the exception of structural members and exterior glazing due to less exterior area being available if larger structural walls were used as discussed in **Section 3.3.1**. The total cost of all wall members, non-wall structural members, drift-sensitive non-structural members, and acceleration-sensitive members are also included in **Table 8.1**.

8.2.2 Room Layouts and Occupancy Details

Three different office-room layouts, labelled Layout A, Layout B, and Layout C, were considered and are shown in **Figures 8.1a** to **8.1c**, respectively. These are based on typical room layouts found at the University of Canterbury. For each case, it is assumed that each floor of the building contains 24 rooms in total; 12 with the orientations shown in **Figure 8.1**, and another 12 with the layout flipped horizontally. Other areas such as stairwells were not considered. The details of the contents present in each of the three room layouts are provided in **Table 8.2**. Note that both the room layouts and content details are identical to that used previously in **Chapter 7** (**Section 7.4.2**).

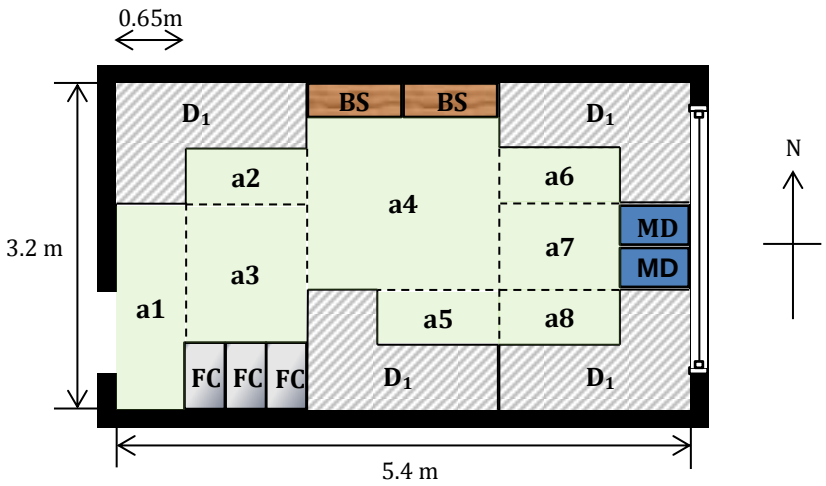

(a)

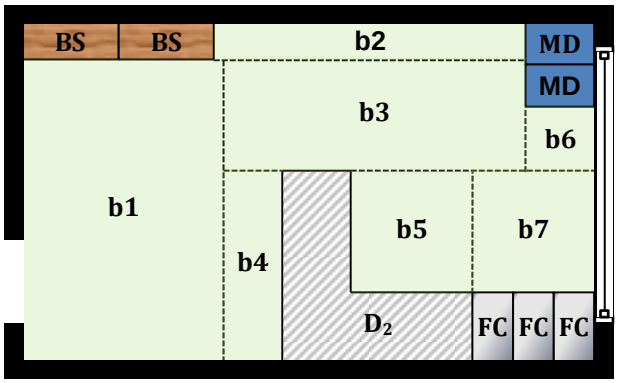

(b)

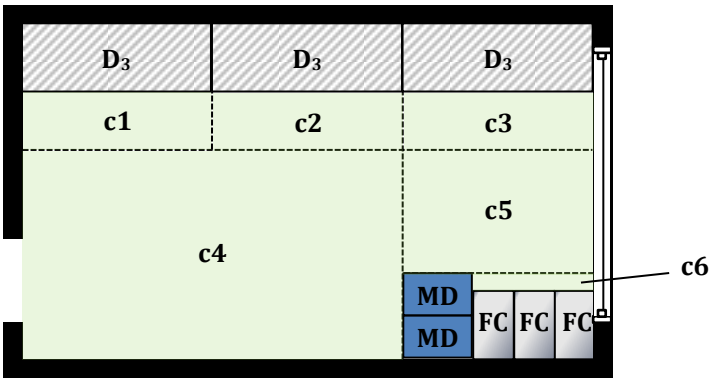

(c)

Figure 8.1. Case study room layouts; (a) Layout A, (b) layout B, and (c) layout C

Table 8.2. Content properties

Content	Rooms	Outer E-W (m)	Outer N-S (m)	Height (m)	μ
Mobile drawers (MD)	A, B, and C	0.65	0.40	0.55	0.1 in E-W 0.45 in N-S
Filing Cabinets (FC)		0.39	0.65	1.65	0.45
Bookshelves (BS)	A and B	0.9	0.2	1.75	
Office desk 1 (D1) [0.65 m depth]	A only	1.80	1.20	0.75	
Office desk 2 (D1) [0.65 m depth]	B only	1.80	1.80	0.75	
Office desk 3 (D3)	C only	1.8	0.65	0.75	

Grids a2, a5, a6, a8, b4, b5, c1, c2, and c3 in **Figure** 8.1 were assigned as sitting-only, while other grids were assumed to be for standing-only. Only one occupant may occupy each sitting-only area, with the exception of grid b4 where two people may be present. In addition, it is assumed that only a maximum of three people in addition to those who are seated may be standing at a given point in time, and that a standing occupant has uniform probability of being located anywhere within the floor area associated to standing-only grids. Finally, the likelihood of a sitting-only grid being occupied is five times the likelihood of a person standing in the room; with the exception of grid b4 where the ratio was 1.25 instead. Reasoning behind these assumptions is provided in **Section 7.4.2**.

Full occupancy was assumed to be 96 occupants per floor in Layout A, 36 occupants per floor in Layout B, and 72 occupants per floor in Layout C, as described in **Section 7.4.3**. The standing height distribution for adult New Zealanders implemented has a median of 1.71 m (from the OECD database [4]), and a lognormal dispersion of 0.07. The effective height of sitting occupants was assumed to be 75% of their standing height. The change in occupancy with time on weekdays was assumed to follow Wong and Mui's [5] transient occupancy model shown in **Figure 8.2**, while no one is assumed to be present on weekends.

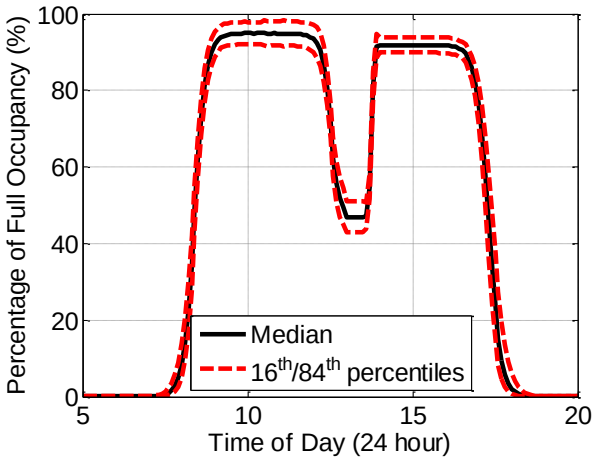

Figure 8.2. Occupancy rate (09:00-17:30 working hours) [5]

8.3 METHODOLOGY

8.3.1 Overall Framework and Injury Prediction

The overall framework implemented for estimating the seismic losses associated with building damage-repair costs, and cost of injury resulting from people falling, contents impacting against people, or building collapse for a single ground-motion record is shown in **Figure 8.3**, which is based off the injury prediction framework proposed in **Section 7.3.1**. Several inputs are required for the framework, such as building and room properties. For each ground motion record, structural analysis is performed to assess the buildings' response and whether it collapsed, and seismic loss assessment is conducted to predict building damage repair costs. If collapse does not occur, content response analyses are performed following **Section 7.2.5**, and the total floor acceleration and content response histories are imported into Monte Carlo simulations for predicting injuries.

The first step of each Monte Carlo simulation is to predict the number of occupants present at the time of shaking following **Section 7.3.2**. If collapse did not occur, injuries were then estimated using the following steps: (i) predict each occupant's location and height (**Section 7.3.3**), (ii) quantify the effect of people falling or being struck by contents (**Section 7.3.4**), and (iii) assess injury severity (**Section 7.2.6**). If collapse occurred, injury rates from HAZUS® [6] were used instead. The final step is to assign injury costs (**Section 7.2.7**) using

datasets by Miller [7] and Zaloshnja et al. [8]. Note that this dataset contains information on direct (i.e. medical treatment costs) and indirect (i.e. decrease in quality of life) aspects of injury cost, of which both are considered in this framework. The possibility of occupants moving and taking cover (i.e. "drop-cover-hold") during strong shaking, and the effect of secondary hazards such as fires and tsunamis are not considered. 5,000 simulations were performed for each ground motion record which was found to provide consistent distributions based on preliminary analyses.

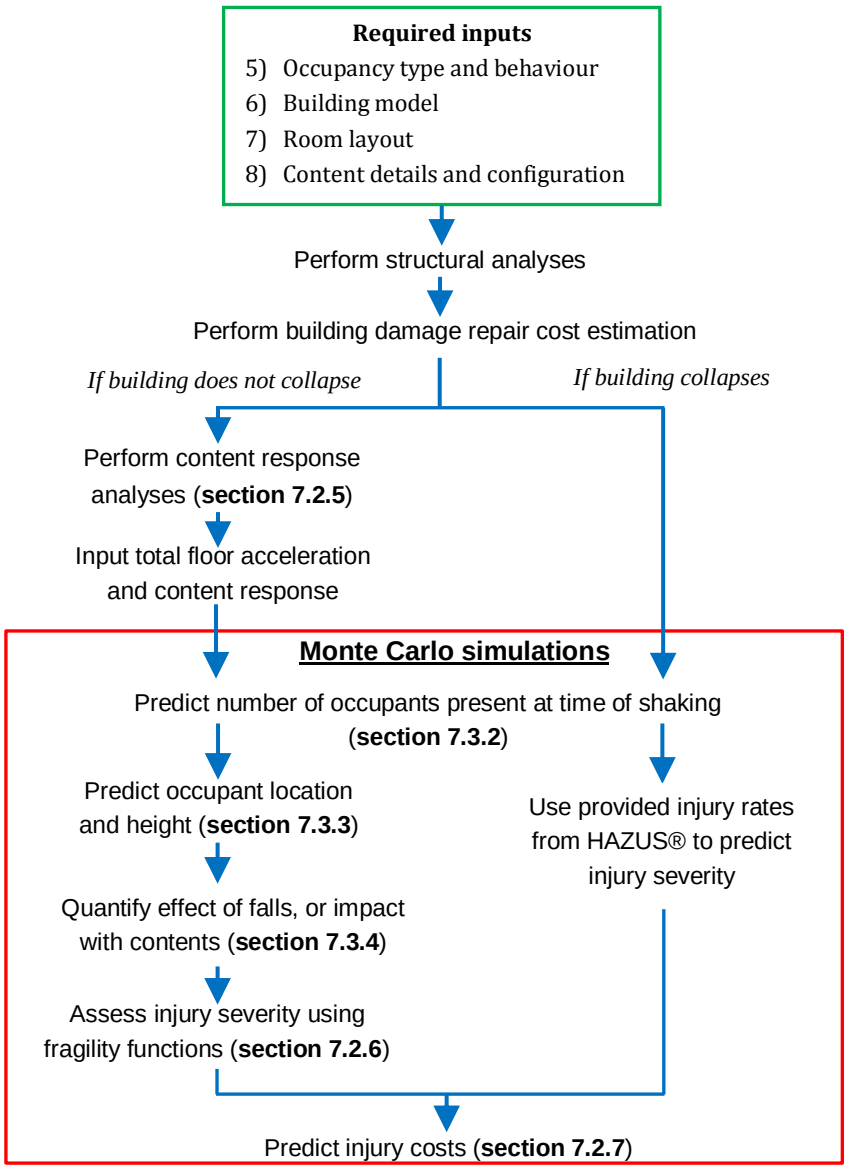

Figure 8.3. Methodology framework

8.3.2 Ground Motion Selection Details

Probabilistic seismic hazard analysis (PSHA) was performed on OpenSHA [9], using New Zealand-specific rupture forecast models [10] and attenuation relationships [11] to obtain the 10% probability of exceedance in 50 years uniform hazard spectra shown in **Figure 8.4a**. This was used to obtain base shear demands, as mentioned in **Section 8.2.1**, rather than the design spectra from NZS1170.5:2004 [12] to ensure consistency with the selected ground motion record selection methodology adopted which required the use of the site's seismic hazard curve shown in **Figure 8.4b**. The Equivalent Static Procedure outlined in NZS1170.5:2004 [12] was followed to distribute lateral loads to each floor.

The ground motion selection methodology adopted was the Generalized Conditioning Intensity Measure approach [13]. Spectral acceleration at 1.25 s, *Sa*(1.25s), was chosen as the conditioning intensity measure. A suite of 11 records were selected, each representing a shaking intensity level ranging from 99% to 0.1% probability of exceedance in 50 years. The 10% in 50 year suite is shown in **Figure 8.4a**. It can be seen that the conditional distribution of other spectral acceleration values of the ground motion record suite matches the theoretical distributions well, indicating that the selected record suite is adequate. Kolmogorov-Smirnov tests [14] were also performed for all non-conditioning intensity measures, such as 5-95% significant duration [15] as shown in **Figure 8.4c**, to ensure that the conditional distributions of the selected suite are reasonable.

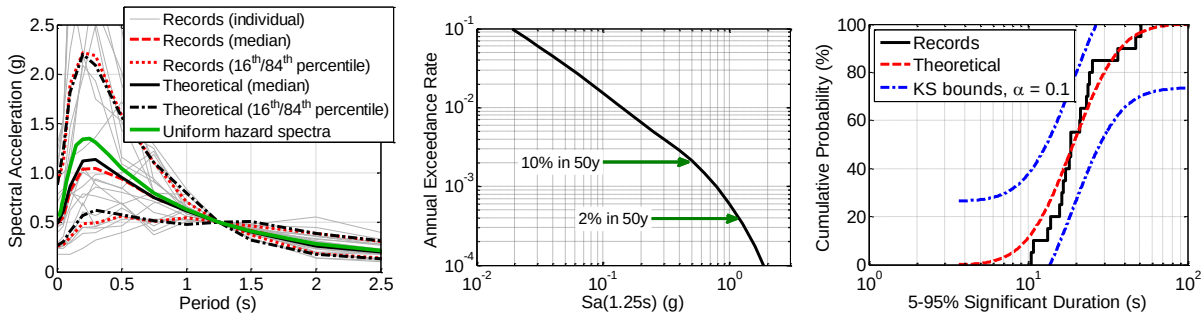

(a) **(b)** **(c)**

Figure 8.4. Seismic hazard and selected records; (a) Spectral curves for 10% in 50 year record suite, (b) Sa(1.25s) hazard, (c) *Ds*595 conditional CDF for 10% in 50 year record suite

8.3.3 Structural Analysis

Dynamic inelastic response analyses were performed on Ruaumoko-2D [16] using: (i) a Caughey damping [17] ratio of 5% for all elastic modes, (ii) large displacement analyses to consider P-delta effects [18], and (iii) the SINA hysteresis rule [19] to model the hysteretic behavior of the reinforced concrete wall members. A limitation of the analytical approach adopted is that local failure modes (i.e. wall buckling) and stiffness/strength degradation were not considered as (i) there is a lack of full-scale shake table experiments of wall buildings in order to calibrate degradation models, and (ii) models to account for local failure modes of wall buildings are still in development [20]. Instead, drift limits from FEMA 356 [21] were used to assess if a building requires full-replacement or has collapsed. These limits are shown in **Table 8.3**, where the first criteria indicates the extent of structural wall damage, while the second is a measure of the building's global stability.

Table 8.3. Criteria to assess full-replacement and collapse damage states

	Building Damage State	
Criteria	**Full-Replacement Drift Limits**	**Collapse Drift Limits**
(1) Difference in inter-storey drift between subsequent floors	>1.0 %	>2.0%
(2) Maximum inter-storey drift on any floor	>2.0 %	>4.0%

8.3.4 Building Damage Repair Cost Estimation

The building's damage cost was estimated using the Seismic Loss Assessment Tool (SLAT) program [22] for each individual ground motion record, which differed from the approach used in **Section 3.2.4** which considered the entire suite of records in loss calculations. This was so that damage cost can be added directly to injury costs for each individual ground motion. Loss distributions were then obtained for each suite of records once injury and damage losses from each individual record were combined together.

Fragility and loss functions available in SLAT were considered, with the exception of wall members which used the Performance Assessment Calculation Tool's (PACT) fragility database (specification B1044.093 [23]). If full-replacement was required, the median

replacement cost is assumed to be equal to the initial building cost of the building, and a dispersion of 0.35 was assumed as described in **Section 3.3.4**. Note that indirect component of building losses (i.e. business interruption or downtime) was not considered.

A key difference in the damage cost and the injury cost assessments is that the extent of content movement was not explicitly considered for the damage cost assessment. This was because damage to contents may not necessarily occur even if its response is severe. For example, overturning of filing cabinets may not lead to any damage. However, if these contents impacted against people, the impact conditions can be used to estimate injuries as described in **Section 7.3.5**. To avoid this complication, fragility and loss functions from SLAT were used for assessing direct damage-repair losses caused by content movement.

8.3.5 Cost Outputs for Decision Making

Once the building's total loss (damage and injury), L_T, has been obtained, several approaches may be carried out to compare the performance of the various buildings, which is similar to the approaches discussed in **Sections 7.6.4** and **7.8.2**. One approach is to assess expected intensity-based loss, $E_{LT|IM}(im)$, using **Eq. 8.1** [24]; where $E_{LT|IM,NC}(im)$, and $E_{LT|IM,C}(im)$ are the expected losses from non-collapse and collapse cases, respectively, at a given intensity measure, $IM = im$; and $P_C(im)$ is the probability of collapse.

$$E_{LT|IM}(im) = E_{LT|IM,NC}(im).[1 - P_C(im)] + E_{LT|IM,C}(im).P_C(im) \quad \textbf{(8.1)}$$

Another approach is to estimate the annual rate of exceeding a given cost, $\lambda_{LT}(l_T)$. This is calculated using **Eq. 8.2** [25]; where $G_{LT|IM,NC}(l_T|im)$, and $G_{LT|IM,C}(l_T|im)$ are total cost exceedance probabilities for non-collapse and collapse-related injuries, respectively; and $P_{NC}(im)$ is the probability of the building not collapsing (i.e. 1-$P_C(im)$).

$$\lambda_{LT}(l_T) = \int \left(G_{LT|IM,NC}(l_T \mid im, NC).P_{NC}(im) + G_{LT|IM,C}(l_T \mid im).P_C(im)\right).\left|\frac{d\lambda_{IM}(im)}{dIM}\right|.dIM \quad \textbf{(8.2)}$$

Finally, net-present cost (*NPC*) analysis from **Eq. 8.3** can be performed for cost-benefit assessment to aid in decision-making. Here, *IC* is the initial construction cost, *N* is the duration in years, *r* is the discount rate, and *EAL* is the expected annual injury loss which is calculated using **Eq. 8.4**.

$$NPC(r,N) = IC + \sum_{t=1}^{N} \frac{EAL}{(1+r)^t} \tag{8.3}$$

$$EAL = E_{LT|IM}(im).\left|\frac{d\lambda_{IM}(im)}{dIM}\right|.dIM \tag{8.4}$$

8.3.6 Derivation of Sample Injury Rates

Sample injury rates used in less advanced injury models, such as that by HAZUS® [6], are generally provided for various injury severity and building damage states. These can be derived using the findings from this case-study by relating injury rates with the building's corresponding damage state. The latter can be defined by a building damage ratio, *BDR*, which may be calculated using **Eq. 8.5**, as discussed in **Section 7.8.1**. Here, ID_{bot} and ID_{top} are the ground-1st floor and 9th-10th floor interstorey drifts, respectively, and is based on the drift limits outlined in **Table 8.3**. This can then be correlated with injury rates in order to estimate injury rates at specific values of *BDR*. Note that *BDR* of 0.125, 0.25, 0.5, and 1.0 corresponds to slight, moderate, extensive, and complete building damage, respectively.

$$BDR = \max\begin{pmatrix} ID_{bot}/2\% \\ ID_{top}/4\% \end{pmatrix} \tag{8.5}$$

8.4 BUILDING RESPONSE

Four key building response parameters were required for estimating damage and injury losses; (i) peak total floor acceleration, A_{FT}, (ii) peak interstorey drifts, *PID*, (iii) probability of the building requiring full-replacement, P_{FR}, and (iv) probability of building collapse, P_C. Of these, only A_{FT} (correlated to occupants falling), and P_C (correlated to building collapse-

related injuries) are relevant to injuries based on the injury prediction framework adopted, and hence only these are discussed here. Information on *PID* and P_{FR} are available in **Section 3.4**. Note that injuries may also occur due to content movement, the response of which is discussed in **Section 8.5**.

The median peak total floor acceleration, A_{FT}, of the buildings subjected to a serviceability level event (SLE), design-basis event (DBE), and maximum credible event (MCE) in the event of non-collapse are shown in **Figures 8.5a** to **8.5c**, respectively. Note that the x-axis limits varied for all three cases so that differences in the building's response can be seen clearer. Under all levels of shaking, the A_{FT}-floor profiles for all cases had a localized peak around the 4th and 5th floor levels, decreased to a minimum on the 8th floor, then peaked at the roof. The 4th and 5th floor localized A_{FT} peak is due to the building's second mode response, as (i) this mode has its largest response around the 4th floor, and (ii) the spectral accelerations at the lower periods representative of the second mode is higher than that of the first mode.

Under SLE shaking (**Figure 8.5a)**, A_{FT} decreases with increasing building flexibility due to higher frequency motion being filtered out for these cases. There are no differences in the A_{FT} response when varying strength due to these buildings barely yielding at this shaking intensity level.

Under DBE shaking (**Figure 8.5b**), the stiffest building still had higher accelerations on most floors compared to more flexible buildings due to the same reasons outlined for the SLE case. In addition, the strongest building had higher A_{FT} compared to weaker buildings due to inertia forces not being limited to the same extent in buildings of higher strength.

Interestingly, the trends are reversed when examining A_{FT} under the MCE event (**Figure 8.5c**). This was because the spectral accelerations of the ground motion records corresponding to cases where only the weakest and the most flexible buildings collapsed

were lower than the median of the record suite at vibration periods less than 1.25 s as shown in **Figure 8.5d**. These cases were not factored in the median A_{FT} response of weaker or more flexible cases since collapse cases are excluded here, resulting in higher median A_{FT} for these cases. The spectral accelerations of these records were however higher than the median of the suite at larger periods, which resulted in greater inelastic behaviour of the weakest and the most flexible building, which correlated to building collapse occurring.

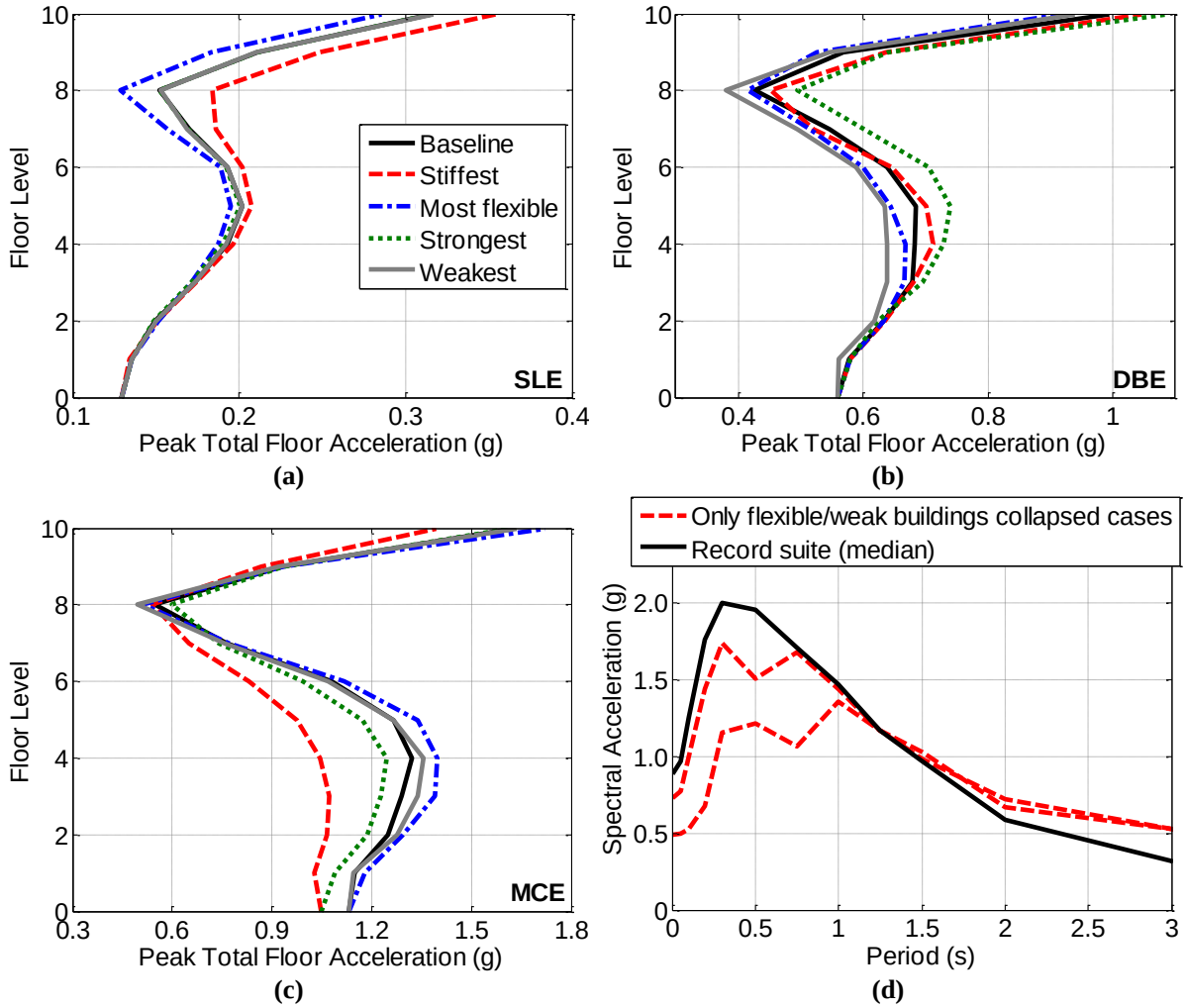

Figure 8.5. Peak total floor acceleration response; (a) SLE median A_{FT}, (b) DBE median A_{FT}, (c) MCE median A_{FT}, and (d) investigation of spectral acceleration under MCE level shaking

The probability of the buildings collapsing is shown in **Figure 8.6**, where stiffer and stronger buildings generally have the lowest probabilities. Stiffer buildings have lower probabilities due to having lesser drifts on all floors. For stronger buildings, the ground-1st floor inter-storey drift is generally lower than that of the weaker building due to having lesser

inelasticity, and thus has greater chance of satisfying the first criteria in **Table 8.3**. However, stronger buildings tend to have larger drifts at the top of the building in more intense seismic shaking as discussed in **Section 3.4.2**, and as such these may fail the second criteria in **Table 8.3** more frequently during more severe shaking events, which explain the higher probability of the stronger building collapsing compared to the stiffer building in **Figure 8.6**.

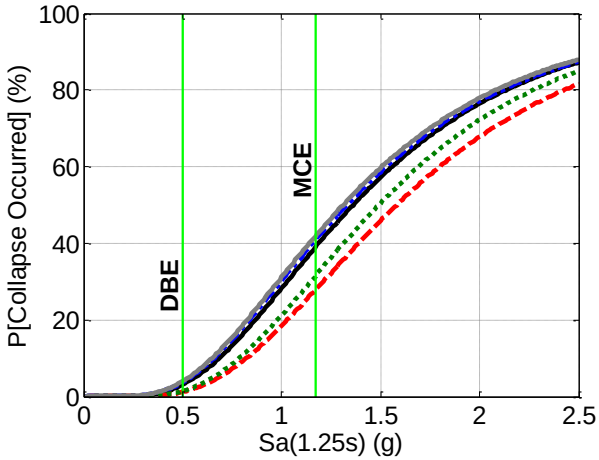

Figure 8.6. Buildings' collapse probability

8.5 CONTENT RESPONSE

Movement of building contents is one possible cause of injury as described in **Section 8.3.1**, with peak total floor accelerations and building collapse being the others. Of the contents considered in **Table 8.2**, only the bookshelves and mobile drawers exhibit noticeable movement. As such, the response of filing cabinets and desks are not discussed here.

The bookshelves' rocking response under DBE shaking is shown in **Figure 8.7a**, where the most flexible building had more contents toppling over within the building's lower half compared to the stiffer building, but lesser on upper floors. The former was due to more flexible buildings having a lower floor response shaking frequency, which enabled bookshelves to have a longer duration to respond. This was despite contents in more flexible buildings being subjected to lower A_{FT} on these floors as shown in **Figure 8.5a**. In contrast, more contents toppled in stronger buildings compared to weaker buildings as A_{FT} was greater

on all floors, while the shaking frequency was similar as they have identical elastic stiffness. These observations were also made at other shaking intensities, though no toppling occurred in events equivalent to, or less severe than, a 50% probability of exceedance in 50 year event (serviceability-level event, SLE).

The mobile drawers' 84th percentile maximum sliding displacement under DBE level shaking is shown in **Figure 8.7b**. The trends observed here were similar to that for the rocking bookshelves, where (i) stiffer buildings had smaller sliding displacements within the lower half of the building, but higher sliding displacements on upper floors; and (ii) stronger buildings have the largest sliding displacements on all floors. Both the observations for rocking and sliding are similar to that discussed in **Section 6.4.2**.

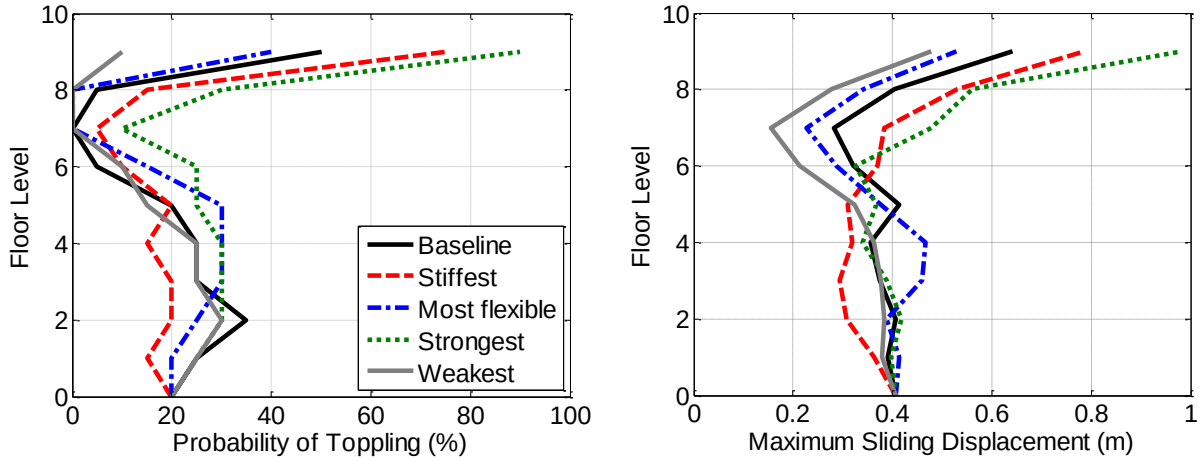

(a) **(b)**

Figure 8.7. Content response in DBE event; (a) Probability of bookshelves overturning, and (b) 84th percentile mobile drawer sliding displacement

8.6 INJURY RATE COMPARISONS

8.6.1 Serviceability-Level Event Injury Rates

The percentage of occupants injured, P_{injury}, on each floor under SLE are shown in **Figures 8.8a** to **8.8c** for room Layouts A to C, respectively. Here, more injuries occurred in the stiffest building compared to most flexible building. This was because stiffer buildings have higher A_{FT} response, which correlated to more people falling. This accounted for virtually all injuries at this shaking intensity level as shown in **Figures 8.8d** to **8.8f** for room

Layouts A to C, respectively, as the chance of contents moving or building collapse was near-zero. It can also be seen from **Figures 8.8a** to **8.8c** that injury rates for buildings of varying strength were identical as these have the same elastic properties and had not yielded under SLE shaking.

One observation from **Figures 8.8d** to **8.8f** is that fall-related injuries occurred more frequently for room Layout B compared to the others. This is due to there being a higher proportion of standing occupants compared to sitting occupants for Layout B; resulting in people having a higher effective height on average. This corresponds to higher impact velocities and hence more severe fall-related injuries occurring as described in **Section 7.3.4**. This observation was also made at other shaking intensity levels.

Figures 8.8g to **8.8i** show that the ratio of minor to moderate injuries at SLE shaking for all room types considered was approximately 2:1, and only a small percentage were serious or fatal. An occupant who fell would therefore have approximately 67% and 33% chance of incurring minor and moderate injuries, respectively.

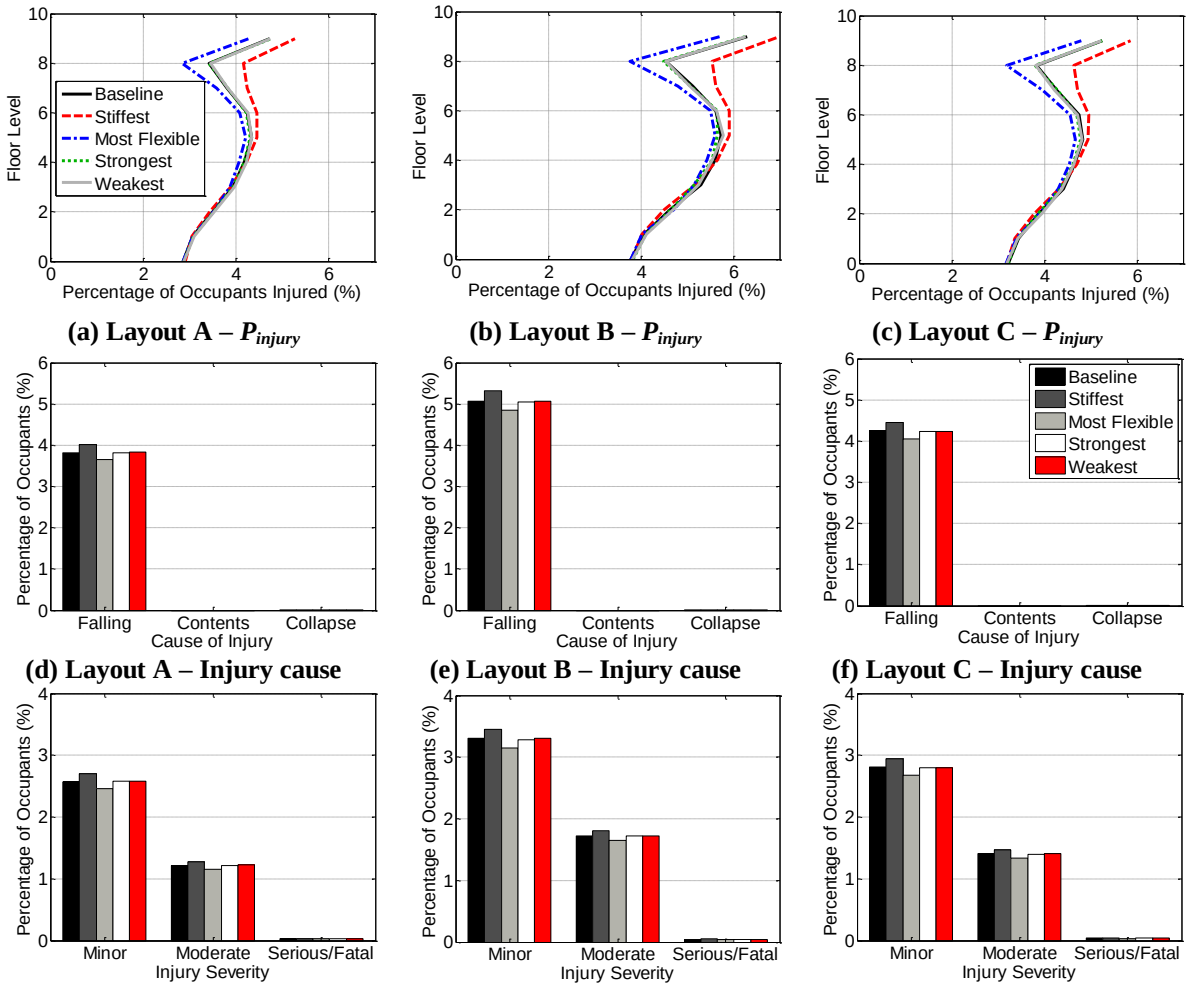

(a) Layout A – P_{injury} **(b) Layout B – P_{injury}** **(c) Layout C – P_{injury}**

(d) Layout A – Injury cause **(e) Layout B – Injury cause** **(f) Layout C – Injury cause**

(g) Layout A – Injury severity **(h) Layout B – Injury severity** **(i) Layout C – Injury severity**

Figure 8.8. Details of injuries incurred during serviceability-level events (SLE)

8.6.2 Design-Basis Event Injury Rates

P_{injury} for each floor of room Layouts A to C under design-basis event, DBE, are shown in **Figures 8.9a** to **8.9c**, respectively. Here, the stiffest building generally had lower injury rates on most floors. This was due to stiffer buildings having a lower probability of collapsing, resulting in less collapse-related injuries as shown in **Figures 8.9d** to **8.9f**. It should be noted that the stiffest building does incur marginally higher falling and content movement-related injuries compared to more flexible buildings. However, the injury framework only estimates injuries from these sources in cases where the building does not collapse. If only non-collapse cases were considered: (i) a similar number of falling injuries would occur regardless of stiffness as A_{FT} in all cases were generally large enough to cause a

similar proportion of occupants to fall under DBE shaking, and (ii) the probability of content-movement related injuries occurring is larger in more flexible buildings due to contents responding more severely on most floors as shown in **Figure 8.7**.

The strongest building also incurs lesser collapse-related injuries, and similar probability of fall-related injuries in non-collapse cases, compared to weaker buildings as shown in **Figures 8.9d** to **8.9f**. However, the strongest building incurred significantly higher content-movement related injuries. This is particularly prominent for Layout A, as shown in **Figure 8.9d**, due to occupants having a high chance of being located in grids a2, a5, a6, and a7, where there is potential for them to fall onto the path of the toppling bookshelves. In contrast, occupants in Layout B are more likely to be located in grid b5 based on the weighting factors assumed, and hence are less likely to have interaction with the bookshelves, resulting lesser content movement-related injuries occurring compared to Layout A as shown in **Figure 8.9e**. No content movement-related injuries occurred in Layout C as shown in **Figure 8.9f** as there were no bookshelves, and mobile drawers were found to have minimal effect on content movement-related injuries.

It can be seen from **Figure 8.9i** that the ratio of minor to moderate injuries for Layout C was approximately 2:1 as most injuries were still caused by falling, which is consistent with the SLE findings. In contrast, **Figure 8.9g** shows that the ratio of minor to moderate injuries was almost 1:1 for room Layout A as content movement-related injuries generally resulted in moderate injuries based on the framework adopted as previously discussed in **Section 7.6.3**. The serious and fatal injury rates for all layouts however were identical as these injuries were generally caused by building collapse, the rate of which was estimated using injury rates provided by HAZUS® [6] as discussed previously.

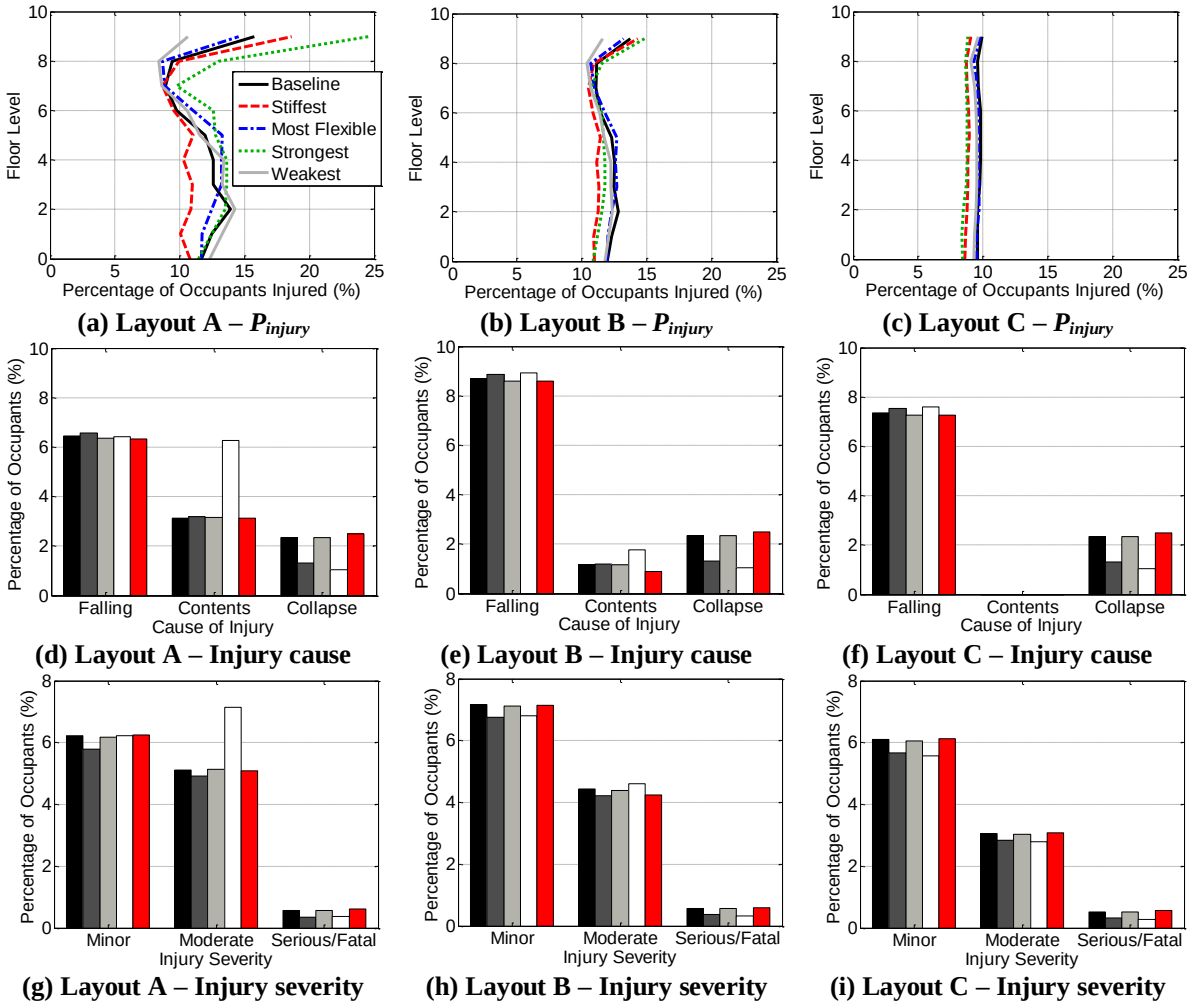

(a) Layout A – P_{injury} **(b) Layout B – P_{injury}** **(c) Layout C – P_{injury}**

(d) Layout A – Injury cause **(e) Layout B – Injury cause** **(f) Layout C – Injury cause**

(g) Layout A – Injury severity **(h) Layout B – Injury severity** **(i) Layout C – Injury severity**

Figure 8.9. Details of injuries incurred during design-basis events (DBE)

8.6.3 Maximum Credible Event Injury Rates

The percentage of occupants injured on each floor level for room Layouts A to C during maximum credible events, MCE, are shown in **Figures 8.10a** to **8.10c**, respectively. In most cases, the stiffest building and the strongest building had the lowest percentage of injuries due to the increased probability of collapse in more flexible and weaker buildings, as shown in **Figures 8.10d** to **8.10f**. The exception was for the strongest building in room Layout A (**Figure 8.10a**) which had a similar proportion of injuries with weaker or more flexible buildings due to contents still having a large contribution to injuries.

The proportion of occupants who were injured in room Layout C was reasonably constant with floor height, as shown in **Figure 8.10c**. This was because under MCE shaking: (i) a similar proportion of occupants fell on all floors across all buildings due to the high A_{FT}

at this intensity level, and (ii) the effect of collapse was irrespective of floor level. In Layouts A and B, there were more variation with floor levels due to content-related injuries.

It can be seen from **Figures 8.10g** to **8.10i** that there is a considerably larger proportion of serious/fatal injuries under MCE level shaking compared to the other shaking intensities observed previously due to increasing probability of collapse. Eventually as the shaking intensity increases, the differences between the injury rates across all buildings and room layout considered will decrease due to building collapse becoming a dominant source of injury.

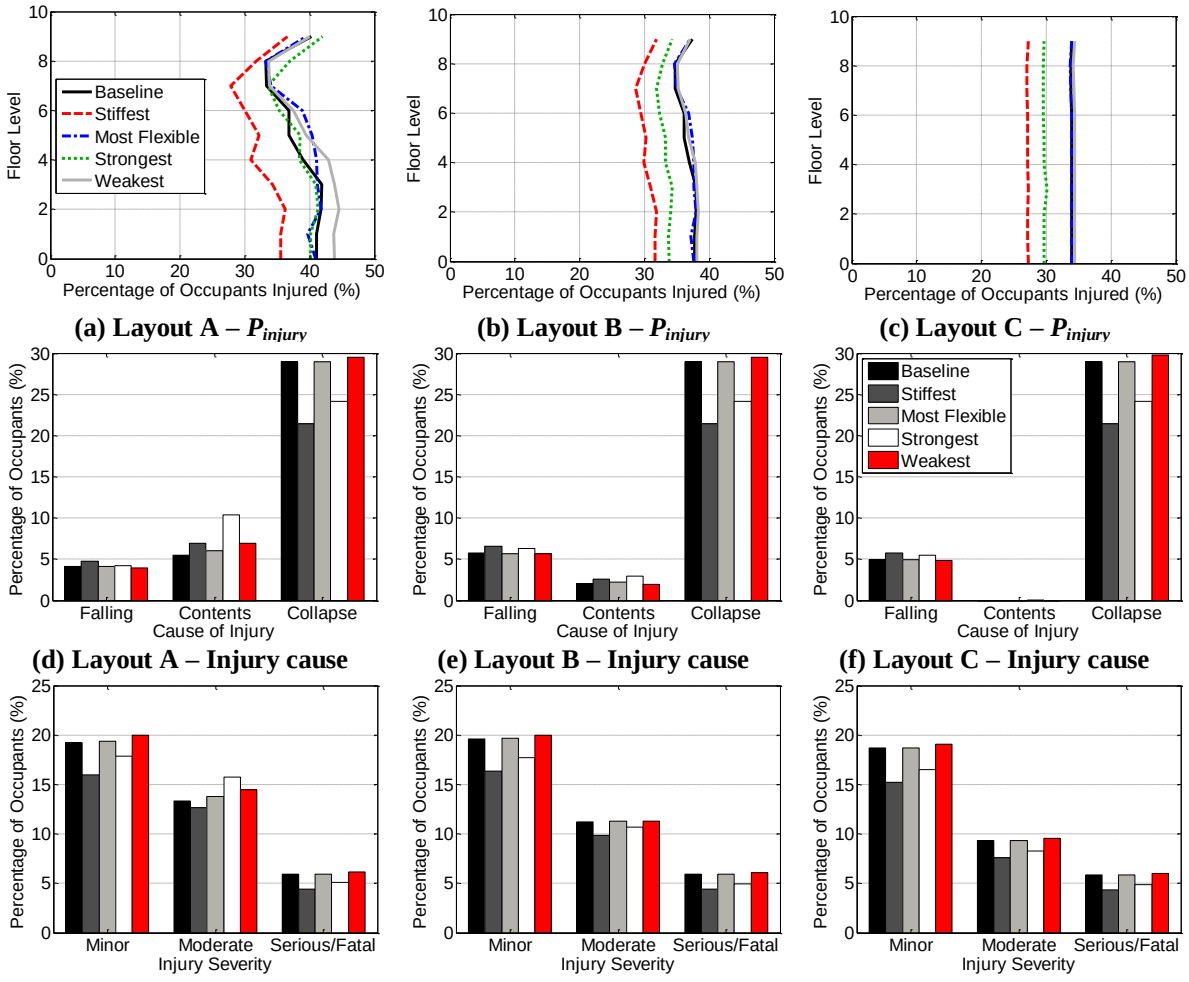

(a) Layout A – P_{injury} **(b) Layout B – P_{injury}** **(c) Layout C – P_{injury}**

(d) Layout A – Injury cause **(e) Layout B – Injury cause** **(f) Layout C – Injury cause**

(g) Layout A – Injury severity **(h) Layout B – Injury severity** **(i) Layout C – Injury severity**

Figure 8.10. Details of injuries incurred during maximum-credible events (MCE)

8.7 INJURY AND DAMAGE COSTS

The expected combined injury and damage repair costs, hereby termed the 'total' cost, with *IM* are shown in **Figures 8.11a** to **8.11c** for room Layouts A to C, respectively. Here, the injury costs were calculated using **Eq. 8.1** while damage repair costs were obtained using SLAT as described in **Section 3.5**. Note that expected costs were used as: (i) this could be deaggregated by cause of injury or building damage, and (ii) the distribution of injury loss at a given *IM* does not follow any obvious statistical distribution due to the amount of time which the building was unoccupied based on the adopted occupancy model from **Figure 8.2**.

For all cases, the stiffest building had the lowest losses overall due to (i) reduced damage losses and lesser need for full-replacement as discussed in **Section 3.5**, and (ii) lower injury rates in larger shaking events as discussed in **Section 8.6**. The strongest building had the second lowest expected losses overall. While many benefits of stiffer buildings also applied to stronger buildings, the latter does incur larger interstorey drifts on its upper floors compared to weaker buildings as described in **Section 3.4.2**. This resulted in greater drift damage on upper floors, and may incur a higher probability of exceeding the second full-replacement or collapse criteria from **Table 8.3** in rarer and more severe events. Considering that stronger buildings also incur a greater number of injuries from content movement, there are lesser benefits to designing for stronger buildings compared to stiffer buildings. Note that while flexible and weaker buildings do generally have greater losses compared to the baseline building, the magnitude of loss is almost identical.

It should be noted that the expected total costs in Layout A is the largest, followed by Layouts C and B. This is due to there being more occupants in room Layout A compared to the other two rooms as discussed in **Section 8.2.2**.

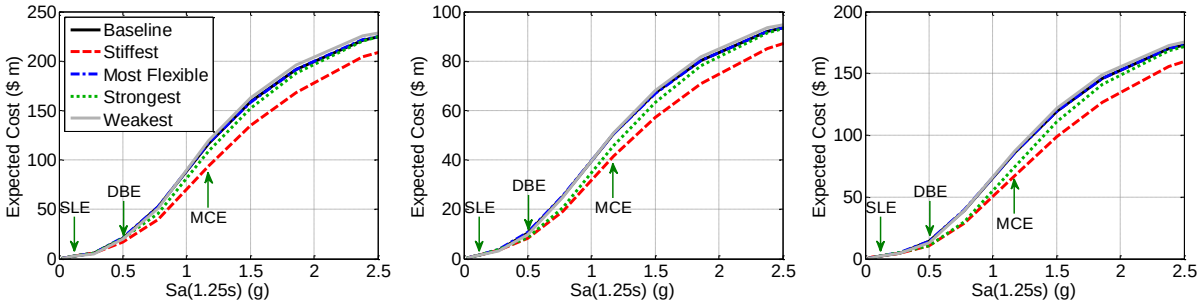

(a) Layout A **(b) Layout B** **(c) Layout C**

Figure 8.11. Buildings' expected total loss (damage and injury) versus IM

The contribution of fall-related injuries, content movement-related injuries, collapse-related injuries, and building damage repair-costs to the expected total loss is shown in **Figure 8.12**. It can be seen that fall-related injuries was the largest contributor to expected losses at events rarer than the SLE shaking, as shown in **Figures 8.12a** to **8.12c** for Layouts A to C, respectively. This was because within this range, the buildings do not incur significant damage, and content movement and building collapse rarely occurred.

Content movement-related losses started having a larger contribution between the SLE and DBE events in Layout A as shown in **Figure 8.12d** due to the increased content response; particularly for the strongest building as observed previously in **Figure 8.9d**. The percentage contribution from content-movement starts decreasing past the DBE event due to the increasing contribution of building collapse, as shown in **Figure 8.12g**, = due to the increasing probability of building collapse which leads to more severe injuries. For Layouts B and C, the contribution from content movement-related injuries was even lower due to the decreased interaction between occupants and contents.

The damage repair loss contribution ranged from 5-50% as shown in **Figures 8.12k** to **8.12l** for Layouts A to C, respectively. This demonstrates the importance of injury-related costs in relation to damage repair losses for this case study using the implemented injury prediction framework. This is especially true when the building had collapsed, as the contribution of collapse-related injuries contributes to 85-95% of total expected losses. To check that this is sensible, the expected cost of collapse injuries for Layout A is calculated.

For this layout, 200 people are expected to be present on average based on the model from **Figure 8.2** and assumptions listed in **Section 8.2.2**. Using injury rates from HAZUS® [6] and implemented cost functions outlined in **Section 7.2.7**, the expected injury cost to a single person due to collapse is approximately $0.89 million, and hence the total expected collapse-related injury cost is $178 million. This is fourteen times that of the full-replacement cost outlined in **Table 8.1**, which is consistent with **Figure 8.12j** and shows the significance of injuries with respect to direct damage-repair costs. Note that similar checks were also performed at other shaking intensity levels.

It should be re-emphasized here that cost estimates for injuries includes both direct (i.e. medical treatment) and indirect (i.e. decrease in quality of life) components. In contrast, only the direct component of building damage-related losses (i.e. repair costs) was considered. The indirect component building damage-related losses, which is related to business interruption costs and is also known as downtime, was not considered. If downtime was considered, or if the indirect component of injury cost (around 85-98% of the total injury cost) was ignored, the contribution of building damage-related losses would be higher.

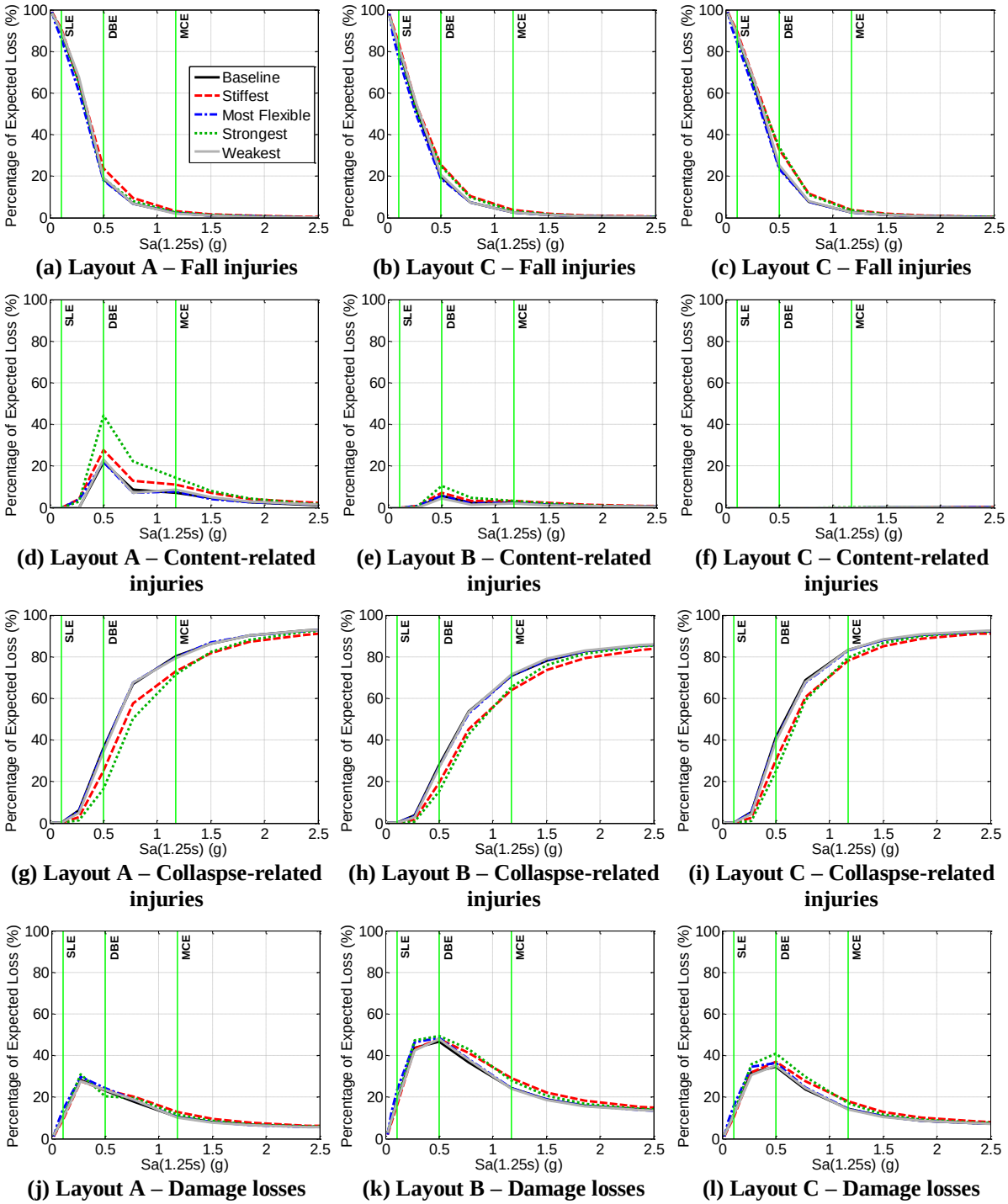

(a) Layout A – Fall injuries **(b) Layout C – Fall injuries** **(c) Layout C – Fall injuries**

(d) Layout A – Content-related injuries **(e) Layout B – Content-related injuries** **(f) Layout C – Content-related injuries**

(g) Layout A – Collaspse-related injuries **(h) Layout B – Collaspse-related injuries** **(i) Layout C – Collaspse-related injuries**

(j) Layout A – Damage losses **(k) Layout B – Damage losses** **(l) Layout C – Damage losses**

Figure 8.12. Deaggregation of buildings' expected total loss by injury cause and damage

8.8 COST-BENEFIT ASSESSMENT

The total expected annual loss, *EAL*, for all cases is shown in **Table 8.4**, and was calculated using **Eq. 8.4**. In all cases, the stiffest building had the lowest *EAL*. This is consistent with observations from **Figure 8.11** as the stiffest building has (i) similar rates of

fall-related injuries in more severe shaking events, (ii) lesser content movement and related injuries, and (iii) lesser building damage and probability of collapse.

The effect of increasing strength varies depending on the room layout, as the strongest building had higher *EAL* compared to weaker buildings for room Layout A, but lower in room Layouts B and C. This was due to more severe content movement in stronger buildings, which resulted in increased number of moderate injuries, particularly in Layout A where there was a higher chance of occupants falling onto the path of toppling contents. Note however that regardless of the room layout, the effect of varying strength on *EAL* is less significant (0.6- 3.3% difference between the strongest and weakest building) compared to varying stiffness (8.1-8.0% difference between the stiffest and most flexible buildings).

Table 8.4. Expected Annual Combined Total Loss

	Expected Annual Loss ($ m)		
Case	**Layout A**	**Layout B**	**Layout C**
Baseline	0.302	0.157	0.240
Stiffest	0.282	0.148	0.222
Most flexible	0.305	0.160	0.242
Strongest	0.310	0.155	0.234
Weakest	0.300	0.156	0.241

Cost-benefit assessment using *EAL* values from **Table 8.4** was performed using **Eq. 8.3**, where the difference in initial construction costs from **Table 8.1** was used as *IC*. The findings for Layouts A to C are shown in **Figures 8.13a** to **8.13c**, respectively. It is shown that the stiffest building has (i) lower net-present-cost, *NPC*, compared to the most flexible case after 8, 21, and 10 years of being in service for room Layouts A to C, respectively, and (ii) the lowest *NPC* among all buildings within 50 years for room Layouts A and C. Note however that the weakest building had a lower *NPC* than the stiffest building in room Layout B. This was due to there being less people being present in this case, resulting in lower injury-related losses and hence smaller differences in *EAL* as shown in **Table 8.4**. The strongest building however had the highest *NPC* of all cases. This was due to the strongest

building having similar *EAL* compared to weaker buildings as shown in **Table 8.4**, yet costs more to construct. Note that additional analyses considering the effect of anchoring contents to prevent movement and related injuries were performed, but had similar trends to that observed in **Figures 8.13a** to **8.13c** and were thus not shown here.

Based on these findings, increasing the building's stiffness would likely result in increased seismic resilience. While increasing strength does not appear to improve the performance on average, it is not the authors' opinion that weaker buildings should be designed for in general, as greater inelastic behaviour and probability of requiring full-replacement or collapsing for weaker buildings may lead to increased business interruption (i.e. downtime) costs which were not considered. In addition, these results should not provide an incentive for designing buildings below minimum allowable standards specified in codes, as inadequate design of buildings may lead to other failure modes not considered here.

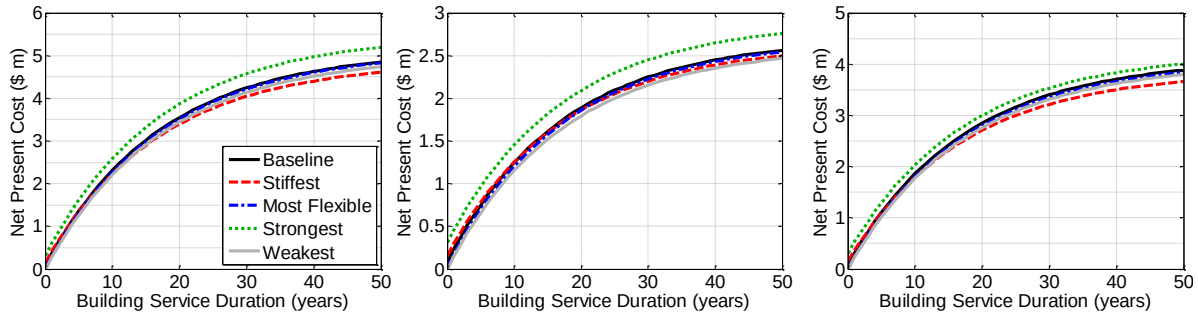

(a) Layout A **(b) Layout B** **(c) Layout C**

Figure 8.13. Cost-benefit assessments using net-present costs considering difference in initial construction costs and expected total annual losses

8.9 COST-HAZARD ASSESSMENT

The annual rate of exceeding a given total loss, λ_{LT}, was calculated using **Eq. 8.2**, and are shown in **Figures 8.14a** to **8.14c** for Layouts A to C, respectively. For Layout A, the total cost for all buildings were similar up until λ_{LiT} = 0.0021 (i.e. 1 in 475 years). The stiffest building had larger costs compared to more flexible buildings between λ_{LiT} = 0.0021 and 0.0004 (i.e. 1 in 2,500 years), due to having a larger A_{FT} and a higher occurrence of occupants falling. After λ_{LiT} = 0.0004, the stiffest building had the lowest losses due to (i) A_{FT} generally

being large enough to cause a similar proportion of occupants to fall, (ii) lesser content response on most floors, and (iii) having a smaller chance of requiring full replacement or incurring collapse. The strongest building for Layout A had larger costs compared to weaker buildings at frequent events, and only incurred lower costs from λ_{LiT} = 0.00014 (i.e. 7,140 years) due to more injuries occurring from content movement, and greater drift-related damage on upper floors compared to weaker buildings.

The trends for Layouts B and C are similar, as can be seen from **Figures 8.14b** to **8.14c**. Here, the losses were similar up until λ_{LiT} = 0.0004 (i.e. 1 in 2,500 years). The stiffest building has the best performance past this point, while the stronger building only has better performance compared to weaker buildings when λ_{LiT} = 0.00017 (i.e. 1 in 5,880 years). There was no sudden increase in losses at λ_{LiT} = 0.0021 as observed for Layout A due to there being less content movement-related injuries.

One approach to make decisions using loss-hazard data is to include the difference in initial construction cost, which aids users of differing risk-appetites to make decisions. However, due to the small difference in construction cost relative to the size of losses, **Figure 8.14** would be sufficient to make this assessment. Therefore, risk-adverse decision makers might tend to favour the stiffest building as this has (i) the lowest losses for events rarer than a 1 in 2,500 year event, and (ii) relatively similar losses in more frequent events. There is however relatively no difference in terms of varying strength, so the decision is less obvious in this case.

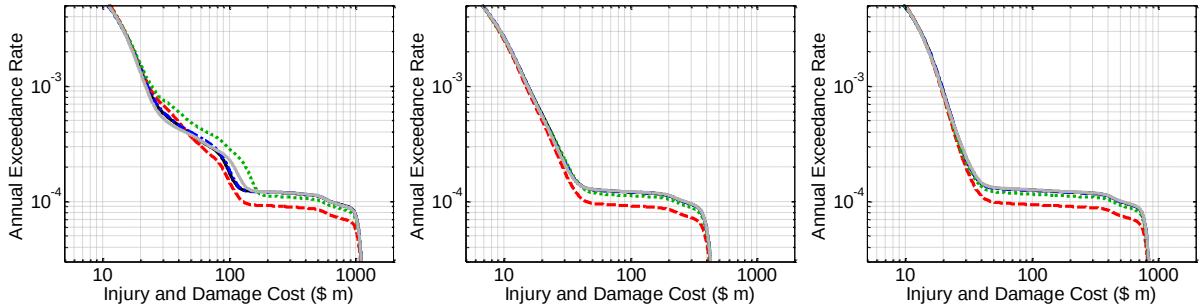

(a) Layout A **(b) Layout B** **(c) Layout C**

Figure 8.14. Annual total loss exceedance rates

8.10 SAMPLE INJURY RATES

8.10.1 Derivation

The findings from this case study were used to derive sample injury rates for usage in less advanced injury prediction models. The first step follows that outlined in **Section 7.8.2**, where the global building damage ratio, *BDR*, was calculated for each ground motion record and building design combination using **Eq. 8.5**. Injury rates for varying injury severity levels were then plotted against *BDR*, as shown in **Figures 8.15a** to **8.15d** for minor, moderate, serious, and fatal injuries, respectively. Interestingly, while the average percentage of occupants who incurred minor injuries was higher than that which causes moderate injuries (i.e. 5.9% against 4.8% for extensive building damage, *BDR* = 0.75), there are cases where there is a higher proportion of moderate injuries compared to minor injuries. This was due to extensive content movement in severe cases, particularly for room Layout A, which lead to more moderate injuries occurring as discussed previously in **Section 8.6.2**.

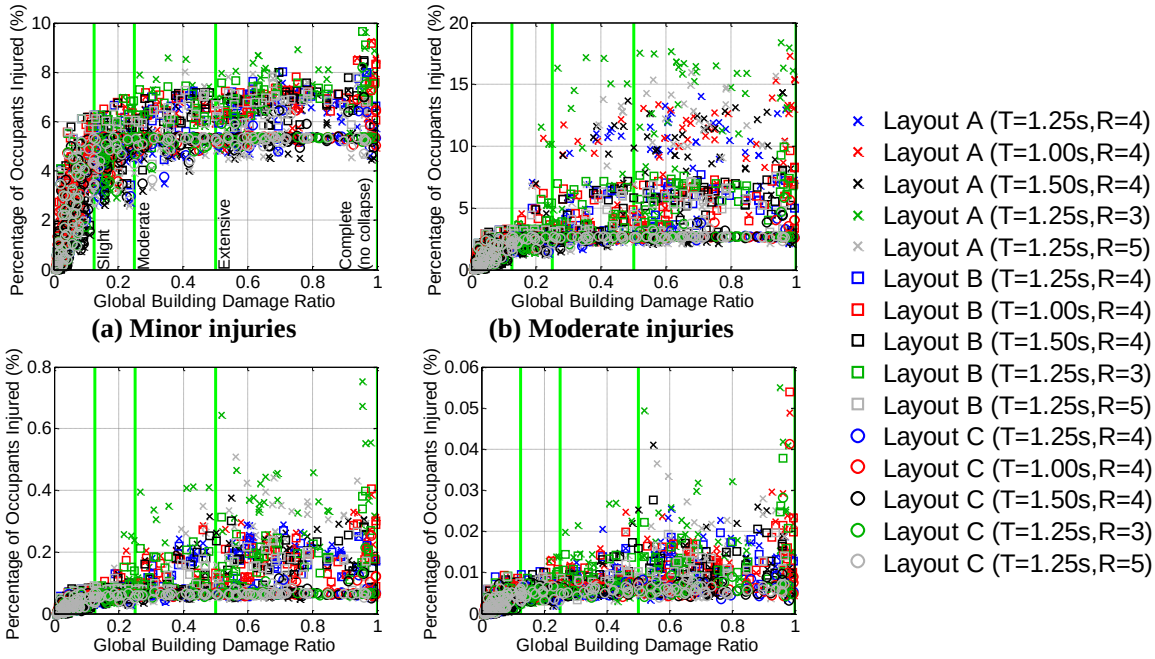

Figure 8.15. Case study injury rates versus global building damage ratio

The next step differs from that implemented in **Section 7.8.2** in that the injury rates at specific levels of building damage (i.e. slight, moderate, extensive, or complete) was used to obtain a lognormal distribution. This was because there are more data points available due to consideration of a wider range of cases. The median and dispersion of injury rates per 1,000 people obtained using this approach are shown in **Table 8.5**. Note that injuries from collapse (i.e. *BDR* > 1.00) are not considered here since injury rates from HAZUS® [6] were used for those cases.

Table 8.5. Median injury rates per 1,000 people from case study (dispersion in brackets)

	Global Building Damage Level			
Injury Severity	**Slight (*BDR* = 0.125)**	**Moderate (*BDR* = 0.25)**	**Extensive (*BDR* = 0.50)**	**Complete – no collapse (*BDR* = 1.00)**
Minor	44.9 (0.20)	50.0 (0.22)	58.5 (0.14)	65.0 (0.19)
Moderate	22.4 (0.22)	28.0 (0.42)	41.7 (0.54)	55.6 (0.64)
Serious	0.55 (0.25)	0.68 (0.44)	1.03 (0.58)	1.44 (0.68)
Fatal	0.05 (0.30)	0.06 (0.40)	0.08 (0.51)	0.11 (0.65)

It should be noted that the values in **Table 8.5** are limited by the effect of furniture movement being smeared. For example, a significantly higher proportion of injuries caused

by furniture movement occurred in room Layout A compared to B and C. This is reflected in the increased dispersion of moderate to fatal injuries with *BDR*. Also, while injury rates were similar in magnitude between the different buildings at a given shaking intensity level as shown in **Section 8.6**, the *BDR* of the buildings corresponding to a specific shaking intensity level can vary, especially for buildings of varying stiffness. For example, stiffer buildings should have lower drifts, so at the same *BDR* level, one would think that the extent of damage should be greater stiffer buildings. Therefore, the effect of a building's stiffness and possibly strength may not be well reflected in **Table 8.5**. Finally, the injury rates here are likely to be conservative as the effects of occupant actions to evade injury, such as "drop-cover-hold", were not considered in the injury prediction framework.

8.10.2 Application of Sample Injury Rates

The following is an example demonstrating the application of sample injury rates for use in predicting injuries. Consider a building which incurred extensive damage (*BDR* = 0.50), and has 300 people present at the time of shaking. Four numbers between 0 and 1 can then be generated assuming uniform distribution to estimate a percentile for the distributions for minor, moderate, serious, and fatal injuries. If these four numbers are 0.81, 0.47, 0.62, and 0.31, these would correspond to probabilities of 6.62%, 4.00%, 0.12%, and 0.01% of occupants incurring minor, moderate, serious, and fatal injuries, respectively, using values from **Table 8.5**. These probabilities can then be multiplied by the population present and rounded to the nearest number to predict the number of injuries that would occur; which is 20 minor and 12 moderate injuries, respectively, in this example.

8.11 DISCUSSION

8.11.1 Validity of Findings for "Drop-Cover-Hold" Considerations

One of the key assumptions made in the derivation of the injury prediction framework was that occupants were assumed to be stationary during the event. In reality, people are likely to take evasive actions such as "drop-cover-hold" to protect themselves from harm, and thus the number of injuries would likely be lower than that estimated using the framework. One method to consider this effect could be to apply a reduction factor to the number of non-collapse-related injuries estimated.

In order to investigate how the conclusions from **Section 8.8** may change if "drop-cover-hold" measures were taken, the *NPC* was recalculated assuming that the number of non-collapse-related injuries and incurred costs were reduced by 80% following **Eq. 8.3**. Collapse-related injuries are assumed to be unaffected by "drop-cover-hold" actions. The resultant curves are shown in **Figures 8.16a** to **8.16c** for room Layouts A to C, respectively. It can be seen that the stiffest building has the lowest *NPC* overall for all room layouts within 6, 14, and 7 years for Layouts A, B, and C, respectively; while the strongest building had the worst performance in all cases. These results are consistent with that observed from **Figure 8.12** when "drop-cover-hold effects were" ignored.

In addition, it can be seen from **Figure 8.16** that the stiffest building's *NPC* after 50 years of being in service is $359,000, $105,000, and $264,000 lower than the most flexible building for Layouts A, B, and C, respectively. This difference is greater than that observed when "drop-cover-hold" was ignored in **Figure 8.12**. The reason for the relatively better performance of the stiffer building when "drop-cover-hold" is considered is that fall-related injuries are more common in stiffer buildings, particularly at lower shaking intensities. Therefore, even if the true reduction in non-collapse-related injuries was greater than 80%, the difference in the *NPC* between the stiffest and the most flexible buildings will only

increase, making stiffer buildings even more economical compared to flexible buildings. Based on these findings, the consideration of "drop-cover-hold" measures further support the fact that it is better to design buildings to be stiffer in order to improve seismic resilience.

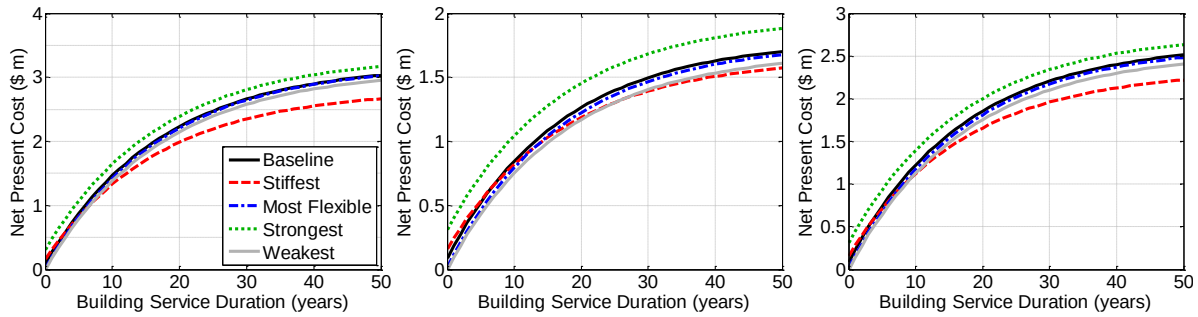

(a) Layout A **(b) Layout B** **(c) Layout C**

Figure 8.16. Cost-benefit assessments using net-present costs considering difference in initial construction costs and expected total annual losses including the effects of "drop-cover-hold"

8.11.2 Validity of Findings for Use of Different Injury Cost Estimation Data

The sample injury cost dataset implemented in the injury prediction framework by Miller [7] and Zaloshnja et al. [8] was selected due to it providing estimates based on which body part was more severely injured, and the injury severity rating based on the Abbreviated Injury Scale (*AIS*). However, many other less comprehensive datasets exists, such as Federal Highway Administration (FHA) [26] or the New Zealand Ministry of Transport [27]. When these datasets were converted to the present day's value of money, the lower-bound cost estimates were all at least equal to half the cost estimates from the implemented dataset.

In order to assess if using other datasets could influence the conclusions from this study, the *NPC* of all buildings were again calculated assuming that all injury-related costs were halved to represent the lower bound estimates of injury cost. The results following this approach, which also included the "drop-cover-hold" effect discussed in **Section 8.11.1**, are shown in **Figures 8.17a** to **8.17c** for room Layouts A to C, respectively. It can be seen here that the stiffest building once again has a better performance compared to more flexible options, and has lowest *NPC* for room Layouts A (**Figure 8.17a**) and C (**Figure 8.17c**), within 50 years of the buildings being in service; though **Figure 8.17b** does show that the

weakest building has the lowest overall *NPC* for room Layout B. These observations are consistent with that from **Section 8.9**; which shows that despite the differences in injury-costs, the findings still indicate that increasing stiffness is generally a financially feasible approach to improve the overall performance of buildings.

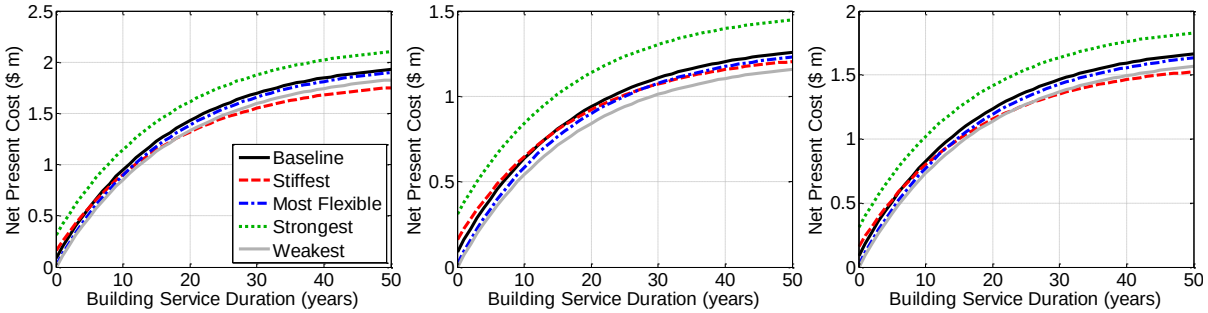

(a) Layout A **(b) Layout B** **(c) Layout C**

Figure 8.17. Cost-benefit assessments using net-present costs considering difference in initial construction costs and expected total annual losses including the effects of "drop-cover-hold" and assuming injury-related losses are halved

8.11.3 Validity of Findings with Inclusion of Downtime

As briefly discussed in **Section 8.7**, a notable difference between the cost estimates for injuries and building damage is that the former includes both direct (i.e. medical treatment) and indirect (i.e. decrease in quality of life) aspects of injury. In contrast, the indirect component of losses with regards to building damage, which is also known as downtime, was ignored. However, it is very likely that stiffer buildings would have lesser downtime losses due to having lower structural damage (**Section 3.5**), and a lower probability of requiring full-replacement (**Section 3.4.3**) or collapsing (**Figure 8.6**). As such, increasing the stiffness of the building is likely to result in even better performance than estimated in this study if downtime-related losses were considered, further indicating that increasing a building's stiffness is a financially feasible method of improving the building's overall performance.

8.12 CONCLUSIONS

Building stiffness and strength effects on injuries are assessed for several office-type room layouts in reinforced concrete cantilever wall buildings. The following are the key conclusions obtained from this study:

1. **Shaking intensity effect**: Where occupants were assumed to remain located at their positions at the start of shaking, occupants falling caused the greatest percentage contribution of injury under serviceability level events (SLE) and design-basis events (DBE). Injuries caused by building collapse were the largest cause of injuries under maximum-credible events (MCE). The contribution of content movement-related injuries varied with it having the second largest contribution in room Layout A in DBE or more severe events, and having almost zero contribution for room Layout C.
2. **Building characteristics effect**: Both the stiffer building and the stronger building had more fall-related injuries compared to weaker or more flexible buildings, which were correlated to their higher peak total floor acceleration, A_{FT}. Content movement-related injuries were greater in stronger buildings compared to weaker buildings due to its higher A_{FT} yet similar floor shaking response frequencies. However, these were generally lower in stiffer buildings compared to more flexible buildings due to its higher floor shaking frequency despite it generally also having higher A_{FT} on most floors. Building collapse-related injuries decreased in stiffer or stronger buildings due to the lower interstorey drift demands, resulting in lower probability of collapse occurring.
3. **Significance of injury-related losses**: 50-95% of total loss (injury and damage repair) resulted from injuries for all shaking levels. Note however that the injury losses included both direct (i.e. medical treatment) and indirect (i.e. decrease in

quality of life) components, whereas the building damage loss only considered direct components (i.e. repair costs).

4. **Cost-benefit assessments**: Increasing the building's stiffness resulted in lower expected net-present-costs, *NPC*, including injury, damage repair, and initial construction costs compared to more flexible buildings for all room layouts considered over a 50 year period of the building being in service. While stronger buildings incurred lower expected annual losses compared to weaker buildings in rooms with fewer content movement-related injuries, its higher construction costs resulted in the strongest building having the highest *NPC* overall. Based on this assessment, stiffening buildings is a financially feasible option to improve seismic resilience. This conclusion was also reached if "drop-cover-hold" effects or different injury cost estimate datasets were considered.
5. **Loss-hazard assessment**: The losses were similar for all buildings regardless of stiffness and strength during events with a return period less than 1,000 years. However, stiffer buildings had the lowest overall losses in rarer events. In contrast, strengthening buildings resulted in minimal reduction in overall losses. Therefore, this assessment approach also highlights that stiffening buildings is a feasible option to improve seismic resilience.
6. **Sample injury rates**: Sample injury rates for use in less advanced injury models were obtained by correlating the building's global damage state to the injury rates estimated in this case study. Rates were provided for various injury severity levels and building damage states; ranging from 45-65 minor injuries, to 0.05-0.11 fatal injuries, per 1,000 people depending on the building's damage state. These rates are can be used in less sophisticated injury models, such as HAZUS®.

8.13 REFERENCES

1. Freeman, J. R. (1932). Earthquake Damage and Earthquake Insurance. New York, US: McGraw-Hill.
2. Berg, G. V. (1983). Seismic Design Codes and Procedures (Vol. 6). Berkeley, California, US: Earthquake Engineering Research Institute.
3. Standards New Zealand. (2004). NZS 1170.5:2004, Structural Design Actions Part 5: Earthquake Actions New Zealand (Commentary): Standards New Zealand, Wellington, New Zealand.
4. OECD. (2009). Society at a Glance 2009: OECD Social Indicators. OECD Publishing, Paris.
5. Wong, L. T., & Mui, K. W. (2011). Modelling Transient Occupant Loads for Offices. Architectural Science Review, 49(1), 53-58.
6. FEMA. (2015). Hazus(R) - MH 2.1 Technical Manual - Earthquake Model: Department of Homeland Security, Mitigation Division, Washington, D.C.
7. Miller, T. R. (1993). Costs and Functional Consequences of U.S. Roadway Crashes. Accident Analysis and Prevention, 25(5), 593-607.
8. Zaloshnja, E., Miller, T. R., Romano, E., & Spicer, R. (2004). Crash costs by body part injured, fracture involvement, and threat-to-life severity, United States, 2000. Accident Analysis and Prevention, 36(3), 415-427.
9. Field, E. H., Jordan, T. H., & Cornell, C. A. (2003). OpenSHA: A Developing Community-Modeling Environment for Seismic Hazard Analysis. Seismological Research Letters, 74(4), 406-419.
10. Stirling, M. W., McVerry, G. H., Gerstenberger, M. C., Litchfield, N. J., Van Dissen, R. J., Berryman, K. R., Barnes, P., Wallace, L. M., Villamor, P., Langridge, R. M., Lamarche, G., Nodder, S., Reyners, M. E., Bradley, B., Rhoades, D. A., Smith, W. D., Nicol, A., Pettinga, J., Clark, K. J., & Jacobs, K. (2012). National seismic hazard model for New Zealand : 2010 update. Bulletin of the Seismological Society of America, 102(4), 1514-1542.
11. Bradley, B. A. (2010). NZ-Specific Pseudo-Spectral Acceleration Ground Motion Prediction Equations based on Foreign Models: Department of Civil and Natural Resources Engineering, University of Canterbury, Christchurch, New Zealand.
12. Standards New Zealand. (2004). NZS 1170.5:2004, Structural Design Actions Part 5: Earthquake Actions New Zealand: Standards New Zealand, Wellington, New Zealand.
13. Bradley, B. A. (2010). A Generalized Conditional Intensity Measure Approach and Holistic Ground Motion Selection. Earthquake Engineering and Structural Dynamics, 39(12), 1324-1342.
14. Ang, A. H. S., & Tang, W. H. (2007). Probability concepts in engineering: Emphasis on applications in civil and environmental engineering: John Wiley & Sons.
15. Bommer, J. J., Stafford, P. J., & Alarcon, J. E. (2009). Empirical Equations for the Prediction of the Significant, Bracketed and Uniform Duration of Earthquake Ground Motion. Bulletin of the Seismological Society of America, 99(6), 3217-3233.
16. Carr, A. J. (2004). Ruaumoko 2D - Inelastic dynamic analysis program. Department of Civil and Natural Resources Engineering, University of Canterbury, Christchurch.
17. Caughey, T. K. (1960). Calssical Normal Modes in Damped Linear Systems. Journal of Applied Mechanics, 27, 269-271.
18. Carr, A. J. (2008). Ruaumoko Manual (Vol. Volumne 2: User Manual for the 2:Dimensional Version Ruaumoko 2D). University of Canterbury, Christchurch, NZ.
19. Saiidi, M., & Sozen, M. A. (1979). Simple and complex models for nonlinear seismic response of reinforced concrete structures. Illinois: University of Illinois.
20. Sedgh, R. E., Dhakal, R. P., & Carr, A. J. (2015). State of the Art: Challenges in analytical modelling of multi-storey shear wall buildings. Paper presented at the 2015 NZSEE Conference, Rotorua.
21. ASCE. (2000). Prestandard and Commentary for the Seismic Rehabilitation of Buildings, FEMA 356. Federal Emergency Management Agency, Washington, D.C.
22. Bradley, B. A. (2011). SLAT:Seismic Loss Assessment Tool (Version 1.16): Department of Civil and Natural Resources Engineering, University of Canterbury.
23. Naeim, F., & Hagie, S. (2012). PACT: Performance Assessment Calculation Tool. John A. Martin & Associates, INC. Los Angeles, California, US.
24. Mitrani-Reiser, J. (2007). An Ounce of Prevention: Probabilistic Loss Estimation for Performance Based Earthquake Design. PhD Thesis, California Institute of Technology, Pasadena, California.
25. Aslani, H., & Miranda, E. (2005). Probabilistic Earthquake Loss Estimation and Loss Disaggregation in Buildings: Department of Civil and Environmental Engineering, Stanford University.
26. Federal Highway Administration. (1994). Technical Advisory: Motor Vehicle Accident Costs, Technical Advisory #7570.2: U.S. Department of Transportation, Washington, D.C.
27. Ministry of Transport. (2016). Social Cost of Road Crashes and Injuries 2015 Update. New Zealand.

9. Conclusions and Recommendations

9.1 OVERVIEW OF WORK PERFORMED

In this thesis, methods for estimating the extent of earthquake-induced content sliding and injuries in buildings were developed and validated, and were then used to assess the seismic sustainability of various injury forms. This involved (i) validating content sliding numerical models by comparing against shake table tests, (ii) deriving and testing parametric equations to predict the maximum sliding displacement of contents using results from numerical models, (iii) develop an injury prediction framework considering injuries due to occupants falling and/or being struck by moving contents, and (iv) investigate the effect of structural forms on damage losses, content movement, and injuries. The key findings, and recommendations for future work, are provided in this chapter.

9.2 KEY FINDINGS

9.2.1 Building Direct Damage-Repair Costs

Influence of structural forms on building damage-repair costs: The relative performance of a reinforced concrete (RC) frame building and an RC wall building was examined considering direct damage-repair costs on its own. It was found that wall buildings had lower expected annual direct damage-repair costs overall due to having lower drifts and a lower probability of requiring full-replacement; though it does experience higher accelerations. Despite the wall buildings incurring lower direct-repair costs, cost-benefit assessments including initial construction costs, but excluding downtime and injuries, showed that these buildings do incur higher life-cycle costs overall. However, evaluation of loss-hazard curves considering initial construction costs showed that wall buildings have lower cost for events equivalent to, or more severe than, a 1 in 910 year event.

A second case-study was examined considering the effect of an RC wall building's stiffness and strength on direct-repair costs. Findings from a comparison between a stiffer and a more flexible building were similar to the wall versus the frame case. However, while stronger buildings did have lower expected annual damage-repair costs compared to weaker buildings, the difference between these cases are lower as the stronger buildings generally incurred larger drifts on upper floors. Cost-benefit assessments, again considering only construction and direct-repair costs, showed that the increased benefits of having a stiffer or stronger building still do not offset the increase in initial construction costs, though the loss-hazard assessments shows that the stiffest building and the stronger building have lower cost for events equivalent to, or more severe than, a 1 in 333 year or a 1 in 588 year event, respectively

9.2.2 Sliding Response of Building Contents

Validation of numerical models: Shake-table test of content sliding was performed to validate numerical content sliding models. It was found that numerical models were able to predict the sliding response of realistic contents (i.e. furniture) on common flooring materials (i.e. carpet or vinyl) subjected to sinusoidal floor motion with an average error of 5%, though the error on a case-by-case basis may be as large as three times. This indicates that numerical models are reliable if analyses were performed considering a suite of ground motions.

Derivation of peak content sliding displacement prediction equation: A parametric equation for predicting the extent of content sliding, shown in **Eq. 5.17**, was derived based on past observations that the content's first sliding excursion (i.e. back-and forth motion) when subjected to sinusoidal floor motion could be used to approximate the maximum sliding displacement of contents subjected to realistic floor excitations. A simpler empirical form has since been developed as shown in **Eq. 6.1**. It was found that the maximum sliding displacement depended on both peak total floor acceleration and peak total floor velocity.

This has repercussions for seismic loss estimation, where damage to generic contents is generally assumed to be acceleration-sensitive.

Predictions using **Eq. 5.17** was compared against findings from a case-study of contents sliding within elastic 5-storey frames of varying periods subjected to the entire Pacific Earthquake Engineering Research Center's ground motion database. It was found that **Eq. 5.17** was more efficient and sufficient compared to other existing equations. A further case-study considering inelastic multi-storey wall buildings of varying heights subjected to ground motion records representative of the Wellington region were examined, where **Eq. 6.1** generally underestimated the displacements by 17% on average. Nonetheless, **Eq. 6.1** still provided more efficient and sufficient predictions compared to considering peak total floor accelerations on its own.

Influence of structural systems on content sliding: The effect of a wall building's stiffness and strength on the extent of content sliding was examined. It was found that contents in stiffer buildings generally have lower response compared to those of more flexible buildings, particularly for cases with low friction coefficients, despite the former incurring higher total floor acceleration response. This was due to the higher frequency of floor response, and hence lower total floor velocities, leading to each sliding excursion being smaller than that of contents within more flexible buildings with higher total floor velocities. In contrast, contents in stronger buildings experience greater sliding due to the frequency of floor response being similar to that of weaker buildings, while also experiencing higher total floor acceleration response. Based on these findings, it is recommended that buildings should be designed to be stiffer in order to minimize the extent of content sliding.

9.2.3 Injury Predictions

Development of an injury prediction framework: A new injury prediction framework was developed, and is an advancement over existing methodologies due to its

ability to consider injuries caused by occupants falling and contents moving, and to account for the effect of injury severity on injury costs. This framework was applied to a 10-storey wall building to demonstrate its usage, where it was found that the deaggregation of injury by severity and cause is similar to observations from past seismic events; demonstrating that the injury prediction framework outputs are reasonable.

Application of framework: The injury prediction framework was used to assess the cost-benefits of anchoring contents to walls during earthquakes, where it was found that anchoring contents resulted in expected injury cost savings over 50 years up to twenty two-times the installation cost. This indicates that it is financially feasible to anchor all contents within a building to limit injuries. In addition, sample injury rates related to varying building damage states and injury severities were derived for use in less advanced injury models. Both of these examples demonstrate the usefulness and versatility of the proposed injury framework.

Influence of structural systems on injuries: The effect of a wall building's stiffness and strength on injury was examined. It was found that stiffer and stronger buildings incurred more fall-related injuries, particularly at less severe shaking intensities, as these were correlated with peak total floor accelerations. Stiffer buildings however generally incurred lower content movement-related injuries compared to more flexible buildings due to it having less severe content movement on most floors, unlike stronger buildings which had more severe content movement on all floors and hence more related injuries compared to weaker buildings. Stiffer and stronger buildings both incur lesser building-collapse-related injuries, particularly at more severe shaking intensities, due to the lower probability of collapse.

9.2.4 Combined Building Damage-Repair and Injury Cost

Influence of structural systems on building damage-repair and injury cost: The influence of the wall building's stiffness and strength on combined building damage-repair

and injury cost was also examined. It was found from cost-benefit assessments that stiffer buildings had the lowest net-present-costs within 50 years of the building being in service, which differs from the case where building damage-repair costs were considered on its own. This finding was consistent even if drop-cover-hold effects were estimated, or if different datasets were used to estimate injury cost. In contrast, stronger buildings are often the most expensive option overall due to it incurring more fall-related and content movement-related injuries compared to weaker buildings.

9.3 RECOMMENDATIONS ON STRUCTURAL FORM SELECTION

Based on the key findings; designing and constructing stiffer buildings will lead to more resilient buildings. This was because in comparison with more flexible buildings, stiffer buildings incur (i) lower building damage and repair costs, (ii) lower severe content movement on most floors, and (iii) lower expected injury costs. In addition, cost-benefit assessment considering construction costs, building damage-repair cost, and injury cost for the office-type buildings considered showed that the improved performance of stiffer buildings justified their increase in construction costs. As such, it is recommended that stiffer buildings be designed for in general.

Stronger buildings however generally do not perform much better than weaker buildings. This is because in addition to higher peak total floor accelerations, stronger buildings generally incur higher drifts on upper floors, and contents within these buildings exhibit more severe movement. Cost-benefit assessment shows that the lower expected annual losses of the strongest building considered was not enough to offset its initial construction costs. Despite these findings however, it is not of the author's opinion that weaker buildings be designed for in general as downtime, which is one of the three major components of losses but was not considered, would have favored stronger buildings due to

its lesser structural damage. In addition, these findings should not be used as justification for designing buildings below the minimum standard as some failure mechanics such as local wall buckling were not considered.

In summary, based on the assumptions and analysis undertaken in this thesis, it is concluded that the initial cost premium of stiffening buildings is worth it based on the indicators considered (i.e. direct-repair and injury costs).

9.4 OPPORTUNITIES FOR FUTURE WORK

9.4.1 Content Movement

The content sliding response investigated in **Chapters 4** to **6** in this thesis was unobstructed, meaning that the contents are free to move without impacting against obstacles. In reality, contents positioned close to interior partitions or walls are likely to impact against them during strong shaking. While this was considered for injury predictions in **Chapters 7** and **8**, the coefficient of restitution assumed was based off experimental studies unrelated to content sliding. To model this properly, typical coefficient of restitution values for sliding cases needs to be investigated, and modifications to **Eq. 5.17** can be derived to account for this effect.

In addition, there are other types of content movement which were not considered, such as projectile motion (e.g. books falling off shelves or bricks falling from buildings). Development of models capable of considering this effect can be used to (i) model injuries caused by items falling onto occupants from height, (ii) identify the severity of shaking based on the distance that contents end up away from a building, or (iii) determine minimum safe distances to place cordons following strong shaking events.

Finally, while the use of content movement numerical models in injury modelling is provided, the damage cost implications was not. This is because even if some contents exhibit

severe movement, the content itself may not necessarily be damaged. An example of this could be bookshelves overturning, which may result in injuries if it impacts against occupants, but it itself may be undamaged. Estimates of potential damage and losses based on the extent of content movement are thus required.

9.4.2 Injury Prediction Framework

One of the major limitations of the proposed injury prediction framework is its assumption that occupants remain stationary during the entirety of ground motion shaking. In reality, many would take evasive actions, such as drop-cover-hold. There are approaches in fire engineering for modelling the thought-process and actions of occupants in the event of hazards. Such approaches may be adapted and calibrated to be relatable for seismic events.

Another limitation is the reliability of the data used in the framework. Examples of these includes (i) the transient occupancy model implemented being specific to Hong Kong conditions, (ii) lack of data required to produce more realistic fragility functions for predicting the peak total floor accelerations that causes loss of balance which results in people tripping and falling over, and (iii) fragility functions for assessing the severity of injuries to the head and extremities not considering the mass of impact. Derivation of more reliable data, such as finite element modelling of impact against body parts to derive more comprehensive fragility functions for predicting injury severity, will aid in making the framework output's even more realistic.

Finally, while some comparisons between the framework's outputs had been made with anecdotal data where possible, a more thorough comparison is required to observe if the framework requires further calibration. Existing studies examining anecdotal injury data from past earthquakes do not provide the level of detail required for such comparisons, such as

relationships linking the cause and severity of injury together. Examination of such data will aid in evaluating the reliability of the injury prediction framework.

9.4.3 Further Extension of Study on Structural Forms and Downtime Considerations

While the influence of a building's stiffness and strength on building damage-repair and injury cost was investigated thoroughly in this thesis, the effect of the selection of structural systems was only briefly touched upon in the frame versus wall comparison in **Chapter 2**. Consideration of a wider range of structural systems, or implementation of low-damage technology such as sliding hinge joints or base-isolation, should also be investigated. This will provide incentives for selecting one structural system over another, and can also aid in subjective performance assessment approaches.

Another research direction of interest is to examine the effects of irregularity on building performance. Examples of irregularity includes, but are not limited to: (i) non-rectangular floor plan geometry, (ii) mass, stiffness, and strength vertical irregularity, and (iii) using differing lateral load resisting systems (i.e. structural walls on one side of the building and a frame in another) which may lead to torsional effects. It would be of interest to observe if these effects outweigh those of stiffness and strength, and if so, additional work can be performed to evaluate the adequacy of current code-provisions regarding irregularity using loss estimation approaches.

On a final note, the comparison studies examined in this thesis were performed excluding the influence of downtime (i.e. business interruption). Consideration of this will provide a more complete assessment of a building's performance in seismic events.

Appendix A. Selected Ground Motion Records

A1. LIMITATIONS OF TRADITIONAL SELECTION APPROACHES

Many current seismic codes allow the use of the Uniform Hazard Spectra (UHS) to select ground motion records. In NZS1170.5 [1] for example, the ground motion records are selected to match the design UHS curve over a period range between $0.4T_1$ and $1.3T_1$, where T_1 is the fundamental mode period of the structure of interest. Constraints are usually applied to implicitly account for duration and frequency content properties of ground motion records. Examples include rejecting records that falls outside a given magnitude range, or specifying an allowable scale factor range for the records.

One limitation of this approach is that rupture distance-magnitude pairings have varying contributions at different periods. An example of this is shown in **Figure A.1**, where smaller magnitude shaking occurring closer to Christchurch, New Zealand, on subsoil class D has a large contribution to the 10% probability of exceedance in 50 year *Sa*(0.5s). In contrast, large magnitude events further away from the site has a greater contribution to the 10% in 50 year *Sa*(1.5s). Thus, if the vibration periods corresponding to both intensity measures are within $0.4T_1$ and $1.3T_1$, it is left up to engineering judgement as to which magnitude and distance limitations to impose.

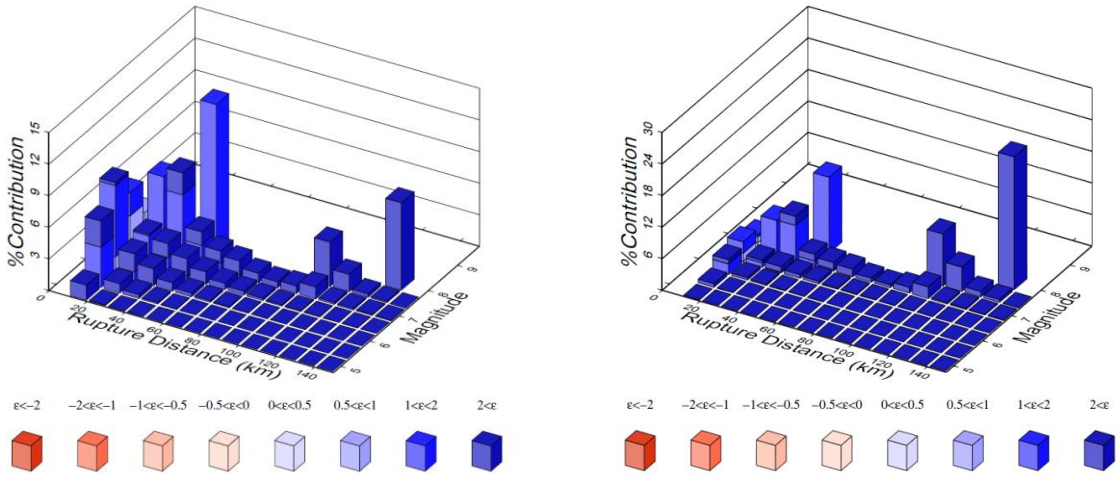

(a) Sa(0.5s) **(b) Sa(1.5s)**

Figure A.1. Deaggregation of 10% in 50 year hazard for Christchurch (*Vs30* = 200m/s)

This discrepancy also highlights the fact that it is unlikely for the same hazard level to be reached across a range of periods in a single rupture event. This issue has been historically documented in several studies, such as the National Research Council [2] and McGuire [3]. An example of this is shown in **Figure A.2**; where *Sa*(0.5s) is the same in two separate events, but noticeable differences were observed at other vibration periods.

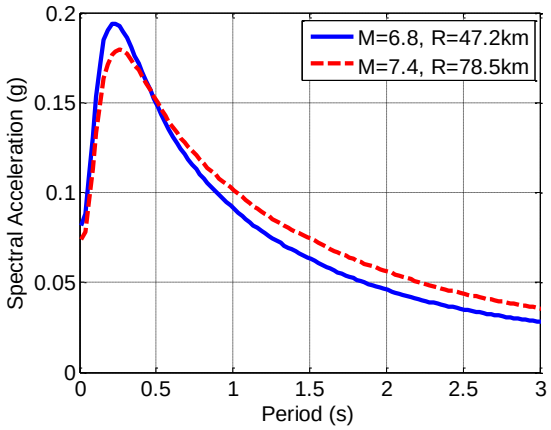

Figure A.2. Comparison of spectral acceleration curves for different ruptures

In addition, a single ground motion record suite is often scaled over a large range of hazard levels when performing probabilistic structural analyses. However, it is unrealistic for ground motion records representative of a frequent event to have the same duration, frequency content, and spectral shapes as ones for rarer events. This may have great influence on building response, especially ones not dominated by the first mode. Other limitations of

traditional ground motion selection approaches are covered in literature (e.g. Vamvatsikos and Cornell [4], Bommer et al. [5]).

A2. GCIM THEORY AND SELECTION ALGORITHM

The Generalized Conditioning Intensity measure approach is a state-of-the-art ground motion selection methodology proposed by Bradley [6]. Using this method, an intensity measure is selected as the conditional intensity measure, IM_j. Lognormal mean and standard deviations at other intensity measures of interest, IM_i, which are conditional to a given value of IM_j, im_j, can then be calculated for a specific rupture, rup_k, as shown in **Eqs. A.1** and **A.2**. Here, ε is the number of standard deviations that $\ln im_j$ is from the average value of $\ln IM_j$, $\mu_{\ln IMj}$; while $\rho_{\ln IMi,\ln IMj}$ is the correlation factor between IM_i and IM_j. The conditional distribution of IM_i given $IM_j = im_j$ considering all ruptures, $f_{IMi|IMj}(im_i| im_j)$, is given in **Eqs. A.3**. An algorithm to derive these distributions has been programmed into OpenSHA [7]. Note that non-amplitude *IM* can also be considered using this approach.

$$\mu_{\ln IM_i|\ln IM_j}(rup_k, im_j) = \mu_{\ln IM_i}(rup_k) + \sigma_{\ln IM_i}(rup_k) \times \varepsilon \times \rho_{\ln IM_i,\ln IM_j} \quad \textbf{(A.1)}$$

$$\sigma_{\ln IM_i|\ln IM_j}(rup_k, im_j) = \sigma_{\ln IM_i}(rup_k)\sqrt{1-\rho^2_{\ln IMi,\ln IMj}} \quad \textbf{(A.2)}$$

$$f_{IMi|IMj}(im_i \mid im_j) = \sum_{k=1}^{N_{Rup}} f_{IM_i|Rup,IM_j}(im_i \mid rup_k, im_j) P_{Rup|IM_j}(rup_k \mid im_j) \quad \textbf{(A.3)}$$

Ground motion records are selected and scaled such that $IM_j = im_j$ and the conditional distribution at other IM_i of the ground motion suite is consistent with the theoretical distributions calculated from **Eqs. A.1** and **A.2**. An algorithm for selecting records and performing statistical tests on the selected ground motion suite is detailed in Bradley [8]. Note that all records were selected from the PEER ground motion database [9].

One limitation of this approach is that the structure's probabilistic response for a given intensity-level shaking, $P_{EDP|IMi,IMj}(edp|im_i,im_j)$, would be biased to the selected IM_j; though

similar limitations also exist when using the UHS to select records. However, convoluting together $P_{EDP|IMi,IMj}(edp|im_i,im_j)$, $f_{IMi|IMj}(IM_i|IM_j)$, and the hazard curve for IM_j, $\lambda_{IMj}(im_j)$ would result in the structural response hazard curve being consistent regardless of the selected IM_j. This is shown mathematically in **Eqs. A.4** and **A.5**. Therefore, the records selected following this approach are consistent with the site's seismic conditions. The unbiasedness of $\lambda_{EDP}(edp)$ to IM_j has been tested for a soil-pile foundation by Bradley [10], where it was shown that the response of the system is independent of the choice of IM_j.

$$P_{EDP|IM_j}(edp \mid im_j) = \int_{IM_i} P_{EDP|IM_i,IM_j}(edp \mid im_i, im_j) f_{IM_i|IM_j}(im_i \mid im_j) dIM_i \quad \textbf{(A.4)}$$

$$\lambda_{EDP}(edp) = \int_{IMj} P_{EDP|IM_j}(edp \mid im_j) \left| \frac{d\lambda_{IM_j}(im_j)}{dIM_j} \right| dIM_j \quad \textbf{(A.5)}$$

A3. CHRISTCHURCH CASE STUDY

A3.1 Selected Records

The records selected for the Christchurch region (43.53°S 172.62°E) for use in **Chapter 2** are listed in **Table A.1**. These records were selected for subsoil class D conditions ($Vs30$ = 300 m/s) using spectral acceleration at 1.50 s, Sa(1.50s), as the conditioning intensity measure. Record suites were selected at 99%, 80%, 50%, 20%, 10% (design-basis event), 5%, 2% (maximum-credible event), 1%, 0.5%, 0.2%, and 0.1% probability of exceedance in 50 years. Other conditioning intensity measures considered, and their respective references, are (i) peak ground acceleration, PGA, and 5% damped spectral acceleration at vibration periods of T = 0.05s, 0.1s, 0.2s, 0.3s, 0.5s, 0.75s, 1.0s, 2.0s, 3.0s and 5.0s [11]; (ii) 5-75% and 5-95% significant durations, D_{s575} and D_{s595}, respectively [12]; and (iii) Cumulative absolute velocity, CAV [13]. Weighting factors of 0.7 and 0.3 were split between all amplitude and non-amplitude intensity measures, respectively.

Table A.1. Selected ground motion records (Christchurch, *Vs30* = 300 m/s, *Sa*(1.50s), ID – NGA number of record, SF – scale factor)

Shaking Intensity Level (Probability of exceedance in 50 years)																					
99%		80%		50%		20%		10%		5%		2%		1%		0.5%		0.2%		0.1%	
ID	SF	ID	SF	ID	SF	ID	SF	ID	SF	ID	SF	ID	SF	ID	SF	ID	SF	ID	SF	ID	SF
96	0.10	150	0.20	164	0.54	164	0.90	269	2.28	178	0.96	165	1.18	159	1.06	130	4.30	1063	0.61	392	7.69
342	0.06	288	0.48	465	0.74	353	1.62	292	0.43	325	3.91	501	3.93	184	0.78	269	5.52	758	0.94	778	2.24
613	0.43	527	0.09	758	0.14	391	1.64	728	0.56	348	1.03	553	3.36	323	4.27	808	1.86	783	1.12	784	1.70
710	0.57	764	0.14	760	0.39	835	0.96	900	0.42	787	0.88	739	1.63	348	1.64	1057	2.62	342	1.68	789	3.15
763	0.11	1074	0.85	778	0.29	933	2.61	1229	1.77	796	1.42	760	1.44	778	1.29	1176	0.86	316	1.88	802	1.55
860	0.26	1218	1.27	836	0.72	1063	0.15	1284	1.81	1119	0.26	835	2.12	1166	1.03	1327	2.49	789	2.69	1136	35.28
963	0.03	1273	1.36	1155	0.39	1155	0.65	1334	0.91	1308	1.99	885	1.77	1257	2.11	1365	4.46	1330	2.80	1373	4.35
1237	0.11	1472	0.19	1368	3.59	1166	0.39	1410	0.43	1330	1.18	1136	16.83	1337	1.37	1414	1.69	1328	2.86	1410	1.52
1486	0.14	1555	0.20	1375	1.36	1295	0.61	1569	2.37	1365	2.34	1253	4.52	1365	3.74	1599	5.61	502	3.05	1504	0.91
1541	0.05	1608	0.67	1411	0.27	1317	0.47	1602	0.42	1430	1.34	1291	3.78	1449	7.99	1759	13.44	1409	3.32	2470	7.25
1837	0.40	1766	0.66	1560	0.72	1337	0.51	2091	6.29	1509	0.24	1330	1.56	1600	21.18	1768	4.58	883	3.67	2489	14.33
2174	1.35	1833	2.59	1608	1.12	1339	1.52	2489	4.08	1529	0.36	1439	3.53	2567	13.22	2091	15.23	1356	3.99	2496	9.37
2464	0.24	2074	6.03	1798	1.59	1352	2.90	2510	1.81	2461	1.18	1592	4.84	2739	4.16	2470	4.99	3490	5.96	2650	2.18
2495	0.04	2456	2.77	2085	3.84	1775	3.03	2884	1.36	2472	1.59	2496	4.47	2762	32.16	2489	9.86	3084	6.91	2926	22.73
2739	0.22	2709	0.36	2107	0.88	2842	7.64	2969	1.70	2489	5.17	2669	13.98	3084	4.66	2669	20.16	3411	7.23	3084	8.08
2781	1.25	2742	0.54	2326	2.96	2930	2.68	3233	5.53	2598	4.49	3230	6.96	3086	4.03	2830	11.77	2496	8.01	3411	8.46
2960	0.31	2806	2.55	2710	0.69	3110	2.08	3268	0.96	2867	5.27	3265	0.91	3110	5.58	3084	5.56	3521	8.74	3490	6.97
3012	2.17	3078	0.97	2946	1.75	3228	2.80	3305	1.71	3083	3.24	3297	4.10	3348	5.96	3236	8.11	3526	8.78	3520	19.75
3039	0.45	3234	1.84	3086	0.90	3396	2.57	3420	7.05	3273	1.04	3411	4.03	3526	5.91	3264	1.91	3544	14.94	3521	10.22
3381	0.31	3460	0.85	3318	2.50	3458	2.10	3425	8.09	3411	3.05	3440	18.21	3526	5.91	3523	4.97	3161	36.80	3523	7.23

A3.2 Design-Basis-Event Suite Check

The record suite for the design-basis event for Christchurch is shown in **Figure A.3**. It can be seen that *Sa*(1.5s) is consistent for all scaled records in the ground motion suite. In addition, the conditional distributions of IM_i of the ground motion suite match the theoretical distributions based on Kolmogorov-Smirnov tests [14] with a 90% confidence level. This indicates that the selection approach is reasonable.

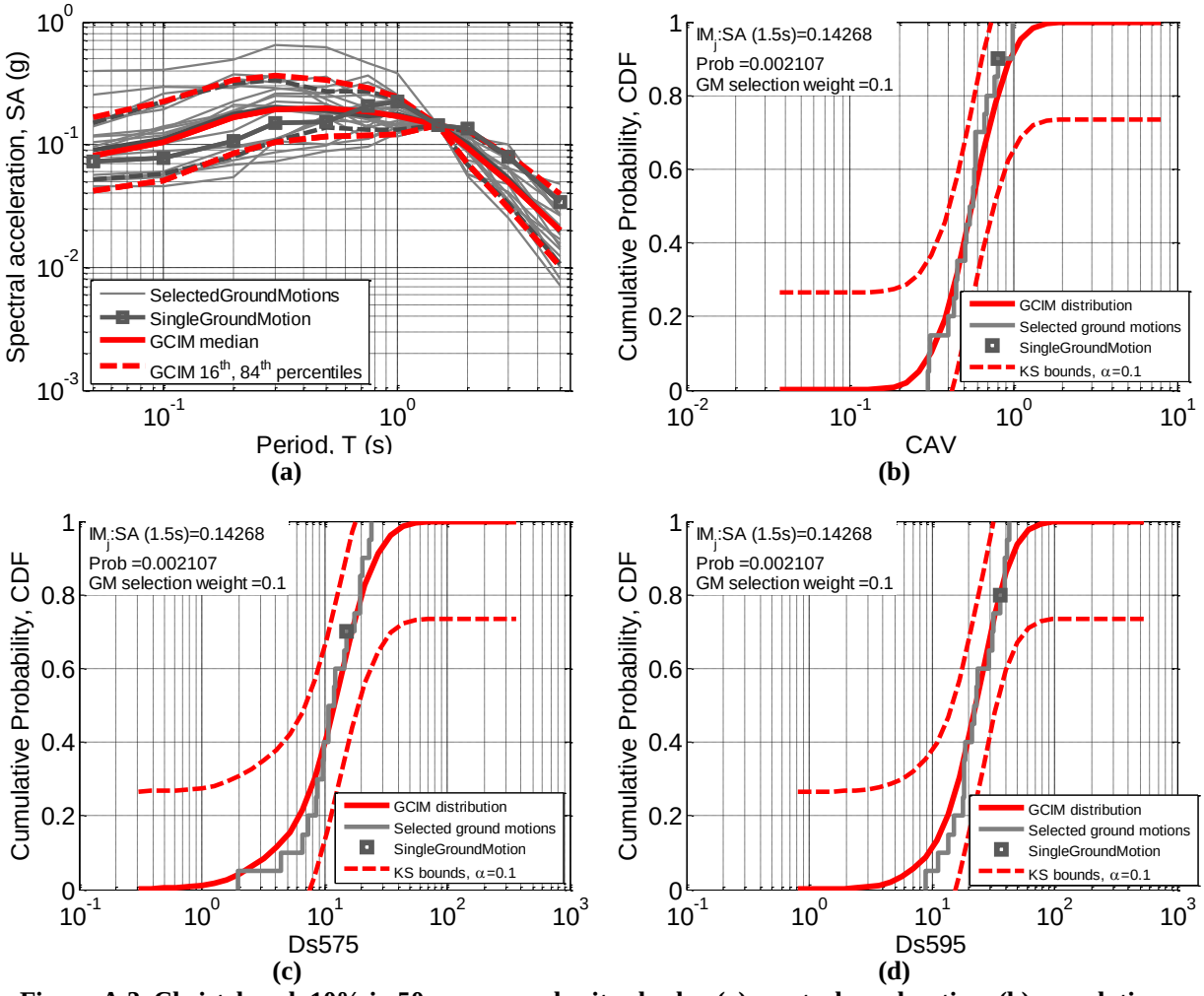

Figure A.3. Christchurch 10% in 50 year record suite checks; (a) spectral acceleration, (b) cumulative absolute velocity, (c) –(d) significant duration for 5-75% and 5-95%, respectively

A3.3 Maximum-Credible-Event Suite Check

The record suite for the maximum-credible event for Christchurch is shown in **Figure A.4**. As with the design-basis case, the conditional distributions of IM_i of the selected record

suite match the theoretical distribution based on Kolmogorov-Smirnov tests [14] with a 90% confidence level. This again indicates that the selection approach is reasonable.

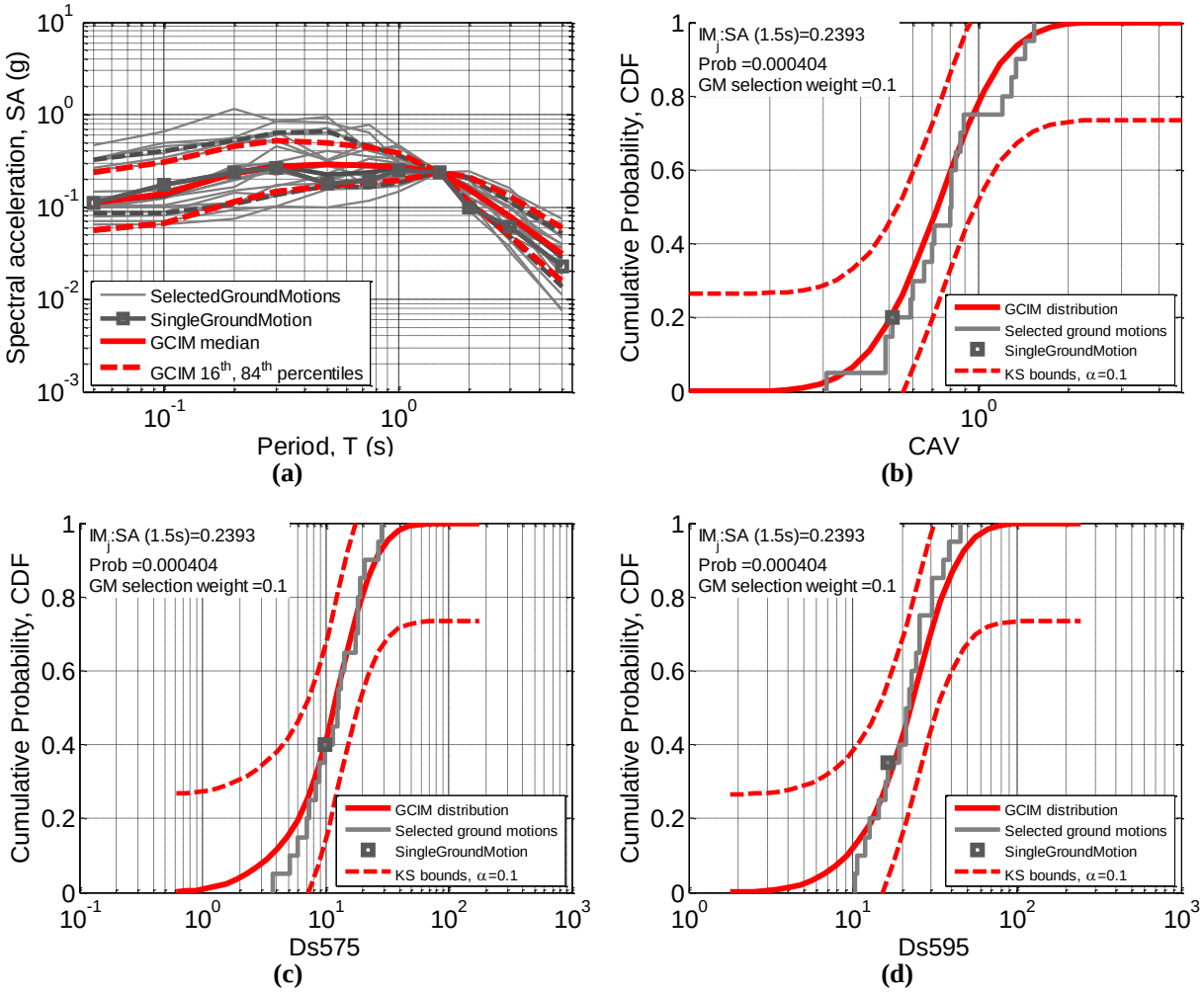

Figure A.4. Christchurch 2% in 50 year record suite checks; (a) spectral acceleration, (b) cumulative absolute velocity, (c) –(d) significant duration for 5-75% and 5-95%, respectively

A4. SELECTED WELLINGTON GROUND MOTION RECORDS

A4.1 Selected Records

The records selected for the Wellington region (41.3°S, 174.8°E) which were used in **Chapters 3**, **6**, **7**, and **8** are listed in **Table A.2**. These records were selected for subsoil class C conditions (*Vs30* = 400 m/s) using spectral acceleration at 1.25 s, *Sa*(1.25s), as the conditioning intensity measure. Record suites were selected at 99%, 80%, 50%, 20%, 10% (design-basis events), 5%, 2% (maximum-credible events), 1%, 0.5%, 0.2%, and 0.1%

probability of exceedance in 50 years. Other conditioning intensity measures considered, and their respective reference, are (i) *PGA* and 5% damped spectral acceleration at vibration periods of T = 0.05s, 0.1s, 0.2s, 0.3s, 0.5s, 0.75s, 1.0s, 1.5s, 2.0s, 3.0s and 5.0s [11], and (ii) 5-75% and 5-95% significant durations, D_{s575} and D_{s595}, respectively [12]. Note that (i) weighting factors of 0.8 and 0.2 were split between all amplitude and non-amplitude intensity measures, respectively; and (ii) cumulative absolute velocity was not selected as an additional intensity measure as attenuation relations for this does not exist for subduction zone ruptures.

Table A.2. Selected ground motion records (Wellington, *Vs30* = 400 m/s, *Sa*(125s), ID – NGA number of record, SF – scale factor)

Shaking Intensity Level (Probability of exceedance in 50 years)																					
99%		80%		50%		20%		10%		5%		2%		1%		0.5%		0.2%		0.1%	
ID	SF	ID	SF	ID	SF	ID	SF	ID	SF	ID	SF	ID	SF	ID	SF	ID	SF	ID	SF	ID	SF
127	0.29	265	0.22	50	3.30	28	4.05	122	5.29	342	2.85	334	4.34	354	15.40	339	11.34	70	14.03	165	10.42
133	0.37	375	3.54	147	0.58	81	8.77	165	1.86	527	1.75	355	14.83	733	8.70	350	14.55	70	14.03	266	15.79
237	0.56	479	1.75	176	0.99	174	1.19	167	8.12	535	18.89	458	6.16	744	5.97	363	11.01	342	8.75	334	10.41
413	0.19	729	0.20	776	0.23	461	1.50	461	2.75	735	5.61	753	3.22	771	5.10	466	15.81	348	12.27	342	10.34
458	0.11	879	0.15	902	0.58	464	2.56	792	9.18	757	4.73	779	1.70	800	18.96	759	4.64	363	14.10	348	14.48
769	0.14	1096	1.23	969	3.77	1042	1.23	795	5.01	829	2.58	850	5.88	841	13.01	760	10.24	527	5.37	744	11.17
1011	0.24	1303	0.87	993	0.92	1263	1.71	797	5.66	839	9.87	902	6.38	963	2.78	795	18.62	728	8.17	796	16.43
1096	0.47	1347	1.06	1093	4.23	1269	1.45	1085	0.72	980	14.12	1071	14.18	1009	7.34	882	10.28	769	15.61	1292	9.85
1132	5.51	1827	0.69	1094	1.79	1303	4.44	1362	5.63	995	3.22	1099	14.10	1019	15.66	988	7.00	783	5.15	1320	17.30
1870	11.25	2009	2.23	1266	0.62	1508	0.48	1440	8.23	1015	10.53	1248	16.67	1039	8.22	1039	10.18	1012	12.17	1329	13.85
1878	9.01	2183	7.33	1564	1.24	1509	0.30	1507	1.14	1057	5.34	1268	12.48	1092	10.21	1053	16.06	1063	2.68	1361	12.99
1921	2.27	2194	14.72	1772	2.08	1783	2.68	1546	1.86	1166	3.13	1297	6.26	1224	15.95	1092	12.65	1092	16.19	1361	12.99
1992	1.88	2415	1.63	1856	13.17	1793	3.71	1626	13.02	1277	5.47	1421	4.97	1258	7.83	1224	19.74	1330	14.10	1410	8.29
2002	1.87	2669	3.22	2316	5.21	1998	16.78	1770	5.70	1513	1.98	1498	3.09	1295	7.09	1292	6.52	1419	7.17	1413	11.01
2277	0.95	2688	3.36	2469	1.70	2508	7.02	1816	4.59	1513	1.98	1551	3.40	2465	10.33	1364	18.13	1459	13.00	2709	18.28
2433	1.51	2795	12.01	2507	0.62	2949	8.39	2221	11.15	2465	5.33	1611	10.18	2648	19.17	1386	19.38	1492	2.86	3259	10.34
2690	4.13	3308	0.47	2903	10.95	3077	5.35	2949	15.42	2889	17.25	1637	8.00	2663	10.16	1419	5.60	1575	13.01	3467	11.36
2946	0.50	3312	1.16	3266	0.92	3329	4.87	3022	16.61	3272	11.35	2714	10.28	3265	5.60	1509	2.04	1791	18.37	3496	16.68
3006	0.78	3430	6.03	3313	1.68	3416	3.06	3296	9.06	3308	6.83	2899	11.49	3345	17.01	1555	8.78	2663	16.11	3504	19.46
3354	0.79	3544	1.57	3432	3.11	3511	4.79	3490	5.74	3323	14.93	3259	4.31	3509	13.76	3493	19.46	3510	13.27	3510	15.66

A4.2 Design-Basis-Event Suite Check

The record suite for the design-basis-event for Wellington is shown in **Figure A.5**. The conditional distributions of IM_i from the ground motion suite match that of the theoretical distributions based on Kolmogorov-Smirnov tests [14] with a 90% confidence level. This indicates that the selection approach is reasonable.

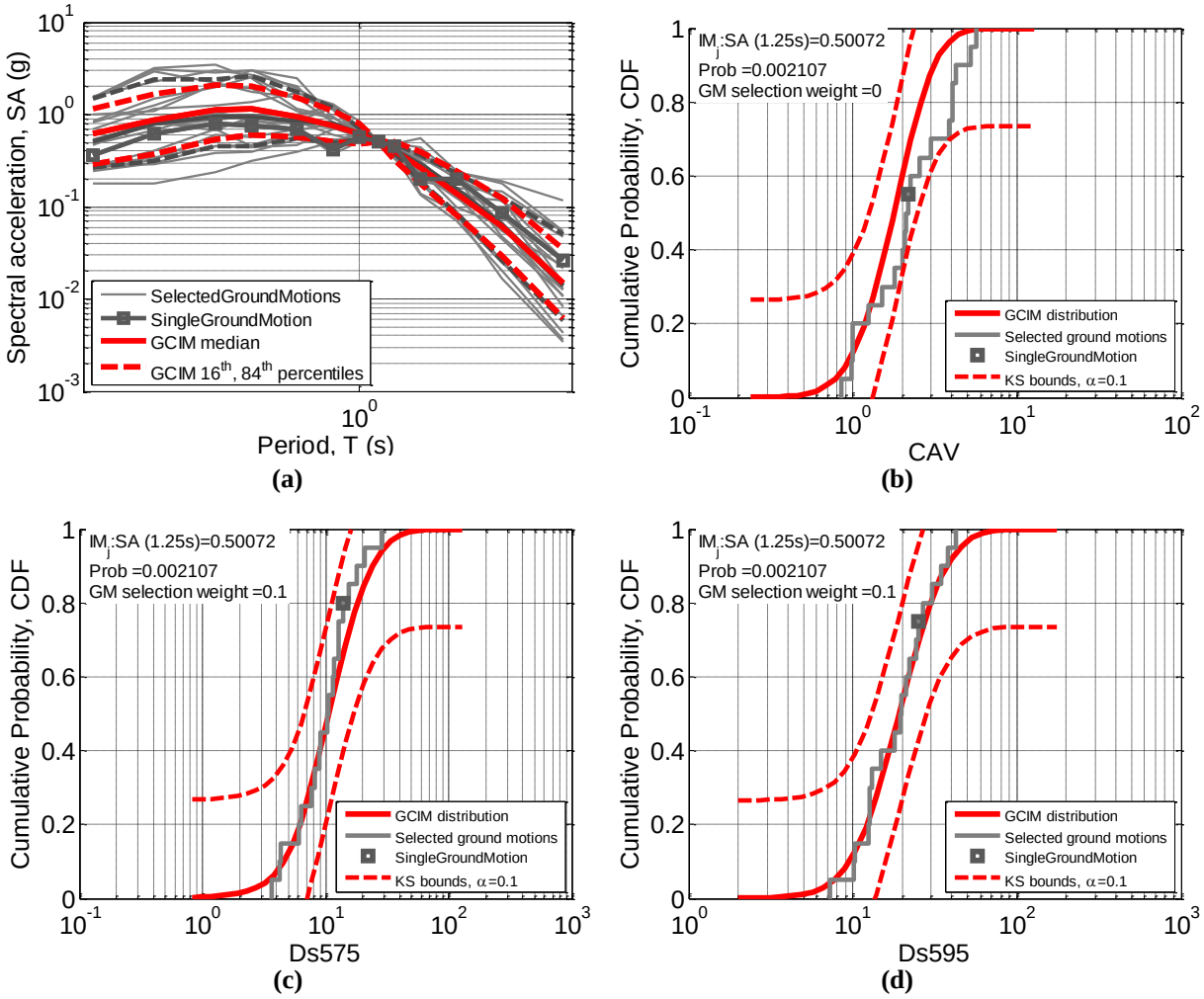

Figure A.5. Wellington 10% in 50 year record suite checks; (a) spectral acceleration, (b) cumulative absolute velocity, (c) –(d) significant duration for 5-75% and 5-95%, respectively

A4.3 Maximum-Credible-Event Suite Check

The record suite for the maximum-credible event for Wellington is shown in **Figure A.6**. Unlike the other suites examined, the conditional distribution for cumulative absolute velocity, *CAV*, of the ground motion suite is a poor fit to the theoretical distributions. This was due to *CAV* not being explicitly considered in ground motion selection as attenuation

relationships are not available for this IM_i for subduction zones. The conditional distributions at other IM_i of the ground motion suite match theoretical distributions.

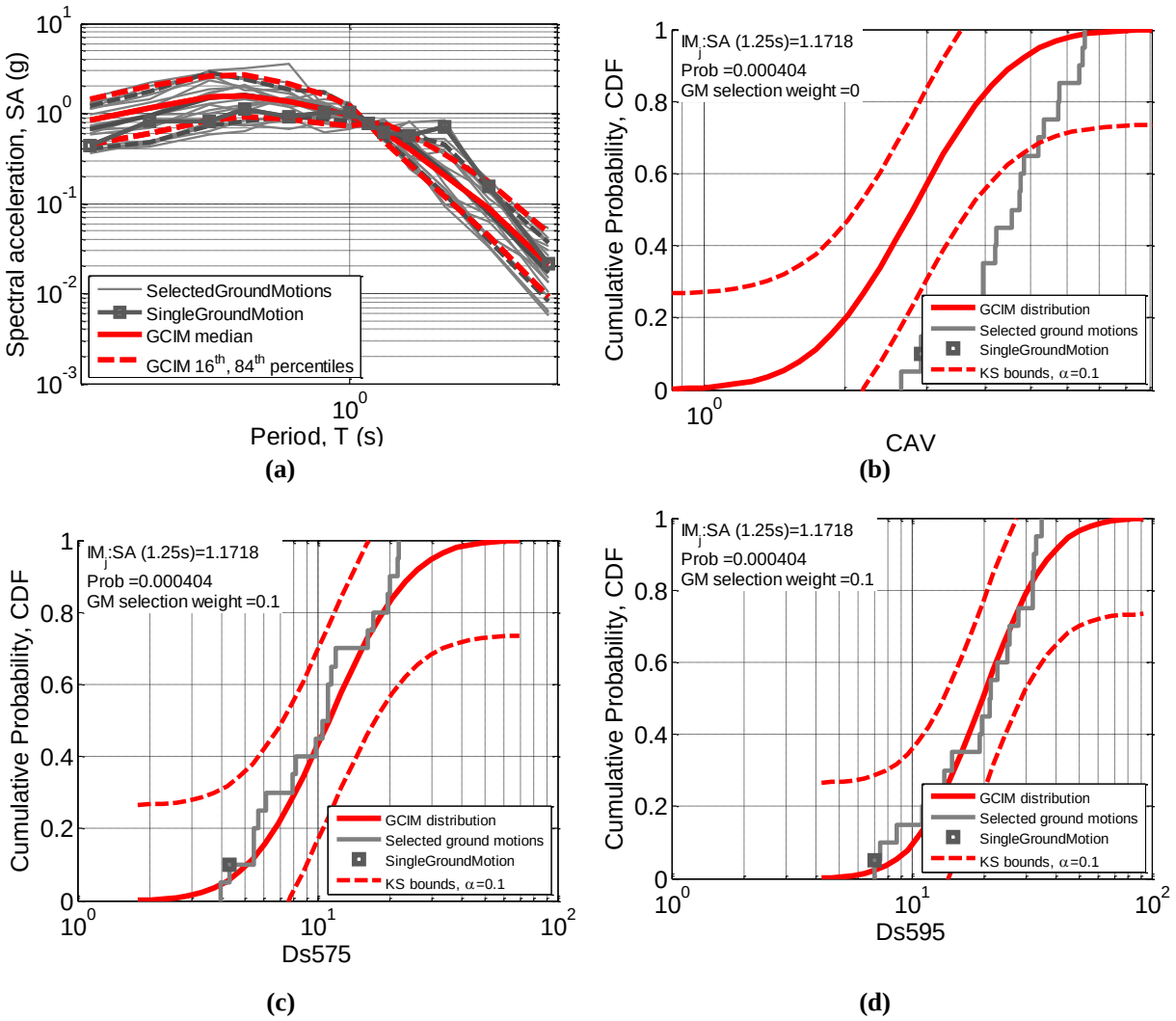

Figure A.6. Wellington 2% in 50 year record suite checks; (a) spectral acceleration, (b) cumulative absolute velocity, (c) –(d) significant duration for 5-75% and 5-95%, respectively

A5. REFERENCES

1. Standards New Zealand. (2004). NZS 1170.5:2004, Structural Design Actions Part 5: Earthquake Actions New Zealand: Standards New Zealand, Wellington, New Zealand.
2. National Research Council. (1988). Probabilistic seismic hazard analysis. National Academy Press, Washington, D.C., 97.
3. McGuire, R. K. (1995). Probabilistic Seismic Hazard Analysis and Design Earthquakes: Closing the Loop. Bulletin of the Seismological Society of America, 85(5), 1275-1284.
4. Vamvatsikos, D., & Cornell, C. A. (2002). Incremental Dyamic Analysis. Earthquake Engineering and Structural Dynamics, 31, 491-514.
5. Bommer, J. J., Scott, S. G., & Sarma, S. K. (2000). Hazard-Consistent Earthquake Scenarios. Soil Dynamics and Earthquake Engineering, 19, 219-231.
6. Bradley, B. A. (2010). A Generalized Conditional Intensity Measure Approach and Holistic Ground Motion Selection. Earthquake Engineering and Structural Dynamics, 39(12), 1324-1342.
7. Field, E. H., Jordan, T. H., & Cornell, C. A. (2003). OpenSHA: A Developing Community-Modeling Environment for Seismic Hazard Analysis. Seismological Research Letters, 74(4), 406-419.

8. Bradley, B. A. (2012). A Ground Motion Selection Algorithm Based on the Generalized Conditional Intensity Measure Approach. Soil Dynamics and Earthquake Engineering, 40, 48-61.
9. Chiou, B. S. J., Darragh, R., Gregor, N., & Silva, W. (2008). NGA Project Strong-Motion Database. Earthquake Spectra, 24(1), 23-44.
10. Bradley, B. A. (2012). The Seismic Demand Hazard and Importance of the Conditioning Intensity Measure. Earthquake Engineering and Structural Dynamics, 41(11), 1417-1437.
11. Bradley, B. A. (2013). A New Zealand-Specific Pseudospectral Acceleration Ground-Motion Prediction Equation for Active Shallow Crustal Earthquakes Based on Foreign Models. Bulletin of the Seismological Society of America, 103(3), 1801-1822.
12. Bommer, J. J., Stafford, P. J., & Alarcon, J. E. (2009). Empirical Equations for the Prediction of the Significant, Bracketed and Uniform Duration of Earthquake Ground Motion. Bulletin of the Seismological Society of America, 99(6), 3217-3233.
13. Campbell, K. W., & Bozorgnia, Y. (2010). A Ground Motion Prediction Equation for the Horizontal Component of Cumulative Absolute Velocity (CAV) Based on the PEER-NGA Strong Motion Database. Earthquake Spectra, 26(3), 635-650.
14. Ang, A. H. S., & Tang, W. H. (2007). Probability concepts in engineering: Emphasis on applications in civil and environmental engineering: John Wiley & Sons.

Appendix B. Ruaumoko Automation Matlab Codes

B1. OVERVIEW

A suite of 440 individual horizontal ground motion record components selected from **Appendix A** was used to analyse each building using Ruaumoko2D [1]. Due to the considerable computation effort required, Matlab [2] was used to automate creation of input files, running the program, and results extraction. The Matlab files written are largely based on similar work by Sadashiva [3], and are described in the following sections.

B2. MASTER SCRIPT FILE

The following script file calls upon other function files written to (i) read ground motion records, (ii) extract out properties of the ground motion records, (iii) write input files and perform structural analyses on Ruaumoko2D [1], (iv) extract out results from summary outputs, and (v) run Dynaplot [4] to extract more detailed building response. More in-depth details of the five functions created are described in the following sections. Note that this code calls ground motion records obtained from the Pacific Earthquake Engineering Center's ground motion database [5]. These records were named NGA#$_1$_#$_2$.txt; where #$_1$ is the NGA ID designation used in the PEER database, and #$_2$ indicates the ground motion component (1 and 2 indicates horizontal components, and 3 indicated vertical).

```
%-----------------------------------------------------------------------
% Purpose - Master MATLAB script to run structural analyses on Ruaumoko
%-----------------------------------------------------------------------

% Inputs

% IM - row of IM values corresponding to hazard levels of interest
IM = [0.021 0.054 0.107 0.273 0.501 0.775 1.17 1.50 1.86 2.38 2.81];

% File/Analyses locations
% Define the directory where (i) the analysis is performed, (ii) the folder
% where outputs will be stored, and (iii) the folder containing ground
% motion records
Analysisfolder = ('C:\Analysisfolder\');
```

```
Outputfolder = ('C:\Outputfolder\');
EQfolder = ('C:\EQfolder\');

% Define building properties
Weight = 1720;  %Weight per floor (in kN)
Period = 1.25;  %Building's Period (for file ID purposes)
Rmod = 4;       %Building's force reduction factor (for file ID purposes)
My = 58300;     %Wall's moment capacity at base (in kNm)
I = 13.72;      %Moment of inertia (m^4)
A = 2.8;        %Wall area (m^2)
As = 2;         %Wall shear area (m^2)

%-------------------------------------------------------------------------

%Create Output Files

% Specify number of type of EDPs of interest
n_ACCEDP = 11;                  %Acc-related EDPs in building
n_DRIFTEDP = 10;                %Drift-related EDPs in building
n_EDP = n_ACCEDP+n_DRIFTEDP;    %Total number of EDPs in building

%Create directory if it doesn't exist
mkdir(Outputfolder)

%Create Accleration Output Files
for i = 1:n_ACCEDP
    FloorAcc = [Outputfolder,'EDPtemp_',num2str(i),'.txt'];
    filetitle = ['EDPIM data for EDP',num2str(i),' - floor ',...
        num2str(i),' acceleration in g'];
    dlmwrite(FloorAcc,filetitle,'delimiter','','newline','pc')
    filepara = ['    ',num2str(nIM),'   20','     (41g12.7)'];
    dlmwrite(FloorAcc,filepara,'-append','delimiter','','newline','pc')
end

% Creating Drift Output Files
for i = n_ACCEDP+1:n_ACCEDP+n_DRIFTEDP
    StoreyDrift = [Outputfolder,'EDPtemp_',num2str(i),'.txt'];
    filetitle = ['EDPIM data for EDP',num2str(i),' - floor ',...
        num2str(i-10),' drift in %'];
    dlmwrite(StoreyDrift,filetitle,'delimiter','','newline','pc')
    filepara = ['    ',num2str(nIM),'   20','     (41g12.7)'];
    dlmwrite(StoreyDrift,filepara,'-append','delimiter','','newline','pc')
end

%-------------------------------------------------------------------------

%Run analyses and extract out results

%Run anlyses for all 11 hazard levels considered
for Z = 1:11

    %Obtain list of ground motions required for this case (see Appendix B.3
    for details)
    [SF,FileIdent] = EQParaSA(Z);

    %Obtaining number of records used in analyses
    Num_Rec = length(SF);

    %Run structural analyses for the given suite of records
```

```
for i = 1:Num_Rec   %Cycling through the ground motion records
    if FileIdent(i)<10,
        Eqlink1 = [EQfolder,'NGA000',num2str(FileIdent(i)),'_1.txt'];
        Eqlink2 = [EQfolder,'NGA000',num2str(FileIdent(i)),'_2.txt'];
    elseif FileIdent(i)<100
        Eqlink1 = [EQfolder,'NGA00',num2str(FileIdent(i)),'_1.txt'];
        Eqlink2 = [EQfolder,'NGA00',num2str(FileIdent(i)),'_2.txt'];
    elseif FileIdent(i)<1000
        Eqlink1 = [EQfolder,'NGA0',num2str(FileIdent(i)),'_1.txt'];
        Eqlink2 = [EQfolder,'NGA0',num2str(FileIdent(i)),'_2.txt'];
    else
        Eqlink1 = [EQfolder,'NGA',num2str(FileIdent(i)),'_1.txt'];
        Eqlink2 = [EQfolder,'NGA',num2str(FileIdent(i)),'_2.txt'];
    end

    for j = 1:2     % Switching record components
        if j == 1
            Eqfilelink = Eqlink1;
        elseif j == 2
            Eqfilelink = Eqlink2;
        end

        % Obtain GM record parameters
        [dt,T] = PullOut_EQ(Eqfilelink);

        % Creating RUAUMOKO data file for Response History Analysis
        [filename] = WallInputNEWSINA2(My,I,A,As,Analysisfolder,...
            Eqfilelink,dt,1/SF(i),T);

        % Run Structural Analysis
        system('Ruaumoko2N.exe JUNK.wri test_0.txt');

        % Specify name and location of output file
        n=[Analysisfolder,'junk.wri'];

        %Identify position of results of interest
        Line = 14;

        % Extract out total acceleration results
        for k = 1:n_ACCEDP
            [MaxAcc, MinAcc] = PullOut_Acc(n,k,Line);
            TEMP1(k,j) = max(abs(MaxAcc),abs(MinAcc));
        end

        % Extract out interstorey drift results
        for k = 1:n_DRIFTEDP
            [MaxID, MinID] = PullOut_ID(n,k,Line);
            TEMP2(k,j) = max(abs(MaxID),abs(MinID));
        end

        % Close all opened output files and erase them
        fclose('all');
        dos('erase JUNK.res');
        dos('erase JUNK.wri');
    end

    %Obtain maximum acceleration and drift considering both horizontal
    %record components
    Acc(:,i) = (max(TEMP1'));
```

```
        Drift(:,i) = (max(TEMP2'))';
    end

    % Storing Acceleration Results
    for k = 1:11
        % Create matrix with IM on left hand column, and acceleration
        % values on others corresponding to each hazard level considered
        LINE = [IM(Z),Acc(k,:)/9.81];
        % Create output acceleration file
        FloorAcc = [Outputfolder,'EDPtemp_',num2str(k),'.txt'];
        % Write data to acceleartion file
        dlmwrite(FloorAcc,LINE,'-append','delimiter','',...
            'precision','%12.7f','newline','pc');
    end

    % Storing Interstorey Drift results
    for k = 1:10
        % Create matrix with IM on left hand column, and drift
        % values on others corresponding to each hazard level considered
        LINE = [IM(Z),Drift(k,:)];
        % Create output drift file
        StoreyDrift = [Outputfolder,'EDPtemp_',num2str(k+11),'.txt'];
        % Write data to drift file
        dlmwrite(StoreyDrift,LINE,'-append','delimiter','',...
            'precision','%12.7f','newline','pc');
    end
end
%-------------------------------------------------------------------------
```

B3. SAMPLE GROUND MOTION DATA FILE

The following function provides an example on specifying the ground motion ID and scale factor. To use this file, the appropriate table detailing the ground motion set of interest from Appendix A should be inserted where mentioned in the function.

```
%-------------------------------------------------------------------------
% Purpose - Obtain ground motion parameters for structural analysis using
% Ruaumoko
%-------------------------------------------------------------------------
% Inputs
% HazLevel - Hazard level of interest
%-------------------------------------------------------------------------

function [SF,FileIdent] = EQParaSA(HazLevel)

%Input
Raw = ['INSERT ID AND SF INFORMATION FROM TABLE FROM APPENDIX A HERE'];

%Obtain size of input
[M N] = size(Raw);

% Extract record IDs and scale factors for use in analyses
for i = 1:M
    FileIdent(i,1) = Raw(i,HazLevel*2-1);
```

```
    SF(i) = Raw(i,HazLevel*2);
End
%-----------------------------------------------------------------------
```

B4. SAMPLE GROUND MOTION READER FILE

The following function is used to extract ground motion record details for use in structural analyses; namely the time-step (*dT*) and number of data points (*Npt*). Note that this code assumes that the ground motion file format of interest is in PEER format.

```
%-------------------------------------------------------------------------
% Obtaining Ground Motion Record Details
%-------------------------------------------------------------------------
% Input
% Eqfile - filename (and directory if required) of ground motion file
%-------------------------------------------------------------------------

function [dT,T] = PullOut_EQ(Eqfile)

%Reading Output File
fid = fopen(Eqfile,'r');

%Discard first three lines of PEER ground motion file
tline = fgetl(fid);
tline = fgetl(fid);
tline = fgetl(fid);

%On fourth line, read timestep (dT) and number of data points (Npt)
dT = str2num(tline(1:7));
Npt = str2num(tline(8:17));

%Obtain duration of ground motion record file
T = (Npt-1)*dT;

fclose('all');
%-------------------------------------------------------------------------
```

B4. SAMPLE RUAUMOKO INPUT FILE

The following function provides an example of creating input files for structural analyses. While some comments have been added to describe the purpose of each section of the input file, details of each individual command are not provided. Users should refer to the Ruaumoko2D manual [6] for these details.

```
%-------------------------------------------------------------------------
% Matlab function to generate Ruaumoko data set to include P-delta and to
```

```
% model Takeda hysteresis models
%-------------------------------------------------------------------------
% Inputs
% My              - Yield moment capacity
% I               - Moment of inertia
% A               - Area of wall member
% As              - Shear area of wall member
% Analysisfolder - Folder where analyses is performed
% Eqfilelink      - Location and name of ground motion file
% dt              - Timestep of ground motion
% SF              - Scale factor for ground motion
% T               - Duration of ground motion
%
% Notes: Please refer to the Ruaumoko manual for full set of instructions
% on input commands
%-------------------------------------------------------------------------

function [filename] = WallInputNEWSINA2(My,I,A,As,Analysisfolder,...
    Eqfilelink,dt,SF,T)

% Create output file
filename=strcat(Analysisfolder,'test_0.txt');

% Analysis Name
line1 = ['WallRuaumoko'];
dlmwrite(filename,line1,'delimiter','','newline','pc')
% Inelastic large displacement response history analyses with 5% damping
% ratio applied to all modes (Coloumb)
line2 = [2 0 1 0 2 0 1 0 0];
dlmwrite(filename,line2,'-append', 'delimiter', ' ', 'newline', 'pc')
% Global building properties (i.e. number of nodes/elements/cross sections)
line3 = [11 10 2 10 1 10 9.81 5 5 0.001 T 1];
dlmwrite(filename,line3,'-append', 'delimiter', ' ', 'newline', 'pc')
% Output parameters (i.e. number of analysis steps to store results
line4 = [0 20 20 0 1 2 1.5 1.5 11 2 1];
dlmwrite(filename,line4,'-append', 'delimiter', ' ', 'newline', 'pc')
% Iteration and error tolerance details
line5 = [5 0 0.001 0 0 0 0 0];
dlmwrite(filename,line5,'-append','delimiter',' ','newline','pc')
dlmwrite(filename,' ','-append','newline','pc')

% Defining Node details (distances in m)
exname = 'NODES ';
line6 = [exname, '0'];
dlmwrite(filename,line6,'-append','delimiter','','newline','pc')
line7 = [1  0   0   1   1   1   0   0   0   1];
dlmwrite(filename,line7,'-append','delimiter',' ','newline','pc')
line8 = [2  0   4   0   0   0   0   0   0   1];
dlmwrite(filename,line8,'-append','delimiter',' ','newline','pc')
line8 = [3  0   7.6 0   0   0   0   0   0   1];
dlmwrite(filename,line8,'-append','delimiter',' ','newline','pc')
line8 = [4  0   11.2    0   0   0   0   0   0   1];
dlmwrite(filename,line8,'-append','delimiter',' ','newline','pc')
line8 = [5  0   14.8    0   0   0   0   0   0   1];
dlmwrite(filename,line8,'-append','delimiter',' ','newline','pc')
line8 = [6  0   18.4    0   0   0   0   0   0   1];
dlmwrite(filename,line8,'-append','delimiter',' ','newline','pc')
line8 = [7  0   22  0   0   0   0   0   0   1];
dlmwrite(filename,line8,'-append','delimiter',' ','newline','pc')
line8 = [8  0   25.6    0   0   0   0   0   0   1];
dlmwrite(filename,line8,'-append','delimiter',' ','newline','pc')
```

```
line8 = [9  0   29.2    0   0   0   0   0   0   1];
dlmwrite(filename,line8,'-append','delimiter',' ','newline','pc')
line8 = [10 0   32.8    0   0   0   0   0   0   1];
dlmwrite(filename,line8,'-append','delimiter',' ','newline','pc')
line8 = [11 0   36.4    0   0   0   0   0   0   1];
dlmwrite(filename,line8,'-append','delimiter',' ','newline','pc')
dlmwrite(filename,' ','-append','newline','pc')

% Defining interstorey drift to track
exname = 'DRIFT A';
line10 = [exname];
dlmwrite(filename,line10,'-append','delimiter','','newline','pc')
line11 = [1 2 3 4 5 6 7 8 9 10 11];
dlmwrite(filename,line11,'-append','delimiter',' ','newline','pc')
dlmwrite(filename,' ','-append','newline','pc')

% Definiting element properties
exname = 'ELEMENTS ';
line12 = [exname,'1'];
dlmwrite(filename,line12,'-append','delimiter','','newline','pc')
line13 = [1 1   1   2   0   0   1];
dlmwrite(filename,line13,'-append','delimiter',' ','newline','pc')
line13 = [2 2   2   3   0   0   1];
dlmwrite(filename,line13,'-append','delimiter',' ','newline','pc')
line13 = [3 2   3   4   0   0   1];
dlmwrite(filename,line13,'-append','delimiter',' ','newline','pc')
line13 = [4 2   4   5   0   0   1];
dlmwrite(filename,line13,'-append','delimiter',' ','newline','pc')
line13 = [5 2   5   6   0   0   1];
dlmwrite(filename,line13,'-append','delimiter',' ','newline','pc')
line13 = [6 2   6   7   0   0   1];
dlmwrite(filename,line13,'-append','delimiter',' ','newline','pc')
line13 = [7 2   7   8   0   0   1];
dlmwrite(filename,line13,'-append','delimiter',' ','newline','pc')
line13 = [8 2   8   9   0   0   1];
dlmwrite(filename,line13,'-append','delimiter',' ','newline','pc')
line13 = [9 2   9   10  0   0   1];
dlmwrite(filename,line13,'-append','delimiter',' ','newline','pc')
line13 = [10    2   10  11  0   0   1];
dlmwrite(filename,line13,'-append','delimiter',' ','newline','pc')
dlmwrite(filename,' ','-append','newline','pc')

% Defining wall properties
line15 = ['PROPS'];
dlmwrite(filename,line15,'-append','delimiter','','newline','pc')
% Define base of wall first (where inelastic action will occur)
exname1 = '1 ';
exname2 = 'FRAME ';
exname3 = 'Wall 1';
line16 = [exname1, exname2,exname3];
dlmwrite(filename,line16,'-append','delimiter','','newline','pc')
line17 = [1 0 0 8 0 0 ];
dlmwrite(filename,line17,'-append','delimiter',' ','newline','pc')
line18 = [25e6 1.31E7 A As I_Tak 0 0 0 0];
dlmwrite(filename,line18,'-append','delimiter',' ','newline','pc')
line19 = [0.02 0.02 36/3 0];
dlmwrite(filename,line19,'-append','delimiter',' ','newline','pc')
line20 = [100000000 -100000000 My -My 100000000 -100000000];
dlmwrite(filename,line20,'-append','delimiter',' ','newline','pc')
line8 = [1 1 My/3 -My/3 My/3 My/3 -My/3 My/3];
dlmwrite(filename,line8,'-append','delimiter',' ','newline','pc')
```

```
dlmwrite(filename,' ','-append','newline','pc')
% Define rest of wall (where response is expected to be elastic)
exname1 = '2 ';
exname2 = 'FRAME ';
exname3 = 'Wall 2';
line16 = [exname1, exname2,exname3];
dlmwrite(filename,line16,'-append','delimiter','','newline','pc')
line17 = [1 0 0 0 0 0 ];
dlmwrite(filename,line17,'-append','delimiter',' ','newline','pc')
line18 = [25e6 1.31E7 A As I_Tak 0 0 0 0];
dlmwrite(filename,line18,'-append','delimiter',' ','newline','pc')
dlmwrite(filename,' ','-append','newline','pc')

% Define nodal weights
exname1 = 'WEIGHTS ';
line29 = [exname1, '0'];
dlmwrite(filename,line29,'-append','delimiter','','newline','pc')
line31 = [1 0   0   0];
dlmwrite(filename,line31,'-append','delimiter',' ','newline','pc')
line31 = [2 1716.75 0   0];
dlmwrite(filename,line31,'-append','delimiter',' ','newline','pc')
line31 = [3 1716.75 0   0];
dlmwrite(filename,line31,'-append','delimiter',' ','newline','pc')
line31 = [4 1716.75 0   0];
dlmwrite(filename,line31,'-append','delimiter',' ','newline','pc')
line31 = [5 1716.75 0   0];
dlmwrite(filename,line31,'-append','delimiter',' ','newline','pc')
line31 = [6 1716.75 0   0];
dlmwrite(filename,line31,'-append','delimiter',' ','newline','pc')
line31 = [7 1716.75 0   0];
dlmwrite(filename,line31,'-append','delimiter',' ','newline','pc')
line31 = [8 1716.75 0   0];
dlmwrite(filename,line31,'-append','delimiter',' ','newline','pc')
line31 = [9 1716.75 0   0];
dlmwrite(filename,line31,'-append','delimiter',' ','newline','pc')
line31 = [10    1716.75 0   0];
dlmwrite(filename,line31,'-append','delimiter',' ','newline','pc')
line31 = [11    1716.75 0   0];
dlmwrite(filename,line31,'-append','delimiter',' ','newline','pc')
dlmwrite(filename,' ','-append','newline','pc')

% Define nodal forces
line33 = 'LOADS';
dlmwrite(filename,line33,'-append','delimiter','','newline','pc')
line34 = [1 0   0   0];
dlmwrite(filename,line34,'-append','delimiter',' ','newline','pc')
line35 = [2 0   -1716.75    0];
dlmwrite(filename,line35,'-append','delimiter',' ','newline','pc')
line35 = [3 0   -1716.75    0];
dlmwrite(filename,line35,'-append','delimiter',' ','newline','pc')
line35 = [4 0   -1716.75    0];
dlmwrite(filename,line35,'-append','delimiter',' ','newline','pc')
line35 = [5 0   -1716.75    0];
dlmwrite(filename,line35,'-append','delimiter',' ','newline','pc')
line35 = [6 0   -1716.75    0];
dlmwrite(filename,line35,'-append','delimiter',' ','newline','pc')
line35 = [7 0   -1716.75    0];
dlmwrite(filename,line35,'-append','delimiter',' ','newline','pc')
line35 = [8 0   -1716.75    0];
dlmwrite(filename,line35,'-append','delimiter',' ','newline','pc')
line35 = [9 0   -1716.75    0];
```

```
dlmwrite(filename,line35,'-append','delimiter',' ','newline','pc')
line35 = [10    0   -1716.75    0];
dlmwrite(filename,line35,'-append','delimiter',' ','newline','pc')
line35 = [11    0   -1716.75    0];
dlmwrite(filename,line35,'-append','delimiter',' ','newline','pc')
dlmwrite(filename,' ','-append','newline','pc')

% Define ground motion properties
exctname = 'EQUAKE ';
exctname2 = Eqfilelink;
line37 = [exctname, exctname2];
dlmwrite(filename,line37,'-append','delimiter','','newline', 'pc')
line38 = [6 1 dt SF -1 0.0 0.0 1.0];
dlmwrite(filename,line38,'-append','delimiter',' ','newline', 'pc')
%-------------------------------------------------------------------------
```

B5. SAMPLE DATA EXTRACTION FILE

The following function is used to extract peak total acceleration results from analyses. A similar file was also written to extract peak interstorey drifts. Note that this file would need calibration depending on the building's properties and specified outputs. For example, if the number of stories in the building is not equal to 10, then the (19+k) from the "for" loop, which identifies the line corresponding to the peak total acceleration results, needs to be modified.

```
%-------------------------------------------------------------------------
%Obtaining Peak Total Floor Acceleration from Outputs
%-------------------------------------------------------------------------
%
% Inputs
% Ruaumokooutputfile - Output file from Ruaumoko analysis
% k                  - Floor level of interest (1 = ground, 11 = roof)
% Line               - Counting number of "1" that appears in the first
%                      entry of each line to skip to the results section of
%                      interest
%-------------------------------------------------------------------------

function [Max_acc1, Max_acc2] = PullOut_Acc(Ruaumokooutputfile,k,Line);

%Opening Ruaumoko Output File
fid = fopen(Ruaumokooutputfile,'r');

%Set counter for "1" in first entry of line (cpt1) to 0
cpt1 = 0;

% Set while loop to read through results
while (1)
    % Read line
    tline = fgetl(fid);
    % If end of file reached, break
```

```
    if (~ischar(tline))
        break
    % If line is empty, move to next line
    elseif (size(tline)==0)
    % If first entry of line is '1', check of cpt1 = Line
    elseif (strcmp(tline(1),'1')==1)
        if (cpt1==Line)
            % If cpt1 = Line, read line containing result of interest
            for i=1:(19+k)
                tline=fgetl(fid);
            end
            % Extract maximum value from positive and negative direction
            Max_acc1 = str2num(tline(19:28));
            Max_acc2 = str2num(tline(51:60));
            % Exit back to main script file
            return
        else
            % Continue reading file
            cpt1=cpt1+1;
        end
    end
end
fclose('all');
```

B6. DYNAPLOT AUTOMATION CODES

Dynaplot [4] is required to extract more detailed results, such as the total floor response history. The following function file was written to perform this, where two files are created; (i) the batch file, and (ii) the input file. Note that for the latter, the output of interest is the total floor acceleration response history of all floors of the building excluding the roof. The input file thus contains the commands required to extract this data if manually inputted into Dynaplot [4]. Modifications to the input file are required to extract other results of interest.

```
%-------------------------------------------------------------------------
% Creating and running batch file for Dynaplot
%-------------------------------------------------------------------------
%
% Inputs
% OutputfileName - File name (and directory if required) of main Ruaumoko
%                  output file (not summary file)
%-------------------------------------------------------------------------

function DynaplotAuto(OutputfileName)

dos('erase junk2.wri')

% Obtain duration of analysis from summary file
Summaryfile = 'junk.wri';
fid = fopen(Summaryfile,'r');
for i = 1:50
    tline=fgetl(fid);
```

```
end
Duration = str2num(tline(26:40));

% Create batch file
Batchfilename = 'DynplotBatch.bat';
Line = ['Dynaplan junk2.wri junk INPUTCOMMAND.txt'];
dlmwrite(Batchfilename,Line,'delimiter','','newline','pc')

% Create input file
Inputcommandname = 'INPUTCOMMAND.txt';
Line = 'No';
dlmwrite(Inputcommandname,Line,'delimiter','','newline','pc')
Line = 't';
dlmwrite(Inputcommandname,Line,'-append','delimiter','','newline','pc')
Line = '10';
dlmwrite(Inputcommandname,Line,'-append','delimiter','','newline','pc')
Line = 'n';
dlmwrite(Inputcommandname,Line,'-append','delimiter','','newline','pc')
Line = '7';
dlmwrite(Inputcommandname,Line,'-append','delimiter','','newline','pc')
Line = '1 2 3 4 5 6 7 8 9 10';
dlmwrite(Inputcommandname,Line,'-append','delimiter','','newline','pc')
Line = 'T';
dlmwrite(Inputcommandname,Line,'-append','delimiter','','newline','pc')
Line = '0.0';
dlmwrite(Inputcommandname,Line,'-append','delimiter','','newline','pc')
Line = '-1 1';
dlmwrite(Inputcommandname,Line,'-append','delimiter','','newline','pc')
Line = '1.0';
dlmwrite(Inputcommandname,Line,'-append','delimiter','','newline','pc')
Line = ['0 ',num2str(ceil(Duration))];
dlmwrite(Inputcommandname,Line,'-append','delimiter','','newline','pc')
Line = '"X Acceleration"';
dlmwrite(Inputcommandname,Line,'-append','delimiter','','newline','pc')
Line = '"Nodes"';
dlmwrite(Inputcommandname,Line,'-append','delimiter','','newline','pc')
Line = 'K';
dlmwrite(Inputcommandname,Line,'-append','delimiter','','newline','pc')
Line = OutputfileName;
dlmwrite(Inputcommandname,Line,'-append','delimiter','','newline','pc')
Line = 'b';
dlmwrite(Inputcommandname,Line,'-append','delimiter','','newline','pc')

% Run batch file
dos(Batchfilename);
%-------------------------------------------------------------------------
```

B7. REFERENCES

1. Carr, A. J. (2004). Ruaumoko 2D - Inelastic dynamic analysis program. Department of Civil and Natural Resources Engineering, University of Canterbury, Christchurch.
2. The MathsWorks Inc. (2012). MATLAB v 7.14 (R2012a). Natick, MA.
3. Sadashiva, V. K. (2010). Quantifying Structural Irregularity Effects for Simple Seismic Design. PhD Thesis, University of Canterbury.
4. Carr, A. J. (2004). Dynaplot - Prost-processor program for Ruaumoko and Ruaumoko3D. Department of Civil and Natural Resources Engineering, University of Canterbury, Christchurch.
5. Chiou, B. S. J., Darragh, R., Gregor, N., & Silva, W. (2008). NGA Project Strong-Motion Database. Earthquake Spectra, 24(1), 23-44.

6. Carr, A. J. (2008). Ruaumoko Manual (Vol. Volumne 2: User Manual for the 2:Dimensional Version Ruaumoko 2D). University of Canterbury, Christchurch, NZ.

Appendix C. SLAT Automation Matlab Codes

C1. OVERVIEW

The computer program 'Seismic Loss Assessment Tool', developed by Bradley [1], was predominantly used in this thesis to perform seismic loss estimation. Due to the large number of cases considered, Matlab [2] script files and functions were written to automatically: (i) create SLAT input files, (ii) run SLAT, (iii) create input files for SLAT's post-processing programme, PostSLAT, and (iv) running PostSLAT to obtain loss results.

C2. MASTER SCRIPT

The following is the master script file used to perform the SLAT automation process as described in **Section C1**. Note here that this code is specific to the baseline building from **Chapter 3**, and that the cost details would differ for other buildings considered.

```
%-------------------------------------------------------------------------
%-------------------------------------------------------------------------
% Script file AUTOSLAT
%-------------------------------------------------------------------------
%-------------------------------------------------------------------------

% Clear workspace and command window
clear;
clc;
fclose('all')
counter = 0;

% Specify directory where files required for analyses are kept (i.e. EDP)
DataLocation = 'C:\SLATTEST\RAWWellyC\SINA_R5_T1p25\';

% Create directory for results output
SLATFOLDER = 'C:\SLATTEST\RAWWellyC\SINA_R5_T1p25\SLAT_Analyses\';
mkdir(SLATFOLDER)

% Specify input and output file names
SLATInputFile = [SLATFOLDER,'SLATRBWALL.txt'];
SLATOutputFile = [SLATFOLDER,'OUTPUT_C'];

% Specify number and cost of elements directly affected by design choice
Wall_Cost=37000;            % Cost to repair damage proportion of wall
Total_Wall_Cost=1419180;    % Cost to construct all walls in building
Num_Walls=8;                % Specify number of walls
Wall_length = 8;            % Length of wall
```

```
Num_Glazing=33;             % Specify amount of glazing (based on wall
                            % layout)
Num_Beams=4;                % Number of seismic beams in building
                            % (connecting walls together)
Total_Beam_Cost=675015;     % Cost to construct all beams in building
Total_Cost=12718717;        % Total cost of building
Glazing_Cost=Num_Glazing*131.7; % Cost of glazing

% Calculate length and cost of each individual beam
Total_Beam_Length = (30-Wall_length*Num_Walls/4);
Avg_beam_length = Total_Beam_Length/(Num_Walls/4+1);
if Avg_beam_length>3.7;
    Seismic_beam_length = (Total_Beam_Length-2*3.7)/(Num_Walls/4-1);
else
    Seismic_beam_length = Avg_beam_length;
end
Beam_Cost = Seismic_beam_length*723;  % Seismic beam cost

% Total construction cost of each element without the building. Note that
% these are based on the fragility functions implemented in the order
% specified in the SLAT manual
Cost_Output = [Total_Beam_Cost  103084.8 1416000 1082922,...
    120407 Glazing_Cost*10  1000000 2009700 112000  600000  930000,...
    2000000 207000  1000000 Total_Wall_Cost];
% Output total cost for post-processing
dlmwrite('Cost_Details.txt',Cost_Output,'delimiter',' ','newline','pc')

% Close all files open in MATLAB, and erase output files from previous
% analyses
fclose('all');
COMMAND = ['erase ',SLATInputFile,'.txt'];
dos(COMMAND);
COMMAND = ['erase ',SLATOutputFile,'.bin'];
dos(COMMAND);

% Create input files
SLATINPUTFILE_C(SLATInputFile,DataLocation,Wall_Cost,Num_Walls,...
    Num_Glazing,Beam_Cost,Num_Beams,Total_Cost)

% Running batch files
SLATBATCH(SLATInputFile,SLATOutputFile,1);
POSTSLATBATCH_NC(SLATOutputFile,SLATFOLDER,1);
%--------------------------------------------------------------------------
```

C3. SAMPLE SLAT INPUT WRITER

The following is a function file for creating a SLAT input file based on the case studies examined in **Chapter 3**. Brief comments were added to describe each section of the input file. The SLAT manual [1] should be examined if definition of the input parameters are sought. Note that fragility functions from the Performance Assessment Calculation Tool (PACT) [3] were borrowed for estimating wall member losses. As both the walls and beams

have different cross sections and length depending on the building design, the construction and repair costs for these elements were estimated using Rawlinson [4], rather than using a predefined cost function.

```
%-------------------------------------------------------------------------
%-------------------------------------------------------------------------
% SLATINPUTFILE_C(SLATInputFile,DataLocation,Wall_Cost,Num_Walls,...
% Num_Glazing,Beam_Cost,Num_Beams,Total_Cost)
%-------------------------------------------------------------------------
% Inputs
% SLATInputFile - filename and directory of slat input file
% DataLocation  - file directory where required data is stored (i.e. EDP)
% Wall_Cost     - Cost of repairing each wall
% Num_Walls     - Number of walls in building
% Num_Glazing   - Number of glazing in building
% Beam_Cost     - Cost of repairing a single beam
% Total_Cost    - Total cost of repairing builing
%-------------------------------------------------------------------------

function SLATINPUTFILE_C(SLATInputFile,DataLocation,Wall_Cost,Num_Walls,...
    Num_Glazing,Beam_Cost,Num_Beams,Total_Cost)

% Section 1 - defining SLAT analysis details
line = '10 storey wall 2D structure - direct losses only';
dlmwrite(SLATInputFile,line,'delimiter','','newline','pc')
line = '    1   21    4  133    0   23    0';
dlmwrite(SLATInputFile,line,'-append','delimiter','','newline','pc')
line = '    1    0    1    0';
dlmwrite(SLATInputFile,line,'-append','delimiter','','newline','pc')
line = '    0    0    0    0    0';
dlmwrite(SLATInputFile,line,'-append','delimiter','','newline','pc')
line = '    1    0     0.005      0.01       300        10';
dlmwrite(SLATInputFile,line,'-append','delimiter','','newline','pc')
line = '    1    1    1    1';
dlmwrite(SLATInputFile,line,'-append','delimiter','','newline','pc')
line = '    1    1    1    1    1    0';
dlmwrite(SLATInputFile,line,'-append','delimiter','','newline','pc')
dlmwrite(SLATInputFile,' ','-append','delimiter','','newline','pc')

% Section 2 - Specify intensity measure details
line = 'INTENSITY';
dlmwrite(SLATInputFile,line,'-append','delimiter','','newline','pc')
line = '    1    0';
dlmwrite(SLATInputFile,line,'-append','delimiter','','newline','pc')
line = '    1    1';
dlmwrite(SLATInputFile,line,'-append','delimiter','','newline','pc')
dlmwrite(SLATInputFile,' ','-append','delimiter','','newline','pc')

% Section 3 - Specify EDP details
line = 'DEMAND';
dlmwrite(SLATInputFile,line,'-append','delimiter','','newline','pc')
line = '    2    0    0';
dlmwrite(SLATInputFile,line,'-append','delimiter','','newline','pc')
line = '    1    1    2    0';
dlmwrite(SLATInputFile,line,'-append','delimiter','','newline','pc')
line = '    2    1    3    0';
dlmwrite(SLATInputFile,line,'-append','delimiter','','newline','pc')
```

```
line = '    3    1    4    0';
dlmwrite(SLATInputFile,line,'-append','delimiter','','newline','pc')
line = '    4    1    5    0';
dlmwrite(SLATInputFile,line,'-append','delimiter','','newline','pc')
line = '    5    1    6    0';
dlmwrite(SLATInputFile,line,'-append','delimiter','','newline','pc')
line = '    6    1    7    0';
dlmwrite(SLATInputFile,line,'-append','delimiter','','newline','pc')
line = '    7    1    8    0';
dlmwrite(SLATInputFile,line,'-append','delimiter','','newline','pc')
line = '    8    1    9    0';
dlmwrite(SLATInputFile,line,'-append','delimiter','','newline','pc')
line = '    9    1   10    0';
dlmwrite(SLATInputFile,line,'-append','delimiter','','newline','pc')
line = '   10    1   11    0';
dlmwrite(SLATInputFile,line,'-append','delimiter','','newline','pc')
line = '   11    1   12    0';
dlmwrite(SLATInputFile,line,'-append','delimiter','','newline','pc')
line = '   12    1   13    0';
dlmwrite(SLATInputFile,line,'-append','delimiter','','newline','pc')
line = '   13    1   14    0';
dlmwrite(SLATInputFile,line,'-append','delimiter','','newline','pc')
line = '   14    1   15    0';
dlmwrite(SLATInputFile,line,'-append','delimiter','','newline','pc')
line = '   15    1   16    0';
dlmwrite(SLATInputFile,line,'-append','delimiter','','newline','pc')
line = '   16    1   17    0';
dlmwrite(SLATInputFile,line,'-append','delimiter','','newline','pc')
line = '   17    1   18    0';
dlmwrite(SLATInputFile,line,'-append','delimiter','','newline','pc')
line = '   18    1   19    0';
dlmwrite(SLATInputFile,line,'-append','delimiter','','newline','pc')
line = '   19    1   20    0';
dlmwrite(SLATInputFile,line,'-append','delimiter','','newline','pc')
line = '   20    1   21    0';
dlmwrite(SLATInputFile,line,'-append','delimiter','','newline','pc')
line = '   21    1   22    0';
dlmwrite(SLATInputFile,line,'-append','delimiter','','newline','pc')
dlmwrite(SLATInputFile,' ','-append','delimiter','','newline','pc')

% Section 4 - Specify fragility and cost functions for analyses
line = 'FRAGILITY';
dlmwrite(SLATInputFile,line,'-append','delimiter','','newline','pc')
line = '   -1    4';  % SEISMIC BEAMS
dlmwrite(SLATInputFile,line,'-append','delimiter','','newline','pc')
line = '     0.005       0.4';
dlmwrite(SLATInputFile,line,'-append','delimiter','','newline','pc')
line = '     0.01       0.45';
dlmwrite(SLATInputFile,line,'-append','delimiter','','newline','pc')
line = '     0.03        0.5';
dlmwrite(SLATInputFile,line,'-append','delimiter','','newline','pc')
line = '     0.06        0.6';
dlmwrite(SLATInputFile,line,'-append','delimiter','','newline','pc')
if 1035/4435*Beam_Cost<1000
    line = ['      ',num2str(ceil(1035/4435*Beam_Cost)),'.      ',...
        num2str(ceil(1035/4435*Beam_Cost)),'.    1  100       0.5'];
else
    line = ['     ',num2str(ceil(1035/4435*Beam_Cost)),'.     ',...
        num2str(ceil(1035/4435*Beam_Cost)),'.    1  100       0.5'];
end
dlmwrite(SLATInputFile,line,'-append','delimiter','','newline','pc')
```

```
if 2909/4435*Beam_Cost<1000
    line = ['      ',num2str(ceil(2909/4435*Beam_Cost)),'.      ',...
        num2str(ceil(2909/4435*Beam_Cost)),'.    1  100       0.5'];
else
    line = ['     ',num2str(ceil(2909/4435*Beam_Cost)),'.     ',...
        num2str(ceil(2909/4435*Beam_Cost)),'.    1  100       0.5'];
end
dlmwrite(SLATInputFile,line,'-append','delimiter','','newline','pc')
for i = 1:2
    if Beam_Cost<1000
        line = ['      ',num2str(ceil(Beam_Cost)),'.      ',...
            num2str(ceil(Beam_Cost)),'.    1  100       0.5'];
    else
    line = ['     ',num2str(ceil(Beam_Cost)),'.     ',...
        num2str(ceil(Beam_Cost)),'.    1  100       0.5'];
    end
    dlmwrite(SLATInputFile,line,'-append','delimiter','','newline','pc')
end
line = '   -2    4';   % GRAVITY COLUMNS
dlmwrite(SLATInputFile,line,'-append','delimiter','','newline','pc')
line = '     0.005       0.4';
dlmwrite(SLATInputFile,line,'-append','delimiter','','newline','pc')
line = '     0.01       0.45';
dlmwrite(SLATInputFile,line,'-append','delimiter','','newline','pc')
line = '     0.03        0.5';
dlmwrite(SLATInputFile,line,'-append','delimiter','','newline','pc')
line = '     0.06        0.6';
dlmwrite(SLATInputFile,line,'-append','delimiter','','newline','pc')
line = '     1966.     1966.    1  100       0.5';
dlmwrite(SLATInputFile,line,'-append','delimiter','','newline','pc')
line = '     5529.     5529.    1  100       0.5';
dlmwrite(SLATInputFile,line,'-append','delimiter','','newline','pc')
line = '     8427.     8427.    1  100       0.5';
dlmwrite(SLATInputFile,line,'-append','delimiter','','newline','pc')
line = '     8427.     8427.    1  100       0.5';
dlmwrite(SLATInputFile,line,'-append','delimiter','','newline','pc')
line = '   -3    4';  % GRAVITY BEAMS
dlmwrite(SLATInputFile,line,'-append','delimiter','','newline','pc')
line = '     0.005       0.4';
dlmwrite(SLATInputFile,line,'-append','delimiter','','newline','pc')
line = '     0.01       0.45';
dlmwrite(SLATInputFile,line,'-append','delimiter','','newline','pc')
line = '     0.03        0.5';
dlmwrite(SLATInputFile,line,'-append','delimiter','','newline','pc')
line = '     0.06        0.6';
dlmwrite(SLATInputFile,line,'-append','delimiter','','newline','pc')
line = '     1113.     1113.    1  100       0.5';
dlmwrite(SLATInputFile,line,'-append','delimiter','','newline','pc')
line = '     3128.     3128.    1  100       0.5';
dlmwrite(SLATInputFile,line,'-append','delimiter','','newline','pc')
line = '     4768.     4768.    1  100       0.5';
dlmwrite(SLATInputFile,line,'-append','delimiter','','newline','pc')
line = '     4768.     4768.    1  100       0.5';
dlmwrite(SLATInputFile,line,'-append','delimiter','','newline','pc')
line = '   -4    3';  % STRUCTURAL WALLS
dlmwrite(SLATInputFile,line,'-append','delimiter','','newline','pc')
line = '    0.0084       0.5';
dlmwrite(SLATInputFile,line,'-append','delimiter','','newline','pc')
line = '     0.012      0.54';
dlmwrite(SLATInputFile,line,'-append','delimiter','','newline','pc')
line = '     0.019       0.5';
```

```
dlmwrite(SLATInputFile,line,'-append','delimiter','','newline','pc')
if 0.174*Wall_Cost<1000
    line = ['      ',num2str(round(0.174*Wall_Cost)),'.      ',...
        num2str(round(0.174*Wall_Cost)),'.    1  100       0.131'];
elseif 0.174*Wall_Cost<10000
    line = ['     ',num2str(round(0.174*Wall_Cost)),'.     ',...
        num2str(round(0.174*Wall_Cost)),'.    1  100       0.131'];
elseif 0.174*Wall_Cost<100000
    line = ['    ',num2str(round(0.174*Wall_Cost)),'.    ',...
        num2str(round(0.174*Wall_Cost)),'.    1  100       0.131'];
else
    line = ['   ',num2str(round(0.174*Wall_Cost)),'.   ',...
        num2str(round(0.174*Wall_Cost)),'.    1  100       0.131'];
end
dlmwrite(SLATInputFile,line,'-append','delimiter','','newline','pc')
if 0.639*Wall_Cost<1000
    line = ['      ',num2str(round(0.639*Wall_Cost)),'.      ',...
        num2str(round(0.639*Wall_Cost)),'.    1  100       0.131'];
elseif 0.639*Wall_Cost<10000
    line = ['     ',num2str(round(0.639*Wall_Cost)),'.     ',...
        num2str(round(0.639*Wall_Cost)),'.    1  100       0.131'];
elseif 0.639*Wall_Cost<100000
    line = ['    ',num2str(round(0.639*Wall_Cost)),'.    ',...
        num2str(round(0.639*Wall_Cost)),'.    1  100       0.131'];
else
    line = ['   ',num2str(round(0.639*Wall_Cost)),'.   ',...
        num2str(round(0.639*Wall_Cost)),'.    1  100       0.131'];
end
dlmwrite(SLATInputFile,line,'-append','delimiter','','newline','pc')
if Wall_Cost<10000
    line = ['     ',num2str(round(Wall_Cost)),'.     ',...
        num2str(round(Wall_Cost)),'.    1  100       0.131'];
elseif Wall_Cost<100000
    line = ['    ',num2str(round(Wall_Cost)),'.    ',...
        num2str(round(Wall_Cost)),'.    1  100       0.131'];
else
    line = ['   ',num2str(round(Wall_Cost)),'.   ',...
        num2str(round(Wall_Cost)),'.    1  100       0.131'];
end
dlmwrite(SLATInputFile,line,'-append','delimiter','','newline','pc')
dlmwrite(SLATInputFile,' ','-append','delimiter','','newline','pc')

% Section 5 - Define performance group
line = 'PGROUP             ! PG_num FRAG_type PG_EDP q_pg';
dlmwrite(SLATInputFile,line,'-append','delimiter','','newline','pc')
for i = 1:10
    if i<10
        line = ['    ',num2str(i),'   -1   ',num2str(11+i),'    ',...
            num2str(Num_Beams),'       0.05                !seimsic beams -
floor ',num2str(i)];
        dlmwrite(SLATInputFile,line,'-append','delimiter','',...
            'newline','pc')
    else
        line = ['   ',num2str(i),'   -1   ',num2str(11+i),'    ',...
            num2str(Num_Beams),'       0.05                !seimsic beams -
floor ',num2str(i)];
        dlmwrite(SLATInputFile,line,'-append','delimiter','',...
            'newline','pc')
    end
end
line = '   11   -2   12    4       0.05                !gravity columns';
```

```
dlmwrite(SLATInputFile,line,'-append','delimiter','','newline','pc')
line = '   12   -2   13    4       0.05                 ';
dlmwrite(SLATInputFile,line,'-append','delimiter','','newline','pc')
line = '   13   -2   14    4       0.05                 ';
dlmwrite(SLATInputFile,line,'-append','delimiter','','newline','pc')
line = '   14   -2   15    4       0.05                 ';
dlmwrite(SLATInputFile,line,'-append','delimiter','','newline','pc')
line = '   15   -2   16    4       0.05                 ';
dlmwrite(SLATInputFile,line,'-append','delimiter','','newline','pc')
line = '   16   -2   17    4       0.05                 ';
dlmwrite(SLATInputFile,line,'-append','delimiter','','newline','pc')
line = '   17   -2   18    4       0.05                 ';
dlmwrite(SLATInputFile,line,'-append','delimiter','','newline','pc')
line = '   18   -2   19    4       0.05                 ';
dlmwrite(SLATInputFile,line,'-append','delimiter','','newline','pc')
line = '   19   -2   20    4       0.05                 ';
dlmwrite(SLATInputFile,line,'-append','delimiter','','newline','pc')
line = '   20   -2   21    4       0.05                 ';
dlmwrite(SLATInputFile,line,'-append','delimiter','','newline','pc')
line = '   21   -3   12    2       0.05                 !gravtiy beam';
dlmwrite(SLATInputFile,line,'-append','delimiter','','newline','pc')
line = '   22   -3   13    2       0.05                 ';
dlmwrite(SLATInputFile,line,'-append','delimiter','','newline','pc')
line = '   23   -3   14    2       0.05                 ';
dlmwrite(SLATInputFile,line,'-append','delimiter','','newline','pc')
line = '   24   -3   15    2       0.05                 ';
dlmwrite(SLATInputFile,line,'-append','delimiter','','newline','pc')
line = '   25   -3   16    2       0.05                 ';
dlmwrite(SLATInputFile,line,'-append','delimiter','','newline','pc')
line = '   26   -3   17    2       0.05                 ';
dlmwrite(SLATInputFile,line,'-append','delimiter','','newline','pc')
line = '   27   -3   18    2       0.05                 ';
dlmwrite(SLATInputFile,line,'-append','delimiter','','newline','pc')
line = '   28   -3   19    2       0.05                 ';
dlmwrite(SLATInputFile,line,'-append','delimiter','','newline','pc')
line = '   29   -3   20    2       0.05                 ';
dlmwrite(SLATInputFile,line,'-append','delimiter','','newline','pc')
line = '   30   -3   21    2       0.05                 ';
dlmwrite(SLATInputFile,line,'-append','delimiter','','newline','pc')
line = '   31    3   12   24                            !slab-column';
dlmwrite(SLATInputFile,line,'-append','delimiter','','newline','pc')
line = '   32    3   13   24                            ';
dlmwrite(SLATInputFile,line,'-append','delimiter','','newline','pc')
line = '   33    3   14   24                            ';
dlmwrite(SLATInputFile,line,'-append','delimiter','','newline','pc')
line = '   34    3   15   24                            ';
dlmwrite(SLATInputFile,line,'-append','delimiter','','newline','pc')
line = '   35    3   16   24                            ';
dlmwrite(SLATInputFile,line,'-append','delimiter','','newline','pc')
line = '   36    3   17   24                            ';
dlmwrite(SLATInputFile,line,'-append','delimiter','','newline','pc')
line = '   37    3   18   24                            ';
dlmwrite(SLATInputFile,line,'-append','delimiter','','newline','pc')
line = '   38    3   19   24                            ';
dlmwrite(SLATInputFile,line,'-append','delimiter','','newline','pc')
line = '   39    3   20   24                            ';
dlmwrite(SLATInputFile,line,'-append','delimiter','','newline','pc')
line = '   40    3   21   24                            ';
dlmwrite(SLATInputFile,line,'-append','delimiter','','newline','pc')
line = '   41  105   12  721                            !drywall partition';
dlmwrite(SLATInputFile,line,'-append','delimiter','','newline','pc')
```

```
line = '   42  105   13  721                          ';
dlmwrite(SLATInputFile,line,'-append','delimiter','','newline','pc')
line = '   43  105   14  721                          ';
dlmwrite(SLATInputFile,line,'-append','delimiter','','newline','pc')
line = '   44  105   15  721                          ';
dlmwrite(SLATInputFile,line,'-append','delimiter','','newline','pc')
line = '   45  105   16  721                          ';
dlmwrite(SLATInputFile,line,'-append','delimiter','','newline','pc')
line = '   46  105   17  721                          ';
dlmwrite(SLATInputFile,line,'-append','delimiter','','newline','pc')
line = '   47  105   18  721                          ';
dlmwrite(SLATInputFile,line,'-append','delimiter','','newline','pc')
line = '   48  105   19  721                          ';
dlmwrite(SLATInputFile,line,'-append','delimiter','','newline','pc')
line = '   49  105   20  721                          ';
dlmwrite(SLATInputFile,line,'-append','delimiter','','newline','pc')
line = '   50  105   21  721                          ';
dlmwrite(SLATInputFile,line,'-append','delimiter','','newline','pc')
line = '   51  106   12  721                          !drywall paint';
dlmwrite(SLATInputFile,line,'-append','delimiter','','newline','pc')
line = '   52  106   13  721                          ';
dlmwrite(SLATInputFile,line,'-append','delimiter','','newline','pc')
line = '   53  106   14  721                          ';
dlmwrite(SLATInputFile,line,'-append','delimiter','','newline','pc')
line = '   54  106   15  721                          ';
dlmwrite(SLATInputFile,line,'-append','delimiter','','newline','pc')
line = '   55  106   16  721                          ';
dlmwrite(SLATInputFile,line,'-append','delimiter','','newline','pc')
line = '   56  106   17  721                          ';
dlmwrite(SLATInputFile,line,'-append','delimiter','','newline','pc')
line = '   57  106   18  721                          ';
dlmwrite(SLATInputFile,line,'-append','delimiter','','newline','pc')
line = '   58  106   19  721                          ';
dlmwrite(SLATInputFile,line,'-append','delimiter','','newline','pc')
line = '   59  106   20  721                          ';
dlmwrite(SLATInputFile,line,'-append','delimiter','','newline','pc')
line = '   60  106   21  721                          ';
dlmwrite(SLATInputFile,line,'-append','delimiter','','newline','pc')
line = ['   61  107   12   ',num2str(Num_Glazing),...
    '                        !exterior glazing'];
dlmwrite(SLATInputFile,line,'-append','delimiter','','newline','pc')
line = ['   62  107   13   ',num2str(Num_Glazing),'                      '];
dlmwrite(SLATInputFile,line,'-append','delimiter','','newline','pc')
line = ['   63  107   14   ',num2str(Num_Glazing),'                      '];
dlmwrite(SLATInputFile,line,'-append','delimiter','','newline','pc')
line = ['   64  107   15   ',num2str(Num_Glazing),'                      '];
dlmwrite(SLATInputFile,line,'-append','delimiter','','newline','pc')
line = ['   65  107   16   ',num2str(Num_Glazing),'                      '];
dlmwrite(SLATInputFile,line,'-append','delimiter','','newline','pc')
line = ['   66  107   17   ',num2str(Num_Glazing),'                      '];
dlmwrite(SLATInputFile,line,'-append','delimiter','','newline','pc')
line = ['   67  107   18   ',num2str(Num_Glazing),'                      '];
dlmwrite(SLATInputFile,line,'-append','delimiter','','newline','pc')
line = ['   68  107   19   ',num2str(Num_Glazing),'                      '];
dlmwrite(SLATInputFile,line,'-append','delimiter','','newline','pc')
line = ['   69  107   20   ',num2str(Num_Glazing),'                      '];
dlmwrite(SLATInputFile,line,'-append','delimiter','','newline','pc')
line = ['   70  107   21   ',num2str(Num_Glazing),'                      '];
dlmwrite(SLATInputFile,line,'-append','delimiter','','newline','pc')
line = '   71  108   12   10                          !generic drift';
dlmwrite(SLATInputFile,line,'-append','delimiter','','newline','pc')
```

```
line = '   72  108   13   10                          ';
dlmwrite(SLATInputFile,line,'-append','delimiter','','newline','pc')
line = '   73  108   14   10                          ';
dlmwrite(SLATInputFile,line,'-append','delimiter','','newline','pc')
line = '   74  108   15   10                          ';
dlmwrite(SLATInputFile,line,'-append','delimiter','','newline','pc')
line = '   75  108   16   10                          ';
dlmwrite(SLATInputFile,line,'-append','delimiter','','newline','pc')
line = '   76  108   17   10                          ';
dlmwrite(SLATInputFile,line,'-append','delimiter','','newline','pc')
line = '   77  108   18   10                          ';
dlmwrite(SLATInputFile,line,'-append','delimiter','','newline','pc')
line = '   78  108   19   10                          ';
dlmwrite(SLATInputFile,line,'-append','delimiter','','newline','pc')
line = '   79  108   20   10                          ';
dlmwrite(SLATInputFile,line,'-append','delimiter','','newline','pc')
line = '   80  108   21   10                          ';
dlmwrite(SLATInputFile,line,'-append','delimiter','','newline','pc')
line = '   81  203    2  693                          !acoustical ceiling';
dlmwrite(SLATInputFile,line,'-append','delimiter','','newline','pc')
line = '   82  203    3  693                          ';
dlmwrite(SLATInputFile,line,'-append','delimiter','','newline','pc')
line = '   83  203    4  693                          ';
dlmwrite(SLATInputFile,line,'-append','delimiter','','newline','pc')
line = '   84  203    5  693                          ';
dlmwrite(SLATInputFile,line,'-append','delimiter','','newline','pc')
line = '   85  203    6  693                          ';
dlmwrite(SLATInputFile,line,'-append','delimiter','','newline','pc')
line = '   86  203    7  693                          ';
dlmwrite(SLATInputFile,line,'-append','delimiter','','newline','pc')
line = '   87  203    8  693                          ';
dlmwrite(SLATInputFile,line,'-append','delimiter','','newline','pc')
line = '   88  203    9  693                          ';
dlmwrite(SLATInputFile,line,'-append','delimiter','','newline','pc')
line = '   89  203   10  693                          ';
dlmwrite(SLATInputFile,line,'-append','delimiter','','newline','pc')
line = '   90  203   11  693                          ';
dlmwrite(SLATInputFile,line,'-append','delimiter','','newline','pc')
line = '   91  204    1    2                          !Hydraulic elevator';
dlmwrite(SLATInputFile,line,'-append','delimiter','','newline','pc')
line = '   92  205   11    4                          !roof equipment';
dlmwrite(SLATInputFile,line,'-append','delimiter','','newline','pc')
line = '   93  208    1   53                          !computers';
dlmwrite(SLATInputFile,line,'-append','delimiter','','newline','pc')
line = '   94  208    2   53                          ';
dlmwrite(SLATInputFile,line,'-append','delimiter','','newline','pc')
line = '   95  208    3   53                          ';
dlmwrite(SLATInputFile,line,'-append','delimiter','','newline','pc')
line = '   96  208    4   53                          ';
dlmwrite(SLATInputFile,line,'-append','delimiter','','newline','pc')
line = '   97  208    5   53                          ';
dlmwrite(SLATInputFile,line,'-append','delimiter','','newline','pc')
line = '   98  208    6   53                          ';
dlmwrite(SLATInputFile,line,'-append','delimiter','','newline','pc')
line = '   99  208    7   53                          ';
dlmwrite(SLATInputFile,line,'-append','delimiter','','newline','pc')
line = '  100  208    8   53                          !';
dlmwrite(SLATInputFile,line,'-append','delimiter','','newline','pc')
line = '  101  208    9   53                          ';
dlmwrite(SLATInputFile,line,'-append','delimiter','','newline','pc')
line = '  102  208   10   53                          ';
```

```
dlmwrite(SLATInputFile,line,'-append','delimiter','','newline','pc')
line = '  103  209    1    5                          !server equipment';
dlmwrite(SLATInputFile,line,'-append','delimiter','','newline','pc')
line = '  104  209    2    5                          ';
dlmwrite(SLATInputFile,line,'-append','delimiter','','newline','pc')
line = '  105  209    3    5                          ';
dlmwrite(SLATInputFile,line,'-append','delimiter','','newline','pc')
line = '  106  209    4    5                          ';
dlmwrite(SLATInputFile,line,'-append','delimiter','','newline','pc')
line = '  107  209    5    5                          ';
dlmwrite(SLATInputFile,line,'-append','delimiter','','newline','pc')
line = '  108  209    6    5                          ';
dlmwrite(SLATInputFile,line,'-append','delimiter','','newline','pc')
line = '  109  209    7    5                          ';
dlmwrite(SLATInputFile,line,'-append','delimiter','','newline','pc')
line = '  110  209    8    5                          ';
dlmwrite(SLATInputFile,line,'-append','delimiter','','newline','pc')
line = '  111  209    9    5                          ';
dlmwrite(SLATInputFile,line,'-append','delimiter','','newline','pc')
line = '  112  209   10    5                          ';
dlmwrite(SLATInputFile,line,'-append','delimiter','','newline','pc')
line = '  113  211    2   23                          !auto sprinkler';
dlmwrite(SLATInputFile,line,'-append','delimiter','','newline','pc')
line = '  114  211    3   23                          ';
dlmwrite(SLATInputFile,line,'-append','delimiter','','newline','pc')
line = '  115  211    4   23                          ';
dlmwrite(SLATInputFile,line,'-append','delimiter','','newline','pc')
line = '  116  211    5   23                          ';
dlmwrite(SLATInputFile,line,'-append','delimiter','','newline','pc')
line = '  117  211    6   23                          ';
dlmwrite(SLATInputFile,line,'-append','delimiter','','newline','pc')
line = '  118  211    7   23                          ';
dlmwrite(SLATInputFile,line,'-append','delimiter','','newline','pc')
line = '  119  211    8   23                          ';
dlmwrite(SLATInputFile,line,'-append','delimiter','','newline','pc')
line = '  120  211    9   23                          ';
dlmwrite(SLATInputFile,line,'-append','delimiter','','newline','pc')
line = '  121  211   10   23                          ';
dlmwrite(SLATInputFile,line,'-append','delimiter','','newline','pc')
line = '  122  211   11   23                          ';
dlmwrite(SLATInputFile,line,'-append','delimiter','','newline','pc')
line = '  123  214    1   10                          !generic acc';
dlmwrite(SLATInputFile,line,'-append','delimiter','','newline','pc')
line = '  124  214    2   10                          ';
dlmwrite(SLATInputFile,line,'-append','delimiter','','newline','pc')
line = '  125  214    3   10                          ';
dlmwrite(SLATInputFile,line,'-append','delimiter','','newline','pc')
line = '  126  214    4   10                          ';
dlmwrite(SLATInputFile,line,'-append','delimiter','','newline','pc')
line = '  127  214    5   10                          ';
dlmwrite(SLATInputFile,line,'-append','delimiter','','newline','pc')
line = '  128  214    6   10                          ';
dlmwrite(SLATInputFile,line,'-append','delimiter','','newline','pc')
line = '  129  214    7   10                          ';
dlmwrite(SLATInputFile,line,'-append','delimiter','','newline','pc')
line = '  130  214    8   10                          ';
dlmwrite(SLATInputFile,line,'-append','delimiter','','newline','pc')
line = '  131  214    9   10                          ';
dlmwrite(SLATInputFile,line,'-append','delimiter','','newline','pc')
line = '  132  214   10   10                          ';
dlmwrite(SLATInputFile,line,'-append','delimiter','','newline','pc')
```

```
line = ['  133   -4   12    ',num2str(Num_Walls),...
        '                          !Wall (bottom 2 floors)'];
dlmwrite(SLATInputFile,line,'-append','delimiter','','newline','pc')
dlmwrite(SLATInputFile,' ','-append','delimiter','','newline','pc')

% Section 6 - Collapse-IM details specification
line = 'COLLAPSE';
dlmwrite(SLATInputFile,line,'-append','delimiter','','newline','pc')
line = '    0    1';
dlmwrite(SLATInputFile,line,'-append','delimiter','','newline','pc')
line = '    1   23';
dlmwrite(SLATInputFile,line,'-append','delimiter','','newline','pc')
line = '    0       0.0      0.00';
dlmwrite(SLATInputFile,line,'-append','delimiter','','newline','pc')
line = [' ',num2str(round(Total_Cost/1e4)/100),'e+06      0.35      0.35
0.0'];
dlmwrite(SLATInputFile,line,'-append','delimiter','','newline','pc')
dlmwrite(SLATInputFile,' ','-append','delimiter','','newline','pc')

% Section 7 - Detailing all the input data files
line = 'DATA';
dlmwrite(SLATInputFile,line,'-append','delimiter','','newline','pc')
line = ['    1     ',DataLocation,'IMrate_data.txt'];
dlmwrite(SLATInputFile,line,'-append','delimiter','','newline','pc')
line = ['    2     ',DataLocation,'EDPv2_1.txt'];
dlmwrite(SLATInputFile,line,'-append','delimiter','','newline','pc')
line = ['    3     ',DataLocation,'EDPv2_2.txt'];
dlmwrite(SLATInputFile,line,'-append','delimiter','','newline','pc')
line = ['    4     ',DataLocation,'EDPv2_3.txt'];
dlmwrite(SLATInputFile,line,'-append','delimiter','','newline','pc')
line = ['    5     ',DataLocation,'EDPv2_4.txt'];
dlmwrite(SLATInputFile,line,'-append','delimiter','','newline','pc')
line = ['    6     ',DataLocation,'EDPv2_5.txt'];
dlmwrite(SLATInputFile,line,'-append','delimiter','','newline','pc')
line = ['    7     ',DataLocation,'EDPv2_6.txt'];
dlmwrite(SLATInputFile,line,'-append','delimiter','','newline','pc')
line = ['    8     ',DataLocation,'EDPv2_7.txt'];
dlmwrite(SLATInputFile,line,'-append','delimiter','','newline','pc')
line = ['    9     ',DataLocation,'EDPv2_8.txt'];
dlmwrite(SLATInputFile,line,'-append','delimiter','','newline','pc')
line = ['   10     ',DataLocation,'EDPv2_9.txt'];
dlmwrite(SLATInputFile,line,'-append','delimiter','','newline','pc')
line = ['   11     ',DataLocation,'EDPv2_10.txt'];
dlmwrite(SLATInputFile,line,'-append','delimiter','','newline','pc')
line = ['   12     ',DataLocation,'EDPv2_11.txt'];
dlmwrite(SLATInputFile,line,'-append','delimiter','','newline','pc')
line = ['   13     ',DataLocation,'EDPv2_12.txt'];
dlmwrite(SLATInputFile,line,'-append','delimiter','','newline','pc')
line = ['   14     ',DataLocation,'EDPv2_13.txt'];
dlmwrite(SLATInputFile,line,'-append','delimiter','','newline','pc')
line = ['   15     ',DataLocation,'EDPv2_14.txt'];
dlmwrite(SLATInputFile,line,'-append','delimiter','','newline','pc')
line = ['   16     ',DataLocation,'EDPv2_15.txt'];
dlmwrite(SLATInputFile,line,'-append','delimiter','','newline','pc')
line = ['   17     ',DataLocation,'EDPv2_16.txt'];
dlmwrite(SLATInputFile,line,'-append','delimiter','','newline','pc')
line = ['   18     ',DataLocation,'EDPv2_17.txt'];
dlmwrite(SLATInputFile,line,'-append','delimiter','','newline','pc')
line = ['   19     ',DataLocation,'EDPv2_18.txt'];
dlmwrite(SLATInputFile,line,'-append','delimiter','','newline','pc')
line = ['   20     ',DataLocation,'EDPv2_19.txt'];
```

```
dlmwrite(SLATInputFile,line,'-append','delimiter','','newline','pc')
line = ['   21     ',DataLocation,'EDPv2_20.txt'];
dlmwrite(SLATInputFile,line,'-append','delimiter','','newline','pc')
line = ['   22     ',DataLocation,'EDPv2_21.txt'];
dlmwrite(SLATInputFile,line,'-append','delimiter','','newline','pc')
line = ['   23     ',DataLocation,'CollapseIMdata.txt'];
dlmwrite(SLATInputFile,line,'-append','delimiter','','newline','pc')
dlmwrite(SLATInputFile,' ','-append','delimiter','','newline','pc')

% Section 8 - Specify all the output data files
line = 'OUTPUT';
dlmwrite(SLATInputFile,line,'-append','delimiter','','newline','pc')
line = '    1   21    1    0';
dlmwrite(SLATInputFile,line,'-append','delimiter','','newline','pc')
line = 'OUTPUTIM';
dlmwrite(SLATInputFile,line,'-append','delimiter','','newline','pc')
line = '    1  100      0.01       1.0';
dlmwrite(SLATInputFile,line,'-append','delimiter','','newline','pc')
line = 'OUTPUTEDP';
dlmwrite(SLATInputFile,line,'-append','delimiter','','newline','pc')
line = '    1  100      0.01       2.0';
dlmwrite(SLATInputFile,line,'-append','delimiter','','newline','pc')
line = '    2  100      0.01       2.0';
dlmwrite(SLATInputFile,line,'-append','delimiter','','newline','pc')
line = '    3  100      0.01       2.0';
dlmwrite(SLATInputFile,line,'-append','delimiter','','newline','pc')
line = '    4  100      0.01       2.0';
dlmwrite(SLATInputFile,line,'-append','delimiter','','newline','pc')
line = '    5  100      0.01       2.0';
dlmwrite(SLATInputFile,line,'-append','delimiter','','newline','pc')
line = '    6  100      0.01       2.0';
dlmwrite(SLATInputFile,line,'-append','delimiter','','newline','pc')
line = '    7  100      0.01       2.0';
dlmwrite(SLATInputFile,line,'-append','delimiter','','newline','pc')
line = '    8  100      0.01       2.0';
dlmwrite(SLATInputFile,line,'-append','delimiter','','newline','pc')
line = '    9  100      0.01       2.0';
dlmwrite(SLATInputFile,line,'-append','delimiter','','newline','pc')
line = '   10  100      0.01       2.0';
dlmwrite(SLATInputFile,line,'-append','delimiter','','newline','pc')
line = '   11  100      0.01       2.0';
dlmwrite(SLATInputFile,line,'-append','delimiter','','newline','pc')
line = '   12  100    0.0001     0.025';
dlmwrite(SLATInputFile,line,'-append','delimiter','','newline','pc')
line = '   13  100    0.0001     0.025';
dlmwrite(SLATInputFile,line,'-append','delimiter','','newline','pc')
line = '   14  100    0.0001     0.025';
dlmwrite(SLATInputFile,line,'-append','delimiter','','newline','pc')
line = '   15  100    0.0001     0.025';
dlmwrite(SLATInputFile,line,'-append','delimiter','','newline','pc')
line = '   16  100    0.0001     0.025';
dlmwrite(SLATInputFile,line,'-append','delimiter','','newline','pc')
line = '   17  100    0.0001     0.025';
dlmwrite(SLATInputFile,line,'-append','delimiter','','newline','pc')
line = '   18  100    0.0001     0.025';
dlmwrite(SLATInputFile,line,'-append','delimiter','','newline','pc')
line = '   19  100    0.0001     0.025';
dlmwrite(SLATInputFile,line,'-append','delimiter','','newline','pc')
line = '   20  100    0.0001     0.025';
dlmwrite(SLATInputFile,line,'-append','delimiter','','newline','pc')
line = '   21  100    0.0001     0.025';
```

```
dlmwrite(SLATInputFile,line,'-append','delimiter','','newline','pc')
line = 'OUTPUTLOSS';
dlmwrite(SLATInputFile,line,'-append','delimiter','','newline','pc')
line = '    1  100     100.0    15.0e6';
dlmwrite(SLATInputFile,line,'-append','delimiter','','newline','pc')
%--------------------------------------------------------------------------
```

C4. SAMPLE SLAT BATCH COMMAND

The following function creates a batch file in order to run the SLAT analyses. This code can be immediately applied to other cases without needing further modifications.

```
%--------------------------------------------------------------------------
%--------------------------------------------------------------------------
% function SLATBATCH
% Written by Trevor Yeow (13/02/2014 v1.0)
%
% Description
% This file is used to create batch files to automate seismic loss analyses
% using SLAT4BATCH.exe.
%
% Input
% SLATInputFile  - Name of input file for SLAT analyses
% SLATOutputFile - Name of output file from SLAT analyses
% RUN_FLAG       - RUN_FLAG = 1   (Run batch file)
%                - RUN_FLAG =/= 1 (Do not run batch file)
%--------------------------------------------------------------------------
%--------------------------------------------------------------------------
% Disclaimer
% SLAT.exe executes a Fortran Pause function at the end of analyses so that
% users can observe analyses details, especially when an error or warning
% has occurred. However, this causes a Microsoft Visual C++ Debug Library
% error at the end of each analyses, which requires the user to manually
% select either "Abort", "Retry" or "Ignore". While this does not have an
% effect on the output files, it does restrict the user from conducting
% fully automated analyses. This may not be an issue if only a handful of
% analyses are being conducted.
%
% An alternate version of SLAT.exe was compiled with the Fortran Pause
% function removed at the end of analyses. This version is called
% SLAT4BATCH.exe. The downside is that users are unable to observe analyses
% details at the end of each analyses if the batch file is run outside of
% the MATLAB environment. If the batch is run within the MATLAB
% environment, the analyses details are displayed in the command window.
% However, if a large number of analyses are conducted, error and warning
% messages from the earlier analyses may be overwritten.
%
% Users are urged to vigorously check and ensure that their analyses run
% correctly prior to batching.
%--------------------------------------------------------------------------
%--------------------------------------------------------------------------

function SLATBATCH(SLATInputFile,SLATOutputFile,RUN_FLAG)

%% TESTING
if nargin == 0
    SLATInputFile = 'E:\SLATTEST\EDPDATA\SLATRBWALL2.txt';
```

```
    SLATOutputFile = 'E:\SLATTEST\EDPDATA\out';
    RUN_FLAG = 1;
end

%% MAIN CODE

% First line of batch file
line = '('; % DO NOT DELETE
dlmwrite('SLATBATCHING.bat',line,'delimiter','','newline','pc') % DO NOT
DELETE

% Opening output file
line = ['echo ',SLATInputFile]; % DO NOT DELETE
dlmwrite('SLATBATCHING.bat',line,'-append','delimiter','','newline','pc') %
DO NOT DELETE

% Extracting out EDP11-hazard data (no collapse)
line = ['echo ',SLATOutputFile];
dlmwrite('SLATBATCHING.bat',line,'-append','delimiter','','newline','pc')

% Final line of batch file
line = ') | SLAT4BATCH.exe'; % DO NOT DELETE
dlmwrite('SLATBATCHING.bat',line,'-append','delimiter','','newline','pc') %
DO NOT DELETE

if RUN_FLAG == 1
% OPTIONAL - run batch file
dos('SLATBATCHING.bat')
end
%--------------------------------------------------------------------------
```

C5. SAMPLE POSTSLAT BATCH COMMAND

The following function provides an example of batching PostSLAT to obtain the roof total acceleration response hazard data. Similar methods are available to obtain other information of interest. Users are encouraged to be familiar with PostSLAT prior to modifying the provided function. Detailed instructions are also provided in the function's description.

```
%--------------------------------------------------------------------------
%--------------------------------------------------------------------------
% function POSTSLATBATCH
% Written by Trevor Yeow (13/02/2014 v1.0)
%
% Description
% This file is used to create batchfiles to automate postprocessing of loss
% data using POSTSLAT.exe. This version was used for a specific case-study
% using a 10 storey RC cantilever wall structure, and is not immediately
% applicable to other cases prior to further modifications
%
% Input
```

```
% SLATOutputFile - Name & location of SLAT output file to postprocess
% OutputLocation - Name of folder where output files from POSTSLAT are
%                  stored
% RUN_FLAG       - RUN_FLAG = 1   (Run batch file)
%                - RUN_FLAG =/= 1 (Do not run batch file)
%--------------------------------------------------------------------------
%--------------------------------------------------------------------------
% Disclaimer
% This batch code was written to obtain the following information (sequence
% of inputs into POSTSLAT listed in brackets).
%  1) EDP11-hazard (5 > 11 > Outputlocation\11.txt)
%
% Commands for additional outputs can be easily created by firstly finding
% out the sequence of inputs required into POSTSLAT.
%  Eg. For Loss-EDP data for Performance Group number 51 considering direct
%      repair costs, the sequence of inputs is:
%         Type of output requestioned = 3 (Loss-EDP relationship data)
%         Performance group number    = 51
%         Type of loss data to output = 1 (direct-repair cost)
%         Output filename to print    = LossEDP51.txt
%
% Once sequence is known, the "echo" function used in Windows batch can be
% used to echo the sequence of inputs into POSTSLAT.exe
%  Eg. echo 3
%      echo 51
%      echo 1
%      echo LossEDP51.txt
%
% Each of the lines can be defined in matlab using the dlmwrite function to
% automatically create batchfiles. This is especially useful if a large
% number of analyses is required.
%  Eg.  line = 'echo 3';
%       dlmwrite('POSTSLATBATCHING.bat',line,'-
append','delimiter','','newline','pc')
%--------------------------------------------------------------------------
%--------------------------------------------------------------------------

function POSTSLATBATCH(SLATOutputFile,POSTSLATOutputLocation,RUN_FLAG)

%% TESTING
if nargin == 0
    SLATOutputFile = 'E:\SLATTEST\EDPDATA\out';
    POSTSLATOutputLocation = 'E:\SLATTEST\EDPDATA\TESTING\';
    RUN_FLAG = 1;
end

%% MAIN CODE

% First line of batch file
line = '('; % DO NOT DELETE
dlmwrite('POSTSLATBATCHING.bat',line,'delimiter','','newline','pc') % DO
NOT DELETE

% Opening output file
line = ['echo ',SLATOutputFile]; % DO NOT DELETE
dlmwrite('POSTSLATBATCHING.bat',line,'-
append','delimiter','','newline','pc') % DO NOT DELETE

% Extracting out EDP11-hazard data
line = 'echo 5';
```

```
dlmwrite('POSTSLATBATCHING.bat',line,'-
append','delimiter','','newline','pc')
line = 'echo 11';
dlmwrite('POSTSLATBATCHING.bat',line,'-
append','delimiter','','newline','pc')
line = ['echo ',POSTSLATOutputLocation,'211.txt'];
dlmwrite('POSTSLATBATCHING.bat',line,'-
append','delimiter','','newline','pc')

% Final line of batch file
line = ') | postSLAT.exe'; % DO NOT DELETE
dlmwrite('POSTSLATBATCHING.bat',line,'-
append','delimiter','','newline','pc') % DO NOT DELETE

if RUN_FLAG == 1
% OPTIONAL - run batch file
dos('POSTSLATBATCHING.bat')
end
%--------------------------------------------------------------------------
```

C6. REFERENCES

1. Bradley, B. A. (2011). SLAT:Seismic Loss Assessment Tool (Version 1.16): Department of Civil and Natural Resources Engineering, University of Canterbury.
2. The MathsWorks Inc. (2012). MATLAB v 7.14 (R2012a). Natick, MA.
3. Naeim, F., & Hagie, S. (2012). PACT: Performance Assessment Calculation Tool. John A. Martin & Associates, INC. Los Angeles, California, US.
4. Rawlinson & Co. (2015). Rawlinsons New Zealand construction handbook. Rawlhouse Publishing, Wellington, New Zealand.

Appendix D. Content Movement Analysis Matlab Codes

D1. THEORY

Modelling of content sliding generally follows Amonton's and Coulomb's dry friction laws [1], which state that (i) friction force is independent of the contact area, (ii) friction force is proportional to the normal force, and (iii) kinetic friction is independent of sliding velocity. Comparison with experimental testing in **Chapter 4** shows that this assumption is reasonable for realistic office-type contents on common flooring surfaces. As such, the generic equation for the total acceleration response of sliding contents, a_{CT} (e.g. Shenton III and Jones [2]), is as shown in **Eq. D.1**. Here, μ_s and μ_k are the static and kinetic friction coefficients, respectively, where $v_{CRF}(t)$ was the contents' velocity relative to the floor with time, and μ_s and μ_k were the static and kinetic friction coefficients, respectively.

$$a_{CT}(t) = \begin{cases} a_{FT}(t) & \text{when } |v_{CRF}(t)| = 0 \text{ and } |a_{FT}(t)| < \mu_s g \\ -\text{sgn}(v_{CRF}(t))\mu_k g & \text{when } |v_{CRF}(t)| > 0 \text{ or } |a_{FT}(t)| \geq \mu_s g \end{cases} \quad \textbf{(D.1)}$$

While the rocking behaviour of furniture was not examined experimentally in this thesis, past studies have shown that the response of rigid rectangular block-like contents provides a good approximation of realistic response [3]. A typical equation for the angular acceleration response of rigid rectangular blocks, $\ddot{\theta}_C$, is given in **Eq. D.2** [3]. Here, θ_C is the block's rotation relative to vertical; a_{FT} is the floor's total acceleration; g is the acceleration due to gravity; and θ^* is given by **Eq. D.3**. Note that $\ddot{\theta}_C$ is zero if neither condition for **Eq. D.2** is satisfied.

$$\ddot{\theta}_C(t) = -\frac{3g}{\sqrt{B^2 + H^2}}\left[\text{sgn}[\theta_C(t)].\sin\left(\theta^*(t)\right) + \frac{a_{FT}(t)}{g}\cos\left(\theta^*(t)\right)\right] \quad \begin{matrix}\text{when } |\theta_C(t)| > 0 \\ \text{and/or } |a_{FT}(t)| > Bg/H\end{matrix} \quad \textbf{(D.2)}$$

$$\theta^*(t) = \tan^{-1}\left(\frac{B}{H}\right) - |\theta_C(t)| \quad \textbf{(D.3)}$$

Energy loss due to the contents impacting against other obstacles is considered using a coefficient of restitution. The coefficient of restitution for rocking cases, e_r, which is the ratio of angular velocity after and before impact, can be obtained using **Eq. D.4** [4]. The sliding coefficient of restitution, e_s, which is the ratio of the content's velocity relative to the floor, v_{CRF}, after and before impact, may be obtained from: (i) rock fall data [5] ($e_s \approx 0.5$); or (ii) experimental studies by Jankowski [6] where a solid ball made of a specific material was dropped onto a rigid surface ($0.6 < e_s < 0.8$).

$$e_r = \left(1 - \frac{3}{2}\sin^2\left[\tan^{-1}\left(\frac{B}{H}\right)\right]\right)^2 \left(1 - \frac{3}{2}\cos^2\left[\tan^{-1}\left(\frac{B}{H}\right)\right]\right) \quad \textbf{(D.4)}$$

D2. MASTER SCRIPT FILE

The following script file demonstrates the usage of sliding analysis function, detailed in **Appendix D3**, to obtain the contents' sliding response history. A similar file can be written for rocking cases.

```
%-------------------------------------------------------------------------
% Purpose - Master script file for content sliding analyses
%-------------------------------------------------------------------------

% Inputs
g = 9.81;                       % Gravity coefficient
B = 1;                          % Width of content base
                                % (in same plane as rocking motion)
H = 0.5;                        % Height of content
mu = 0.1;                       % Friction coefficient
COR = -0.5;                     % Coefficient of restitution
Filename = '01_01_1.txt';       % Acceleration filename
dt_Slide = 0.0001;              % Time step for sliding analyses

%-------------------------------------------------------------------------
% Import data
Acc = importdata(Filename);  % Input acceleteration data
%-------------------------------------------------------------------------
% Perform sliding analyses
SLIDINGCALCULATOR(g,B,H,mu,COR,Acc,Floor);
%-------------------------------------------------------------------------
```

D3. SLIDING ANALYSIS FUNCTION

The following function was written to perform sliding analyses based on **Eq. D.1**, and the outputs (sliding displacement and content's velocity relative to the floor) are exported in a text file. This version of the function was for obstructed sliding where the gap between the content and the obstruction is zero; and can be easily modified for other cases. The trapezium rule [7] is used for numerical integration in this code, though Newton's integration schemes [8] was also implemented in other versions. Note that an iterative procedure was not implemented when the content impacts against obstacles, as this can be accurately captured using a time step of 0.001 s or less based on preliminary assessments.

```
%-------------------------------------------------------------------------
% function SLIDINGCALCULATOR(g,B,H,mu,COR,Acc,Floor,dt_Slide)
%-------------------------------------------------------------------------
% Inputs
% g         - Gravity coefficient
% B         - Width of content base in same plane as rocking motion
% H         - Height of content
% mu        - Friction coefficient
% COR       - Coefficient of restitution
% Acc       - Total floor acceleration history. Note that this is taken
%             directly from Dynaplot outputs. Thus, the first column
%             contains time values, while the rest contains accelerations
%             at each floor level. This might have to be modified
%             accordingly if a different acceleration format was
%             considered. Also note that acceleration values should be in
%             units of gravity.
% Floor     - Building floor level of interest
% dt_Slide  - Timestep for sliding analyses
%-------------------------------------------------------------------------

function SLIDINGCALCULATOR(g,B,H,mu,COR,Acc,Floor,dt_Slide)

% Obtain time information
[M N]=size(Acc);                    % Obtain number of datapoints from Acc
dt = Acc(2,1)-Acc(1,1);             % Obtain stepsize
T0 = Acc(1,1);                      % Initial time
TF = dt*(M-1);                      % Final time
Time1 = T0:dt_Slide:TF;             % Time vector for analysis

% Obtain acceleration values for use in analyses
af1 = interp1([T0:dt:TF],Acc(:,1+Floor),Time1)/-9.81;
af1(isnan(af1))=0;

%-------------------------------------------------------------------------

% Performing sliding analyses

% Identify if sliding occurs
```

```
if max(abs(af1))<mu;            % No sliding as mu>acceleration
    SlideDisp = zeros(length(Acc(:,1)),1);  % Slide displacement output
    SlideVel = zeros(length(Acc(:,1)),1);   % Slide velocity output
else                            % Sliding as mu<acceleration
    vf1 = 0;                    % Initial total floor velocity
    df1 = 0;                    % Initial total floor displacement
    ac1 = 0;                    % Initial total content acceleration
    vc1 = 0;                    % Initial total content velocity
    dc1 = 0;                    % Initial total content displacement
    Flag = 0;                   % No initial sliding

    for i = 1:length(Time1)-1
        % Floor response
        % Numerical integration to obtain total floor velocity
        vf1(i+1)=vf1(i)+mean(af1(i:i+1))*dt_Slide*g;
        % Numerical integration to obtain total floor displacement
        df1(i+1)=df1(i)+mean(vf1(i:i+1))*dt_Slide;

        % Content response
        % Note that the state of content sliding is defined by Flag, where
        % Flag = 0, 1, and 2 represents (i) no sliding, (ii) sliding in
        % postive direction, and (iii) sliding in negative direction,
        % respectively.
        if Flag == 0                % If no sliding occurs
            if abs(af1(i))<=mu      % No slide, content and floor
                % response identical
                ac1(i+1)=af1(i+1);
                vc1(i+1)=vf1(i+1);
            elseif af1(i)>mu        % Slide occurs in positive direction,
                % floor acceleration equals mu
                ac1(i+1)=mu;
                vc1(i+1)=vc1(i)+mean(ac1(i:i+1))*dt_Slide*g;
                Flag = 1;
            elseif af1(i)<-mu       % Slide occurs in negative direction,
                % floor acceleration equals -mu
                ac1(i+1)=-mu;
                vc1(i+1)=vc1(i)+mean(ac1(i:i+1))*dt_Slide*g;
                Flag = 2;
            end
        elseif Flag == 1            % If sliding in positive direction
            if vc1(i)>vf1(i)        % Check if content switches direction
                if af1(i)<-mu       % Check if sliding reverses
                    ac1(i+1)=-mu;
                    vc1(i+1)=vc1(i)+mean(ac1(i:i+1))*dt_Slide*g;
                    Flag = 2;
                else                % Check if sliding terminates
                    ac1(i+1)=af1(i+1);
                    vc1(i+1)=vf1(i+1);
                    Flag = 0;
                end
            else                    % Check if sliding continues in
                % positive direction
                ac1(i+1)=mu;
                vc1(i+1)=vc1(i)+mean(ac1(i:i+1))*dt_Slide*g;
            end
        elseif Flag == 2            % If sliding in negative direction
            if vc1(i)<vf1(i)        % Check if content switches direction
                if af1(i)>mu        % Check if sliding reverses
                    ac1(i+1)=mu;
                    vc1(i+1)=vc1(i)+mean(ac1(i:i+1))*dt_Slide*g;
                    Flag = 1;
```

```
                else                % Check if sliding terminates
                    ac1(i+1)=af1(i+1);
                    vc1(i+1)=vf1(i+1);
                    Flag = 0;
                end
            else                    % Check if sliding continues in
                % positive direction
                ac1(i+1)=-mu;
                vc1(i+1)=vc1(i)+mean(ac1(i:i+1))*dt_Slide*g;
            end
        end

        % Calculate content's total displacement
        dc1(i+1)=dc1(i)+mean(vc1(i:i+1))*dt_Slide;

        % Check if content has impacted against obstacle. If so, set
        % displacement to be equal to that of the obstacle, and apply
        % coefficient of restitution to velocity response
        if Flag >0
            if dc1(i+1)<df1(i+1)
                dc1(i+1)=df1(i+1);
                vc1(i+1)=COR*(vc1(i+1)-vf1(i+1))+vf1(i+1);
            end
        end
    end
    SlideDisp = dc1'-df1';      % Slide displacement output
    SlideVel = vc1'-vf1';       % Slide velocity output
end

% Export out sliding displacement
dlmwrite(['SlideDisp_',Filename,'.TXT'],SlideDisp,...
    'delimiter',' ','newline','pc')
% Export out sliding velocity
dlmwrite(['SlideVel_',Filename,'.TXT'],SlideVel,...
    'delimiter',' ','newline','pc')
%-------------------------------------------------------------------------
```

D4. ROCKING ANALYSIS

The following function was written to perform rocking analyses based on **Eqs. D.2-D.3**, and the coefficient of restitution for this case is given in **Eq. D.4**. Unlike for the sliding analyses, a higher-order numerical integration approach was required due to the non-linearity of the content's rocking response. As such, a 4^{th}-Order Runge-Kutta approach [7] was implemented.

```
%-------------------------------------------------------------------------
% function RockOneWay(g,B,H,Acc,Floor,dt_Rock)
%-------------------------------------------------------------------------
% Inputs
% g         - Gravity coefficient
% B         - Width of content base in same plane as rocking motion
% H         - Height of content
```

```
% Acc       - Total floor acceleration history. Note that this is taken
%             directly from Dynaplot outputs. Thus, the first column
%             contains time values, while the rest contains accelerations
%             at each floor level. This might have to be modified
%             accordingly if a different acceleration format was
%             considered. Also note that acceleration values should be in
%             units of gravity.
% Floor     - Building floor level of interest
% dt_Rock   - Timestep for rocking analysis
%-------------------------------------------------------------------------

function Rotation = RockOneWay(g,B,H,Acc,dt_Rock)

% Content parameters
alpha = atan(B/H);          % Maximum angle before overturning occurs
R = sqrt((B/2)^2+(H/2)^2);  % Distance from corner to centre of content
P = sqrt(3*g/4/R);          % Content coefficient for analyses

% Coefficient of restitution
COR = (1-3/2*(sin(alpha))^2)^2*(1-3/2*(cos(alpha))^2);

% Time data
[M N]=size(Acc);                    % Obtain size of Acc
dt = Acc(2,1)-Acc(1,1);             % Obtain stepsize
T0 = Acc(1,1);                      % Initial time
TF = dt*(length(Acc(:,1))-1);       % Final time
Time1 = T0:dt_Rock:TF;                  % Time vector for analysis

% Obtain acceleration values for use in analyses
af1 = interp1([T0:dt:TF],Acc(:,2),Time1)/9.81;
af1(isnan(af1))=0;

%-------------------------------------------------------------------------

% Performing rocking analyses

% Initial Conditions
x(:,1) = [0;0];     % Initial rotation and angular velocity
Flag = 0;           % Flag assessing if overturning had occurred

% Content extra parameters
if min(af1)<-B/H                    % Check if rocking occurs in postive
                                    % direction
for i = 1:length(Time1)-1
    if Flag == 0 && af1(i)>-B/H     % If no rocking occuurs
        x(:,i+1)=x(:,i);
    else
        % Perform 4th order Runge-Kutta numerical integration
        k1 = myode(x(:,i),af1(i),P,alpha);
        k2 = myode(x(:,i)+k1*dt_Rock/2,mean(af1(i:i+1)),P,alpha);
        k3 = myode(x(:,i)+k2*dt_Rock/2,mean(af1(i:i+1)),P,alpha);
        k4 = myode(x(:,i)+k3*dt_Rock,af1(i+1),P,alpha);
        x(:,i+1)=x(:,i)+dt_Rock/6*(k1+2*k2+2*k3+k4);
        Flag = 1;

        % If angular rotation reaches 0 (i.e. impacts with wall), apply
        % coefficient of restitution to angular velocity, and set angular
        % rotation to 0.
        if x(1,i+1)<0
```

```
            x(2,i+1)=x(2,i+1)*COR;
            x(1,i+1)=0;
        end
    end

    % Stop analyses if content overturns
    if abs(x(1,i))>pi/2
        break
    end
end
else    % If rocking does not occur, set response to 0
    x=zeros(2,length(Time1));
end

% Export out rotation data
dlmwrite(['BS2Rot_',Filename,'.TXT'],[x(1,:)]',...
    'delimiter',' ','newline','pc')
% Export out angular velocity data
dlmwrite(['BS2Vel_',Filename,'.TXT'],[x(2,:)]',...
    'delimiter',' ','newline','pc')


%-------------------------------------------------------------------------

function dxdt = myode(x,ug,P,alpha)

% Differential equation for rocking case
dxdt = [x(2);
    -P^2*(sign(x(1))*sin(alpha-abs(x(1)))+ug*cos(alpha-abs(x(1))))];

%-------------------------------------------------------------------------
```

D4. REFERENCES

1. Meyer, E., Overney, R. M., Dransfeld, K., & Gyalog, T. (1998). Nanoscience - friction and rheology on the nanometer scale. Singapore: World Scientific Publishing.
2. Shenton III, H. W., & Jones, N. P. (1992). Base Excitation of Rigid Bodies. Part I: Formulation. Journal of Engineering Mechanics, 117(10), 2286-2306.
3. Konstantinidis, D. A. (2008). Experimental and Analytical Studies on the Seismic Response of Freestanding and Anchored Building Contents. Civil and Environmental Engineering, University of California, Berkeley.
4. Sorrentino, L., AlShawa, O., & Decanini, L. D. (2011). The relevance of energy damping in unreinforced masonry rocking mechanisms. Experimental and analytic investigations. Bulletin of Earthquake Engineering, 9(5), 1617-1642.
5. Rocscience. (2015). RocFall - Statistical Analysis of Rockfalls.
6. Jankowski, R. (2010). Experimental study on earthquake-induced pounding between structural elements made of different building materials. Earthquake Engineering and Structural Dynamics, 39(3), 343-354.
7. Atkinson, K. E. (1989). An Introduction to Numerical Analysis (2nd ed): John Wiley & Sons, New York.
8. Newmark, N. M. (1959). A Method of Computation for Structural Dynamics. Journal of Engineering Mechanics, 85(EM3), 67-94.

Appendix E. Injury Prediction Matlab Codes

E1. OVERVIEW

The script files and functions described herein are based on the injury prediction framework described in **Chapter 7**. Note that while an effort was made to write the functions in a manner which can be applied to every possible scenario, these have only been tested for cases specific to **Chapter 7** and **8**. Users are encouraged to test each script file prior to using it in analyses.

E2. MASTER SCRIPT FILE

The following script file is the main file required for running the injury prediction framework. The example from **Chapter 7** is also included.

```
%-------------------------------------------------------------------------
% Purpose - main script file for injury modelling
%-------------------------------------------------------------------------
% Inputs
% ContentCoordinate - matrix with two rows, where the top row contains
%                     the name of the contents, the second row contains
%                     a matrix of content coordinates and height, while
%                     each column represents each individual content. The
%                     matrix should contain the following information:
%                       Row 1 - Content height and number of coordinates
%                       (nc)
%                       Row 2 - x and y coordinates of first point
%                       Row nc+1 - x and y coordinates of point nc
%                     NOTE: coordinates should be specified going in either
%                     a clockwise or anticlockwise direction. Any other
%                     specification (e.g. left-right, then up-down) will
%                     cause the code to misinterpret the dimensions of the
%                     content.
%       e.g.     DeskProp = [0.5,4;0 0;1 0;1 1;0 1];
%                ContentCoordinate = {'Desk';DeskProp};
%
%               Point 4(0,1) _______ Point 3(1,1)
%                           |       |
%                           | Desk  |
%                           |       |
%               Point 1(0,0)|_______|Point 2(1,0)
%
% ContentBehaviour - Similar format to ContentCoordinate, except that the
%                    second row should contain a row of 5 numbers, where
%                       first entry - type of content (1 = rocking, 2 =
%                                     sliding)
```

```
%                       second entry - direction (1 = N-S, 2 = E-w)
%                        third entry - file ID for displacement/rotation
%                                      response
%                       fourth entry - file ID for velocity/angular velocity
%                                      response
%                        fifth entry - maximum allowable rotation response.
%                                      Note that this is only used for
%                                      rocking cases, as it is assumed this
%                                      would've been accounted for in
%                                      sliding analyses
%                        sixth entry - content's mass
%
% AreaD      - Information for each grid
%                        first entry - Grid number
%                       second entry - Standing or sitting
%                        third entry - Standing grid ID
%                       fourth entry - west-most coordinate
%                        fifth entry - east-west length
%                        sixth entry - south-most coordinate
%                      seventh entry - noth-south length
%
% OC         - Occupant location's coordinate
% Height     - Occupant's height
% Floor      - Floor which room is being considered
%--------------------------------------------------------------------------

% Building/Room/Maximum occupancy information
Rooms = 24;                 % Number of rooms per floor
NumF = 10;                  % Number of floors in building
MaxOcc=96*ones(NumF,1);     % Maximum occupancy per floor

% Room and occupant spatial distribution weighting factor
NumSeat = 4;                % Number of sitting vacancies
NumStand = 3;               % Number of standing vacancies
RateSeat = 1;               % Rating applied per seat
RateStand = 0.2;            % Rating applied per standing occupant

% Input information for grids (see script description)
AreaD = [1 1 0 0 0 0.65 2
    2 2 1 0.65 2 1.15 0.55
    3 1 0 0.65 0.65 1.15 1.35
    4 1 0 1.8 1.2 1.8 1.65
    5 2 2 2.45 0.65 1.15 0.55
    6 2 3 3.6 2 1.15 0.55
    7 1 0 3.6 1.2 1.15 0.8
    8 2 4 3.6 0.65 1.15 0.55];

% Input content coordinate information (see script description)
Wall = [10 4;0 0;5.4 0;5.4 3.2;0 3.2];
D1C = [0.75 6;0 2;0.65 2;0.65 2.55;1.8 2.55;1.8 3.2;0 3.2];
D2C = [0.75 6;3.6 2.55;4.75 2.55;4.75 2;5.4 2;5.4 3.2;3.6 3.2];
D3C = [0.75 6;1.8 0;3.6 0;3.6 0.65;2.45 0.65;2.45 1.2;1.8 1.2];
D4C = [0.75 6;3.6 0;5.4 0;5.4 1.2;4.75 1.2;4.75 0.65;3.6 0.65];
MD2C = [0.55 4;4.75 1.2;5.4 1.2;5.4 1.6;4.75 1.6];
MD1C = [0.55 4;4.75 1.6;5.4 1.6;5.4 2;4.75 2];
FC1C = [1.65 4;0.65 0;1.15/3+0.65 0;1.15/3+0.65 0.65;0.65 0.65];
FC2C = [1.65 4;1.15/3+0.65 0;2*1.15/3+0.65 0;2*1.15/3+0.65 0.65;1.15/3+0.65
0.65];
FC3C = [1.65 4;2*1.15/3+0.65 0;1.8 0;1.8 0.65;2*1.15/3+0.65 0.65];
BS1C = [1.8 4;1.8 2.85;2.7 2.85;2.7 3.2;1.8 3.2];
```

```
BS2C = [1.8 4;2.7 2.85;3.6 2.85;3.6 3.2;2.7 3.2];
ContentCoordinate={'D1','D2','D3','D4','MD1','MD2','FC1','FC2','FC3','BS1',
'BS2','Wall';
    D1C,D2C,D3C,D4C,MD1C,MD2C,FC1C,FC2C,FC3C,BS1C,BS2C,Wall};

% Input content behaviour information (see script description)
D1B = [0 0 0 0 0 0.03];
D2B = [0 0 0 0 0 0.03];
D3B = [0 0 0 0 0 0.03];
D4B = [0 0 0 0 0 0.03];
MD1B = [2 4 2 3 0 0.04];
MD2B = [2 4 2 3 0 0.04];
FC1B = [1 1 6 7 0 0.09];
FC2B = [1 1 6 7 0 0.09];
FC3B = [1 1 6 7 0 0.09];
BS1B = [1 2 4 5 1.1 0.075];
BS2B = [1 2 4 5 0 0.075];
Wall = [0 0 0 0 0 0];
ContentBehaviour={'D1','D2','D3','D4','MD1','MD2','FC1','FC2','FC3','BS1','
BS2','Wall';
    D1B,D2B,D3B,D4B,MD1B,MD2B,FC1B,FC2B,FC3B,BS1B,BS2B,Wall};

% Occupant height distribution
HeightM = 1.71;         % Median height
HeightD = 0.07;         % Dispersion

% Specify number of analyses to perform
nmc = 5000;

% Specify input files (Note that this corresponds to file IDs in
% ContentBehaviour input, except for first entry which is floor total
% acceleration)
Fileinputs = {'FloorAcc\05_01.txt';
    'Sliding\MDDispn_05_01_2.txt';
    'Sliding\MDVeln_05_01_2.txt';
    'Rocking\BS2Rot_05_01_1.txt';
    'Rocking\BS2Vel_05_01_1.txt';
    'Rocking\FC2Rot_05_01_1.txt';
    'Rocking\FC2Vel_05_01_1.txt'};
 %-------------------------------------------------------------------------

% Create output file for deaggregation results. Note that results are
% presented in the following order
% Area>Severity>Bodypart>Source
Output = zeros(NumF,(6*4*6+1)*length(AreaD(:,1)));

% Read input files
for i = 1:length(Fileinputs)
    Datainputs{i} = importdata(Fileinputs{i});
end

% Identify number of occupants present
[OccTotal,Time] = INJURYOccupancyNum(nmc,NumF,MaxOcc);

% Identify location and height of all occupants present in room
[OCX,OCY,Height,Area] = INJURYLocation(Rooms,AreaD,NumSeat,NumStand,...
    RateSeat,RateStand,HeightM,HeightD,OccTotal);
[M N] = size(OCX);
% Perform Monte Carlo simulations
for i = 1:N
```

```
    for j = 1:M
        % If occupant is present in the room
        if OCX(j,i+(k-1)*N/length(RecordInfo))~=-1
            % Calculate floor
            Floor = ceil(j/Rooms)-1;
            % Determine falling acceleration "capacity"
            Afall = exp(icdf('norm',rand,log(0.17),0.69));
            % Identify fall direction
            FallAngle = rand(1)*2*pi;

            % Perform assessment to identify source of injury
            [ImpactV,BIR]=INJURYSource(ContentCoordinate,...
                ContentBehaviour,Height(j,i+(k-1)*N/length(RecordInfo)),...
                Afall,[OCX(j,i+(k-1)*N/length(RecordInfo)),...
                OCY(j,i+(k-1)*N/length(RecordInfo))],Datainputs,Floor);

            % Injury severity assessment
            [Source,AIS,BodyPart] =...
                INJURYSeverityAssessment(ImpactV(find(BIR(:,1)>=-1),:),...
                BIR(find(BIR(:,1)>=-1),:));

            % Sort data into deaggregation table
            if AIS == 0     %If no injury occurs
                Output(Floor+1,(Area(j,i+(k-1)*N/length(RecordInfo))-1)*...
                    145+1)=Output(Floor+1,(Area(j,i+(k-1)*...
                    N/length(RecordInfo))-1)*145+1)+1;
            else            %If injury occurs
                Output(Floor+1,(Area(j,i+(k-1)*N/length(RecordInfo))-1)*...
                    145+1+(AIS-1)*24+(BodyPart-1)*6+Source)=...
                    Output(Floor+1,(Area(j,i+(k-1)*...
                    N/length(RecordInfo))-1)*145+1+(AIS-1)*24+...
                    (BodyPart-1)*6+Source)+1;
            end

            % Estimate cost based on injury severity
            InjuryCost(j,i+(k-1)*N/length(RecordInfo)) = ...
                INJURYCostEstimate(AIS,BodyPart,CFlag);
        else
            InjuryCost(j,i+(k-1)*N/length(RecordInfo))=0;
        end
    end
end

% Store data into cost matrix
for i = 1:NumF
    for j = 1:nmc
        %Cost per floor
        FloorCost(i,j)=sum(sum(InjuryCost(Rooms*(i-1)+1:Rooms*i,...
            (NumSeat+NumStand)*(j-1)+1:(NumSeat+NumStand)*j)));
    end
end

% Export deaggregation details
dlmwrite(['Hazard ',num2str(Hazardlvl),' Trial ',num2str(num),...
    ' - DeaggInfo.txt'],Output,'delimiter',' ','newline','pc')
% Export floor cost details
dlmwrite(['Hazard ',num2str(Hazardlvl),' Trial ',num2str(num),...
    ' - FloorCost.txt'],FloorCost,'delimiter',' ','newline','pc')
```

E3. TRANSIENT OCCUPANCY MODEL FUNCTION

The following function was used to estimate the number of occupants present on each floor of the building at the time of shaking. This was done by (i) predicting time of event, (ii) obtaining occupancy distribution based on predicted time, and (iii) using probabilistic approaches to estimate the number of occupants present.

```
%-------------------------------------------------------------------------
%-------------------------------------------------------------------------
% function [OccTotal,Time] = INJURYOccupancyNum(nmc,NumF,MaxOcc)
% Version 1.0 (08 Sept 2015)
%-------------------------------------------------------------------------
% Purpose
% For determmining time of earthquake, and number of occupants at time of
% earthquake.
%
% Inputs
% nmc    - number of Monte Carlo iterations
% NumF   - number of floors
% MaxOcc - maximum number of occupants on each floor
%
% Outputs
% OccTotal - total number of occupants per trial
% Time     - time of event
%-------------------------------------------------------------------------

function [OccTotal,Time] = INJURYOccupancyNum(nmc,NumF,MaxOcc)

% Determine time of EQ for each trial
TimeTemp = rand(1,nmc);              %For assessing if working day or not
Time = rand(1,nmc)*24;               %Randomly generated time
Time(find(TimeTemp>240/356))=25;     %If earthquake occrs on weekends
                                     %or public holidays, set to 25 hours

% Setting up matrix for determining number of occupants
OccTotal = zeros(NumF,nmc);
OccTotalTemp = rand(NumF,nmc);

% INSERT OCCUPANCY MODEL DETAILS HERE. DATA(:,1) IS TIME OF DAY, DATA(:,2)
% IS MEDIAN OCCUPANCY, AND DATA(:,3) IS OCCUPANCY DISPERSION

% Interpolate to obtain median and dispersion of occupancy rate at time of
% earthquake
OccMed = ones(NumF,1)*interp1(Data(:,1),Data(:,2),Time);
OccDisp = ones(NumF,1)*interp1(Data(:,1),Data(:,3),Time);

% Use random number generator to obtain occupancy rate
OccTotal = round((MaxOcc*ones(1,length(Time))).*...
    exp(icdf('norm',OccTotalTemp,log(OccMed),OccDisp)));
%-------------------------------------------------------------------------
```

E4. OCCUPATION SPATIAL DISTRIBUTION FUNCTION

The following function was used to estimate the location of occupants. This was done by (i) applying weighting factors based on the likelihood of a person sitting, (ii) use probabilistic approaches to identify the grid which the occupant is occupying, and (iii) the occupant's coordinates.

```
%--------------------------------------------------------------------------
% function [OCX,OCY,Height] = INJURYLocation(Rooms,AreaD,NumSeat,...
%    NumStand,RateSeat,RateStand,HeightM,HeightD,OccTotal)
%--------------------------------------------------------------------------
% Purpose
% For determmining location of occupants
%
% Inputs
% Rooms         - Number of rooms per floor
% Area D        - Grid area properties
% NumSeat       - Number of sitting vacancies
% NumStand      - Number of standing vacancies
% RateSeat      - Rating factor assigned to sitting vacancies
% RateStand     - Rating factor assigned to standing vacancies
% HeightM       - Median occupant height
% HeightD       - Occupant height dispersion
% OccTotal      - Total number of occupants present
%--------------------------------------------------------------------------

function [OCX,OCY,Height,Area] = INJURYLocation(Rooms,AreaD,NumSeat,...
    NumStand,RateSeat,RateStand,HeightM,HeightD,OccTotal)

%--------------------------------------------------------------------------
% Analysis set up

% Matrix for occupant location
OccLoc = zeros(Rooms*length(OccTotal(:,1)),(NumSeat+NumStand)*...
    length(OccTotal(1,:)));

% Number of iterations (M) and number of floors (N)
M = length(OccTotal(:,1));
N = length(OccTotal(1,:));

% Matrix for occupant coordinates
OCY = zeros(M,N);           % y coordinate matrix
OCX = zeros(M,N);           % x coordinate matrix
Area = zeros(M,N);          % grid area ID matrix

% Determine standing heights of occupants
Trial = rand(M,N);
Height = exp(icdf('norm',Trial,log(HeightM),HeightD));

% Set up a row of vacancy numbers for using bsxfun in following part
Trow = [0:1:N-1]*(Rooms*(NumSeat+NumStand));
%--------------------------------------------------------------------------
% Determining if vacancies have been filled
for m = 1:M
```

```
    % Obtain number of occupants for this trial
    OccTrial = OccTotal(m,:);
    % Set up temporary occupant location file
    OccLocTemp = zeros(Rooms,(NumStand+NumSeat)*N);
    % Assigning rates to each vacancy
    Rating=[RateSeat*ones(Rooms*NumSeat,N);RateStand*...
        ones(Rooms*NumStand,N)];

    % Calculating normalized rate, and identify location
    for j = 1:max(OccTrial)
        % Calculate noramlized cumulative rat
        CummRate=cumsum(Rating);
        CummRate=bsxfun(@rdivide,CummRate,...
            CummRate(length(CummRate(:,1)),:));
        % Use probabilistic methods to identify location of occupant
        row=(Rooms*(NumSeat+NumStand)-...
            sum(bsxfun(@gt,CummRate,rand(1,N)))+1+Trow).*(OccTrial>=j);
        OccLocTemp(row(find(row>0)))=1;
        % Reset weighting of individual rating to 0 before assigning the
        % next occupant to a location
        Rating(row(find(row>0)))=0;
    end
    %Store findings in row and repeat for next iteration
    OccLoc((m-1)*Rooms+1:m*Rooms,:)=OccLocTemp;
end
%-------------------------------------------------------------------------
% Determining location of standing occupant
%
% Only consider standing-only grids
AreaSTD = [zeros(1,7);AreaD(find(AreaD(:,2)==1),:)];
% Calculate floor area of each standing-only grid
AreaSTV = AreaSTD(:,6).*AreaSTD(:,7);
% Determine the cumulative probability that a single occupant would be
% located within the affected grid
ProbSTV = [[1:length(AreaSTD(:,1))]',cumsum(AreaSTV)];
ProbSTV(:,2) = ProbSTV(:,2)/max(ProbSTV(:,2));

% Use random number generators to determine a standing occupant's grid
% location
% Create matrix of random numbers of faster processing
Trial = rand(M,N);
% ID grid where standing occupants were related
AreaIDS = ceil(interp1(ProbSTV(:,2),ProbSTV(:,1),Trial));

% Assume that an occupant have uniform probability of being located
% anywhere within a given grid
Trial = rand(M,N);
Trial2 = rand(M,N);
for i = 1:length(AreaSTV(:,1))-1
    OCX(find(AreaIDS==i+1))=Trial(find(AreaIDS==i+1))*...
        AreaSTD(i+1,6)+AreaSTD(i+1,4);
    OCY(find(AreaIDS==i+1))=Trial2(find(AreaIDS==i+1))*...
        AreaSTD(i+1,7)+AreaSTD(i+1,5);
    Area(find(AreaIDS==i+1))=AreaSTD(i+1,1);
end

%-------------------------------------------------------------------------
% Determine location of sitting occupants

% Only consider sitting occupants
```

```
AreaSID = [AreaD(find(AreaD(:,2)==2),:)];

% Repeat similar analyses for standing occupants as for sititng occuapnts
for i = 1:length(AreaSID(:,1))
OCX(:,i:NumSeat+NumStand:N-NumSeat-NumStand+i)=Trial(:,i:NumSeat+...
NumStand:N-NumSeat-NumStand+i)*AreaSID(i,6)+AreaSID(i,4);
OCY(:,i:NumSeat+NumStand:N-NumSeat-NumStand+i)=Trial2(:,i:NumSeat+...
    NumStand:N-NumSeat-NumStand+i)*AreaSID(i,7)+AreaSID(i,5);
Area(:,i:NumSeat+NumStand:N-NumSeat-NumStand+i)=AreaSID(i,1);
% Note that a sitting occupant's height was assumed to be 70% of their
% standing height based on typical body proportions
Height(:,i:NumSeat+NumStand:N-NumSeat-NumStand+i)=Height(:,i:NumSeat+...
    NumStand:N-NumSeat-NumStand+i)*0.7;
end
%-------------------------------------------------------------------------
```

E5. IMPACT ASSESSMENT FUNCTIONS

The following function details the overall procedure to evaluate injuries arising from occupants falling or contents moving. This used several other more detailed functions files; (i) NoFallInjury, (ii) PreFallInjury, (iii) ContentsRearrange, (iv) FallInjury, (v) PostFallInjuryRock, and (vi) PostFallInjurySlide. The latter four functions were also provided in detail, while the first two were simply variants of (v) and (vi).

```
%-------------------------------------------------------------------------
%-------------------------------------------------------------------------
% function [ImpactV,BIR]=INJURYSource(ContentCoordinate,...
%    ContentBehaviour,Height,Afall,OC,Datainputs,Floor)
% Written by Trevor Yeow (31 August 2015)
% Version 1.0
%
% Purpose
% This function performs analyses to identify if occupants fell or were
% struck by moving contents, and the resultant impact properties (i.e.
% velocity and mass) for use in predicting injury severity
%
% Inputs (see main script file for detailed information on formatting)
% ContentCoordinate - Information on location and position of contents
% ContentBehaviour  - Information on likely behaviour of contents
% Height            - Occupant's height
% Afall             - Acceleration that causes occupant to fall
% OC                - Occupant's coordinates
% Datainputs        - Input data of interest (defined in
%                     ContentBehaviour)
%
% Outputs
% ImpactV           - Velocities at each end of distributed impact
% BIR               - N by 5 matrix detailing the boundary impact
%                     conditions. (1) Location of lower impact on occupant
%                     as a ratio of total occupant height, (ii) location of
%                     upper impact, (iii)impact mass, (iv) impact type
%                     (i.e. occuapnts fell first before getting stuck by
%                     contents, and (v) source of injury
```

```
%-------------------------------------------------------------------------

function [ImpactV,BIR]=INJURYSource(ContentCoordinate,...
    ContentBehaviour,Height,Afall,OC,Datainputs,Floor)

% Initial setup
Acc = Datainputs{1};     % Read acceleration data (first entry of
                         % Datainputs)
Flag = 0;                % Flag = 0 indicates no injury.
BIR = zeros(1,5);        % Setup BIR matrix
ImpactV = zeros(1,5);    % Setup ImpactV matrix

%-------------------------------------------------------------------------
% Main code

if Afall>max(Acc(:,Floor+2))     % Check if falling does not occur
    [ImpactV1,BIR1,Flag1]=NoFallInjury(ContentCoordinate,...
        ContentBehaviour,Datainputs,OC,Height,Floor);
    Flag = 1;                    % This indicates that potential injuries
                                 % that occur here are caused by content
                                 % movement while the occupant was upright

else                             % If falling occurs
    % Find time at which occupant falls
    tf = Acc(min(find(Acc(:,Floor+2)>Afall)),1);
    % Perform analysis of content impact prior to falling
    [ImpactV1,BIR1,Flag1]=PreFallInjury(ContentCoordinate,...
        ContentBehaviour,Datainputs,OC,Height,Floor,tf);
    % There are three outcomes from this analysis as indicated by Flag1,
    % (i) no injuries occur (Flag1 = 0), (ii) occupants were struck by
    % toppling contetns (Flag1 = 1), and (iii) occupants were struck by
    % sliding contents (Flag1 = 2).

    % It is assumed here that if Flag1 = 1, the content would pin the
    % occupant to the ground, and thus further analyses was not required.
    % Hence, check if occupant was not struck by toppling contents
    if Flag1 == 0||Flag1 == 2
        % Rearrange content layout in room at time of falling
        [ContentCoordinate2,ContentBehaviour2]=...
            ContentsRearrange(ContentCoordinate,ContentBehaviour,...
            Datainputs,tf,Floor);
        % Predict direction that occupants fell
        FallAngle = rand(1)*2*pi;
        % Perform falling analysis
        [BodyAngle,ImpactV2,BIR2,Flag2]=FallInjury(ContentCoordinate2,...
            Height,FallAngle,OC);
        % Assess injuries due to toppling contents after occupant falls
        [ImpactV3,BIR3,Flag3] = PostFallInjuryRock(ContentCoordinate2,...
            ContentBehaviour2,Height,OC,FallAngle,Datainputs,Floor,...
            BodyAngle);
        % Note that there are two possible outcomes from using
        % PostFallInjuryRock, either (i) the occupant was struck by
        % toppling contents (Flag3>0), or (ii) they weren't. In the latter
        % case, further sliding analyses is required
        if Flag3 == 0
            [ImpactV3,BIR3,Flag3] = ...
                PostFallInjurySlide(ContentCoordinate,ContentBehaviour,...
                Height,OC,FallAngle,Datainputs,Floor,tf,BodyAngle);
        end
    end
```

```
end

% If the occupant falls, then the sequence of events needs to be considered
% in ImpactV and BIR.
if Flag==0||Flag1==0||Flag1==2  % If occupant falls before being injured
    BIR=[BIR1,ones(length(BIR1(:,1)),1)*1,ones(length(BIR1(:,1)),1)*Flag1;
        BIR2,ones(length(BIR2(:,1)),1)*0,ones(length(BIR2(:,1)),1)*Flag2;
        BIR3,ones(length(BIR3(:,1)),1)*2,ones(length(BIR3(:,1)),1)*Flag3];
    ImpactV = [ImpactV1;ImpactV2;ImpactV3];
elseif Flag==0||Flag1 == 1      % If occupant was struck by toppling
                                % contents prior to falling
    BIR=[BIR1,ones(length(BIR1(:,1)),1)*1,ones(length(BIR1(:,1)),1)*Flag1];
    ImpactV = ImpactV1;
end
%--------------------------------------------------------------------------
%--------------------------------------------------------------------------

%--------------------------------------------------------------------------
%--------------------------------------------------------------------------
% function [ContentCoordinate2,ContentBehaviour2]=...
% ContentsRearrange(ContentCoordinate,ContentBehaviour,Fileinputs,tf,Floor)
%
% Purpose
% To update the position of contents at the time which the occupant fell
% Inputs
% ContentCoordinate - Information on location and position of contents
% ContentBehaviour  - Information on likely behaviour of contents
% Datainputs        - Input data of interest (defined in
%                     ContentBehaviour)
% tf                - Time at which occupants fell
% Floor             - Floor level of interest
%
% Outputs
% ContentCoordinate2- Updated content location/position information
% ContentBehaviour2 - Updated content behaviour information
%--------------------------------------------------------------------------

function [ContentCoordinate2,ContentBehaviour2]=...
    ContentsRearrange(ContentCoordinate,ContentBehaviour,Datainputs,...
    tf,Floor)

%Retain first line in new output, which contains description of file input
ContentCoordinate2(1,:)=ContentCoordinate(1,:);
ContentBehaviour2(1,:)=ContentBehaviour(1,:);

%Run for each content
for i = 1:length(ContentBehaviour(1,:))
    % Read content behaviour data
    CB = ContentBehaviour{2,i};

    % Retain data if content is not able to topple or slide
    if CB(1)==0
        ContentCoordinate2(2,i)=ContentCoordinate(2,i);
        ContentBehaviour2(2,i)=ContentBehaviour(2,i);

    % Consideration of contents prone to toppling
    elseif CB(1)==1
        % Read content response file
        Temp = Datainputs{CB(3)};
        % If content does not fully topple by tf, retain data
```

```
        if max(abs(Temp(find(Temp(:,1)<tf),Floor+2)))<1.56||CB(5)~=0
            ContentCoordinate2(2,i)=ContentCoordinate(2,i);
            ContentBehaviour2(2,i)=ContentBehaviour(2,i);
        else
            % If content fell in south direction
            if CB(2)==2
                Temp = ContentCoordinate{2,i};
                NewH=max(Temp(2:length(Temp(:,1)),2))...
                    -min(Temp(2:length(Temp(:,1)),2));
                Temp(find(Temp(2:Temp(1,2)+1,2)==...
                    max(Temp(2:Temp(1,2)+1,2)))+1,2)=...
                    min(Temp(2:Temp(1,2)+1,2))-Temp(1,1);
                Temp(1,1)=NewH;
                ContentCoordinate2{2,i}=Temp;
                CB(1)=0;     % Change content behaviour to static, since it
                             % already toppled
                ContentBehaviour2{2,i}=CB;
            % If content fell in north direction
            elseif CB(2)==1
                Temp = ContentCoordinate{2,i};
                NewH=max(Temp(2:length(Temp(:,1)),2))-...
                    min(Temp(2:length(Temp(:,1)),2));
                Temp(find(Temp(2:Temp(1,2)+1,2)==...
                    min(Temp(2:Temp(1,2)+1,2)))+1,2)=...
                    max(Temp(2:Temp(1,2)+1,2))+Temp(1,1);
                Temp(1,1)=NewH;
                ContentCoordinate2{2,i}=Temp;
                CB(1)=0;     % Change content behaviour to static, since it
                             % already toppled
                ContentBehaviour2{2,i}=CB;
            end
            % NOTE - contents falling in east and west direction not
            % considered at this stage due to it not being required for the
            % case studies
        end

    % Consideration of sliding contents
    elseif CB(1)==2
        % Read content response file
        Temp = Datainputs{CB(3)};
        % Obtain slide displacement at time of occupants falling
        Disp = interp1(Temp(:,1),Temp(:,Floor+2),tf);
        % If content slid in west direction
        if CB(2)==4
            Temp = ContentCoordinate{2,i};
            Temp(2:Temp(1,2)+1,1)=Temp(2:Temp(1,2)+1,1)+Disp;
            ContentCoordinate2{2,i}=Temp;
            ContentBehaviour2(2,i)=ContentBehaviour(2,i);
        end
        % NOTE - contents sliding in north, south, and est direction not
        % considered at this stage due to it not being required for the
        % case studies
    end
end
%--------------------------------------------------------------------------
%--------------------------------------------------------------------------

%--------------------------------------------------------------------------
%--------------------------------------------------------------------------
% function [BodyAngle,ImpactV,BIR,Flag]=...
%     FallInjury(ContentCoordinate,Height,FallAngle,OC)
```

```
%
% Purpose
% To assess the consequence of injuries caused by occupants falling
%
% Inputs
% ContentCoordinate - Information on location and position of contents
% Height            - Occupant's height
% FallAngle         - Angle at which occupants fell
% OC                - Occupant's coordinates
%
% Outputs
% BodyAngle         - Occupant's body position after falling relative to
%                     vertical
% ImpactV           - Impact velocity
% BIR               - N by 3 matrix detailing the boundary impact
%                     conditions. (1) Location of lower impact on occupant
%                     as a ratio of total occupant height, (ii) location of
%                     upper impact, and (iii)impact mass
%-------------------------------------------------------------------------

function [BodyAngle,ImpactV,BIR,Flag]=...
    FallInjury(ContentCoordinate,Height,FallAngle,OC)

% Initial setup
BIR = [-2 -2 0];
ImpactV = 0;

% Convert fall direction to slope in 2D plane (birds eye view perspective)
m1 = 1/tan(FallAngle);

% Set body angle to pi/2 relative to vertical. Update with analyses
% (should decrease or remain pi/2)
BodyAngle = pi/2;

% Identifying if there are any contents present in the direction which the
% occupant falls in
[M N] = size(ContentCoordinate);        % Determining number of contents
for i = 1:N                             % Cycle analyses for all contents
    TempC = ContentCoordinate{2,i};     % Read content information
    NumC = TempC(1,2);                  % Number of corners of content
    TempC(NumC+2,:) = TempC(2,:);       % Extracting coordinates
    CC = TempC(2:length(TempC(:,1)),:);
    CC(NumC+1,:) = CC(1,:);
    Test = 0;                           % Check if content is in direction
                                        % of occupant falling (remain 0
                                        % if not)

    % Check if any contents present if occupant fell in NE direction
    if FallAngle<=pi/2
        % Check if any of the content's corners are in direction which
        % occupant fell
        if max(CC(:,1))>OC(1)&&max(CC(:,2))>OC(2)&&...
                min(CC(:,1))<OC(1)+Height*abs(sin(FallAngle))&&...
                min(CC(:,2))<OC(2)+Height*abs(cos(FallAngle))
            if min(CC(:,1))<OC(1)
                CC(find(CC(:,1)<OC(1)),1)=OC(1);
            end
            if min(CC(:,2))<OC(2)
                CC(find(CC(:,2)<OC(2)),2)=OC(2);
            end
```

```
        % Check if angle which occupant fell is possible to impact
        % content (not accounting for distance yet)
        CCAngle = atan((CC(:,1)-OC(1))./(CC(:,2)-OC(2)));
        if min(CCAngle)<FallAngle && max(CCAngle)>FallAngle
            Test = 1;
        end
    end
% Check if any contents present if occupant fell in SE direction
elseif FallAngle<=pi
    % Check if any of the content's corners are in direction which
    % occupant fell
    if max(CC(:,1))>OC(1)&&min(CC(:,2))<OC(2)&&...
            min(CC(:,1))<OC(1)+Height*abs(sin(FallAngle))&&...
            max(CC(:,2))>OC(2)-Height*abs(cos(FallAngle))
        if min(CC(:,1))<OC(1)
            CC(find(CC(:,1)<OC(1)),1)=OC(1);
        end
        if max(CC(:,2))>OC(2)
            CC(find(CC(:,2)>OC(2)),2)=OC(2);
        end
        % Check if angle which occupant fell is possible to impact
        % content (not accounting for distance yet)
        CCAngle = atan((CC(:,1)-OC(1))./(CC(:,2)-OC(2)));
        CCAngle(find(CCAngle<0))=CCAngle(find(CCAngle<0))+pi;
        if min(CCAngle)<FallAngle && max(CCAngle)>FallAngle
            Test = 2;
        end
    end
% Check if any contents present if occupant fell in SW direction
elseif FallAngle<=3*pi/2
    % Check if any of the content's corners are in direction which
    % occupant fell
    if min(CC(:,1))<OC(1)&&min(CC(:,2))<OC(2)&&...
            max(CC(:,1))>OC(1)-Height*abs(sin(FallAngle))&&...
            max(CC(:,2))>OC(2)-Height*abs(cos(FallAngle))
        if max(CC(:,1))>OC(1)
            CC(find(CC(:,1)>OC(1)),1)=OC(1);
        end
        if max(CC(:,2))>OC(2)
            CC(find(CC(:,2)>OC(2)),2)=OC(2);
        end
        % Check if angle which occupant fell is possible to impact
        % content (not accounting for distance yet)
        CCAngle = abs(atan((CC(:,1)-OC(1))./(CC(:,2)-OC(2))))+pi;
        if min(CCAngle)<FallAngle && max(CCAngle)>FallAngle
            Test = 3;
        end
    end
% Check if any contents present if occupant fell in NW direction
else
    % Check if any of the content's corners are in direction which
    % occupant fell
    if min(CC(:,1))<OC(1)&&max(CC(:,2))>OC(2)&&...
            max(CC(:,1))>OC(1)-Height*abs(sin(FallAngle))&&...
            min(CC(:,2))<OC(2)+Height*abs(cos(FallAngle))
        if max(CC(:,1))>OC(1)
            CC(find(CC(:,1)>OC(1)),1)=OC(1);
        end
        if min(CC(:,2))<OC(2)
            CC(find(CC(:,2)<OC(2)),2)=OC(2);
        end
```

```
        % Check if angle which occupant fell is possible to impact
        % content (not accounting for distance yet)
        CCAngle = atan((CC(:,1)-OC(1))./(CC(:,2)-OC(2)))+2*pi;
        if min(CCAngle)<FallAngle && max(CCAngle)>FallAngle
            Test = 4;
        end
    end
end

% Checking if occupant had fallen onto contents (Note, only comments
% were included for this case. Subsequent cases follow the same
% approach)
if Test>0
    for j = 1:NumC
        % Check cases where line joining 2 coordinates is horizontal
        if TempC(j+1,2)-TempC(j+2,2)==0
            y = TempC(j+1,2);           % y coordinate is constant
            x = (y-OC(2))/m1+OC(1);     % required x coordinate if
                                        % occupant were to land on
                                        % contents
            if x<=max(TempC(j+1:j+2,1))&&x>=min(TempC(j+1:j+2,1))
                % If occupant fell in NE direction
                if Test==1
                    % Check if there is potential for occupant to land
                    % onto content
                    if x>=OC(1)&&y>=OC(2)
                        % Calculate distance between occupant and
                        % content
                        Dist = sqrt((x-OC(1))^2+(y-OC(2))^2);
                        % Check if occupant lands on content
                        if Dist<Height
                            % Determine the height of impact from
                            % ground
                            ImpactHeight = sqrt(Height^2-Dist^2);
                            % If impact height was less than height of
                            % content, calculate respective body angles
                            % and location of impact
                            if ImpactHeight<TempC(1,1)
                                NewBodyAngle=atan(Dist/ImpactHeight);
                                NewBodyImpact = ImpactHeight/...
                                    cos(NewBodyAngle);
                            % If impact height was greater than height
                            % of content, calculate respective body
                            % angles and location of impact
                            else
                                NewBodyAngle=atan(Dist/TempC(1,1));
                                NewBodyImpact = TempC(1,1)/...
                                    cos(NewBodyAngle);
                            end
                            % Update body angle, and define body impact
                            % locations
                            if NewBodyAngle<BodyAngle
                                BodyAngle=NewBodyAngle;
                                BIR(1,:) = [NewBodyImpact,...
                                    NewBodyImpact -1];
                                % Set Flag to 3 to indicate that
                                % occupants fell onto contents
                                Flag = 3;
                            end
                        end
                    end
```

```
% If occupant fell in SE direction
elseif Test==2
    if x>=OC(1)&&y<=OC(2)
        Dist = sqrt((x-OC(1))^2+(y-OC(2))^2);
        if Dist<Height
            ImpactHeight = sqrt(Height^2-Dist^2);
            if ImpactHeight<TempC(1,1)
                NewBodyAngle=atan(Dist/ImpactHeight);
                NewBodyImpact = ImpactHeight/...
                    cos(NewBodyAngle);
            else
                NewBodyAngle=atan(Dist/TempC(1,1));
                NewBodyImpact = TempC(1,1)/...
                    cos(NewBodyAngle);
            end
            if NewBodyAngle<BodyAngle
                BodyAngle=NewBodyAngle;
                BIR(1,:) = [NewBodyImpact,...
                    NewBodyImpact -1];
                Flag = 3;
            end
        end
    end
% If occupant fell in SW direction
elseif Test==3
    if x<=OC(1)&&y<=OC(2)
        Dist = sqrt((x-OC(1))^2+(y-OC(2))^2);
        if Dist<Height
            ImpactHeight = sqrt(Height^2-Dist^2);
            if ImpactHeight<TempC(1,1)
                NewBodyAngle=atan(Dist/ImpactHeight);
                NewBodyImpact = ImpactHeight/...
                    cos(NewBodyAngle);
            else
                NewBodyAngle=atan(Dist/TempC(1,1));
                NewBodyImpact = TempC(1,1)/...
                    cos(NewBodyAngle);
            end
            if NewBodyAngle<BodyAngle
                BodyAngle=NewBodyAngle;
                BIR(1,:) = [NewBodyImpact,...
                    NewBodyImpact -1];
                Flag = 3;
            end
        end
    end
% If occupant fell in NW direction
elseif Test==4
    if x<=OC(1)&&y>=OC(2)
        Dist = sqrt((x-OC(1))^2+(y-OC(2))^2);
        if Dist<Height
            ImpactHeight = sqrt(Height^2-Dist^2);
            if ImpactHeight<TempC(1,1)
                NewBodyAngle=atan(Dist/ImpactHeight);
                NewBodyImpact = ImpactHeight/...
                    cos(NewBodyAngle);
            else
                NewBodyAngle=atan(Dist/TempC(1,1));
                NewBodyImpact = TempC(1,1)/...
                    cos(NewBodyAngle);
            end
```

```
                    if NewBodyAngle<BodyAngle
                        BodyAngle=NewBodyAngle;
                        BIR(1,:) = [NewBodyImpact,...
                            NewBodyImpact -1];
                        Flag = 3;
                    end
                end
            end
        end
    end

% Check cases where line joining 2 coordinates is vertical
elseif TempC(j+1,1)-TempC(j+2,1)==0
    x = TempC(j+1,1);           % x coordinate is constant
    y = m1*(x-OC(1))+OC(2);     % Required y coordinate if
                                % occupant were to land on
                                % contents
    if y<=max(TempC(j+1:j+2,2))&&y>=min(TempC(j+1:j+2,2))
        % If occupant fell in NE direction
        if Test==1
            if x>=OC(1)&&y>=OC(2)
                Dist = sqrt((x-OC(1))^2+(y-OC(2))^2);
                if Dist<Height
                    ImpactHeight = sqrt(Height^2-Dist^2);
                    if ImpactHeight<TempC(1,1)
                        NewBodyAngle=atan(Dist/ImpactHeight);
                        NewBodyImpact = ImpactHeight...
                            /cos(NewBodyAngle);
                    else
                        NewBodyAngle=atan(Dist/TempC(1,1));
                        NewBodyImpact = TempC(1,1)...
                            /cos(NewBodyAngle);
                    end
                    if NewBodyAngle<BodyAngle
                        BodyAngle=NewBodyAngle;
                        BIR(1,:) = [NewBodyImpact,...
                            NewBodyImpact -1];
                        Flag = 3;
                    end
                end
            end
        % If occupant fell in SE direction
        elseif Test==2
            if x>=OC(1)&&y<=OC(2)
                Dist = sqrt((x-OC(1))^2+(y-OC(2))^2);
                if Dist<Height
                    ImpactHeight = sqrt(Height^2-Dist^2);
                    if ImpactHeight<TempC(1,1)
                        NewBodyAngle=atan(Dist/ImpactHeight);
                        NewBodyImpact = ImpactHeight/...
                            cos(NewBodyAngle);
                    else
                        NewBodyAngle=atan(Dist/TempC(1,1));
                        NewBodyImpact = TempC(1,1)/...
                            cos(NewBodyAngle);
                    end
                    if NewBodyAngle<BodyAngle
                        BodyAngle=NewBodyAngle;
                        BIR(1,:) = [NewBodyImpact,...
                            NewBodyImpact -1];
                        Flag = 3;
```

```
                        end
                    end
                end
            % If occupant fell in SW direction
            elseif Test==3
                if x<=OC(1)&&y<=OC(2)
                    Dist = sqrt((x-OC(1))^2+(y-OC(2))^2);
                    if Dist<Height
                        ImpactHeight = sqrt(Height^2-Dist^2);
                        if ImpactHeight<TempC(1,1)
                            NewBodyAngle=atan(Dist/ImpactHeight);
                            NewBodyImpact = ImpactHeight/...
                                cos(NewBodyAngle);
                        else
                            NewBodyAngle=atan(Dist/TempC(1,1));
                            NewBodyImpact = TempC(1,1)/...
                                cos(NewBodyAngle);
                        end
                        if NewBodyAngle<BodyAngle
                            BodyAngle=NewBodyAngle;
                            BIR(1,:) = [NewBodyImpact,...
                                NewBodyImpact -1];
                            Flag = 3;
                        end
                    end
                end
            % If occupant fell in NW direction
            elseif Test==4
                if x<=OC(1)&&y>=OC(2)
                    Dist = sqrt((x-OC(1))^2+(y-OC(2))^2);
                    if Dist<Height
                        ImpactHeight = sqrt(Height^2-Dist^2);
                        if ImpactHeight<TempC(1,1)
                            NewBodyAngle=atan(Dist/ImpactHeight);
                            NewBodyImpact = ImpactHeight/...
                                cos(NewBodyAngle);
                        else
                            NewBodyAngle=atan(Dist/TempC(1,1));
                            NewBodyImpact = TempC(1,1)/...
                                cos(NewBodyAngle);
                        end
                        if NewBodyAngle<BodyAngle
                            BodyAngle=NewBodyAngle;
                            BIR(1,:) = [NewBodyImpact,...
                                NewBodyImpact -1];
                            Flag = 3;
                        end
                    end
                end
            end
        % Note that cases wherethe line connecting two coordinates
        % is neither horizontal nor vertical is not currently
        % considered
    end
end
end

% Calculate angular velocity based on Body Angle
vel=sqrt((1-cos(BodyAngle))*16*9.81/4.7/Height);
```

```
% Format results for output into INJURYSource function file
if BIR(2)>0                             % If occupants fell onto contents
    ImpactV = vel*BIR(1:2);             % Convert angular velocity to impact
                                        % velocity
    BIR(:,1:2)=BIR(:,1:2)/Height;       % Obtain impact locations on occupant
                                        % based on a ratio of occupant's height

else                                    % If occupants fel onto floor instead
    if rand<0.5                         % Assume 50% chance of them landing on
                                        % their hips
        BIR(1,:) = [4.35/8 4.35/8 -1];
    else                                % Assume 50% chance of them landing
                                        % on their hands/shoulders
        BIR(1,:) = [-1 6.7/8 -1];
    end
    % Calculate impact velocity for cases were occupants fell to floor
    ImpactV = vel*BIR(2)*ones(1,2)*Height;
    % Set Flag to 4 to indicate that occupants fell to floor
    Flag = 4;
end
%--------------------------------------------------------------------------
%--------------------------------------------------------------------------

%--------------------------------------------------------------------------
%--------------------------------------------------------------------------
% function [BIR,ImpactV] = PostFallInjuryRock(ContentCoordinate,...
%     ContentBehaviour,Height,OC,FallAngle,Fileinputs,Floor)
% Written by Trevor Yeow
% Version 0.5 - WORK IN PROGRESS
%
% Purpose
% This code assesses the potental for injury from contents toppling onto
% occupants who had previously fallen onto the floor.
%
% Inputs
% ContentCoordinate - {} matrix with two rows, where the top row contains
%                     the name of the contents, the second row contains
%                     a matrix of content coordinates and height, while
%                     each column represents each individual content. The
%                     matrix should contain the following information:
%                       Row 1 - Content height and number of coordinates
%                       (nc)
%                       Row 2 - x and y coordinates of first point
%                       Row nc+1 - x and y coordinates of point nc
%                     NOTE: coordinates should be specified going in either
%                     a clockwise or anticlockwise direction. Any other
%                     specification (e.g. left-right, then up-down) will
%                     cause the code to misinterpret the dimensions of the
%                     content.
%       e.g.     DeskProp = [0.5,4;0 0;1 0;1 1;0 1];
%                ContentCoordinate = {'Desk';DeskProp};
%
%               Point 4(0,1) _______ Point 3(1,1)
%                           |       |
%                           | Desk  |
%                           |       |
%               Point 1(0,0)|_______|Point 2(1,0)
%
% ContentBehaviour - Similar format to ContentCoordinate, except that the
%                    second row should contain a row of 5 numbers, where
```

```
%                       first entry - type of content (1 = rocking, 2 =
%                                     sliding)
%                       second entry- direction (1 = N-S, 2 = E-w)
%                       third entry - file ID for displacement/rotation
%                                     response
%                       fourth entry- file ID for velocity/angular velocity
%                                     response
%                       fifth entry - maximum allowable rotation response.
%                                     Note that this is only used for
%                                     rocking cases, as it is assumed this
%                                     would've been accounted for in
%                                     sliding analyses
%                       sixth entry - content's mass
%
% Fileinputs - input of data files. The first file should contain peak
%              total floor acceleration response history. The rest is up to
%              the user, as long as it is consistent with the entries in
%              ContentBehaviour
%
% OC         - Occupant location's coordinate
% Height     - Occupant's height
% Floor      - Floor which room is being considered
%--------------------------------------------------------------------------
% Outputs
%
% ImpactV    - impact velocity for each impact occurrence
%               Entry 1 - impact velocity at lowest point of contact
%               Entry 2 - impact velocity at highest point of contact
% BIR        - A row of three numbers describing the impact scenario
%               Entry 1 - lowest point of contact on body
%               Entry 2 - highest point of contact on body
%               Entry 3 - effective mass acting on body
%--------------------------------------------------------------------------
%--------------------------------------------------------------------------

function [ImpactV,BIR,Flag] = PostFallInjuryRock(ContentCoordinate,...
    ContentBehaviour,Height,OC,FallAngle,Datainputs,Floor,BodyAngle)

% Set initial parameters
counterC = 0;       % Check number of impact cases (set to 0 initially)
BIR = [-2 -2 0];    % Initial BIR data
ImpactV = [0 0];    % Impact velocity initial setup
Flag = 0;           % Set injury type flag to 0
EffHeight = Height*sin(BodyAngle);  % Obtain occupant's effective height

%--------------------------------------------------------------------------
% Cycle through all contents
for i = 1:length(ContentBehaviour(1,:))
  counter = 0;                    % Set initial counter to 0 for use in
                                  % cases where occupants were located
                                  % outside of fallzones
  IVTemp = 0;                     % Initial impact velocity = 0
  BIRTemp = 0;                    % Initial impact location = 0
  CB = ContentBehaviour{2,i};     % Read content behaviour details
  if CB(1)==1                     % Only consider contents prone to
                                  %toppling
     Temp = Datainputs{CB(3)};
     RotRH = Temp(:,Floor+2);           % Obtain rotation response
                                        % history
     if max(abs(RotRH))>1.56&&CB(5)==0  % Only consider contents that
                                        % overturned fully
```

```
if CB(2)==1      %Content topples in N direction (VERIFIED)
   %Fallzone Details (i.e. coordinates if content had toppled)
   FZ = ContentCoordinate{2,i};
   FZ(find(FZ(2:FZ(1,2)+1,2)==min(FZ(2:FZ(1,2)+1,2)))+1,2)...
      =max(FZ(2:FZ(1,2)+1,2))+FZ(1,1);
   FZ(FZ(1,2)+2,:) = FZ(2,:);

   %Check if occupant is already within fallzone
   if OC(1)<=max(FZ(2:FZ(1,2)+1,1))&&...
      OC(1)>=min(FZ(2:FZ(1,2)+1,1))&&...
      OC(2)<=max(FZ(2:FZ(1,2)+1,2))&&...
      OC(2)>=min(FZ(2:FZ(1,2)+1,2))

      %Check direction of content falling
      for j = 1:FZ(1,2)
          %Check intercept to horizontal lines in north
          %direction
          if FZ(j+1,2)-FZ(j+2,2)==0
             if FZ(j+1,2)==max(FZ(2:FZ(1,2)+2,2))
                if FallAngle<pi/2||FallAngle>=3*pi/2
                   % Obtain x and y coordinates
                   y = FZ(j+1,2)-OC(2);
                   x = y*tan(FallAngle);
                   % Check if occupant's body does cross
                   % the horizontal line
                   if sqrt(y^2+x^2)<EffHeight&&...
                      OC(1)+x<max(FZ(2:FZ(1,2)+2,1))&&...
                      OC(1)+x>min(FZ(2:FZ(1,2)+2,1))
                      % Check that the intercept does
                      % occur in the North direction
                      if (FallAngle<=pi&&x>=0)||...
                          (FallAngle>=pi&&x<=0)
                         % Impact occurs, increase counter
                         counter = counter+1;
                         Temp = Datainputs{CB(4)};
                         % Obtain impact angular velocity
                         RotVH = Temp(:,Floor+2);
                         counterC = counterC+1;
                         % Obtain impact mass
                         Mass = (max(FZ(2:FZ(1,2)+2,2))*3/4-...
                             min(FZ(2:FZ(1,2)+2,2))/2-OC(2)/4)/...
                             (max(FZ(2:FZ(1,2)+2,2))-...
                             min(FZ(2:FZ(1,2)+2,2)))*CB(6);
                         % Obtain impact location and mass
                         BIR(counterC,:) = [0, sqrt(x^2+y^2),...
                             Mass];
                         % Calculate impact velocity acting on
                         % occupant
                         ImpactV(counterC,:) =...
                             abs(RotVH(length(RotVH(:,1))))*...
                             [(OC(2)-...
                             min(FZ(2:length(FZ(:,1)),2))),...
                             max(FZ(2:FZ(1,2)+2,2))-...
                             min(FZ(2:FZ(1,2)+2,2))];
                         % Flag to indicate that occupants were
                         % struck by contents after they had
                         % previously fallen
                         Flag = 5;
                      end
                   end
```

```
            end
         end
      %Check intercept to vertical lines (note that process is
      %similar to intercept with horizontal lines. As such no
      %comments are given here)
      elseif FZ(j+1,1)-FZ(j+2,1)==0
         x = FZ(j+1,1)-OC(1);
         if (FallAngle<=pi&&x>=0)||(FallAngle>=pi&&x<=0)
            y = x/tan(FallAngle);
            if sqrt(y^2+x^2)<EffHeight&&...
               OC(2)+y<max(FZ(2:length(FZ(:,1)),2))&&...
               OC(2)+y>min(FZ(2:length(FZ(:,1)),2))
               if (FallAngle<pi&&x>0)||(FallAngle>pi&&x<0)
                  counter = counter+1;
                  Temp = Datainputs{CB(4)};
                  RotVH = Temp(:,Floor+2);
                  counterC = counterC+1;
                  Mass = (max(FZ(2:length(FZ(:,1)),2))-...
                         min(FZ(2:length(FZ(:,1)),2))/2-...
                         (OC(2)+y/2)/2)/...
                         (max(FZ(2:length(FZ(:,1)),2))-...
                         min(FZ(2:length(FZ(:,1)),2)))*...
                         CB(6);
                  BIR(counterC,:) = [0 sqrt(x^2+y^2) Mass];
                  if y<0
                     ImpactV(counterC,:) =...
                         abs(RotVH(length(RotVH(:,1))))*...
                         [(OC(2)-...
                         min(FZ(2:length(FZ(:,1)),2))+y),...
                         (OC(2)-min(FZ(2:length(FZ(:,1)),2)))];
                  else
                     ImpactV(counterC,:) =...
                        abs(RotVH(length(RotVH(:,1))))*...
                        [(OC(2)-...
                        min(FZ(2:length(FZ(:,1)),2))),...
                        (OC(2)-min(FZ(2:length(FZ(:,1)),2))+y)]
                  end
                  Flag = 5;
               end
            end
         end
      end
   end

   %If whole of occupant's body is trapped under content
   if counter == 0
      counterC = counterC+1;
      Temp = Datainputs{CB(4)};
      RotVH = Temp(:,Floor+2);
      % Calculate impact mass
      y = min(FZ(2:length(FZ(:,1)),2))-OC(2);
      Mass = (max(FZ(2:length(FZ(:,1)),2))-...
              OC(2)/2-max(y,EffHeight*cos(FallAngle))/4-...
              min(FZ(2:length(FZ(:,1)),2))/2)/...
             (max(FZ(2:length(FZ(:,1)),2))-...
              min(FZ(2:length(FZ(:,1)),2)))*CB(6);
      BIR(counterC,:) = [0 EffHeight Mass];
      % Determine impact velocity if occupant's head is resting
      % against content
      if EffHeight>=OC(2)-min(FZ(2:length(FZ(:,1)),2))
         ImpactV(counterC,:) =...
```

```
                [abs(RotVH(length(RotVH(:,1))))*...
                abs(OC(2)-min(FZ(2:length(FZ(:,1)),2))) 0];
        else
            % Determine impact velocity if occupant's head is not
            % resting against content
            ImpactV(counterC,:) =...
                abs(RotVH(length(RotVH(:,1))))*...
                [abs(OC(2)-min(FZ(2:length(FZ(:,1)),2))),...
                abs(OC(2)+EffHeight*cos(FallAngle)-...
                min(FZ(2:length(FZ(:,1)),2)))];
        end
        Flag = 5;
    end

%For cases where occupant was outside of fallzone
else
    for j = 1:FZ(1,2)
        % Check for intercept with vertical
        if FZ(j+1,2)-FZ(j+2,2)==0
            if FZ(j+1,2)==max(FZ(2:FZ(1,2)+2,2))
                % Same process as before for crossing vertical line
                y = FZ(j+1,2)-OC(2);
                x = y*tan(FallAngle);
                if (FallAngle<=pi&&x>0)||(FallAngle>=pi&&x<0)
                    if x+OC(1)>min(FZ(2:FZ(1,2)+2,1))&&...
                        x+OC(1)<max(FZ(2:FZ(1,2)+2,1))&&...
                        sqrt(x^2+y^2)<EffHeight
                        counter = counter+1;
                        Temp = Datainputs{CB(4)};
                        RotVH = Temp(:,Floor+2);
                        BIRTemp(counter)=sqrt(x^2+y^2);
                        IVTemp(counter)=...
                            abs(RotVH(length(RotVH(:,1))))*...
                            (max(FZ(2:FZ(1,2)+2,2))-...
                            min(FZ(2:FZ(1,2)+2,2)));
                    end
                end
            end
            % Check for intercept with horizontal
        elseif FZ(j+1,1)-FZ(j+2,1)==0
            x = FZ(j+1,1)-OC(1);
            y = x/tan(FallAngle);
            % Same process as before for crossing horizontal line
            if (FallAngle<pi&&x>0)||(FallAngle>pi&&x<0)
                if y+OC(2)>min(FZ(2:FZ(1,2)+2,2))&&...
                    y+OC(2)<max(FZ(2:FZ(1,2)+2,2))&&...
                    sqrt(x^2+y^2)<EffHeight
                    counter = counter+1;
                    Temp = Datainputs{CB(4)};
                    RotVH = Temp(:,Floor+2);
                    BIRTemp(counter)=sqrt(x^2+y^2);
                    IVTemp(counter)=...
                        abs(RotVH(length(RotVH(:,1))))*...
                        (-min(FZ(2:length(FZ(:,1)),2))+OC(2)+y);
                end
            end
        end
    end

    % Calculate impact mass and velocity if occupant only crosses
    % one of the content's edges
```

```
                if counter == 1
                   counterC = counterC+1;
                   MAXY = max(FZ(2:length(FZ(:,1)),2));
                   MINY = min(FZ(2:length(FZ(:,1)),2));
                   Mass = (MAXY-MINY/2-OC(2)/2-BIRTemp*cos(FallAngle)/4-...
                          max(EffHeight*cos(FallAngle),...
                          MINY-OC(2))/4)/(MAXY-MINY)*CB(6);
                   BIR(counterC,:) = [BIRTemp EffHeight Mass];
                   ImpactV(counterC,:) =...
                       [IVTemp,abs(RotVH(length(RotVH(:,1))))*...
                       (max(FZ(2:length(FZ(:,1)),2))-...
                       OC(2)-min(EffHeight*cos(FallAngle),...
                       max(FZ(2:length(FZ(:,1)),2))-OC(2)))];
                   Flag = 5;
                % Calculate impact mass and velocity if occupant crosses
                % two of the content's edges
                elseif counter == 2
                   counterC = counterC+1;
                   Mass = (max(FZ(2:length(FZ(:,1)),2))-...
                          min(FZ(2:length(FZ(:,1)),2))/2-...
                          (OC(2)+mean(BIRTemp)*cos(FallAngle))/2)/...
                          (max(FZ(2:length(FZ(:,1)),2))-...
                          min(FZ(2:length(FZ(:,1)),2)))*CB(6);
                   BIR(counterC,:) = [min(BIRTemp) max(BIRTemp) Mass];
                   ImpactV(counterC,:) =...
                       [IVTemp(find(BIRTemp==min(BIRTemp)))...
                       IVTemp(find(BIRTemp==max(BIRTemp)))]; %#ok<FNDSB>
                   Flag = 5;
                end
             end
%-------------------------------------------------------------------------
          %Content topples in S direction (VERIFIED, note that process is
          %similar to that in N direction, so no detailed comments provided
          %herein)
          elseif CB(2)==2
             %Fallzone Details
                FZ = ContentCoordinate{2,i};
                FZ(find(FZ(2:FZ(1,2)+1,2)==max(FZ(2:FZ(1,2)+1,2)))+1,2)=...
                    min(FZ(2:FZ(1,2)+1,2))-FZ(1,1);
                FZ(FZ(1,2)+2,:) = FZ(2,:);

                %Check if occupant is already within fallzone
                if OC(1)<=max(FZ(2:FZ(1,2)+1,1))&&...
                   OC(1)>=min(FZ(2:FZ(1,2)+1,1))&&...
                   OC(2)<=max(FZ(2:FZ(1,2)+1,2))&&...
                   OC(2)>=min(FZ(2:FZ(1,2)+1,2))

                   %Check direction of content falling
                   for j = 1:FZ(1,2)
                      %Check intercept to horizontal lines
                      if FZ(j+1,2)-FZ(j+2,2)==0
                         if FZ(j+1,2)==min(FZ(2:FZ(1,2)+2,2))
                            if FallAngle>pi/2&&FallAngle<=3*pi/2
                               y = FZ(j+1,2)-OC(2);
                               x = y*tan(FallAngle);
                               if sqrt(y^2+x^2)<EffHeight&&...
                                  OC(1)+x<max(FZ(2:FZ(1,2)+2,1))&&...
                                  OC(1)+x>min(FZ(2:FZ(1,2)+2,1))
                                  if (FallAngle<=pi&&x>=0)||...
                                          (FallAngle>=pi&&x<=0)
                                     counter = counter+1;
```

```
                    Temp = Datainputs{CB(4)};
                    RotVH = Temp(:,Floor+2);
                    counterC = counterC+1;
                    Mass = (max(FZ(2:FZ(1,2)+2,2))/2-...
                           min(FZ(2:FZ(1,2)+2,2))+...
                           (OC(2)+y/2)/2)/...
                           (max(FZ(2:FZ(1,2)+2,2))-...
                           min(FZ(2:FZ(1,2)+2,2)))*CB(6);
                    BIR(counterC,:) =...
                        [0 sqrt(x^2+y^2) Mass];
                    ImpactV(counterC,:) =...
                        abs(RotVH(length(RotVH(:,1))))*...
                        [(max(FZ(2:length(FZ(:,1)),2))...
                        -OC(2)),max(FZ(2:FZ(1,2)+2,2))-...
                        min(FZ(2:FZ(1,2)+2,2))];
                    Flag = 5;
                end
            end
        end
    end
    %Check intercept to vertical lines
    elseif FZ(j+1,1)-FZ(j+2,1)==0
        x = FZ(j+1,1)-OC(1);
        if (FallAngle<=pi&&x>=0)||(FallAngle>=pi&&x<=0)
            y = x/tan(FallAngle);
            if sqrt(y^2+x^2)<EffHeight&&...
               OC(2)+y<max(FZ(2:length(FZ(:,1)),2))&&...
               OC(2)+y>min(FZ(2:length(FZ(:,1)),2))
               if (FallAngle<pi&&x>0)||(FallAngle>pi&&x<0)
                  counter = counter+1;
                  Temp = Datainputs{CB(4)};
                  RotVH = Temp(:,Floor+2);
                  counterC = counterC+1;
                  Mass = (max(FZ(2:length(FZ(:,1)),2))/2-...
                         min(FZ(2:length(FZ(:,1)),2))+...
                         (OC(2)+y/2)/2)/...
                         (max(FZ(2:length(FZ(:,1)),2))-...
                         min(FZ(2:length(FZ(:,1)),2)))*CB(6);
                  BIR(counterC,:) = [0 sqrt(x^2+y^2) Mass];
                  if y<0
                     ImpactV(counterC,:) =...
                         abs(RotVH(length(RotVH(:,1))))*...
                         [(max(FZ(2:length(FZ(:,1)),2))...
                         -OC(2)),...
                         (max(FZ(2:length(FZ(:,1)),2))...
                         -OC(2))-y];
                  else
                     ImpactV(counterC,:) =...
                         abs(RotVH(length(RotVH(:,1))))*...
                         [(max(FZ(2:length(FZ(:,1)),2))-...
                         OC(2)-y),...
                         (max(FZ(2:length(FZ(:,1)),2))...
                         -OC(2))];
                  end
                  Flag = 5;
               end
            end
        end
    end
end
%If whole of occupant's body is trapped under content
```

```
    if counter == 0
        counterC = counterC+1;
        Temp = Datainputs{CB(4)};
        RotVH = Temp(:,Floor+2);
        y = max(FZ(2:length(FZ(:,1)),2))-OC(2);
        Mass = (max(FZ(2:length(FZ(:,1)),2))-...
               min(FZ(2:length(FZ(:,1)),2))-...
               (max(FZ(2:length(FZ(:,1)),2))-...
               OC(2)-min(y,EffHeight*cos(FallAngle))/2))/...
               (max(FZ(2:length(FZ(:,1)),2))-...
               min(FZ(2:length(FZ(:,1)),2)))*CB(6);
        BIR(counterC,:) = [0 EffHeight Mass];
        if EffHeight>=max(FZ(2:length(FZ(:,1)),2))-OC(2)
            ImpactV(counterC,:) =...
                [abs(RotVH(length(RotVH(:,1))))*abs(OC(2)-...
                max(FZ(2:length(FZ(:,1)),2))) 0];
        else
            ImpactV(counterC,:) =...
                abs(RotVH(length(RotVH(:,1))))*[abs(OC(2)...
                -max(FZ(2:length(FZ(:,1)),2))),...
                abs(max(FZ(2:length(FZ(:,1)),2))-OC(2)-...
                EffHeight*cos(FallAngle))];
        end
        Flag = 5;
    end
else
    %If occupant is outside fallzone
    for j = 1:FZ(1,2)
        if FZ(j+1,2)-FZ(j+2,2)==0
            if FZ(j+1,2)==min(FZ(2:FZ(1,2)+2,2))
                %Impact vertical line
                y = FZ(j+1,2)-OC(2);
                x = y*tan(FallAngle);
                if (FallAngle<pi&&x>0)||(FallAngle>pi&&x<0)
                    if x+OC(1)>min(FZ(2:FZ(1,2)+2,1))&&...
                       x+OC(1)<max(FZ(2:FZ(1,2)+2,1))&&...
                       sqrt(x^2+y^2)<EffHeight
                       counter = counter+1;
                       Temp = Datainputs{CB(4)};
                       RotVH = Temp(:,Floor+2);
                       BIRTemp(counter)=sqrt(x^2+y^2);
                       IVTemp(counter)=...
                           abs(RotVH(length(RotVH(:,1))))*...
                           (max(FZ(2:FZ(1,2)+2,2))-...
                           min(FZ(2:FZ(1,2)+2,2)));
                    end
                end
            end
        elseif FZ(j+1,1)-FZ(j+2,1)==0
            %Impact horizontal line
            x = FZ(j+1,1)-OC(1);
            y = x/tan(FallAngle);
            if (FallAngle<=pi&&x>0)||(FallAngle>=pi&&x<0)
                if y+OC(2)>min(FZ(2:FZ(1,2)+2,2))&&...
                   y+OC(2)<max(FZ(2:FZ(1,2)+2,2))&&...
                   sqrt(x^2+y^2)<EffHeight
                   counter = counter+1;
                   Temp = Datainputs{CB(4)};
                   RotVH = Temp(:,Floor+2);
                   BIRTemp(counter)=sqrt(x^2+y^2);
                   IVTemp(counter)=...
```

```
                                abs(RotVH(length(RotVH(:,1))))*...
                                (max(FZ(2:length(FZ(:,1)),2))-OC(2)-y);
                            end
                        end
                    end
                end
                % Calculate impact mass and velocity if occupant only
                % crosses one of the content's edges
                if counter == 1
                    counterC = counterC+1;
                    MAXY = max(FZ(2:length(FZ(:,1)),2));
                    MINY = min(FZ(2:length(FZ(:,1)),2));
                    Mass = (MAXY-MINY-...
                           (MAXY-OC(2)-BIRTemp*cos(FallAngle)/2-...
                           min(EffHeight*cos(FallAngle),...
                           MAXY-OC(2))/2)/2)/(MAXY-MINY)*CB(6);
                    BIR(counterC,:) = [BIRTemp EffHeight Mass];
                    ImpactV(counterC,:) = [IVTemp,...
                            abs(RotVH(length(RotVH(:,1))))*...
                            (max(FZ(2:length(FZ(:,1)),2))-...
                            OC(2)-min(EffHeight*cos(FallAngle),...
                            max(FZ(2:length(FZ(:,1)),2))-OC(2)))];
                    Flag = 5;
                % Calculate impact mass and velocity if occupant crosses
                % two of the content's edges
                elseif counter == 2
                        counterC = counterC+1;
                        Mass = (max(FZ(2:length(FZ(:,1)),2))-...
                            min(FZ(2:length(FZ(:,1)),2))-...
                            (max(FZ(2:length(FZ(:,1)),2))-...
                            OC(2)-mean(BIRTemp)*cos(FallAngle))/2)/...
                            (max(FZ(2:length(FZ(:,1)),2))-...
                            min(FZ(2:length(FZ(:,1)),2)))*...
                            CB(6);
                        BIR(counterC,:) = [min(BIRTemp) max(BIRTemp) Mass];
                        ImpactV(counterC,:) =...
                            [IVTemp(find(BIRTemp==min(BIRTemp))),...
                            IVTemp(find(BIRTemp==max(BIRTemp)))];
                        Flag = 5;
                end
            end
        end
    end
end
% Normalize impact locations by occupant height
BIR(:,1:2)=BIR(:,1:2)/EffHeight;
%--------------------------------------------------------------------------
%--------------------------------------------------------------------------

%--------------------------------------------------------------------------
%--------------------------------------------------------------------------
% function [BIR,ImpactV] = PostFallInjurySlide(ContentCoordinate,...
%     ContentBehaviour,Height,OC,FallAngle,Fileinputs,Floor,tf)
% Written by Trevor Yeow
% Version 0.1a - WORK IN PROGRESS
%
% Purpose
% This code assesses the potental for injury from contents sliding and
% impacting occupants who had previously fallen onto the floor.
%
```

```
% !!!!!!!!!!!!!!!!!!!!!!!!!!!!!!!
% WARNING - CURRENTLY THIS VERSION ONLY CONSIDERS CONTENTS SLIDING IN THE
% WEST DIRECTION. THE ABILITY TO CONSIDER CONTENTS SLIDING IN OTHER
% DIRECTIONS ARE STILL IN PROGRESS
% !!!!!!!!!!!!!!!!!!!!!!!!!!!!!!!
%
% Inputs
% ContentCoordinate - {} matrix with two rows, where the top row contains
%                     the name of the contents, the second row contains
%                     a matrix of content coordinates and height, while
%                     each column represents each individual content. The
%                     matrix should contain the following information:
%                       Row 1 - Content height and number of coordinates
%                       (nc)
%                       Row 2 - x and y coordinates of first point
%                       Row nc+1 - x and y coordinates of point nc
%                     NOTE: coordinates should be specified going in either
%                     a clockwise or anticlockwise direction. Any other
%                     specification (e.g. left-right, then up-down) will
%                     cause the code to misinterpret the dimensions of the
%                     content.
%       e.g.     DeskProp = [0.5,4;0 0;1 0;1 1;0 1];
%                ContentCoordinate = {'Desk';DeskProp};
%
%               Point 4(0,1) _______ Point 3(1,1)
%                           |       |
%                           | Desk  |
%                           |       |
%               Point 1(0,0)|_______|Point 2(1,0)
%
% ContentBehaviour - Similar format to ContentCoordinate, except that the
%                    second row should contain a row of 5 numbers, where
%                       first entry - type of content (1 = rocking, 2 =
%                                     sliding)
%                       second entry- direction (1 = N-S, 2 = E-w)
%                       third entry - file ID for displacement/rotation
%                                     response
%                       fourth entry- file ID for velocity/angular velocity
%                                     response
%                       fifth entry - maximum allowable rotation response.
%                                     Note that this is only used for
%                                     rocking cases, as it is assumed this
%                                     would've been accounted for in
%                                     sliding analyses
%                       sixth entry - content's mass
%
% Fileinputs - input of data files. The first file should contain peak
%              total floor acceleration response history. The rest is up to
%              the user, as long as it is consistent with the entries in
%              ContentBehaviour
%
% OC         - Occupant location's coordinate
% Height     - Occupant's height
% Floor      - Floor which room is being considered
%-------------------------------------------------------------------------
% Outputs
%
% ImpactV    - impact velocity for each impact occurrence
%               Entry 1 - impact velocity at lowest point of contact
%               Entry 2 - impact velocity at highest point of contact
% BIR        - A row of three numbers describing the impact scenario
```

```
%               Entry 1 - lowest point of contact on body
%               Entry 2 - highest point of contact on body
%               Entry 3 - effective mass acting on body
%--------------------------------------------------------------------------
%--------------------------------------------------------------------------

function [ImpactV,BIR,Flag] = PostFallInjurySlide(ContentCoordinate,...
    ContentBehaviour,Height,OC,FallAngle,Datainputs,Floor,tf,BodyAngle)

% Set initial parameters
counterC = 0;       % Check number of impact cases (set to 0 initially)
BIR = [-2 -2 0];    % Initial BIR data
ImpactV = [0 0];    % Impact velocity initial setup
Flag = 0;           % Set injury type flag to 0
EffHeight = Height*sin(BodyAngle);  % Obtain occupant's effective height

% Cycle through contents
for i=1:length(ContentBehaviour(2,:))
    FlagS = 0;
    CB = ContentBehaviour{2,i};
    % Only consider contents prone to sliding
    if CB(1)==2
        if CB(2)==4     % If content slides to the west
            CC = ContentCoordinate{2,i};
            CC(CC(1,2)+2,:)=CC(2,:);
            % Perform analyses if occupants do not fall in north and south
            % as this causes error in analyses (very rare for fall angles
            % to be exactly 0 and pi as well)
            if FallAngle~=0||FallAngle~=pi
            % Obtain occupant's coordinates
            OCY1 = OC(2);
            OCY2 = OC(2)+cos(FallAngle)*EffHeight;
            OCX1 = OC(1);
            OCX2 = OC(1)+sin(FallAngle)*EffHeight;
            % Obtain content's coordinates
            MAXY = max(CC(2:CC(1,2)+2,2));
            MINY = min(CC(2:CC(1,2)+2,2));
            MAXX = max(CC(2:CC(1,2)+2,1));
            MINX = min(CC(2:CC(1,2)+2,1));
            % Check that occupant is located to the west of the content
            if max(OCX1,OCX2)<MINX
            % Consider case where part of occupant is located north of
            % impact
            if max(OCY1,OCY2)>MAXY&&min(OCY1,OCY2)<MAXY
                % Consider case where another part of occupant is located
                % south of impact
                if min(OCY1,OCY2)>MINY
                    % Check distance required to cause impact
                    x1 = (MAXY-OC(2))*tan(FallAngle);
                    x2 = (min(OCY1,OCY2)-OC(2))*tan(FallAngle);
                    % Compute sliding displacement
                    SD = max(x1,x2)+OC(1)-min(CC(2:CC(1,2)+2,1));
                    % Determine impact location and mass
                    if max(x1,x2)==x1
                        BIRTEMP = [x1/sin(FallAngle), x1/sin(FallAngle),...
                            CB(6)];
                    else
                        BIRTEMP = [x2/sin(FallAngle), x2/sin(FallAngle),...
                            CB(6)];
                    end
                    FlagS = FlagS+1;
```

```
    % Consider case where rest of occupant's body was subjected
    % to impact (same process as previous)
    elseif min(OCY1,OCY2)<=MINY
        x1 = (MAXY-OC(2))*tan(FallAngle);
        x2 = (MINY-OC(2))*tan(FallAngle);
        SD = max(x1,x2)+OC(1)-min(CC(2:CC(1,2)+2,1));
        if max(x1,x2)==x1
            BIRTEMP = [x1/sin(FallAngle), x1/sin(FallAngle),...
                CB(6)];
        else
            BIRTEMP = [x2/sin(FallAngle), x2/sin(FallAngle),...
                CB(6)];
        end
        FlagS = FlagS+1;
    end
% Consider case where no part of the occupant's body was
% located north of the impact
elseif max(OCY1,OCY2)<=MAXY&&max(OCY1,OCY2)>=MINY
    % Consider case where whole of occupant's body was
    % subjected to impact
    if min(OCY1,OCY2)>MINY
        x1 = (max(OCY1,OCY2)-OC(2))*tan(FallAngle);
        x2 = (min(OCY1,OCY2)-OC(2))*tan(FallAngle);
        SD = max(x1,x2)+OC(1)-min(CC(2:CC(1,2)+2,1));
        if max(x1,x2)==x1
            BIRTEMP = [x1/sin(FallAngle), x1/sin(FallAngle),...
                CB(6)];
        else
            BIRTEMP = [x2/sin(FallAngle), x2/sin(FallAngle),...
                CB(6)];
        end
        FlagS = FlagS+1;
    % Consider case where part of occupant's body was
    % located south of impact
    elseif min(OCY1,OCY2)<=MINY
        x1 = (max(OCY1,OCY2)-OC(2))*tan(FallAngle);
        x2 = (MINY-OC(2))*tan(FallAngle);
        SD = max(x1,x2)+OC(1)-min(CC(2:CC(1,2)+2,1));
        if max(x1,x2)==x1
            BIRTEMP = [x1/sin(FallAngle), x1/sin(FallAngle),...
                CB(6)];
        else
            BIRTEMP = [x2/sin(FallAngle), x2/sin(FallAngle),...
                CB(6)];
        end
        FlagS = FlagS+1;
    end
end

% If any of the above conditions were satisfied
if FlagS == 1
    % Import sliding content response (i.e. velocity,
    % displacement)
    TEMP1 = Datainputs{CB(3)};
    TEMP2 = Datainputs{CB(4)};
    % Combine both velocity and displacement to single matrix
    % for processing
    SlideRHTemp = [TEMP1(find(TEMP1(:,1)>tf),Floor+2),...
        TEMP2(find(TEMP1(:,1)>tf),Floor+2)];
    % Find the velocity value at the time of impact
    SlideRH=SlideRHTemp(min(find(SlideRHTemp(:,1)>SD)):...
```

```
                length(SlideRHTemp(:,1)),:);
                % Identify if impact occurs at all in the first place
                if min(SlideRH)<SD
                    counterC=counterC+1;
                    % Calculate impact velocity
                    ImpactV(counterC,:)=...
                        interp1(abs(SlideRH(min(find(SlideRH(:,1)<SD))-...
                        1:min(find(SlideRH(:,1)<SD)),1)),...
                        abs(SlideRH(min(find(SlideRH(:,1)<SD))-1:...
                        min(find(SlideRH(:,1)<SD)),2)),abs(SD))*ones(1,2);
                    % Calculate impact locations
                    BIR(counterC,:)=BIRTEMP;
                end
            end
            end
            end
        end
    end
end
% Normalize impact locations by occupant height
if BIR(1)>=0
BIR(:,1:2)=BIR(:,1:2)/EffHeight;
% Flag to indicate that injuries due to content sliding had occurred
Flag = 6;
End
%--------------------------------------------------------------------------
%--------------------------------------------------------------------------
```

E6. INJURY SEVERITY FUNCTIONS

The following function takes the impact velocity and mass information obtained from impact assessment for use in predicting the severity of injuries. Note that several smaller functions were written to incorporate severity fragility functions. An example of this for lower extremity injuries is also detailed.

```
%--------------------------------------------------------------------------
% function [Source,AIS,BodyPart] = INJURYSeverityAssessment(ImpactV,BIR)
% Written by Trevor Yeow
% Version 1.0 (27th August 2015)
%--------------------------------------------------------------------------
% Purpose
% This code predicts the severity of injury based on the impact velocity
% and mass acting on the occupant
%
% Inputs
% ImpactV           - N by 2 matrix detailing the impact velocities at both
%                     ends of the Nth distributed load. If the impact was
%                     concentrated, then both ImpactV values in a row are
%                     the same
% BIR               - N by 5 matrix detailing the boundary impact
%                     conditions. (1) Location of lower impact on occupant
%                     as a ratio of total occupant height, (ii) location of
%                     upper impact, (iii)impact mass, (iv) impact type
%                     (i.e. occuapnts fell first before getting stuck by
```

```
%                     contents, and (v) source of injury
%
% Outputs
% Source            - Indicator of type of injury which occured
% AIS               - AIS rating of injury
% BodyPart          - Body part which is most severely injured
%--------------------------------------------------------------------------

function [Source,AIS,BodyPart] = INJURYSeverityAssessment(ImpactV,BIR)

% Define body part boundary for head, lower extremity, upper extremity, and
% chest respectively.
BPR = [6.7/8 1;0.5 4.7/8;0 0.5;2 3;4.7/8 6.7/8];

% Define initial parameters
m1 = zeros(length(BIR(:,1)),1);          %For storing mass information
Type = zeros(length(BIR(:,1)),1);        %For identifying injury source
IVAnalysis = zeros(length(BIR(:,1)),5); %For obtaining impact velocity

% Cycle through all impact cases
for i = 1:length(BIR(:,1))
    if BIR(i,1)>=0
        % Cycle through all body parts
        for j = 1:5
            % If the impact was distributed
            if BIR(i,1)~=BIR(i,2)
                %Identify if impact covers entire body part
                if BIR(i,1)<=BPR(j,1)&&BIR(i,2)>=BPR(j,2)
                    %Intepolate to obtain mean impact velocity across body
                    %part
                    IVAnalysis(i,j)=mean(interp1(BIR(i,1:2),...
                        ImpactV(i,:),BPR(j,:)));
                    %Note that for chest injuries, impact mass is also
                    %required. Example for this given below.
                    if j == 5
                        if BIR(i,3)~=-1
                            m1(i)=BIR(i,3)/(BIR(i,2)-BIR(i,1))*...
                                (BPR(j,2)-BPR(j,1));
                            Type(i) = BIR(i,4);
                        end
                    end
                %Identify if lower point of impact is below body part of
                %interest, yet if higher impact point is within body part
                elseif BIR(i,1)<=BPR(j,1)&&BIR(i,2)<=...
                        BPR(j,2)&&BIR(i,2)>=BPR(j,1)
                    IVAnalysis(i,j)=(interp1(BIR(i,1:2),ImpactV(i,:),...
                        BPR(j,1))+ImpactV(i,2))/2;
                    if j == 5
                        if BIR(i,3)~=-1
                            m1(i)=BIR(i,3)/(BIR(i,2)-BIR(i,1))*...
                                (BIR(i,2)-BPR(j,1));
                            Type(i) = BIR(i,4);
                        end
                    end
                %Identify both points of impact occur within the same body
                %part
                elseif BIR(i,1)<=BPR(j,2)&&BIR(i,1)>=...
                        BPR(j,1)&&BIR(i,2)<=BPR(j,2)
                    IVAnalysis(i,j)=mean(ImpactV(i,:));
                    if j == 5
```

```
                        if BIR(i,3)~=-1
                            m1(i)=BIR(i,3)/(BIR(i,2)-BIR(i,1))*...
                                (BIR(i,2)-BIR(i,1));
                            Type(i) = BIR(i,4);
                        end
                    end
                %Identify if upper point of impact is above body part of
                %interest, yet if higher impact point is within body part
                elseif BIR(i,1)<=BPR(j,2)&&BIR(i,1)>=...
                        BPR(j,1)&&BIR(i,2)>=BPR(j,2)
                    IVAnalysis(i,j)=(ImpactV(i,1)+interp1(BIR(i,1:2),...
                        ImpactV(i,1:2),BPR(j,2)))/2;
                    if j == 5
                        if BIR(i,3)~=-1
                            m1(i)=BIR(i,3)/(BIR(i,2)-BIR(i,1))*...
                                (BPR(j,2)-BIR(i,1));
                            Type(i) = BIR(i,4);
                        end
                    end
                end
            else %For single impact cases
                if BIR(i,1)<=BPR(j,2)&&BIR(i,1)>=BPR(j,1)
                    IVAnalysis(i,j)=ImpactV(i,1);
                    if j == 5
                        if BIR(i,3)~=-1
                            m1(i)=BIR(i,3);
                            Type(i) = BIR(i,4);
                        end
                    end
                end
            end
        end
    elseif BIR(i,1)==-1 %If occupant fell onto arm
        IVAnalysis(i,4)=max(IVAnalysis(4),ImpactV(i,2));
    end
end

% Injury severity assessments
for i = 1:length(Type)
    if IVAnalysis(i,1)>0;       % Head injuries
        AISHead = SeverityHead(IVAnalysis(i,1));
    else
        AISHead = 0;
    end
    if IVAnalysis(i,2)>0        % Pelvis injuries
        AISPelvis = SeverityPelvis(IVAnalysis(i,2));
    else
        AISPelvis = 0;
    end
    if IVAnalysis(i,3)>0        % Lower limb injuries
        AISLL = SeverityLL(IVAnalysis(i,3));
    else
        AISLL = 0;
    end
    if IVAnalysis(i,4)>0        % Upper limb injuries
        AISUL = SeverityUL(IVAnalysis(i,4));
    else
        AISUL = 0;
    end
    if IVAnalysis(i,5)>0        % Chest injuries
        AISChest = SeverityChest(Type(i),m1(i),IVAnalysis(i,5));
```

```
    else
        AISChest = 0;
    end
    % Store AIS results
    AISTemp(i,:) = [AISHead,max(AISPelvis,AISLL),AISUL,AISChest];
end

% Identify if any injuries even occurred in the first place
if max(max(AISTemp))>0
    for i = 1:4
        % Identifying which body part has the largest AIS and is highest on
        % heirachy, and the source of injury
        if max(AISTemp(:,i))==max(max(AISTemp))
            BodyPart = i;
            Source = BIR(min(find(AISTemp(:,i)==max(max(AISTemp)))),5);
            AIS = max(max(AISTemp));
            break
        end
    end
else
    % If no injury occurs, just export out 0 for all values of interest
    AIS = 0;
    BodyPart = 0;
    Source = 0;
end
%--------------------------------------------------------------------------


%--------------------------------------------------------------------------
% function AIS = SeverityLL(ImpactV)
%--------------------------------------------------------------------------
% Purpose
% To obtain an AIS rating for lower extremity injuries for a given impact
% velocity
%--------------------------------------------------------------------------

function AISLL = SeverityLL(ImpactV)

% If impact velocity is 0, reset to 1e-6 so that lognormal distribution can
% be used for the gravility functions
if ImpactV<=0
    ImapctV=1e-6;
end

% Fragility function for three damage states
Prob(1)=cdf('norm',log(ImpactV),log(4.3),0.15);
Prob(2)=cdf('norm',log(ImpactV),log(5),0.15);
Prob(3)=cdf('norm',log(ImpactV),log(6.5),0.15);

% Random trial to obtain AIS severity
Temp = rand;

% Cycle through cases to identify the AIS corresponding to the injury
% specified
i = 1;
while Prob(i)>Temp
    i = i+1;
    if i == 3
        i = 4;
        break
```

```
    end
end
AISLL = i-1;
%-------------------------------------------------------------------------
```

E7. INJURY COST FUNCTIONS

The following function was used to obtain injury cost. Note here that the injury costs were deaggregated into smaller categories based on Miller [1] and Zaloshnja et al. [2]; such as medical cost and decrease in quality of life, among others. Note that a dispersion of 0.15 was assumed for each category.

```
%-------------------------------------------------------------------------
% function InjuryCost = CostEstimate(AIS)
% Written by Trevor Yeow
% Version 1.0 (27th August 2015)
%
% Purpose
% This code predicts cost of injury to a single occupant based on the
% Abbreviated Injury Scale rating for each body part. This version only
% considers the brain/head, lower extremities (legs, knees, ankle, pelvis),
% upper extremities (arms, shoulders, elbows), and chest/torso area.
%
% Input
% AIS     - A row with four entries [X1 X2 X3 X4]
%               X1 = AIS rating for brain/head
%               X2 = AIS rating for lower extremities
%               X3 = AIS rating for upper extremities
%               X4 = AIS rating for chest/torso area
% CFlag   - A row with 7 entries. If entry > 0, cost component is
%             considered
%               Entry 1 - Medical cost
%               Entry 2 - Emergency services cost
%               Entry 3 - Household productivity loss
%               Entry 4 - Loss of wages
%               Entry 5 - Workplace productivity loss
%               Entry 6 - Insurance administration
%               Entry 7 - Quality of life
%
% Output
% Injury cost - Cost of injury in USD (year 2015)
%
% Notes
% The median data was adjusted from Miller [1] and Zaloshnja et al. [2] to
% 2015 values assuming a 4% discount rate. A dispersion of 0.15 was assumed
% for all individual parameters.
%
% References
% [1] Miller TR. (1993). "Costs and functional consequences of U.S.
%     roadway crashes". Accident Analysis and Prevention, Vol 25(5), pp
%     593-607.
% [2] Zaloshnja E, Miller TR, Romano E, & Spicer R. (2004). "Crash costs by
% body part injured, fracture involvement, and threat-to-life severity,
% United States, 2000". Accident Analysis and Prevention, Vol 36(3), pp
```

```
% 415-427.
%--------------------------------------------------------------------------

function [InjuryCost] = INJURYCostEstimate(AIS,BodyPart,CFlag)

% Identify most severely injurred body part
i = BodyPart;

% If body part was injured
if i>0
j = AIS;

    % Medical costs (across is varying AIS, downwards is body part in order
    % of head/lower extremities/upper extremities/chest - same applies for
    % remainder of categories, also note that all cost values here are
    % median cost)
    Medical = [26000    43400   154000  273000  605000  27100
        2150    18900   60900   74000   378000  27100
        2040    11800   25200   25200   25200   27100
        2220    14500   45600   76400   103000  27100];

    % Emergency services cost
    ES = [262 579 914 2070 2120 1960];

    % Household productivity loss
    HW = [3700  9390    27700   58100   356000  385000
        625 13600   39900   67300   230000  385000
        1110    11900   28400   28400   28400   385000
        1020    11100   23100   30600   65300   385000];

    % Workplace wages loss
    Wages = [12300  34300   102000  224000  977000  1340000
        1890    44600   144000  347000  757000  1340000
        3680    39100   99100   99100   99100   1340000
        3110    42300   84200   112000  209000  1340000];

    % Workplace productivity loss
    WP = [513   2930    6720    7760    15900   17800
        409 3330    7920    10300   10300   17800
        505 3750    7240    7240    7240    17800
        433 2530    5150    7080    8000    17800];

    % Insurance administration
    IA = [5290  9490    31300   61400   149000  95600
        1020    10800   30900   50000   107000  95600
        1230    6980    19700   19700   19700   95600
        1210    9850    21600   29200   44300   95600];

    % Decrease in quality of life
    QL = [47800 407000 768000 2170000 4190000 4230000
        7620 84600 610000 643000 643000 4230000
        10500 123000 453000 453000 453000 4230000
        7100 68800 453000 920000 876000 4230000];

    % Calculate injury cost for given AIS and body part, assuming a
    % dispersion of 0.15 for all loss categories considered
    InjuryCost = exp(icdf('norm',rand,log(Medical(i,j)),0.15))*CFlag(1)+...
        exp(icdf('norm',rand,log(ES(j)),0.15))*CFlag(2)+...
        exp(icdf('norm',rand,log(HW(i,j)),0.15))*CFlag(3)+...
```

```
        exp(icdf('norm',rand,log(Wages(i,j)),0.15))*CFlag(4)+...
        exp(icdf('norm',rand,log(WP(i,j)),0.15))*CFlag(5)+...
        exp(icdf('norm',rand,log(IA(i,j)),0.15))*CFlag(6)+...
        exp(icdf('norm',rand,log(QL(i,j)),0.15))*CFlag(7);
end
%-------------------------------------------------------------------------
```

E8. REFERENCES

1. Miller, T. R. (1993). Costs and Functional Consequences of U.S. Roadway Crashes. Accident Analysis and Prevention, 25(5), 593-607.
2. Zaloshnja, E., Miller, T. R., Romano, E., & Spicer, R. (2004). Crash costs by body part injured, fracture involvement, and threat-to-life severity, United States, 2000. Accident Analysis and Prevention, 36(3), 415-427.